WHP I08N REVISIT/I07S IN 2019/2020 DATA BOOK

Field Activity of JAMSTEC towards a Sustained Global Survey of the Ocean Interior

WHP I08N REVISIT/I07S
in 2019/2020

Towards
a Sustained Global Survey
of the Ocean Interior

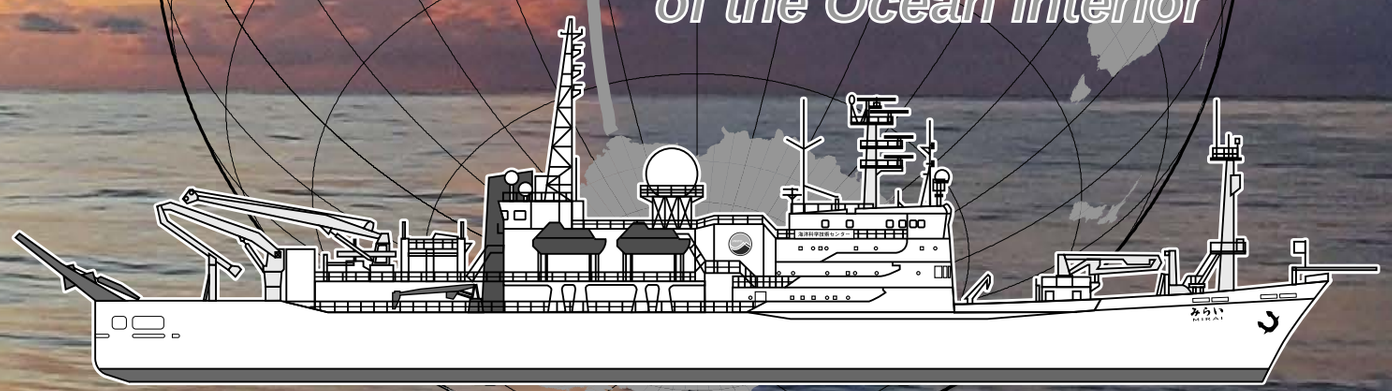

WHP I08N REVISIT/I07S IN 2019/2020 DATA BOOK

Edited by
Hiroshi Uchida (JAMSTEC),
Akihiko Murata (JAMSTEC),
Katsuro Katsumata (JAMSTEC),
Kanapathipillai Arulananthan (NARA),
Toshimasa Doi (JAMSTEC)

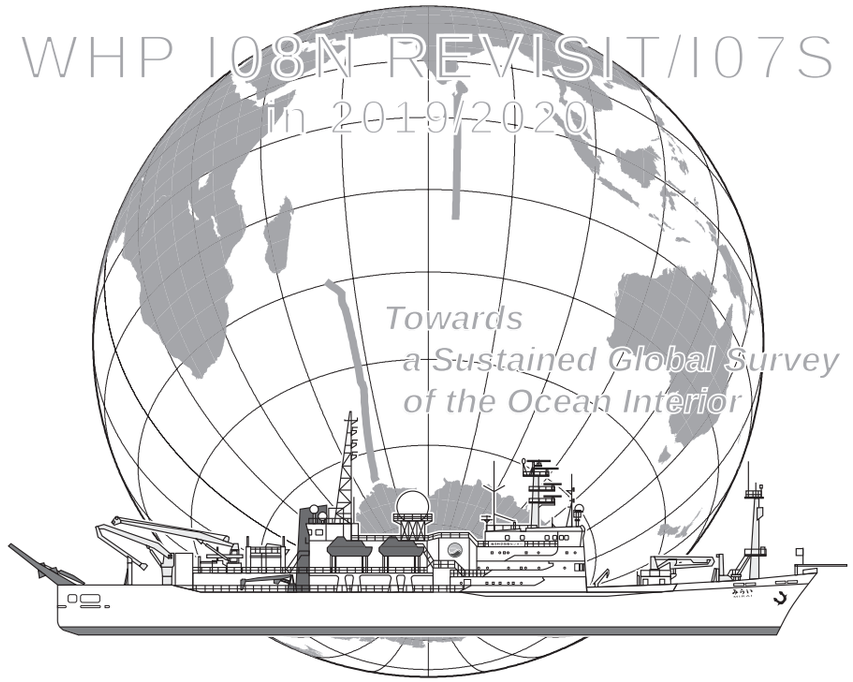

The photograph on the front and back cover of a cumulonimbus above the Indian Ocean was taken by Mr. Koki Miyakawa.
The photograph on the inside cover of Antarctica was taken by Mr. David Snider.

WHP I08N REVISIT/I07S IN 2019/2020 DATA BOOK

March 12, 2021 Published
Edited by Hiroshi Uchida (JAMSTEC), Akihiko Murata (JAMSTEC), Katsuro Katsumata (JAMSTEC), Kanapathipillai Arulananthan (NARA) and Toshimasa Doi (JAMSTEC)

Japan Agency for Marine-Earth Science and Technology
2-15 Natsushima, Yokosuka, Kanagawa. 237-0061, Japan
Phone +81-46-867-9474, Fax +81-46-867-9835

ISBN 987-4-901833-47-9

DOI: 10.17596/0002162

Printed by Aiwa Enterprise, Ltd.
3-22-4 Takanawa, Minato-ku, Tokyo 108-0074, Japan

Contents

Preface

I am pleased to announce that we finally publish the data book on our cruise conducted in 2019/2020. The cruise was conducted under the framework of Global Ocean Ship-based Hydrographic Investigations Program (GO-SHIP). We usually have a GO-SHIP cruise basically every second year using the R/V *Mirai*. However, the GO-SHIP cruise in 2019/2020 was somewhat different from the previous ones; First, we could not conduct water samplings at every CTD stations, because we did not have a ship time enough for water sampling. Second, the observation section in the South Indian was a new one (named as I07S), which was not set in the World Ocean Circulation Experiment (WOCE) Hydrographic Program (WHP). Despite these differences, high-quality hydrographic measurements were successfully made in the cruise.

In the leg from Columbo, Sri Lanka to Port Louis, Mauritius, we re-occupied the WOCE WHP I08N section for the first time in 25 years. In fact, we intended to the re-occupation of the section in 2011, but we had to postpone the observation because of the big earthquake occurred in Japan in March 2011. For the re-occupation cruise, we had planned the observation also in the EEZ of Sri Lanka in co-operation with National Aquatic Resources Research and Development Agency (NARA) in Sri Lanka. When we had to give up the cruise in 2011, we promised the re-occupation in the future to Sri Lanka. Thus, we are very happy that we could fulfill the promise.

In the cruise from Port Louis to the coast of the Antarctic, as we entered the so-called Roaring 40s, Furious 50s and Screaming 60s, we often had to change cruise schedules due to rough weather. Because of this, data gaps along the section, especially for water sampling properties,

Through the cruise, as a general, we could perform high-quality measurements. Nevertheless, data on nutrients seem to be somewhat inferior to the data collected in the previous GO-SHIP cruises by the R/V *Mirai*. Nutrients data provided by the *Mirai*'s GO-SHIP cruises has been one of the leading measurements in the ocean community. In this data book, the reason why the nutrients measurements became inferior is described in detail. We hope that the descriptions and data could be helpful for a better measurement in the future not only for us but also for people who aim to produce high-quality data, together with those for other properties.

I am now writing this preface on 2nd January, 2021, when a pandemic of COVID-19 is still predominant in the world. Fortunately, little influences existed for our cruise in 2019/2020. I hope the pandemic ends as soon as possible so that we can conduct with no restrictions ship-based observations, which are indispensable for coping with global environmental issues.

Readers may find contents of this data book, and links to other WHP revisit data books, on the web site http://www.jamstec.go.jp/iorgc/ocorp/data/post-woce.html. Updates and corrections will be found online. The data book published since 2018 is assigned a DOI (Digital Object Identifier), and all the previously published data books will also be assigned a DOI in a near future.

Akihiko Murata

Physical and Chemical Oceanography Research Group

Global Ocean Observation Research Center (GOORC)

Research Institute for Global Changes (RIGC)

Japan Agency for Marine-Earth Science and Technology (JAMSTEC)

1 Cruise Narrative

Akihiko Murata (JAMSTEC)

Katsuro Katsumata (JAMSTEC)

1.1 Highlight

Cruise track: See Fig. 1.1.1

Cruise code: MR19-04

Expedition Designation: Leg 2, 49NZ20191205

Leg 3, 49NZ20191229

GHPO section designation: Leg 2, I08N

Leg 3, I07S

Ship name: R/V Mirai

Ports of Call: Leg 1, Hachinohe, Japan – Singapore, Singapore – Colombo, Sri Lanka

Leg 2, Colombo, Sri Lanka – Port Lois, Mauritius

Leg 3, Port Louis, Mauritius – Singapore, Singapore

Leg 4, Singapore, Singapore – Koror, Palau

Cruise Dates: Leg 1, 15 November 2019 – 4 December 2019

Leg 2, 5 December 2019 – 27 December 2019

Leg 3, 29 December 2019 – 10 February 2020

Leg 4, 13 February 2020 – 21 February 2020

Chief Scientist and Affiliation:

Leg 2, Akihiko Murata (murataa@jamstec.go.jp)

Leg 3, Katsuro Katsumata (k.katsumata@jamstec.go.jp)

Global Ocean Observation Research Center,

Research Institute for Global Change,

Japan Agency for Marine-Earth Science and Technology (JAMSTEC)

2-15 Natsushima, Yokosuka, Kanagawa, Japan 237-0061

Fax: +81-46-867-9835

Number of Stations: Leg 1, none

Leg 2, 69 CTD stations

Leg 3, 79 CTD stations,

23 XCTD deployments (16 XCTD only + 7 side-by-side with CTD)

Leg 4, none

Floats and drifter deployed: 1 Argo float, 3 Deep Argo floats, 1 BGC Argo float (Leg 2)

17 Argo floats, 1 Deep Argo float, 8 BGC Argo floats (Leg 3)

Mooring recovery: none

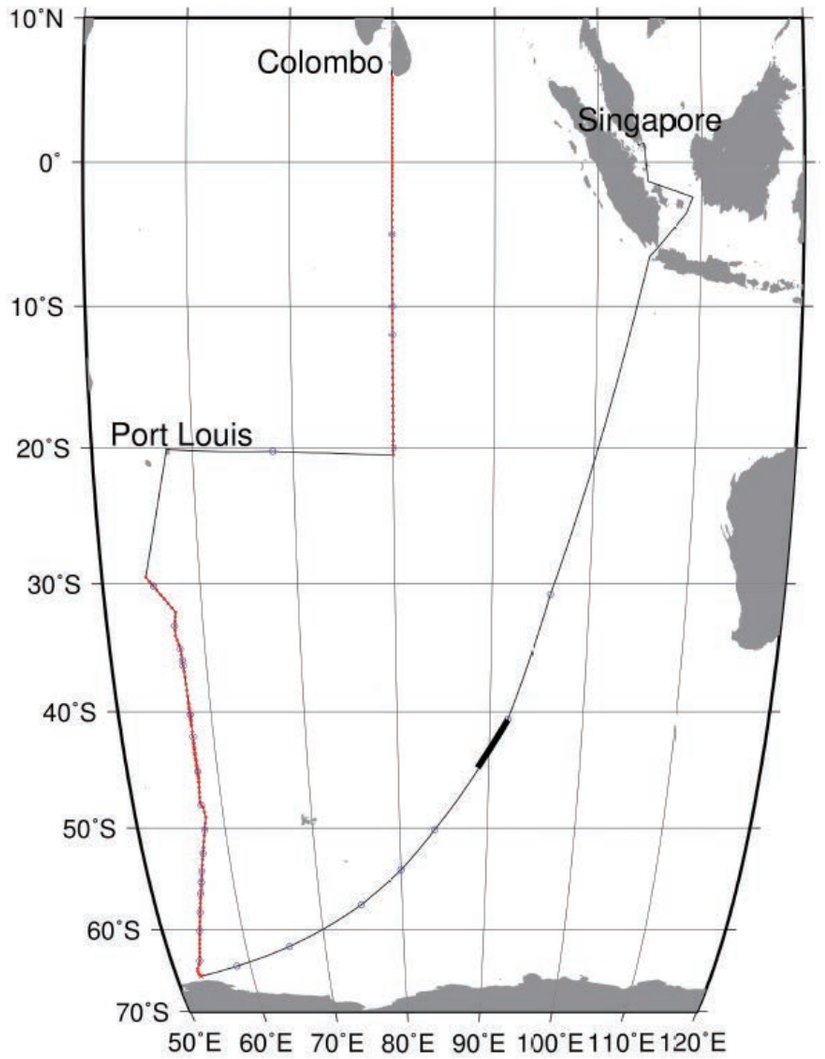

Fig. 1.1.1 MR19-04 cruise track (Legs 2 and 3). The red dots show CTD and/or Niskin sampling stations. Blue circles show float deployments. Thick black segment shows geophysical survey.

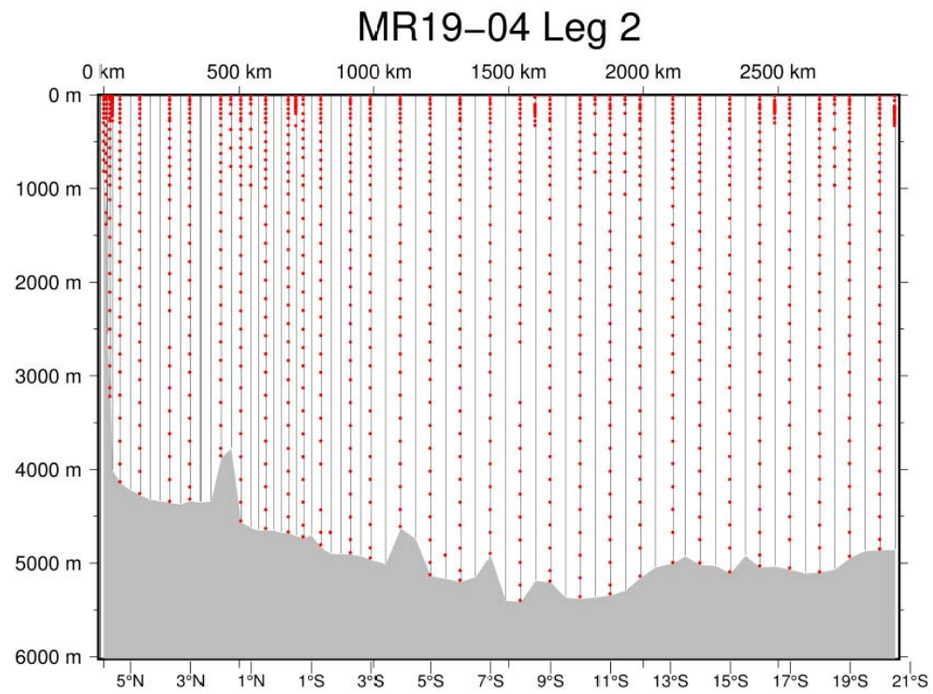

Fig. 1.1.2 Water sampling positions for leg 2 (I08N revisit). Blue lines show CTD trace and red dots show Niskin sampling. Gray is ocean bottom bathymetry.

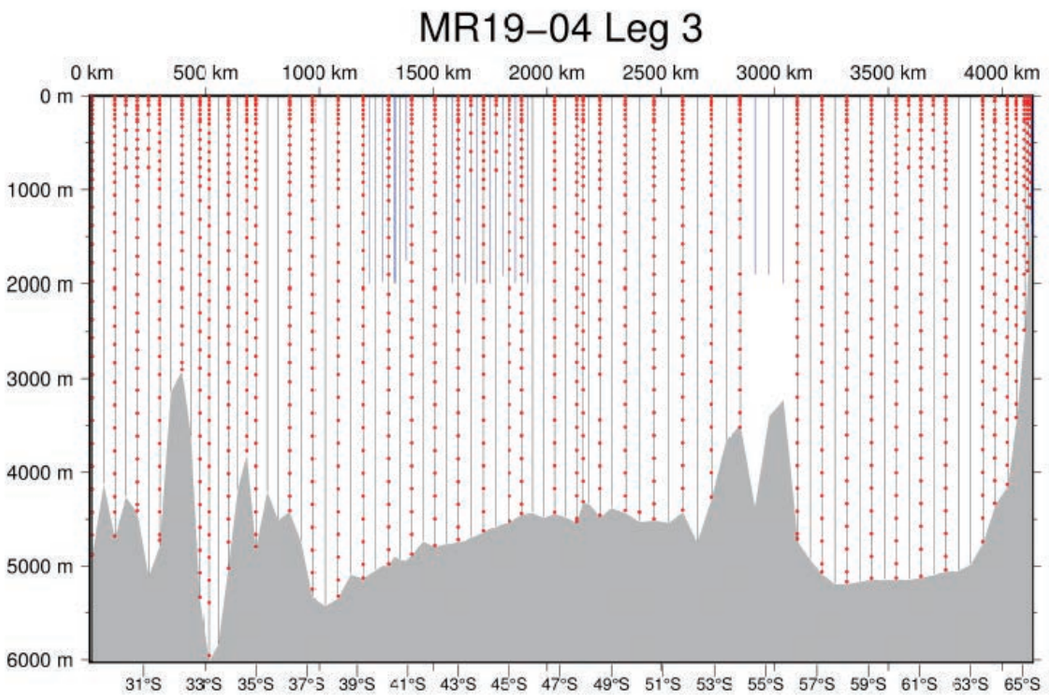

Fig. 1.1.3 Water sampling positions for leg 3 (I07S first visit). Blue lines show CTD/XCTD trace and red dots show Niskin sampling. Gray is ocean bottom bathymetry

1.2 Cruise Description

Indian and Southern Oceans are logistically challenging for large scale ship observation despite their large amplitude variability with intraseasonal to decadal time scales owing to the complicated wind system and topography. World Ocean Circulation Experiment (WOCE) established a number of hydrographic sections to monitor this important ocean. As JAMSTEC contribution towards the Global Ocean Ship-based Hydrographic Investigation Program (GO-SHIP), decadal reoccupation of the WOCE section I8N (nominally along 80°E, 6°N to 24°S, previously occupied in 1995) and new occupation of the section I7S (nominally along 57.5°E, 28°S to ice edge) are proposed. All GO-SHIP level 1 and selected level 2 water samples will be collected from the surface to near the bottom along with continuous CTD observation. In addition to providing baseline hydrographic data to describe the ocean circulation in this relatively unknown part of the Indian and Southern Oceans, the data will contribute to clarify subsurface decadal changes in water properties associated with climate change and to improve the carbon budget by measuring the subsurface carbon distribution in this mode/intermediate water source region. Other items including ocean-atmosphere fluxes and biogeochemical parameters will also be measured interaction among mantle, ocean ridge, and subduction system. This cruise has been endorsed by IIOE-2 (International Indian Ocean Expedition).

1.3 Principal Investigators and personnel in charge onboard

The principal investigators (PI) and the persons responsible for major parameters are listed in Table 1.3.1.

Table 1.3.1. List of principal investigator and person in charge on the ship.

Item	Principal Investigator	Person in Charge on the Ship
Underway		
Navigation	Katsuro Katsumata (JAMSTEC)	Masanori Murakami (NME) (leg 2)
	k.katsumata@jamstec.go.jp	Kazuho Yoshida (NME) (leg 3)
Bathymetry	Katsuro Katsumata (JAMSTEC)	Masanori Murakami (NME) (leg 2)
	k.katsumata@jamstec.go.jp	Kazuho Yoshida (NME) (leg 3)
Magnetic Field	Katsuro Katsumata (JAMSTEC)	Masanori Murakami (NME) (leg 2)
	k.katsumata@jamstec.go.jp	Kazuho Yoshida (NME) (leg 3)
Gravity	Katsuro Katsumata (JAMSTEC)	Masanori Murakami (NME) (leg 2)
	k.katsumata@jamstec.go.jp	Kazuho Yoshida (NME) (leg 3)

Meteorology	Katsuro Katsumata (JAMSTEC) *k.katsumata@jamstec.go.jp*	Masanori Murakami (NME) (leg 2) Kazuho Yoshida (NME) (leg 3)
TSG	Hiroshi Uchida (JAMSTEC) *huchida@jamtec.go.jp*	Erii Irie (MWJ)
Underway pCO_2	Akihiko Murata (JAMSTEC) *murataa@jamstec.go.j*p	Nagisa Fujiki (MWJ)
ADCP	Katsuro Katsumata (JAMSTEC) *k.katsumata@jamstec.go.jp*	Masanori Murakami (NME) (leg 2) Kazuho Yoshida (NME) (leg 3)
Ceilometer	Katsuro Katsumata (JAMSTEC) *k.katsumata@jamstec.go.jp*	Masanori Murakami (NME) (leg 2) Kazuho Yoshida (NME) (leg 3)
Sky Radiometer	Kazuma Aoki (Univ. of Toyama) *kazuma@sci.u-toyama.ac.jp*	Masanori Murakami (NME) (leg 2) Kazuho Yoshida (NME) (leg 3)
C-band Weather Radar	Masaki Katsumata (JAMSTEC) *katsu@jamstec.go.jp*	Masanori Murakami (NME) (leg 2) Kazuho Yoshida (NME) (leg 3)
Lidar	Masaki Katsumata (JAMSTEC) *katsu@jamstec.go.jp*	Masanori Murakami (NME) (leg 2) Kazuho Yoshida (NME) (leg 3)
Disdrometer	Masaki Katsumata (JAMSTEC) *katsu@jamstec.go.jp*	
Micro Rain Radar	Masaki Katsumata (JAMSTEC) *katsu@jamstec.go.j*p	
GNSS Precipitable Water	Masaki Katsumata (JAMSTEC) *katsu@jamstec.go.jp*	
Satellite Image	Katsuro Katsumata (JAMSTEC) *k.katsumata@jamstec.go.jp*	Masanori Murakami (NME) (leg 2) Kazuho Yoshida (NME) (leg 3)
Tropospheric Gases and Particles		
	Yugo Kanaya (JAMSTEC) *yugo@jamstec.go.jp*	Masanori Murakami (NME) (leg 2) Kazuho Yoshida (NME) (leg 3)
CH_4 Isotope Ratio	Eiji Tasumi (JAMSTEC) *etasumi@jamstec.go.jp*	Eiji Tasumi (JAMSTEC)
Microplastic	Ryota Nakajima (JAMSTEC) *nakajimar@jamstec.go.jp*	Hiroshi Uchida (JAMSTEC)

Hydrography

CTD/O_2	Hiroshi Uchida (JAMSTEC) *huchida@jamstec.go.jp*	Shinsuke Toyoda (MWJ) (leg 2) Rio Kobayashi (MWJ) (leg 3)
Salinity	Hiroshi Uchida (JAMSTEC) *huchida@jamstec.go.jp*	Hiroki Ushiromura (MWJ) (leg 3) Shungo Oshitani (MWJ) (leg 2)
LADCP	Shinya Kouketsu (JAMSTEC) *skouketsu@jamstec.go.jp*	Shinya Kouketsu (JAMSTEC)
Micro Ridar	Shinya Kouketsu (JAMSTEC) *skouketsu@jamstec.go.jp*	Shinya Kouketsu (JAMSTEC)
Oxygen	Yuichiro Kumamoto (JAMSTEC) *kumamoto@jamstec.go.jp*	Erii Irie (MWJ)
Nutrients	Michio Aoyama (JAMSTEC) *michioaoyama1953@jamstec.go.jp*	Keitaro Matsumoto (MWJ) (leg 2) Shinichiro Yokogawa (MWJ) (leg 3)
Density	Hiroshi Uchida (JAMSTEC) *huchida@jamstec.go.jp*	Hiroshi Uchida (JAMSTEC)
$CFCs/SF_6$	Masahito Shigemitsu (JAMSTEC) *ma-shige@jamstec.go.jp*	Masahiro Orui (MWJ) (leg 2) Katsunori Sagishima (MWJ) (leg 3)
Carbon Properties	Akihiko Murata (JAMSTEC) *murataa@jamstec.go.jp*	Nagisa Fujiki (MWJ)

Chlorophyll *a*	Kosei Sasaoka (JAMSTEC) *sasaoka@jamstec.go.jp*	Misato Kuwahara (MWJ)
CDOM/Absorption Coefficients	Kosei Sasaoka (JAMSTEC) *sasaoka@jamstec.go.jp*	Kosei Sasaoka (JAMSTEC)
Radiocesium	Yuichiro Kumamoto (JAMSTEC) *kumamoto@jamstec.go.jp*	Yuichiro Kumamoto (JAMSTEC)
Nitrogen Cycles	Akiko Makabe (JAMSTEC) *makabea@jamstec.go.jp*	Eiji Tasumi (JAMSTEC)
DOC and FDOM	Masahito Shigemitsu (JAMSTEC) *ma-shige@jamstec.go.jp*	Masahito Shigemitsu (JAMSTEC)
N_2/O_2/Ar	Yutaka Watanabe (Hokkaido Univ.) *yywata@ees.hokudai.ac.jp*	Bofeng Li (Hokkaido Univ.) (leg 2) Chenye Wang (Hokkaido Univ.) (leg 2)
$\Delta^{14}C/\delta^{13}C$	Yuichiro Kumamoto (JAMSTEC) *kumamoto@jamstec.go.jp*	Yuichiro Kumamoto (JAMSTEC)
$\delta^{18}O$	Shigeru Aoki (Hokkaido Univ.) *shigeru@lowtem.hokudai.ac.jp*	Katsuro Katsumata (JAMSTEC)
Urea/Iodine	Peter Croot (NUI Galway) *peter.croot@nuigalway.ie*	Peter Croot (NUI Galway) (leg 2) Maija Heller (PCUV) (leg 3)
Radon Sensor	Kiminori Shitashima (TUMSAT) *kshita0@kaiyodai.ac.jp*	Kiminori Shitashima (TUMSAT)
pH/pCO_2 Sensor	Kiminori Shitashima (TUMSAT) *kshita0@kaiyodai.ac.jp*	Kiminori Shitashima (TUMSAT)
Iodine Isotopes	Satoko Owari (TUMSAT) *sowari0@kaiyodai.ac.jp*	Yuichiro Kumamoto (JAMSTEC) (leg3)
Microbiology	Taichi Yokokawa (JAMSTEC) *taichi.yokokawa@jamstec.go.jp*	Masahito Shigemitsu (JASMTEC)
Refractive Index Density Sensor/Sound Velocity Sensor	Hiroshi Uchida (JAMSTEC) *huchida@jamstec.go.jp*	Hiroshi Uchida (JAMSTEC)
XCTD	Katsuro Katsumata (JAMSTEC) *k.katsumata@jamstec.go.jp*	Kazuho Yoshida (NME) (leg 3)
RBR Optode	Hiroshi Uchida (JAMSTEC) *huchida@jamstec.go.jp*	Hiroshi Uchida (JAMSTEC)
Sampling for SOCCOM	Lynne Talley (SIO) *ltalley@ucsd.edu* Stephen Riser (Univ.Washington) *riser@ocean.washington.edu* Ken Johnson (MBARI) *johnson@mbari.org*	Melissa Miller (SIO)

Floats, Drifters, Moorings

JAMSTEC ARGO Float	Shigeki Hosoda (JAMSTEC) *hosodas@jamstec.go.jp*	Keisuke Takeda (MWJ) (leg 2) Hiroyuki Hayashi (MWJ) (leg 3)
SOCCOM BGC Float	Stephen Riser (Univ.Washington) *riser@ocean.washington.edu* Lynne Talley (SIO) *ltalley@ucsd.edu* Ken Johnson (MBARI) *johnson@mbari.org*	Melissa Miller (SIO)

CSIRO ARGO Float

Peter Oke (CSIRO) Katsuro Katsumata (JAMSTEC) (leg 3)

Peter.Oke@csiro.au

1.4 Cruise Participants

List of Participants for leg 2

Akihiko Murata	Chief Scientist	JAMSTEC
Katsuro Katsumata	CTD/LADCP/Water sampling	JAMSTEC
Yuichiro Kumamoto	DO/Cs/Ra/^{14}C/^{13}C/Water sampling	JAMSTEC
Hiroshi Uchida	Salinity/Density/Microplastic/Water sampling	JAMSTEC
Shinya Kouketsu	CTD/LADCP/Water sampling	JAMSTEC
Sayaka Yasunaka	Water sampling	JAMSTEC
Masahito Shigemitsu	CFCs/FDOM/DOC	JAMSTEC
Kosei Sasaoka	Chl-a/CDOM/Water sampling	JAMSTEC
Minoru Hamana	Water sampling	JAMSTEC
Taichi Yokokawa	CH_4/N_2O/Bacteria/DNA/Water sampling	JAMSTEC
Eiji Tasumi	CH_4/N_2O/Bacteria/DNA/Water sampling	JAMSTEC
Akiko Makabe	CH_4/N_2O/Bacteria/DNA/Water sampling	JAMSTEC
Kiminori Shitashima	Radon, pH, pCO_2 sensors/Water sampling	TUMSAT
Satoko Owari	^{129}I/Water sampling	TUMSAT
Peter Croot	Iodate/Urea/Water sampling	NUI Galway
Li Bofeng	N_2/O_2/Ar/Water sampling	Hokkaido Univ.
Wang Chenye	N_2/O_2/Ar/Water sampling	Hokkaido Univ.
Yusuke Sasaki	microrider/Water sampling	Tokyo Univ.
K. Arulananthan	observer/Water sampling	NARA
Adikari Appuhami lage Upul	observer/Water sampling	NARA
Kasumi Yamauchi	FDOM	JAMATEC
Koki Miyakawa	DNA/Water sampling	JAMSTEC
Soichiro Sueyoshi	Meteorology/Geophysics/ADCP	NME
Yutaro Murakami	Meteorology/Geophysics/ADCP	NME
Masanori Murakami	Meteorology/Geophysics/ADCP	NME
Yasuhiro Arii	Water sampling	MWJ
Masahiro Orui	Water sampling	MWJ
Shinsuke Toyoda	CTD/Argo	MWJ
Misato Kuwahara	DO/TSG/Chl-a	MWJ
Tun Htet Aung	CTD/Argo	MWJ
Tomoyuki Tanaka	Nutrients	MWJ
Hiroki Ushiromura	Salinity	MWJ
Keisuke Takeda	CTD/Argo	MWJ
Yuta Oda	DIC/TA	MWJ
Katsunori Sagishima	CFCs	MWJ
Nagisa Fujiki	DIC/TA/pCO_2	MWJ
Hiroshi Hoshino	CFCs	MWJ
Keitaro Matsumoto	Nutrients	MWJ
Atsushi Ono	DIC/TA/pCO_2	MWJ
Tomomi Sone	Water sampling (Nutrients)	MWJ
Erii Irie	DO/TSG/Chl-a	MWJ
Yuko Miyoshi	DO/TSG/Chl-a	MWJ

List of Participants for leg 3

Katsuro Katsumata	Chief scientist	JAMSTEC
Yuichiro Kumamoto	DO/Cs/Ra/^{14}C/^{13}C/Water sampling	JAMSTEC
Hiroshi Uchida	Salinity/Density/Microplastic/Water sampling	JAMSTEC
Shinya Kouketsu	CTD/LADCP/Water sampling	JAMSTEC
Masahito Shigemitsu	CFCs/DFOM/DOC	JAMSTEC
Kosei Sasaoka	Chl-a/CDOM/Water sampling	JAMSTEC
Minoru Hamana	Water sampling	JAMSTEC
Maija Heller	Iodate/Urea/Water sampling	PCUV
Melissa Miller	SOCCOM floats/Water sampling	SIO
Sasaki Yusuke	Microrider/Water sampling	Tokyo University
Kasumi Yamauchi	FDOM	JAMSTEC
Koki Miyakawa	DNA/Water sampling	JAMSTEC
Kazuho Yoshida	Meteorology/Geophysics/ADCP	NME
Wataru Tokunaga	Meteorology/Geophysics/ADCP	NME
Satomi Ogawa	Meteorology/Geophysics/ADCP	NME
Yasuhiro Arii	Water sampling	MWJ
Katsunori Sagishima	CFCs	MWJ
Masanori Enoki	DIC/TA/ pCO_2	MWJ
Shinichiro Yokogawa	Nutrients	MWJ
Misato Kuwahara	DO/TSG/Chl-a	MWJ
Hiroshi Hoshino	CFCs	MWJ
Atsushi Ono	CFCs/ pCO_2	MWJ
Tomomi Sone	Nutrients	MWJ
Erii Irie	DO/TSG/Chl-a	MWJ
Yuko Miyoshi	DO/TSG/Chl-a	MWJ
Nagisa Fujiki	DIA/TA/pCO_2	MWJ
Hiroyuki Hayashi	CTD/Argo	MWJ
Rio Kobayashi	CTD/Argo	MWJ
Kento Fukahori	CTD/Argo	MWJ
Daiki Kawata	DIA/TA/pCO_2	MWJ
Shungo Oshitani	Salinity/Argo	MWJ
Ko Morita	Nutrients	MWJ
Shuntaro Hyogo	Water sampling	MWJ
Takuma Matsumoto	Water sampling	MWJ
Mikio Hasegawa	Water sampling	MWJ
Misaki Otsuka	Water sampling	MWJ

CSIRO	Commonwealth Scientific and Industrial Research Organization
JAMSTEC	Japan Agency for Marine-Earth Science and Technology
MBARI	Monterey Bay Aquarium Research Institute
MWJ	Marine Works Japan, Ltd.
NARA	National Aquatic Resources Research and Development Agency
NME	Nippon Marine Enterprises, Ltd.
NUI	National University of Ireland
PCUV	Pontifical Catholic University of Valparaíso
SIO	Scripps Institution of Oceanography
TUMSAT	Tokyo University of Marine Science and Technology

2 Underway Measurements

2.1 Navigation

(1) Personnel

Akihiko Murata	JAMSTEC: Principal investigator	- leg 2 -
Katsuro Katsumata	JAMSTEC: Principal investigator	- leg 3 -
Yutaro Murakami	Nippon Marine Enterprises Ltd., (NME)	- leg 2 -
Souichiro Sueyoshi	NME	- leg 2 -
Masanori Murakami	NME	- leg 2 -
Kazuho Yoshida	NME	- leg 3 -
Wataru Tokunaga	NME	- leg 3 -
Satomi Ogawa	NME	- leg 3 -
Takehito Hattori	MIRAI crew	- leg 2, 3 -

(2) System description

Ship's position and velocity were provided by Navigation System on R/V MIRAI. This system integrates GNSS position, Doppler sonar log speed, Gyro compass heading and other basic data for navigation. This system also distributed ship's standard time synchronized to GPS time server via Network Time Protocol. These data were logged on the network server as "SOJ" data every 5 seconds. Sensors for navigation data are listed below;

i) GNSS system:

R/V MIRAI has four GNSS systems, all GNSS positions were offset to radar-mast position, datum point. Anytime changeable manually switched as to GNSS receiving state.

a) StarPack-D & Multi-Fix (version 10.01.03), Differential GNSS system.
Antenna: Located on compass deck, starboard.

b) StarPack-D & Multi-Fix (version 09.10.05), Differential GNSS system.
Antenna: Located on compass deck, portside.

c) Standalone GPS system.
Receiver: Trimble SPS751
Antenna: Located on navigation deck, starboard.

d) Standalone GPS system.
Receiver: Trimble SPS751
Antenna: Located on navigation deck, portside.

ii) Doppler sonar log:

FURUNO DS-30, which use three acoustic beam for current measurement under the hull.

iii) Gyro compass:

TOKYO KEIKI TG-8000, Sperry type mechanical gyrocompass.

iv) GPS time server:

SEIKO TS-2550 Time Server, synchronizing to GPS satellites every 1 second.

(3) Data period (Time in UTC)

Leg2: 05:00, 05 Dec. 2019 to 05:40, 27 Dec. 2019

Leg3: 11:20, 29 Dec. 2019 to 00:30, 10 Feb. 2020

(4) Remarks

The firmware of both StarPack-D systems was updated to version 10.03.02 in 27 Dec. 2019 due to advance preparation against GLONASS week rollover at the end of Dec. 2019

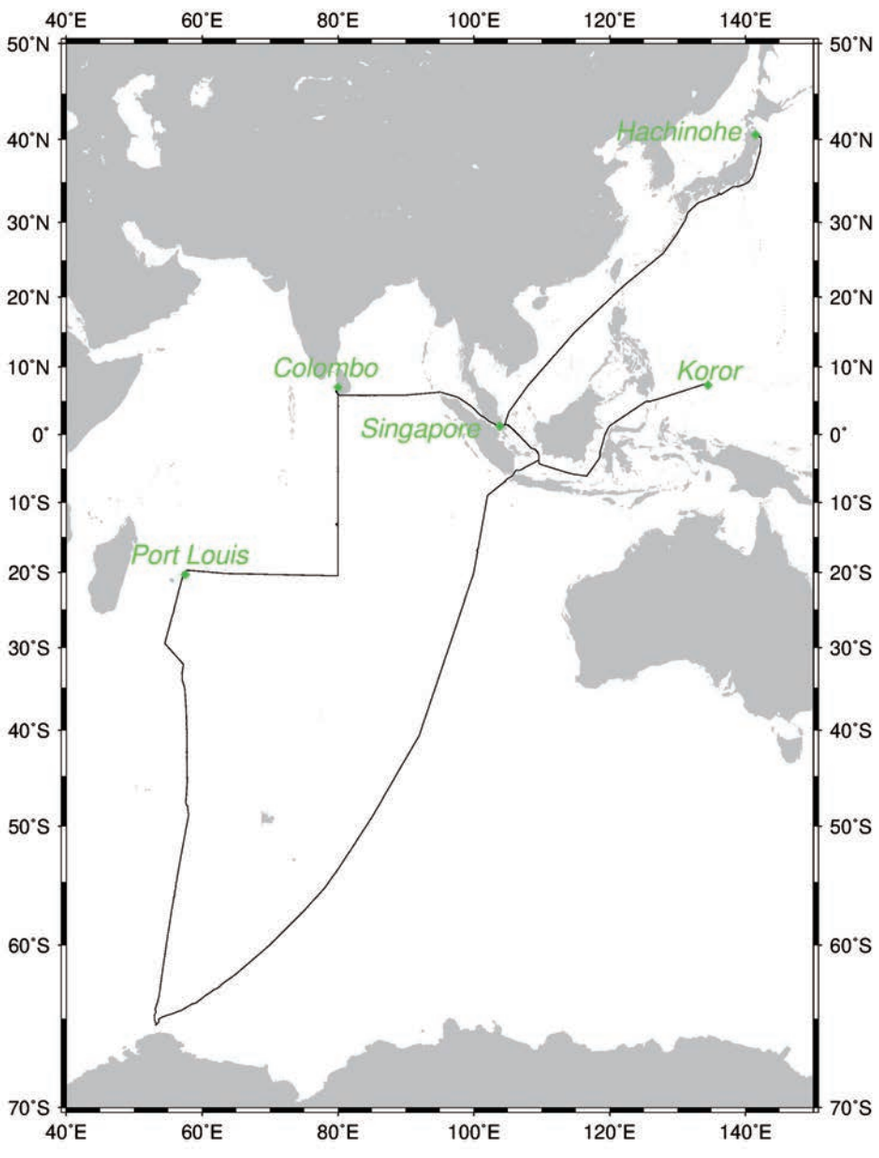

Fig. 2.1.1 Cruise track of MR19-04.

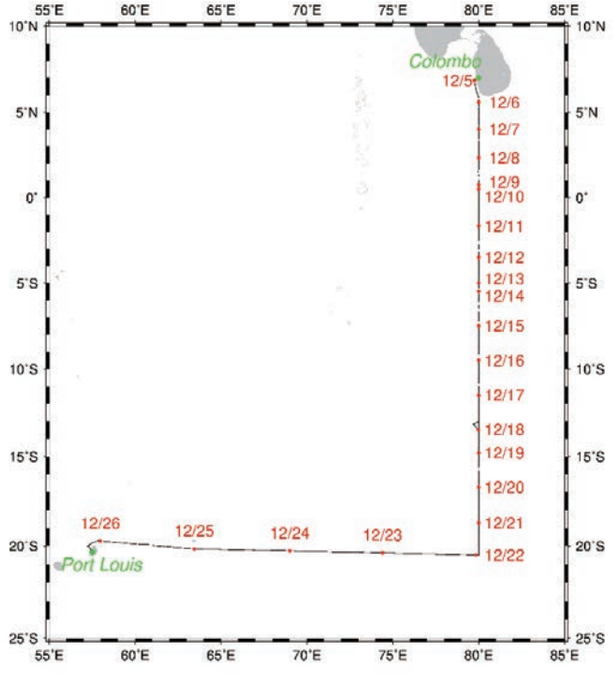

Fig. 2.1.2 Same as Fig. 2.1.1, but for Leg 2.

Fig. 2.1.3 Same as Fig. 2.1.1, but for Leg 3.

2.2 Swath Bathymetry

(1) Personnel

Akihiko Murata	JAMSTEC: Principal investigator	- leg 2 -
Katsuro Katsumata	JAMSTEC: Principal investigator	- leg 3 -
Masakaze Fujii	National Institute of Polar Research	Not onboard
Yutaro Murakami	Nippon Marine Enterprises Ltd., (NME)	- leg 2 -
Souichiro Sueyoshi	NME	- leg 2 -
Masanori Murakami	NME	- leg 2 -
Kazuho Yoshida	NME	- leg 3 -
Wataru Tokunaga	NME	- leg 3 -
Satomi Ogawa	NME	- leg 3 -
Takehito Hattori	MIRAI crew	- leg 2,3 -

(2) Introduction

R/V MIRAI is equipped with a Multi narrow Beam Echo Sounding system (MBES), SEABEAM 3012 (L3 Communications, ELAC Nautik). The objective of MBES is collecting continuous bathymetric data along ship's track to make a contribution to geological and geophysical investigations and global datasets.

(3) Data Acquisition

The "SEABEAM 3012" on R/V MIRAI was used for bathymetry mapping during the cruise.

To get accurate sound velocity of water column for ray-path correction of acoustic multibeam, we used Surface Sound Velocimeter (SSV) data to get the sea surface sound velocity (at 6.62 m), and the deeper depth sound velocity profiles were calculated by temperature and salinity profiles from CTD and XCTD data by the equation in Del Grosso (1974) during these cruises. Table 2.2.1 shows system configuration and performance of SEABEAM 3012.

Table 2.2.1 SEABEAM 3012 system configuration and performance

Frequency:	12 kHz
Transmit beam width:	2.0 degree
Transmit power:	4 kW
Transmit pulse length:	2 to 20 msec.
Receive beam width:	1.6 degree
Depth range:	50 to 11,000 m
Number of beams:	301 beams
Beam spacing:	Equi-angle
Swath width:	60 to 150 degrees
Depth accuracy:	< 1 % of water depth (average across the swath)

(4) Data processing of MBES (leg 3)

We processed bathymetry data along I08N and I07S observation lines as below.

i) Sound velocity correction

Sound velocity correction in post-processing was carried out by using the HIPS software version 10.2 (Teledyne CARIS, Canada). Each bathymetry data were corrected with sound velocity profiles calculated from the nearest CTD and XCTD data in the distance. The equation of Del Grosso (1974) was used for calculating sound velocity.

ii) Editing and Gridding

Editing for the bathymetry data was carried out using the HIPS. Firstly, the bathymetry data during ship's turning were basically deleted, and spike noise of swath data was removed. Then the bathymetry data were checked by "BASE surface (resolution: 50 m averaged grid)".

Finally, all accepted data were exported as XYZ ASCII data (longitude [degree], latitude [degree], depth [m]), and converted to 150 m grid data using "nearneighbor" utility of GMT (Generic Mapping Tool) software (Table 2.2.2).

Table 2.2.2 Parameters for gridding on "nearneighbor" in GMT

Gridding mesh size:	150 m
Search radius size:	150 m
Number of sectors around grid point	16
Minimum number of sectors with data required for averaging	1

(5) Data Archives

These data obtained in this cruise will be submitted to the Data Management Group (DMG) in JAMSTEC, and will be opened to the public via "Data Research System for Whole Cruise Information in JAMSTEC (DARWIN)" in JAMSTEC web site (http://www.godac.jamstec.go.jp/darwin/e).

(6) Remarks (Time in UTC)

i) The following periods, the MBES observations were carried out.

Leg2: 11:47, 05 Dec. 2019 to 16:03, 24 Dec. 2019

Leg3: 13:35, 30 Dec. 2019 to 03:15, 04 Feb. 2020

ii) The following period, the geophysical line survey was carried out from 44-40S 88-45E to 91-55S 40-40E in Leg3 cruise.

02:23, 28 Jan. 2020 to 06:14, 29 Jan. 2020.

2.3 Surface Meteorological Observations

(1) Personnel

Akihiko Murata	JAMSTEC: Principal investigator	- leg 2 -
Katsuro Katsumata	JAMSTEC: Principal investigator	- leg 3 -
Yutaro Murakami	Nippon Marine Enterprises Ltd., (NME)	- leg 2 -
Souichiro Sueyoshi	NME	- leg 2 -
Masanori Murakami	NME	- leg 2 -
Kazuho Yoshida	NME	- leg 3 -
Wataru Tokunaga	NME	- leg 3 -
Satomi Ogawa	NME	- leg 3 -
Takehito Hattori	MIRAI crew	- leg 2,3 -

(2) Objectives

Surface meteorological parameters are observed as a basic dataset of the meteorology. These parameters provide the temporal variation of the meteorological condition surrounding the ship.

(3) Methods

Surface meteorological parameters were observed during this cruise, except for the Democratic Socialist Republic of Sri Lankan territorial waters, the Republic of Mauritius EEZ, French Relle Union EEZ, the Republic of Indonesia EEZ and the Republic of Singapore EEZ. In this cruise, we used two systems for the observation.

i) MIRAI Surface Meteorological observation (SMet) system

Instruments of SMet system are listed in Table 2.3.1 and measured parameters are listed in Table 2.3.2. Data were collected and processed by KOAC-7800 weather data processor made by Koshin-Denki, Japan. The data set consists of 6-second averaged data.

ii) Shipboard Oceanographic and Atmospheric Radiation (SOAR) measurement system

SOAR system designed by BNL (Brookhaven National Laboratory, USA) consists of major five parts.

a) Portable Radiation Package (PRP) designed by BNL – short and long wave downward radiation.

b) Analog meteorological data sampling with CR1000 logger manufactured by Campbell Inc. Canada – wind, pressure, and rainfall (by a capacitive rain gauge) measurement.

c) Digital meteorological data sampling from individual sensors - air temperature, relative humidity and rainfall (by ORG (optical rain gauge)) measurement.

d) Photosynthetically Available Radiation (PAR) sensor manufactured by Biospherical Instruments Inc. (USA) - PAR measurement.

e) Scientific Computer System (SCS) developed by NOAA (National Oceanic and Atmospheric Administration, USA) – centralized data acquisition and logging of all data sets.

SCS recorded PRP, CR1000 data every 6 seconds, CR1000 data every second, air temperature and relative humidity data every 2 seconds, ORG data every 6 seconds and PAR data every 6 seconds. SCS composed "Event data (JamMet_PARUV)" from these data and ship's navigation data. Instruments and their locations are listed in Table 2.3.3 and measured parameters are listed in Table 2.3.4.

For the quality control as post processing, we checked the following sensors, before and after the cruise.

i. Capacitive rain gauge (SMet and SOAR)

Inspect of the linearity of output value from the rain gauge sensor to change input value by adding fixed quantity of test water.

ii. Barometer (SMet and SOAR)

Comparison with the portable barometer value, PTB220, VAISALA

iii. Thermometer (air temperature and relative humidity) (SMet and SOAR)

Comparison with the portable thermometer value, HM70, VAISALA

(4) Preliminary results

Fig. 2.3.1 to Fig. 2.3.4 show the time series of the following parameters;

Wind (SOAR)

Air temperature (SMet)

Relative humidity (SMet)

Precipitation (SOAR, ORG)

Short/long wave radiation (SMet)

Pressure (SMet)

Sea surface temperature (SMet)

Significant wave height (SMet)

(5) Data archives

These data obtained in these cruises will be submitted to the Data Management Group of JAMSTEC, and will be opened to the public via “Data Research System for Whole Cruise Information in JAMSTEC (DARWIN)” in JAMSTEC web site (http://www.godac.jamstec.go.jp/darwin/e).

(6) Remarks (Times in UTC)

i) The following periods, the observation were carried out.

Leg2: 11:21 05 Dec. 2019 - 16:03 24 Dec. 2019

Leg3: 13:35 30 Dec. 2019 - 03:15 05 Feb. 2020

ii) The following periods, sea surface temperature of SMet data were available.

Leg2: 11:21 05 Dec. 2019 - 16:03 24 Dec. 2019

Leg3: 13:35 30 Dec. 2019 - 03:15 05 Feb. 2020

iii) The following time, increasing of SMet capacitive rain gauge data were invalid due to transmitting MF/HF radio.

07:11 14 Dec. 2019

21:11 14 Dec. 2019

04:30 23 Jan. 2020

iv) FRSR data was not available in this cruise due to the system trouble.

v) The following period, PSP and PIR data were invalid due to mechanical trouble.

11:21 05 Dec. 2019 - 06:00 13 Dec. 2019

vi) The following period, PRP data acquisition was stopped due to operation PC trouble.

14:35 15 Dec. 2019 - 19:03 15 Dec.2010

vii) The following period, SMet wind speed/direction were measured by KE-500, the wind vane on the foremast due to instrument trial.

11:33 18 Jan. 2020 - 11:35 18 Jan 2020

viii) The following days, short wave radiation amount contained invalid value in nighttime, more than 0.01kW/m^2.

01 Feb. 2020 - 02 Feb. 2020

ix) The following period, SOAR PIR data were invalid due to mechanical trouble.

08:49 06 Jan. 2020 - 09:32 06 Jan 2020

x) The following period, SOAR wind speed and direction data were invalid due to seabirds perching.

06:15 04 Feb. 2020 - 23:10 04 Feb. 2020

Table 2.3.1 Instruments and installation locations of MIRAI Surface Meteorological observation system

Sensors	Type	Manufacturer	Location (altitude from surface)
Anemometer	KS-5900	Koshin Denki, Japan	Foremast (25 m)
Tair/RH	HMP155	Vaisala, Finland	Compass deck (21 m)
with aspirated radiation shield	43408 Gill	R.M. Young, USA	starboard and portside
Thermometer: SST	RFN2-0	Koshin Denki, Japan	4th deck (-1m, inlet -5m)
Barometer	Model-370	Setra System, USA	Captain deck (13 m)
			weather observation room
Capacitive rain gauge	50202	R. M. Young, USA	Compass deck (19 m)
Optical rain gauge	ORG-815DS	Osi, USA	Compass deck (19 m)
Radiometer (short wave)	MS-802	Eko Seiki, Japan	Radar mast (28 m)
Radiometer (long wave)	MS-202	Eko Seiki, Japan	Radar mast (28 m)
Wave height meter	WM-2	Tsurumi-seiki, Japan	Bow (10 m)
			Stern (8m)

Table 2.3.2 Parameters of MIRAI Surface Meteorological observation system

Parameter	Units	Remarks
1 Latitude	degree	
2 Longitude	degree	
3 Ship's speed	knot	MIRAI log
4 Ship's heading	degree	MIRAI gyro
5 Relative wind speed	m/s	6sec./10min. averaged
6 Relative wind direction	degree	6sec./10min. averaged
7 True wind speed	m/s	6sec./10min. averaged
8 True wind direction	degree	6sec./10min. averaged
9 Barometric pressure	hPa	adjusted to sea surface level
		6sec. averaged
10 Air temperature (starboard side)	degC	6sec. averaged
11 Air temperature (port side)	degC	6sec. averaged
12 Dewpoint temperature (starboard side)	degC	6sec. averaged
13 Dewpoint temperature (port side)	degC	6sec. averaged
14 Relative humidity (starboard side)	%	6sec. averaged
15 Relative humidity (port side)	%	6sec. averaged
16 Sea surface temperature	degC	6sec. averaged
17 Rain rate (optical rain gauge)	mm/hr	hourly accumulation
18 Rain rate (capacitive rain gauge)	mm/hr	hourly accumulation
19 Down welling shortwave radiation	W/m^2	6sec. averaged
20 Down welling infra-red radiation	W/m^2	6sec. averaged
21 Significant wave height (bow)	m	hourly
22 Significant wave height (aft)	m	hourly
23 Significant wave period (bow)	second	hourly
24 Significant wave period (aft)	second	hourly

Table 2.3.3 Instruments and installation locations of SOAR system

Sensors (Meteorological)	Type	Manufacturer	Location (altitude from surface)
Anemometer	05106	R.M. Young, USA	Foremast (25 m)
Barometer	PTB210	Vaisala, Finland	
with 61002 Gill pressure port		R.M. Young, USA	Foremast (23 m)
Rain gauge	50202	R.M. Young, USA	Foremast (24 m)
Tair/RH	HMP155	Vaisala, Finland	
with 43408 Gill aspirated radiation shield		R.M. Young, USA	Foremast (23 m)
Optical rain gauge	ORG-815DR	Osi, USA	Foremast (24 m)

Sensors (PRP)	Type	Manufacturer	Location (altitude from surface)
Radiometer (short wave)	PSP	Epply Labs, USA	Foremast (25 m)
Radiometer (long wave)	PIR	Epply Labs, USA	Foremast (25 m)
Fast rotating shadowband radiometer		Yankee, USA	Foremast (25 m)

Sensor (PAR)	Type	Manufacturer	Location (altitude from surface)
PAR sensor	PUV-510	Biospherical Instruments Inc., USA	Navigation deck (18m)

Table 2.3.4 Parameters of SOAR system (JamMet)

Parameter	Units	Remarks
1 Latitude	degree	
2 Longitude	degree	
3 SOG	knot	
4 COG	degree	
5 Relative wind speed	m/s	
6 Relative wind direction	degree	
7 Barometric pressure	hPa	
8 Air temperature	degC	
9 Relative humidity	%	
10 Rain rate (optical rain gauge)	mm/hr	
11 Precipitation (capacitive rain gauge)	mm	reset at 50 mm
12 Down welling shortwave radiation	W/m^2	
13 Down welling infra-red radiation	W/m^2	
14 Defuse irradiance	W/m^2	
15 PAR	$microE/cm^2/sec$	
16 UV 305 nm	$microW/cm^2/nm$	
17 UV 320 nm	$microW/cm^2/nm$	
18 UV 340 nm	$microW/cm^2/nm$	
19 UV 380 nm	$microW/cm^2/nm$	

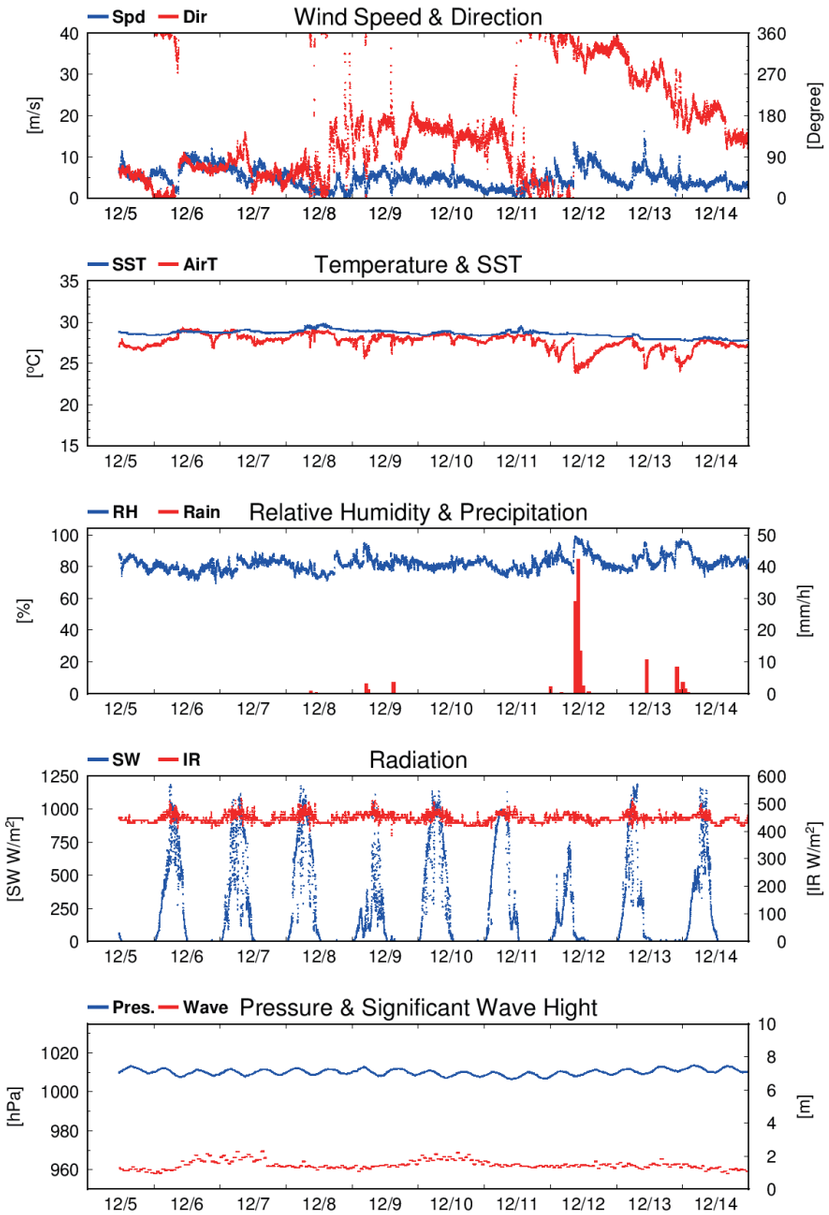

Fig. 2.3.1 Time series of surface meteorological parameters during the MR19-04 Leg2 cruise.

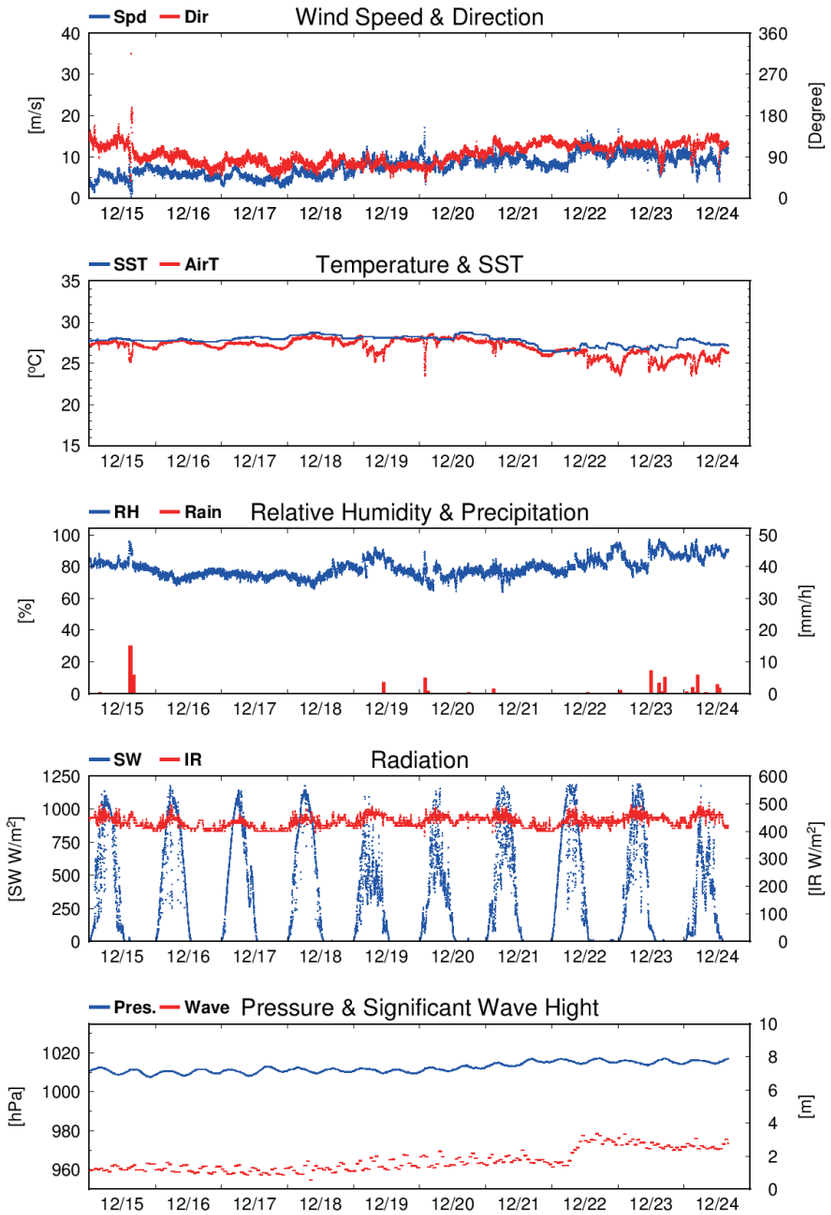

Fig. 2.3.1 (Continued)

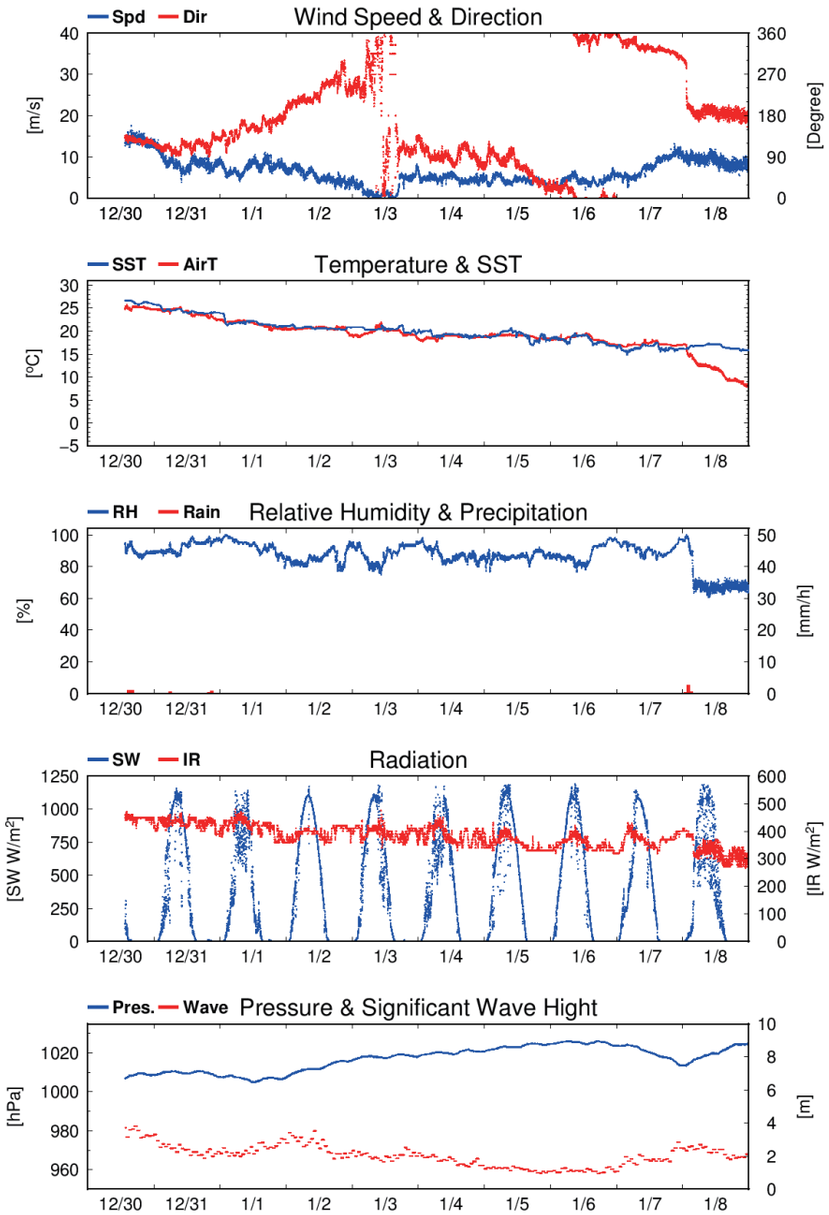

Fig. 2.3.2 Time series of surface meteorological parameters during the MR19-04 Leg3 cruise.

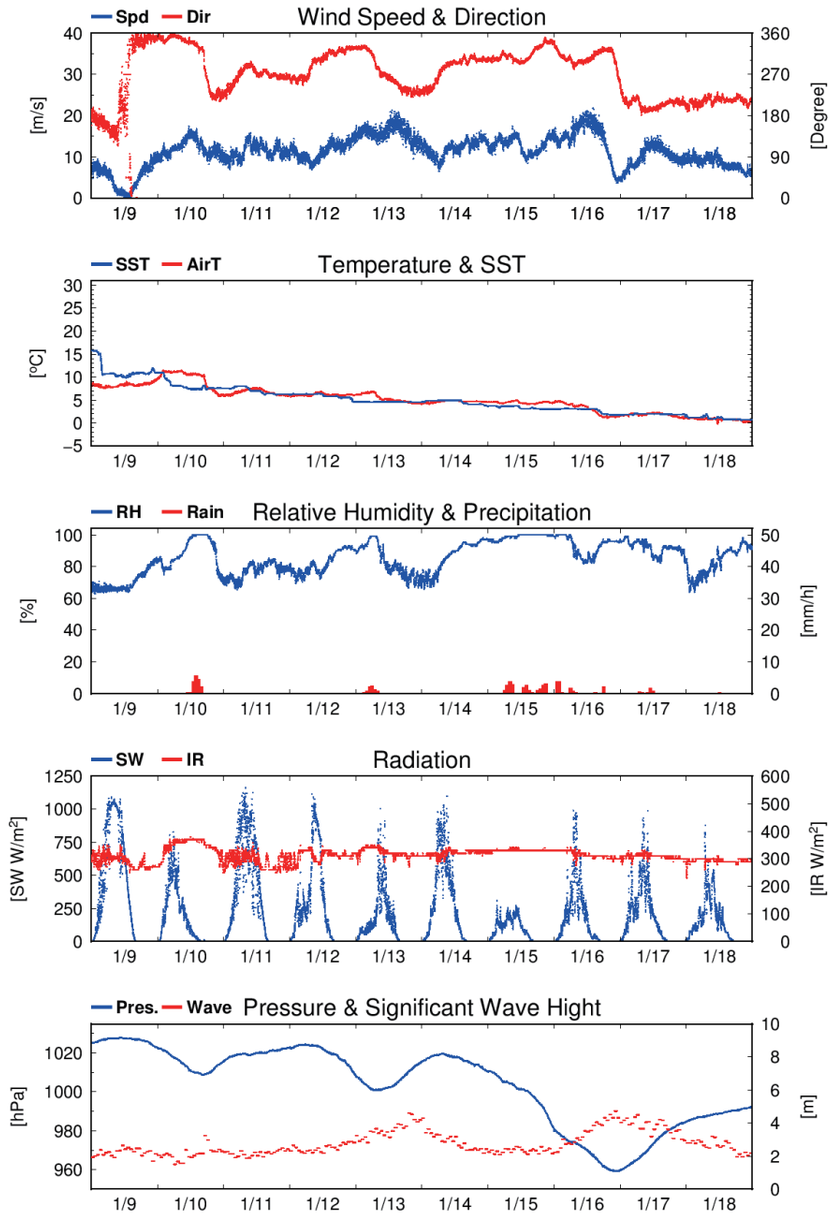

Fig. 2.3.2 (Continued)

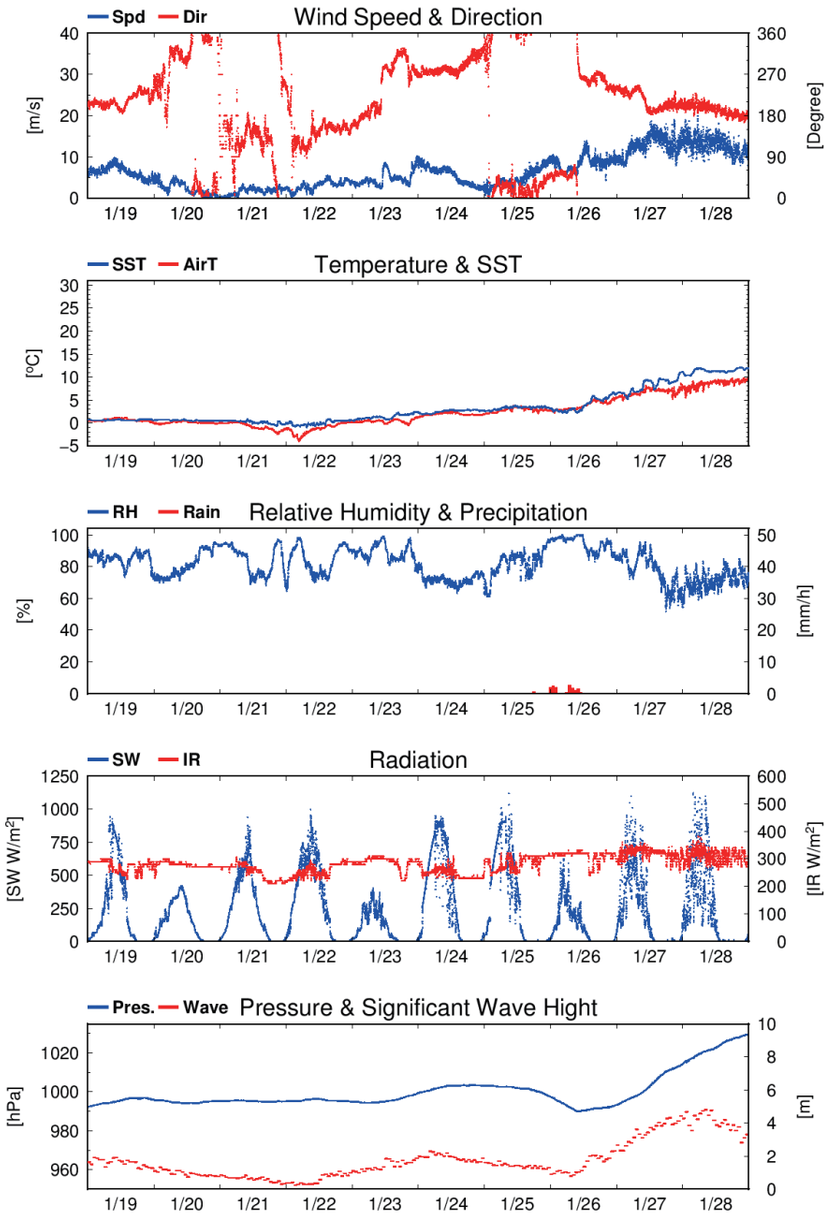

Fig. 2.3.2 (Continued)

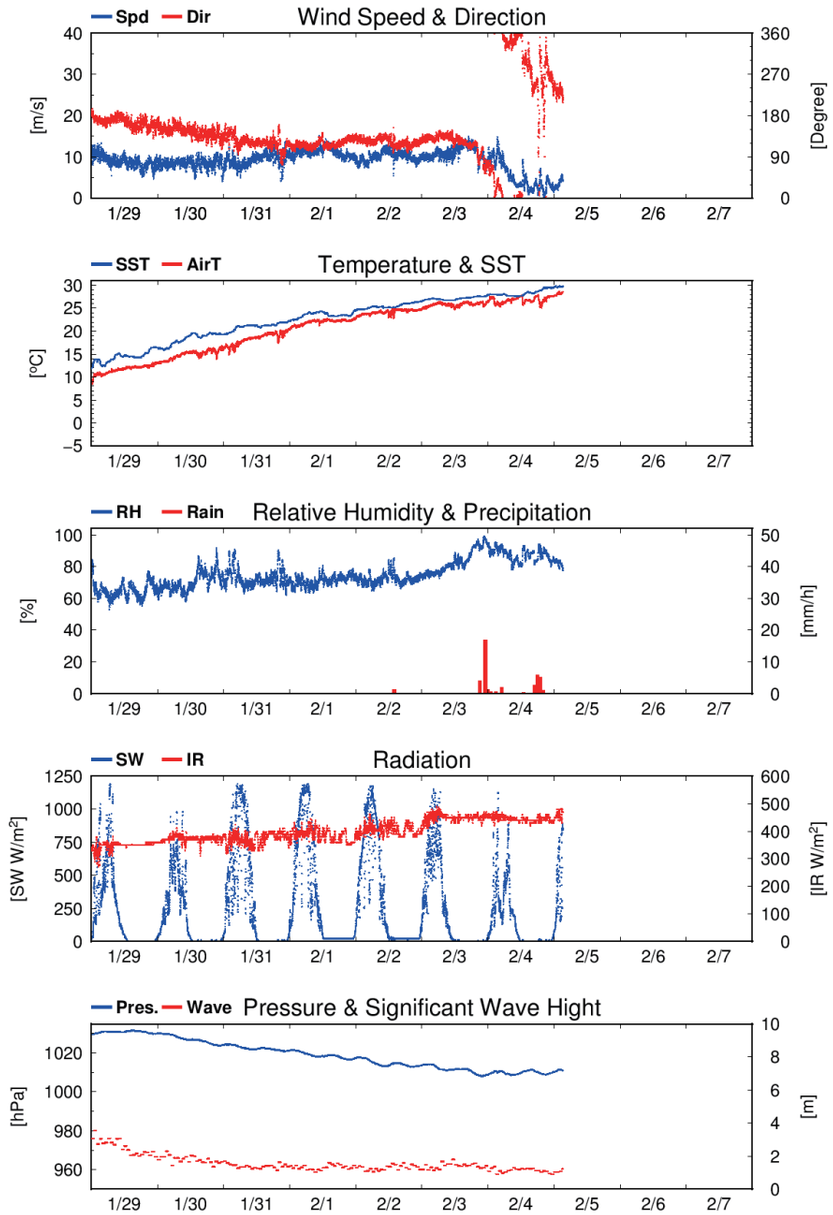

Fig. 2.3.2 (Continued)

2.4 Thermo-Salinograph and Related Properties

January 15, 2021

(1) Personnel

Hiroshi Uchida (JAMSTEC): Principal investigator

Erii Irie (MWJ): Operation leader

Misato Kuwahara (MWJ)

Yuko Miyoshi (MWJ)

(2) Objective

The objective of this measurements is to collect sea surface salinity, temperature, dissolved oxygen, fluorescence and total dissolved gas pressure data continuously along the cruise track.

(3) Instruments and method

The Continuous Sea Surface Water Monitoring System (Marine Works Japan Co, Ltd., Yokosuka, Kanagawa, Japan) automatically measures salinity, temperature, dissolved oxygen, fluorescence, turbidity, total dissolved gas pressure in sea surface water every one minute. This system is installed in the sea surface monitoring laboratory and bottom of the ship and connected to shipboard LAN system. Measured data along with time and location of the ship were displayed on a monitor and stored in a personal computer. Seawater was continuously pumped up to the laboratory from about 5 m water depth and flowed into the system through a vinyl-chloride pipe or a tube. One thermometer is located just before the sea water pump at bottom of the ship. Flow rate in the system was controlled to be about 1.2 L/min.

Materials used in this cruise are as follows:

Temperature (bottom of the ship), SBE 38, Sea-Bird Scientific, Inc., Bellevue, Washington, USA

Serial no. 3857820-0540 (pre-cruise calibration date: September 20, 2019)

Temperature and conductivity, SBE 45, Sea-Bird Scientific, Inc.

Serial no. 4557820-0319 (pre-cruise calibration date: June 19, 2019)

Dissolved oxygen, RINKO II, JFE Advantech, Co., Ltd., Osaka, Japan

Serial no. 0013 (pre-cruise calibration date: April 27, 2018 [at JAMSTEC])

Chlorophyll fluorometer, C3, Turner Designs, Inc., Sunnwale, California, USA

Serial no. 2300123 (2 chlorophyll fluorometers) (pre-cruise calibration date: April 19, 2019)

Total dissolved gas pressure, HGTD-Pro, Pro Oceans, Bridgewater, Nova Scotia, Canada

Serial no. 37-394-10 (pre-cruise calibration date: unknown)

Data acquisition software, SeaMoni, Marine Works Japan, Co., Ltd.

Version 1.2.0.0

(4) Pre-cruise calibration

Pre-cruise sensor calibrations for the SBE 38, SBE 45, C3 and HGTD-Pro were performed by the manufacturer.

Pre-cruise sensor calibration for C3 was performed by Marine Works Japan, Co., Ltd. The C3 primary chlorophyll fluorometer was calibrated with 100 ppb uranine solution, then the Secondary Solid Standard (SSS) was calibrated using the calibrated primary chlorophyll fluorometer. The secondary chlorophyll fluorometer was calibrated using thus calibrated SSS.

Pre-cruise sensor calibration for RINKO was performed at JAMSTEC. The oxygen sensor was immersed in fresh water in a 1-L semi-closed glass vessel, which was immersed in a temperature-controlled water bath. Temperature of the water bath was set to 1, 10, 20 and 29°C. Temperature of the fresh water in the vessel was measured by a thermistor of the portable dissolved oxygen sensor (expanded uncertainty of smaller than 0.01°C, ARO-PR, JFE Advantech, Co., Ltd.). At each temperature, the fresh water in the vessel was bubbled with standard gases (4, 10, 17 and 25% oxygen consisted of the oxygen-nitrogen mixture, whose relative expanded uncertainty is 0.5%, Japan Fine Products, Tochigi, Japan). Absolute pressure of the vessel's headspace was measured by a reference quartz crystal barometer (expanded uncertainty of 0.01% of reading,

RPM4 BA100Ks, Fluke Co., Phoenix Arizona, USA) and ranged from about 1040 to 1070 hPa. The data were averaged over 5 minutes at each calibration point (a matrix of 24 points). As a reference, oxygen concentration of the fresh water in the calibration vessel was calculated from the oxygen concentration of the gases, temperature and absolute pressure at the water depth (about 6 cm) of the sensor's sensing foil as follows:

$$O_2\ (\mu mol/L) = \{1000 \times c(T) \times (A_p - pH_2O)\} / \{0.20946 \times 22.3916 \times (1013.25 - pH_2O)\}$$

where $c(T)$ is the oxygen solubility, A_p is absolute pressure (in hPa), and pH_2O is the water vapor pressure (in hPa). The RINKO was calibrated by the modified Stern-Volmer equation slightly modified from a method by Uchida et al. (2010):

$$O_2\ (\mu mol/L) = [(V_0 / V)^E - 1] / K_{sv}$$

where V is raw phase difference, V_0 is raw phase difference in the absence of oxygen, K_{sv} is Stern-Volmer constant. The coefficient E corrects nonlinearity of the Stern-Volmer equation. The V_0 and the K_{sv} are assumed to be functions of temperature as follows.

$$K_{sv} = C_0 + C_1 \times T + C_2 \times T^2$$

$$V_0 = 1 + C_3 \times T$$

$$V = C_4 + C_5 \times (N/10000)$$

where T is temperature (°C) and N is raw output. The calibration coefficients are as follows:

C_0 = 3.633746e-03, C_1 = 1.622265e-04, C_2 = 2.926342e-06, C_3 = -1.070016e-03,

C_4 = -3.082474e-02, C_5 = 2.139890e-01, E = 1.2

(5) Data collection

Data from the Continuous Sea Surface Water Monitoring System were obtained at 1-minute intervals. Periods of measurement, maintenance and problems are listed in Table 2.4.1. Seawater samples for salinity, dissolved oxygen and chlorophyll-a analysis were taken from the the Continuous Sea Surface Water Monitoring System basically once in a day to calibrate the sensors in situ. Details of the analysis are described in elsewhere of the cruise report.

Table 2.4.1. Events of the Continuous Sea Surface Water Monitoring System operation.

System Date [UTC]	System Time [UTC]	Events
Leg 2		
2019/12/05	11:21	Start logging
2019/12/15	16:58-17:14	Filter maintenance
2019/12/18	20:59-21:09	Logging stop only for C3
2019/12/18	20:58	Logging stop due to leak
2019/12/24	11:30	End logging
Leg 3		
2019/12/30	13:35	Start logging
2020/01/03	01:59-02:19	Filter maintenance
2020/01/07	04:41-05:02	Filter maintenance
2020/01/09	0:46-01:03	Filter maintenance
2020/01/12	05:01-05:16	Filter maintenance
2020/01/14	05:50-06:37	RINKO and filter maintenance
2020/01/14	06:37-07:05	C3 maintenance
2020/01/16	06:20-06:35	Filter maintenance
2020/01/18	02:50-03:06	Filter maintenance
2020/01/26	08:28-08:50	Filter maintenance
2020/01/27	09:41-10:43	C3 maintenance
2020/02/05	03:15	End logging

(6) Post-cruise calibration

Data from the Continuous Sea Surface Water Monitoring System were processed as follows. Spikes in the temperature and salinity data were removed using a median filter with a window of 3 scans (3 minutes) when difference between the original data and the median filtered data was larger than 0.1°C for temperature and 0.5 for salinity. Data gaps were linearly interpolated when the gap was ≤ 13 minutes. Fluorometer and turbidity data were low-pass filtered using a median filter with a window of 3 scans (3 minutes) to remove spikes. Raw data from the RINKO oxygen sensor and fluorometer data were low-pass filtered using a Hamming filter with a window of 15 scans (15 minutes).

Salinity (S [PSU]), dissolved oxygen (O [μmol/kg]), and fluorescence (Fl [RFU]) data were corrected using the water sampled data. Corrected salinity (S_{cor}), dissolved oxygen (O_{cor}), and estimated chlorophyll *a* (Chl-a) were calculated from following equations:

$$S_{cor}\ [PSU] = c_0 + c_1 S + c_2 t$$

$$O_{cor}\ [\mu mol/kg] = c_0 + c_1 O + c_2 T + c_3 t$$

$$\text{Chl-a}\ [\mu g/L] = c_0 + c_1 Fl \quad (\text{for Latitude} <= -31^o \text{ or Latitude} >= -30^o)$$

$$= \{1 - (\text{Latitude}+31)\}\ \text{Chl-a}_1 + (\text{Latitude}+31)\ \text{Chl-a}_1 \quad (\text{for } -31^o < \text{Latitude} < -30^o)$$

where S is practical salinity, t is days from a reference time (2019/12/05 11:21 [UTC]), T is temperature in °C. The best fit sets of calibration coefficients (c_0~c_3) were determined by a least square technique to minimize the deviation from the water sampled data. Chl-a_1 and Chl-a_2 are chlorophyll-a calibrated using the coefficients for latitude smaller than –31° and for latitude greater than –30°, respectively. The calibration coefficients were listed in Table 2.4.2. Comparisons between the Continuous Sea Surface Water Monitoring System data and water sampled data are shown in Figs. 2.4.1, 2.4.2 and 2.4.3.

For fluorometer data, water sampled data obtained at night [PAR (Photosynthetically Available Radiation) < 50 μE/(m^2 sec)] were used for the calibration, since sensitivity of the fluorometer to chlorophyll *a* is different at nighttime and daytime (Section 2.4 in Uchida et al., 2015).

For the HGTD-Pro, pressure data obtained in air were compared with a portable barometer (model PTB220, Vaisala, calibration date: April 1, 2019) to check the HGTD-Pro pressure sensor drift (Table 2.4.3). Post-cruise quality check for the HGTD-Pro data is not yet finished.

Table 2.4.2. Calibration coefficients for the salinity, dissolved oxygen, and chlorophyll *a*.

	c_0	c_1	c_2	c_3
Salinity				
Leg 2	1.308692e–2	0.9996418	8.239194e–4	
Leg 3	4.242270e–1	0.9882574	3.819200e–4	
Dissolved oxygen				
Leg 2	79.72396	0.7292034	–0.9451510	–8.384717e–2
Leg 3 (for ~2020/01/14 07:00)				
	78.75307	0.6800804	–1.380412	0.3642751
Leg 3 (for 2020/01/14/07:00~)				
	–1.192846	0.9191097	0.3601672	0.3155845
Chlorophyll a				
Legs 2,3	1.971706e–2	6.797531e–2	(for Latitude <= –31°)	
	1.971706e–2	0.1635513	(for Latitude >= –30°)	

Table 2.4.3. Comparison between the HGTD-Pro pressure in air and the portable barometer.

Date of comparison	HGTD-Pro pressure (hPa)	Portable barometer (hPa)
December 2, 2019	1008.343 ± 0.010	1008.21 ± 0.02
February 7, 2020	1008.669 ± 0.017	1008.19 ± 0.05

(7) References

Uchida, H., G. C. Johnson, and K. E. McTaggart (2010): CTD oxygen sensor calibration procedures, The GO-SHIP Repeat Hydrography Manual: A collection of expert reports and guidelines, IOCCP Rep., No. 14, ICPO Pub. Ser. No. 134.

Uchida, H., K. Katsumata, and T. Doi (2015): WHP P14S, S04I Revisit Data Book, JASTEC, Yokosuka, 187 pp., doi:10.17596/0000030.

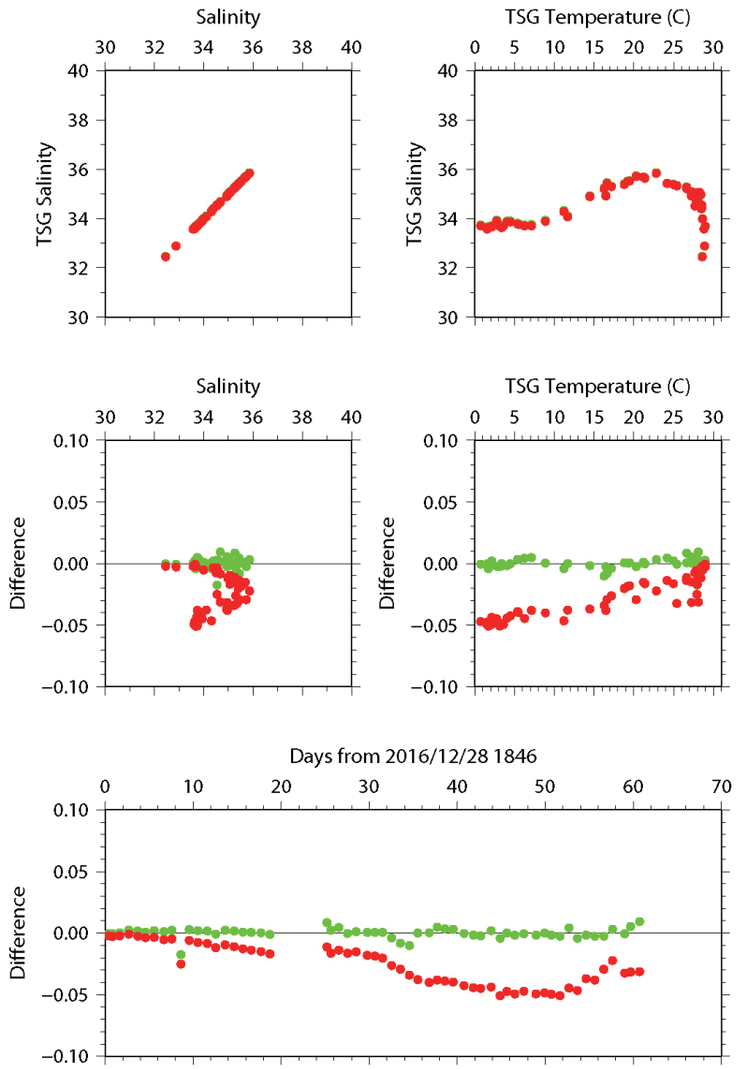

Fig. 2.4.1. Comparison between TSG salinity (red: before correction, green: after correction) and sampled salinity.

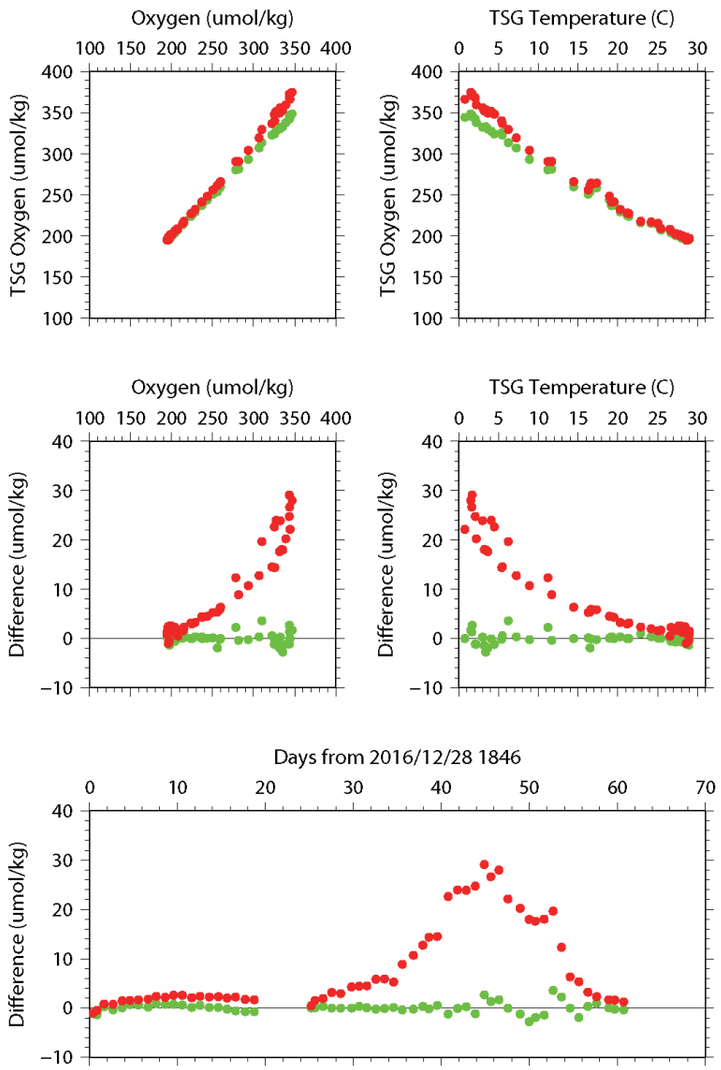

Fig. 2.4.2. Same as Fig. 2.4.1, but for dissolved oxygen.

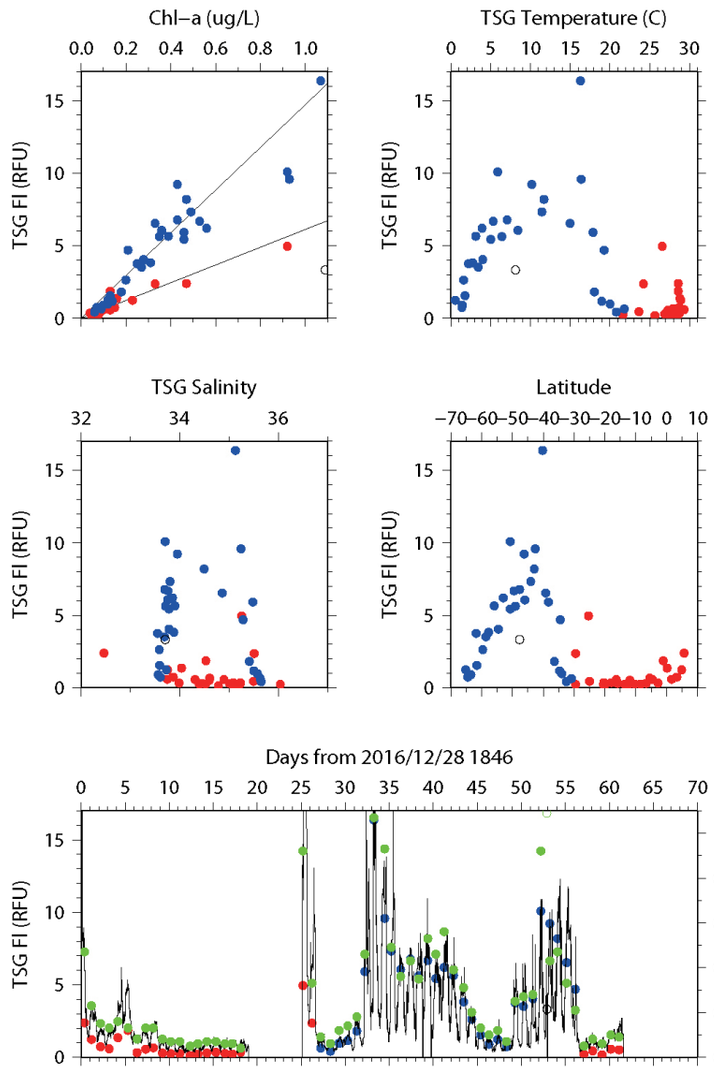

Fig. 2.4.3. Comparison between TSG fluorescence (red: latitude > –30°, blue: latitude < –30°) and sampled chlorophyll-a. Open dots show that PAR data were greater than 50 μE/(m^2 sec). Green dots and lines in the lowest panel are sampled chlorophyll-*a* and estimated chlorophyll-*a* from TSG fluorescence, respectively.

2.5 Underway pCO_2

November 25, 2020

(1) Personnel

Akihiko Murata (JAMSTEC)

Nagisa Fujiki (MWJ)

Atsushi Ono (MWJ)

Masanori Enoki (MWJ)

Yuta Oda (MWJ)

Daiki Kawata (MWJ)

(2) Introduction

Concentrations of CO_2 in the atmosphere are now increasing at a rate of about 2.0 ppmv yr^{-1} owing to human activities such as burning of fossil fuels, deforestation, and cement production. It is an urgent task to estimate as accurately as possible the absorption capacity of the oceans against the increased atmospheric CO_2, and to clarify the mechanism of the CO_2 absorption, because the magnitude of the anticipated global warming depends on the levels of CO_2 in the atmosphere, and because the ocean currently absorbs 1/3 of the 6 Gt of carbon emitted into the atmosphere each year by human activities.

In this cruise, we were aimed at quantifying how much atmospheric CO_2 is absorbed in the surface ocean in the Indian Ocean and the Southern Ocean. For the purpose, we measured partial pressure of CO_2 (pCO_2) in the atmosphere and surface seawater along the cruise tracks of WHP I08N line and a newly-set observation line of ~56°E.

(3) Apparatus and shipboard measurement

Continuous underway measurements of atmospheric and surface seawater pCO_2 were made with the CO_2 measuring system (Nihon ANS, Inc.) installed in the R/V *Mirai* of JAMSTEC. The system comprises of a non-dispersive infrared gas analyzer (Li-COR LI-7000, modified by Nihon ANS, Inc.), an air-circulation module and a showerhead-type equilibrator. To measure concentrations (mole fraction) of CO_2 in dry air (xCO_2a), air sampled from the bow of the ship (approx. 13 m above the sea level) was introduced into the NDIR through a dehydrating route with an electric dehumidifier (kept at ~2 °C) and a starling cooler. The flow rate of the air was approx. 500 ml min^{-1}. To measure surface seawater concentrations of CO_2 in dry air (xCO_2s), the air equilibrated with seawater within the equilibrator was introduced into the NDIR through the same flow route as the dehydrated air used in measuring xCO_2a. The flow rate of the equilibrated air was 600 – 800 ml min^{-1}. The seawater was taken by a pump from the intake placed at the approx. 4.5 m below the sea surface. The flow rate of seawater in the equilibrator was 4000 – 5000 ml min^{-1}.

The CO_2 measuring system was set to repeat the measurement cycle such as 4 kinds of CO_2 standard gases (Table 1), xCO_2a (twice), xCO_2s (7 times). This measuring system was run automatically throughout the cruise by a PC control.

(4) Quality control

Concentrations of CO_2 of the standard gases are listed in Table 1, which were calibrated before and after the cruise by the JAMSTEC primary standard gases. The CO_2 concentrations of the primary standard gases were calibrated by the Japan Meteorological Agency, and traceable to the WMO 2007 scale.

In actual shipboard observations, the signals of NDIR usually reveal a trend. The trends were adjusted linearly using the signals of the standard gases analyzed before and after the sample measurements.

Effects of water temperature increased between the inlet of surface seawater and the equilibrator on xCO_2s were adjusted based on Takahashi *et al.* (1993), although the temperature increases were slight, being usually < 0.1 °C.

We checked values of xCO_2a and xCO_2s by examining signals of the NDIR by plotting the xCO_2a and xCO_2s as a function of sequential day, longitude, sea surface temperature and sea surface salinity.

(5) Reference

Takahashi, T., J. Olafsson, J. G. Goddard, D. W. Chipman, and S. C. Southerland (1993) Seasonal variation of CO_2 and nutrients in the high-latitude surface oceans: a comparative study, *Global Biogeochem. Cycles*, 7, 843–878.

Table 2.5.1. Concentrations of CO_2 standard gases used during the cruise.

Cylinder no.	Concentrations (ppmv)
CQB05955	249.65
CQB06029	320.00
CQB06029	389.77
CQB06034	460.20

2.6 Shipboard ADCP

(1) Personnel

Akihiko Murata	JAMSTEC: Principal investigator	- Leg 2 -
Katsuro Katsumata	JAMSTEC: Principal investigator	- Leg 3 -
Yutaro Murakami	Nippon Marine Enterprises, Ltd. (NME)	- Leg 2 -
Souichiro Sueyoshi	NME	- Leg 2 -
Masanori Murakami	NME	- Leg 2 -
Kazuho Yoshida	NME	- Leg 3 -
Wataru Tokunaga	NME	- Leg 3 -
Satomi Ogawa	NME	- Leg 3 -
Takehito Hattori	MIRAI crew	- Leg 2, Leg 3-
Shinya Kouketsu	JAMSTEC	- Leg 2, Leg 3-

(2) Objectives

To obtain continuous measurement data of the current profile along the ship's track.

(3) Instruments and methods

Upper ocean current measurements were made in this cruise, using the hull-mounted Acoustic Doppler Current Profiler (ADCP) system. For most of its operation, the instrument was configured for water-tracking mode. Bottom-tracking mode, interleaved bottom-ping with water-ping, was made to get the calibration data for evaluating transducer misalignment angle in the shallow water. The system consists of following components;

i) R/V MIRAI has installed the Ocean Surveyor for vessel-mount ADCP (frequency 76.8 kHz; Teledyne RD Instruments, USA). It has a phased-array transducer with single ceramic assembly and creates 4 acoustic beams electronically. We mounted the transducer head rotated to a ship-relative angle of 45 degrees azimuth from the keel.

ii) For heading source, we use ship's gyro compass (Tokyo Keiki, Japan), continuously providing heading to the ADCP system directory. Additionally, we have Inertial Navigation System (Phins, IXBLUE SAS, France) which provide high-precision heading, attitude information, pitch and roll. They are stored in ".N2R" data files with a time stamp.

iii) Differential GNSS system (StarPack-D, Fugro, Netherlands) providing precise ship's position.

iv) We used VmDas software version 1.49(TRDI) for data acquisition.

v) To synchronize time stamp of ping with Computer time, the clock of the logging computer is adjusted to GPS time server continuously by the application software.

vi) Fresh water is charged in the sea chest to prevent bio fouling at transducer face.

vii) The sound speed at the transducer does affect the vertical bin mapping and vertical velocity measurement, and that is calculated from temperature, salinity (constant value; 35.0 PSU) and depth (6.5 m; transducer depth) by equation in Medwin (1975).

Data was configured for "8 m" layer intervals starting about 23m below sea surface, and recorded every ping as raw ensemble data (.ENR). Additionally, 15 seconds averaged data were recorded as short-term average (.STA). 300 seconds averaged data were long-term average (.LTA), respectively.

(4) Parameters

Major parameters for the measurement, Direct Command, are shown in Table 2.6.1.

Table 2.6.1. Major parameters

Environmental Sensor Commands

EA = 04500	Heading Alignment (1/100 deg)
ED = 00065	Transducer Depth (0 - 65535 dm)
EF = +001	Pitch/Roll Divisor/Multiplier (pos/neg) [1/99 - 99]
EH = 00000	Heading (1/100 deg)
ES = 35	Salinity (0-40 pp thousand)
EX = 00000	Coordinate Transform (Xform:Type; Tilts; 3Bm; Map)
EZ = 10200010	Sensor Source (C; D; H; P; R; S; T; U)

C (1): Sound velocity calculates using ED, ES, ET (temp.)

D (0): Manual ED

H (2): External synchro

P (0), R (0): Manual EP, ER (0 degree)

S (0): Manual ES

T (1): Internal transducer sensor

U (0): Manual EU

EV = 0	Heading Bias (1/100 deg)

Water-Track Commands

WA = 255	False Target Threshold (Max) (0-255 count)
WC = 120	Low Correlation Threshold (0-255)
WD = 111 100 000	Data Out (V; C; A; PG; St; Vsum; Vsum^2; #G; P0)
WE = 1000	Error Velocity Threshold (0-5000 mm/s)
WF = 0800	Blank After Transmit (cm)
WN = 100	Number of depth cells (1-128)
WP = 00001	Pings per Ensemble (0-16384)
WS = 800	Depth Cell Size (cm)
WV = 0390	Mode 1 Ambiguity Velocity (cm/s radial)

(5) Data in the databook

ADCP-coordinate velocities were converted to the earth-coordinate velocities using ship attitude data from INU, and then the 5-minute mean current velocities were obtained by subtracting ship velocities based on GPS from the ADCP-coordinate velocities with misalignment and scale corrections for ADCP measurements. Corrections of misalignment (0.004 radian) and scale factors (0.99) were made using the bottom track data.

(6) Raw data archives

All the raw data obtained in this cruise will be submitted to the Data Management Group of JAMSTEC and will be opened to the public via “Data Research System for Whole Cruise Information in JAMSTEC (DARWIN)” in JAMSTEC web site.

http://www.godac.jamstec.go.jp/darwin/e

(7) Remarks (Times in UTC)

i) The following days, “NMEA1 Time Out” happened in N1R data due to onboard GNSS system error.

08 Jan. 2020 - 15 Jan. 2020

ii) The following days, N3R data recorded as spare NMEA data.

13 Jan. 2020 - 05 Feb. 2020

3 Hydrographic Measurements

3.1 $CTDO_2$

February 9, 2020

(1) Personnel

Hiroshi Uchida (JAMSTEC)

Katsuro Katsumata (JAMSTEC)

Shinya Kouketsu (JAMSTEC)

Shinsuke Toyoda (MWJ) (leg 2)

Keisuke Takeda (MWJ) (leg 2)

Tun Htet Aung (MWJ) (leg 2)

Rio Kobayashi (MWJ) (leg 3)

Hiroyuki Hayashi (MWJ) (leg 3)

Kento Fukahori (MWJ) (leg 3)

(2) Objective

The $CTDO_2$/water sampling measurements were conducted to obtain vertical profiles of seawater properties by sensors and water sampling.

(3) Instruments and method

Materials used in this cruise are as follows:

Winch, cable, and frame

Traction winch system (4.5 ton), Dynacon, Inc., Bryan, Texas, USA (Fukasawa et al., 2004)

8,080 m of 9.53 mm armored cable, Rochester Wire & Cable, LLC, Culpeper, Virginia, USA

(routinely cut 400 m after the leg 2)

Compact underwater slip ring swivel, Hanayuu Co., Ltd., Shizuoka, Japan (Uchida et al., 2018)

Deck unit

SBE 11plus, Sea-Bird Scientific, Bellevue, Washington, USA

Serial no. 11P54451-0872

Frame, water sampler

460 kg stainless steel frame for 36-position 12-L water sample bottles

with an aluminum rectangular fin (54 × 90 cm) to resist frame's rotation

(weight of the full CTD/water sampling package was about 930 kg)

36-position carousel water sampler, SBE 32, Sea-Bird Scientific

Serial no. 3254451-0826

12-L Niskin-X water sample bottle, model 1010X, General Oceanic, Inc., Miami, Florida, USA

(No TEFLON coating)

12-L sample bottle, model OTE 110, OceanTest Equipment, Inc., Fort Lauderdale, Florida, USA

(No TEFLON coating)

Underwater unit

Pressure sensor, SBE 9plus, Sea-Bird Scientific

Serial no. 09P54451-1027 (117457) (calibration date: April 18, 2019)

Deep standard reference thermometer, SBE 35, Sea-Bird Scientific

Serial no. 0045 (calibration date: April 1, 2019)

Temperature sensor, SBE 3F, Sea-Bird Scientific

Primary serial no. 031525 (calibration date: June 1, 2019)

Secondary serial no. 031359 (calibration date: June 27, 2019)

Conductivity sensor, SBE 4C, Sea-Bird Scientific

Primary serial no. 042435 (calibration date: June 25, 2019)

Secondary serial no. 042854 (calibration date: June 26, 2019)

Dissolved oxygen sensor

primary, RINKO III, JFE Advantech Co., Ltd., Osaka, Japan

Serial no. 037, Sensing foil no. 182822 (calibration date: September 18, 2019)

Secondary, SBE 43, Sea-Bird Scientific

Serial no. 432211 (calibration date: June 19, 2019)

Transmissometer, C-Star, WET Labs, Inc., Philomath, Oregon, USA

Serial no. 1727DR

Chlorophyll fluorometer, Seapoint Sensors Inc., Exeter, New Hampshire, USA

Serial no. 3618, Gain: 30X (0-5 ug/L) for stations 001 – 097,

Gain: 10X (0-15 ug/L) for stations 098 – 153

Ultraviolet fluorometer, Seapoint Sensors Inc.

Serial no. 6223, Gain 30X (0-50 QSU)

Turbidity meter, Seapoint Sensors Inc.

Serial no. 14953, Gain 100X (0-25 FTU)

Photosynthetically Active Radiation (PAR) sensor, PAR-Log ICSW,

Satlantic, LP, Halifax, Nova Scotia, Canada

Serial no. 1025 (calibration date: July 6, 2015)

Altimeter, PSA-916T, Teledyne Benthos, Inc.

Serial no. 1157

Pump, SBE 5T, Sea-Bird Scientific

Primary serial no. 055816

Secondary serial no. 054598

Other additional sensors

Lowered acoustic Doppler current profilers

Micro Ridar

Refractive index density sensor

Sound velocity profiler

RBR TD/ODO sensors

Radon (gamma-ray) sensor

pH/pCO_2 sensors

Software

Data acquisition software, SEASAVE-Win32, version 7.23.2

Data processing software, SBEDataProcessing-Win32, version 7.23.2 and some original modules

(4) Pre-cruise calibration

(4.1) Pressure sensor

Pre-cruise sensor calibration for linearization was performed at Sea-Bird Scientific. The time drift of the pressure sensor was adjusted by periodic recertification corrections by using electric dead-weight testers (model E-DWT-H A70M and A200M, Fluke Co., Phoenix, Arizona, USA) and a barometer (model RPM4 BA100Ks, Fluke Co.):

Serial no. 181 (A70M) (for 10-70 MPa) (calibration date: January 19, 2019)

Serial no. 1305 (A200M) (for 90 to 100 MPa) (calibration date: January 19, 2019)

Serial no. 1453 (BA100Ks) (for 0 MPa) (calibration date: January 15, 2019)

These reference pressure sensors were calibrated by Ohte Giken, Inc. (Ibaraki, Japan) traceable to National Institute of Standards and Technology (NIST) pressure standards. The pre-cruise correction was performed at JAMSTEC (Kanagawa, Japan) by Marine Works Japan Ltd. (MWJ) (Kanagawa, Japan) (Fig. 3.1.1).

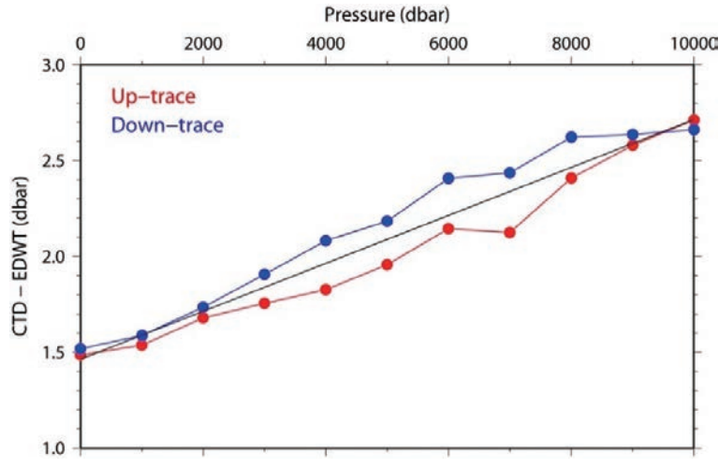

Fig. 3.1.1. Pre-cruise comparison of the CTD pressure and the reference pressure (E-DWT).

(4.2) Temperature sensors

Pre-cruise sensor calibrations of the SBE 3s were performed at Sea-Bird Scientific. Pre-cruise sensor calibration of the SBE 35 for linearization was also performed at Sea-Bird Scientific. The slow time drift of the SBE 35 was adjusted by periodic recertification corrections by measurements in thermodynamic fixed-point cells (water triple point [0.01 °C] and gallium melt point [29.7646 °C]) (Uchida et al., 2015). Since 2016, pre-cruise calibration was performed at JAMSTEC by using fixed-point cells traceable to National Metrology Institute of Japan (NMIJ) temperature standards (Fig. 3.1.2).

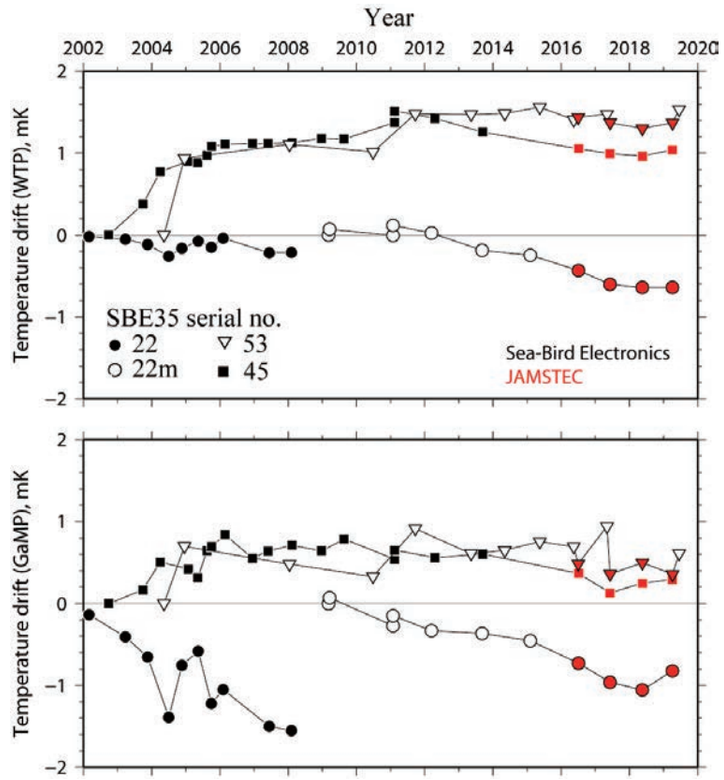

Fig. 3.1.2. Time drifts (temperature offsets relative to the first calibration) of four SBE 35s based on laboratory calibrations in fixed-point cells (water triple point: WTP, gallium melt point: GaMP).

(4.3) Conductivity sensors

Pre-cruise sensor calibrations were performed at Sea-Bird Scientific.

(4.4) Dissolved oxygen sensors

Pre-cruise sensor calibration of RINKO was performed at JAMSTEC by using O_2/N_2 standard gases (JCSS Grande 1, Taiyo Nippon Sanso Co., Japan):

3.978% of O_2, chamber no. 3MK-61964 (certification date: May 29, 2018)

9.979% of O_2, chamber no. 1MK-52697 (certification date: May 29, 2018)

16.97% of O_2, chamber no. 3MK-35986 (certification date: May 29, 2018)

24.96% of O_2, chamber no. MK-84510 (certification date: May 24, 2018)

The standard gas-saturated pure water was measured by the RINKO at temperature of 1, 10, 20 and 29 °C. Oxygen saturation was calculated from oxygen concentration of the standard gases, water temperature, and the atmospheric pressure in the calibration vessel and used to calibrate the RINKO (Fig. 3.1.3) by using the modified Stern-Volmer equation slightly modified from a method by Uchida et al. (2010). The calibration coefficients for the pressure dependency were determined from the results from the previous cruises. Details of the calibration equations are described in the sub-section of the post-cruise calibration.

Pre-cruise sensor calibration of SBE 43 was performed at Sea-Bird Scientific.

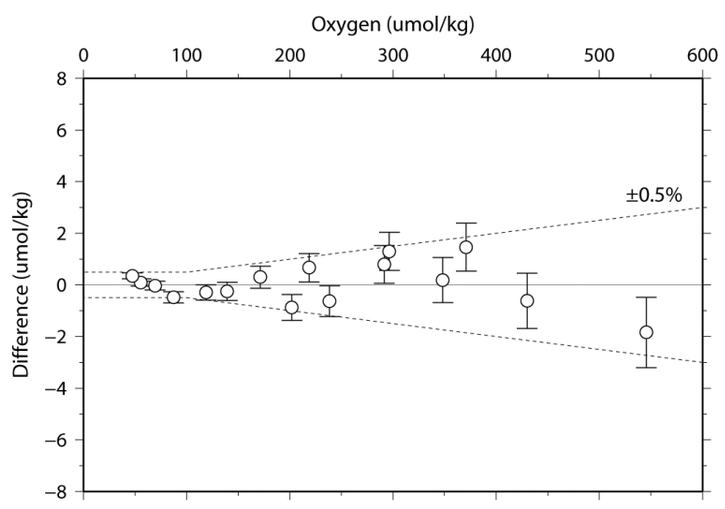

Fig. 3.1.3. Result of pre-cruise calibration of the RINKO-III (serial no. 0037). Difference between the calibrated oxygen sensor data and the reference dissolved oxygen values are shown.

(4.5) Ultraviolet fluorometer

Periodic recertification was not performed by the manufacturer for the ultraviolet fluorometer. However, the ultra pure water and the Multi-parametric Standard Seawater (MSSW) (lot PRE18) were periodically measured at JAMSTEC (Fig. 3.1.4). The MSSW is currently under development jointly by KANSO CO., Ltd. (Osaka, Japan) (Uchida et al., 2020), and fluorescent dissolved organic matter (FDOM) will be measured after this cruise to calibrate the ultraviolet fluorometer in the laboratory.

Temperature dependency of the ultraviolet fluorometer following the method by Yamashita et al. (2015):

$$CTDUVFLUORcorr = CTDUVFLUOR / (1.0 + \rho \times [T - T_r])$$

$$\rho = -0.0065$$

$$T_r = 20$$

where T is temperature (in °C), T_r is reference temperature (in °C) and ρ is the correction coefficient determined from the laboratory measurement (Fig. 3.1.4).

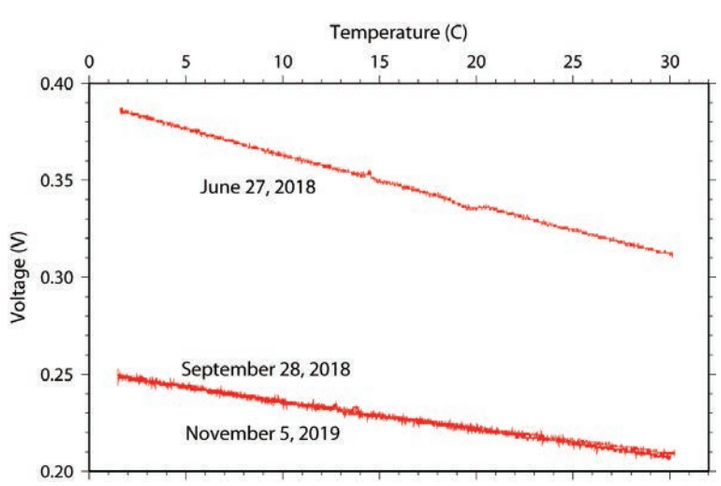

Fig. 3.1.4. Temperature dependency of the ultraviolet fluorometer for the MSSW (PRE18). The sensor output was suddenly shifted in the deep ocean during the CTD cast in July-August 2018 (RV Mirai cruise MR18-04).

(4.6) Transmissometer

Light transmission (T_r in %) is calibrated as

$$T_r = (V - V_d) / (V_r - V_d) \times 100$$

where V is the measured signal (voltage), V_d is the dark offset for the instrument, and V_r is the signal for clear water. V_d can be obtained by blocking the light path. The calibration coefficients (V_d and V_r) estimated from the previous cruise were used, because periodic recertification was not performed by the manufacturer for the transmissometer.

(4.7) Turbidity meter, chlorophyll fluorometer, PAR, altimeter

Periodic recertification was not performed by the manufacturer for these sensors.

(5) Data collection and processing

(5.1) Data collection

The CTD system was powered on at least 20 minutes in advance of the data acquisition to stabilize the pressure sensor. The data was acquired at least two minutes before and after the CTD cast to collect atmospheric pressure data on the ship's deck.

The CTD package was lowered into the water from the starboard side and held 10 m beneath the surface in order to activate the pump. After the pump was activated, the package was lifted to the surface and lowered at a rate of 1.0 m/s to 200 m (or 300 m when significant wave height was high) then the package was stopped to operate the heave compensator of the crane. The package was lowered again at a rate of 1.2 m/s to the bottom. For the up cast, the package was lifted at a rate of 1.1 m/s except for bottle firing stops. As a rule, the bottle was fired after waiting from the stop for more than 30 seconds and the package was stayed at least 5 seconds for measurement of the SBE 35 at each bottle firing stops. For depths where vertical gradient of water properties was expected to be large (from surface to thermocline), the bottle was fired after waiting from the stop for 60 seconds to enhance exchanging the water between inside and outside of the bottle. At 200 m (or 300 m) from the surface, the package was stopped to stop the heave compensator of the crane.

The water sample bottles and the stainless-steel frame of the CTD package were wiped with acetone before a cast taken water for CFCs.

(5.2) Data collection problems

There were many leaks of the water sample bottles because the top or bottom cap of the bottle did not close correctly, especially for the bottles model OTE 110 (OceanTest Equipment, Inc.).

At station 86, data quality of the primary temperature and conductivity was bad at depths deeper than 378 dbar probably due to jellyfish in the TC duct. Therefore, the secondary temperature and conductivity data were used for station 86.

At station 97, the chlorophyll fluorometer data were not obtained at the chlorophyll max layer (9-24 dbar in the down cast) due to low measurement range (0-5 µg/L) of the sensor.

At station 126, the water sample bottles were closed without bottle firing stops at depths shallower than 2730 dbar to finish the CTD cast urgently due to rough weather. The bottle data obtained without bottle firing stops were averaged over ±1 second of the bottle firing time.

At station 132, the RINKO data were not obtained because the cap of the sensing foil was not removed before the cast. Therefore, the SBE 43 data were used for station 132.

For the transmissometer, the sensor output was shifted at 581 dbar in the down cast of station 22. Offset correction (+0.006 V) was applied to the sensor output for depths deeper than 580 dbar. Data quality of the sensor output was bad in the down cast between 205 to 4660 dbar of station 36 and between 1135 to 4978 dbar of station 55 probably because of the effect of jellyfish, and the data quality flag was set to 4 (bad measurement) for the data.

(5.3) Data processing

The following are the data processing software (SBEDataProcessing-Win32) and original software data processing module sequence and specifications used in the reduction of CTD data in this cruise.

DATCNV converted the raw data to engineering unit data. DATCNV also extracted bottle information

where scans were marked with the bottle confirm bit during acquisition. The duration was set to 4.4 seconds, and the offset was set to 0.0 second. The hysteresis correction for the SBE 43 data (voltage) was applied for both profile and bottle information data.

TCORP (original module, version 1.1) corrected the pressure sensitivity of the SBE 3 for both profile and bottle information data.

RINKOCOR (original module, version 1.0) corrected the time-dependent, pressure-induced effect (hysteresis) of the RINKO for both profile data.

RINKOCORROS (original module, version 1.0) corrected the time-dependent, pressure-induced effect (hysteresis) of the RINKO for bottle information data by using the hysteresis-corrected profile data.

BOTTLESUM created a summary of the bottle data. The data were averaged over 4.4 seconds.

ALIGNCTD converted the time-sequence of sensor outputs into the pressure sequence to ensure that all calculations were made using measurements from the same parcel of water. For a SBE 9plus CTD with the ducted temperature and conductivity sensors and a 3000-rpm pump, the typical net advance of the conductivity relative to the temperature is 0.073 seconds. So, the SBE 11plus deck unit was set to advance the primary and the secondary conductivity for 1.73 scans (1.75/24 = 0.073 seconds). Oxygen data are also systematically delayed with respect to depth mainly because of the long time constant of the oxygen sensor and of an additional delay from the transit time of water in the pumped plumbing line. This delay was compensated by 5 seconds advancing the SBE 43 oxygen sensor output (voltage) relative to the temperature data. Delay of the RINKO data was also compensated by 1 second advancing sensor output (voltage) relative to the temperature data. Delay of the transmissometer data was also compensated by 2 seconds advancing sensor output (voltage) relative to the temperature data.

WILDEDIT marked extreme outliers in the data files. The first pass of WILDEDIT obtained an accurate estimate of the true standard deviation of the data. The data were read in blocks of 1000 scans. Data greater than 10 standard deviations were flagged. The second pass computed a standard deviation over the same 1000 scans excluding the flagged values. Values greater than 20 standard deviations were marked bad. This process was applied to pressure, temperature, conductivity, and SBE 43 output.

CELLTM used a recursive filter to remove conductivity cell thermal mass effects from the measured conductivity. Typical values used were thermal anomaly amplitude alpha = 0.03 and the time constant 1/beta = 7.0.

FILTER performed a low pass filter on pressure with a time constant of 0.15 seconds. In order to produce zero phase lag (no time shift) the filter runs forward first then backwards.

WFILTER performed as a median filter to remove spikes in fluorometer, turbidity meter, transmissometer, and ultraviolet fluorometer data. A median value was determined by 49 scans of the window. For the ultraviolet fluorometer data, an additional box-car filter with a window of 361 scans was applied to remove noise.

SECTIONU (original module, version 1.1) selected a time span of data based on scan number in order to reduce a file size. The minimum number was set to be the start time when the CTD package was beneath the sea-surface after activation of the pump. The maximum number was set to be the end time when the depth of the package was 1 dbar below the surface. The minimum and maximum numbers were automatically calculated in the module.

LOOPEDIT marked scans where the CTD was moving less than the minimum velocity of 0.0 m/s (traveling backwards due to ship roll).

DESPIKE (original module, version 1.0) removed spikes of the data. A median and mean absolute deviation was calculated in 1-dbar pressure bins for both down- and up-cast, excluding the flagged values. Values greater than 4 mean absolute deviations from the median were marked bad for each bin. This process was performed 2 times for temperature, conductivity, SBE 43, and RINKO output.

DERIVE was used to compute oxygen (SBE 43).

BINAVG averaged the data into 1-dbar pressure bins. The center value of the first bin was set equal to the bin size. The bin minimum and maximum values are the center value plus and minus half the bin size. Scans with pressures greater than the minimum and less than or equal to the maximum were averaged. Scans were interpolated so that a data record exist every dbar.

BOTTOMCUT (original module, version 0.1) deleted the deepest pressure bin when the averaged scan

number of the deepest bin was smaller than the average scan number of the bin just above.

DERIVE was re-used to compute salinity, potential temperature, and density

SPLIT was used to split data into the down cast and the up cast.

Remaining spikes in the CTD data were manually eliminated from the 1-dbar-averaged data. The data gaps resulting from the elimination were linearly interpolated with a quality flag of 6.

(6) Post-cruise calibration

(6.1) Pressure sensor

The CTD pressure sensor offset in the period of the cruise was estimated from the pressure readings on the ship's deck. For best results the Paroscientific sensor was powered on for at least 20 minutes before the operation. In order to get the calibration data for the pre- and post-cast pressure sensor drift, the CTD deck pressure was averaged over first and last one minute, respectively. Then the atmospheric pressure deviation from a standard atmospheric pressure (1013.25 hPa) was subtracted from the CTD deck pressure to check the pressure sensor time drift. The atmospheric pressure was measured at the captain deck (20 m high from the base line) and sub-sampled one-minute interval as a meteorological data.

Time series of the CTD deck pressure is shown in Figs. 3.1.5 and 3.1.6. The CTD pressure sensor offset was estimated from the deck pressure. Mean of the pre- and the post-casts data over the whole period gave an estimation of the pressure sensor offset (0.07 and 0.03 dbar for leg 2 and leg 3, respectively) from the pre-cruise calibration. The post-cruise correction of the pressure data is not deemed necessary for the pressure sensor.

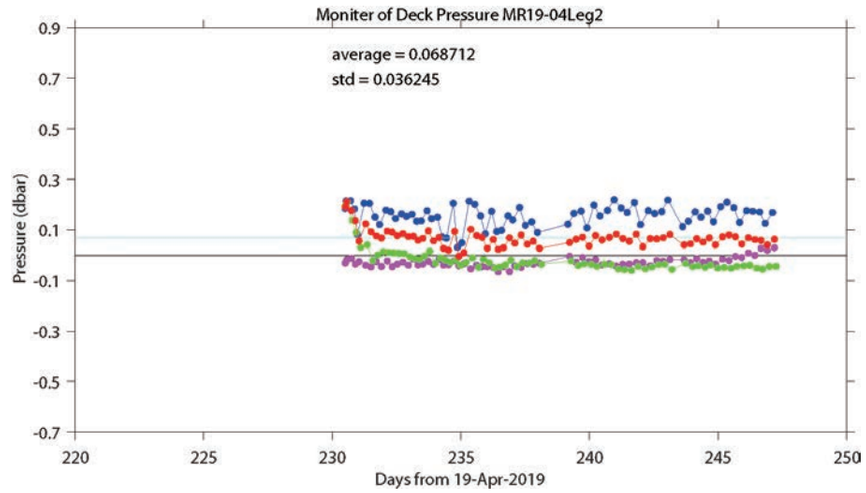

Fig. 3.1.5. Time series of the CTD deck pressure for leg 2. Atmospheric pressure deviation (magenta dots) from a standard atmospheric pressure was subtracted from the CTD deck pressure. Blue and green dots indicate pre- and post-cast deck pressures, respectively. Red dots indicate averages of the pre- and the post-cast deck pressures.

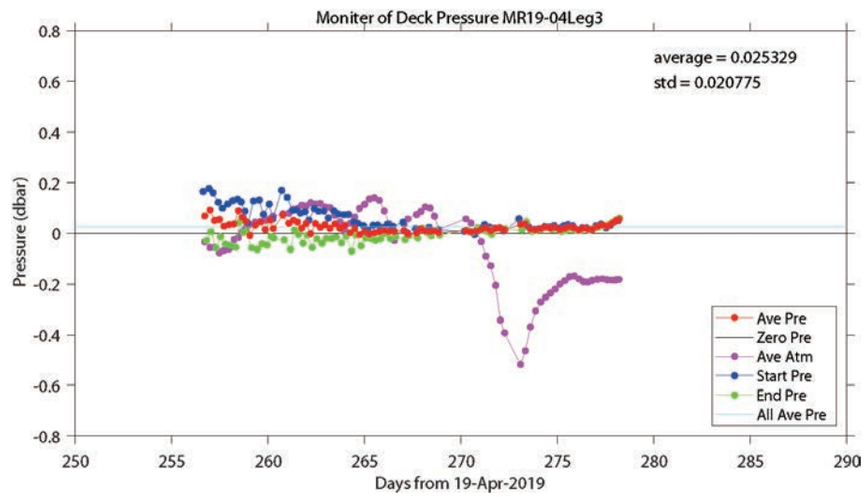

Fig. 3.1.6. Same as Fig. 3.1.5, but for leg 3.

(6.2) Temperature sensors

The CTD temperature sensors (SBE 3) were calibrated with the SBE 35 under the assumption that discrepancies between SBE 3 and SBE 35 data were due to pressure sensitivity, the viscous heating effect, and time drift of the SBE 3 (Uchida et al., 2015).

Post-cruise sensor calibration for the SBE 35 will be performed at JAMSTEC in August 2020.

The CTD temperature was calibrated as

Calibrated temperature = $T - (c_0 \times P + c_1 \times t + c_2)$

where T is CTD temperature in °C, P is pressure in dbar, t is time in days from pre-cruise calibration date of the CTD temperature and c_0, c_1, and c_2 are calibration coefficients. The coefficients were determined using the data for the depths deeper than 1950 dbar.

The primary temperature data were basically used for the post-cruise calibration. The secondary temperature sensor was also calibrated and used instead of the primary temperature data when the data quality of the primary temperature data was bad (station 86). The results of the post-cruise calibration for the CTD temperature are shown in Table 3.1.1, Figs. 3.1.7, 3.1.8, and 3.1.9, and the calibration coefficients are as follows:

c_0 = 5.19734252e-08, c_1 = 4.49880e-06, c_2 = -9.6313e-04 [for leg 2, primary]

c_0 = 1.13549796e-08, c_1 = 2.72736e-05, c_2 = -5.7034e-03 [for leg 3, primary]

c_0 = -3.56735208e-08, c_1 = 3.41359e-07, c_2 = -5.1565e-04 [for leg 3, secondary]

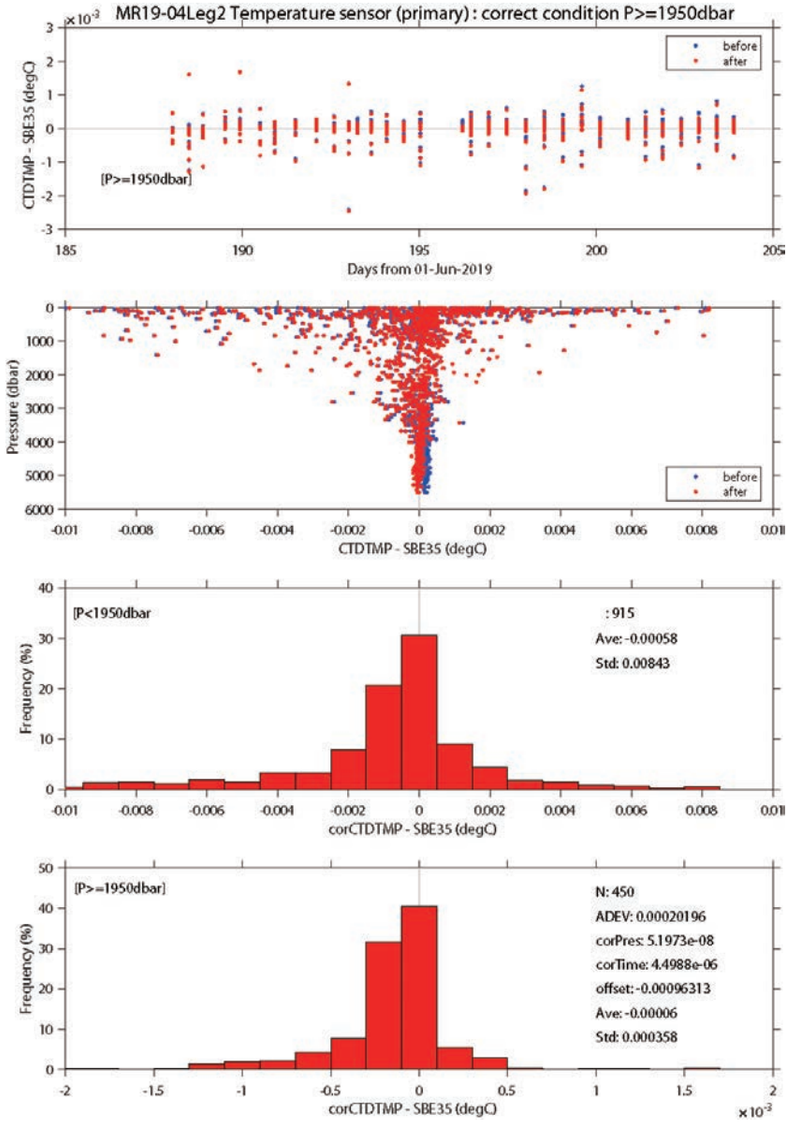

Fig. 3.1.7. Difference between the CTD temperature (primary) and the SBE 35 for leg 2. Blue and red dots indicate before and after the post-cruise calibration using the SBE 35 data, respectively. Lower two panels show histogram of the difference after the calibration.

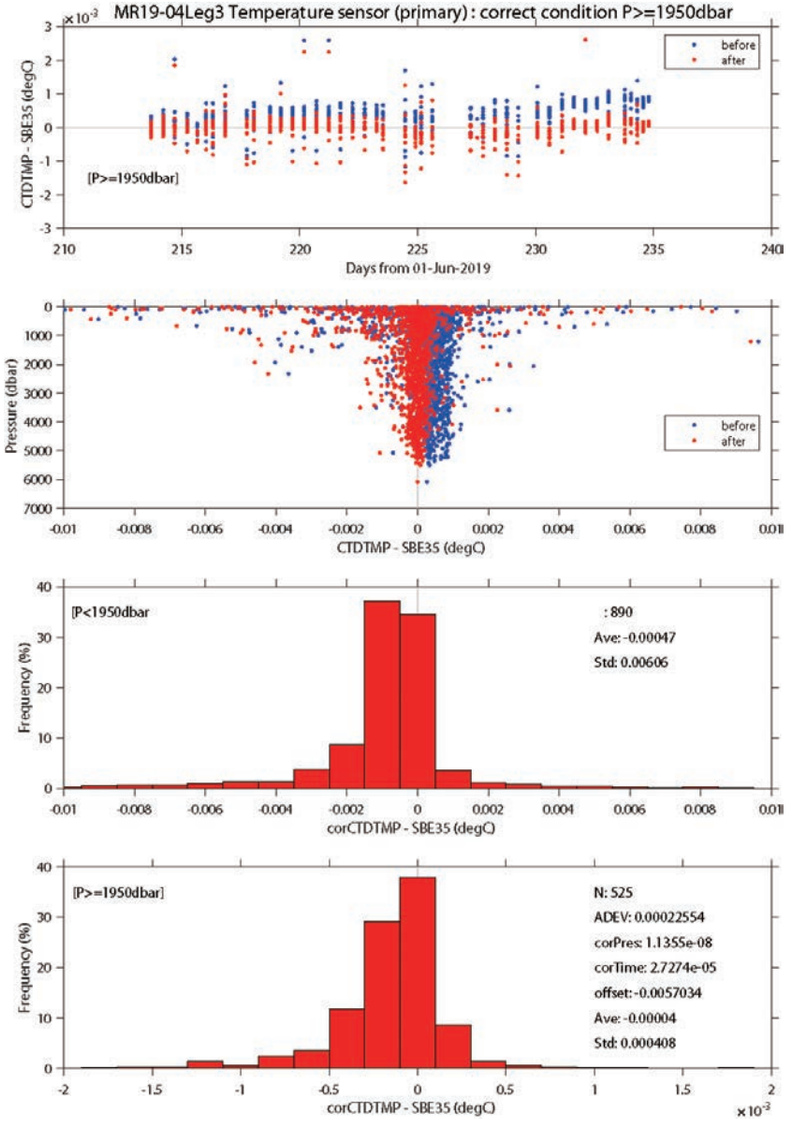

Fig. 3.1.8. Same as Fig. 3.1.7, but for leg 3 (primary temperature).

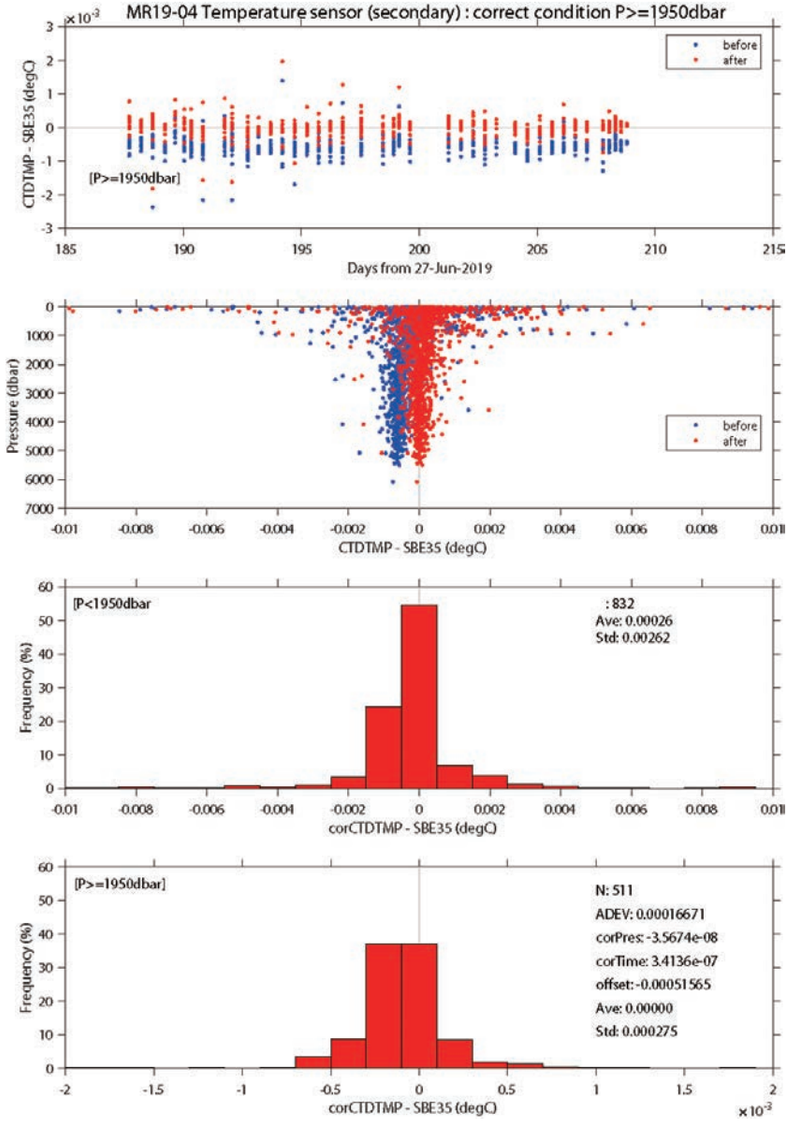

Fig. 3.1.9. Same as Fig. 3.1.7, but for leg 3 (secondary temperature).

Table 3.1.1. Difference between the CTD temperature and the SBE 35 after the post-cruise calibration. Mean and standard deviation (Sdev) are calculated for the data below and above 1950 dbar. Number of data used is also shown.

Leg	Sensor	Pressure ≥ 1950 dbar			Pressure < 1950 dbar		
		Number	Mean (mK)	Sdev (mK)	Number	Mean (mK)	Sdev (mK)
2	Primary	450	–0.1	0.4	915	–0.6	8.4
3	Primary	525	–0.0	0.4	890	–0.5	6.1
3	Secondary	511	0.0	0.3	832	0.3	2.6

(6.3) Conductivity sensor

The discrepancy between the CTD conductivity and the conductivity calculated from the bottle salinity data with the CTD temperature and pressure data is considered to be a function of conductivity, pressure and time. The CTD conductivity was calibrated as

Calibrated conductivity =

$$C - (c_0 \times C + c_1 \times P + c_2 \times C \times P + c_3 \times P^2 + c_4 \times P^2 \times C + c_5 \times P^2 \times C^2 + c_6 \times t + c_7)$$

where C is CTD conductivity in S/m, P is pressure in dbar, t is time in days and c_0, c_1, c_2, c_3, c_4, c_5, c_6 and c_7 are calibration coefficients. The best fit sets of coefficients were determined by a least square technique to minimize the deviation from the conductivity calculated from the bottle salinity data.

The primary conductivity data created by the software module ROSSUM were used after the post-cruise calibration for the temperature data. The results of the post-cruise calibration for the CTD salinity are summarized in Table 3.1.2 and shown in Figs 3.1.10, 3.1.11 and 3.1.12. The calibration coefficients are as follows:

c_0 = 5.1161481588e-05, c_1 = -2.9852469268e-07, c_2 = 8.6423667125e-08,

c_3 = -7.8216002143e-11, c_4 = 1.5213293009e-10, c_5 = -3.9207472832e-11,

c_6 = 5.5962247644e-08, c_7 = 1.8345172035e-04 [for leg 2, primary]

c_0 = 8.4059171088e-05, c_1 = 3.9805334321e-07, c_2 = -1.0817725126e-07,

c_3 = -6.6727430535e-10, c_4 = 4.3600536612e-10, c_5 = -7.1667314964e-11,

c_6 = 5.3289917898e-06, c_7 = -6.1688283232e-05 [for leg 3, primary]

c_0 = 9.2155745106e-05, c_1 = 3.2725052723e-07, c_2 = -8.7940015706e-08,

c_3 = -2.8014029332e-10, c_4 = 1.9319180823e-10, c_5 = -3.3675443715e-11,

c_6 = 4.4847233878e-06, c_7 = -2.4324855043e-04 [for leg 3, secondary]

Table 3.1.2. Difference between the CTD salinity and the bottle sampled salinity after the post-cruise calibration. Mean and standard deviation (Sdev) are calculated for the data below and above 1950 dbar. Number of data used is also shown.

Leg	Sensor	Pressure ≥ 1950 dbar			Pressure < 1950 dbar		
		Number	Mean (10^{-3})	Sdev (10^{-3})	Number	Mean (10^{-3})	Sdev (10^{-3})
2	Primary	435	0.1	0.5	601	0.1	8.3
3	Primary	522	0.1	0.4	843	–0.4	4.9
3	Secondary	501	0.0	0.5	824	–0.4	4.8

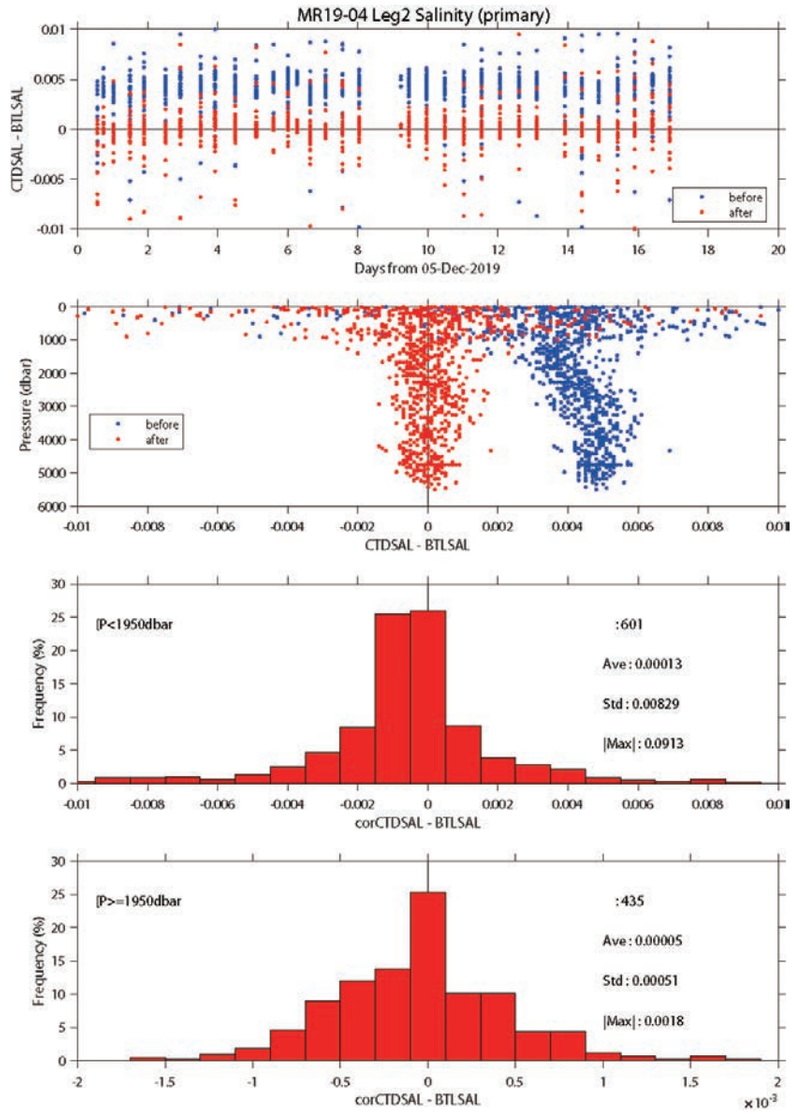

Fig. 3.1.10. Difference between the CTD salinity (primary) and the bottle salinity for leg 2. Blue and red dots indicate before and after the post-cruise calibration, respectively. Lower two panels show histogram of the difference after the calibration.

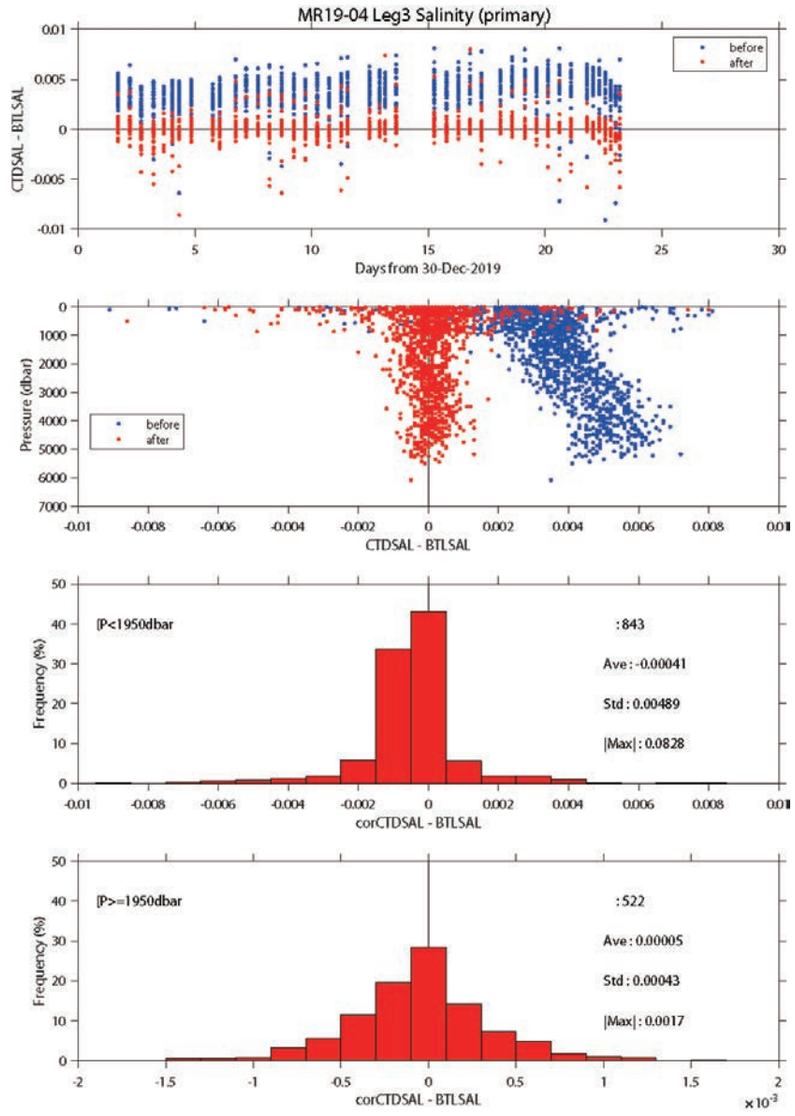

Fig. 3.1.11. Same as Fig. 3.1.10, but for leg 3 (primary salinity).

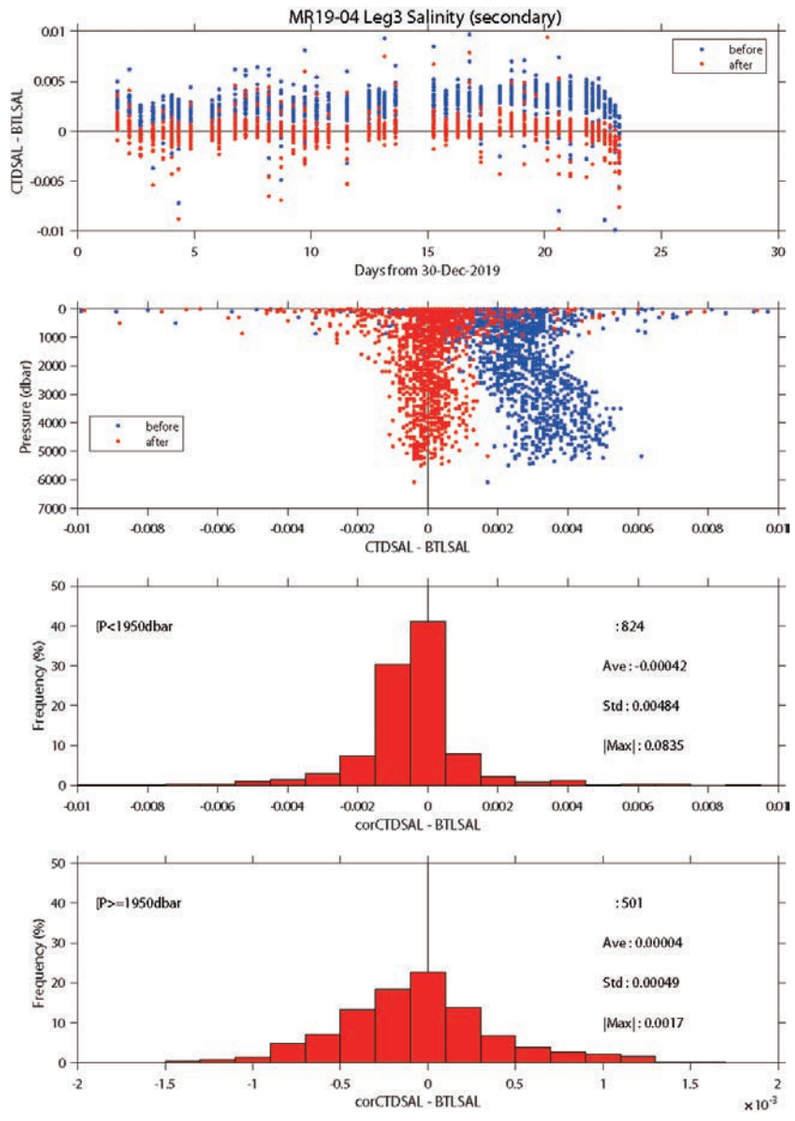

Fig. 3.1.12. Same as Fig. 3.1.10, but for leg 3 (secondary salinity).

(6.4) Dissolved oxygen sensors

(6.4.1) Primary oxygen sensor, RINKO

Data from the RINKO can be corrected for the time-dependent, pressure-induced effect by means of the same method as that developed for the SBE 43 (Edwards et al., 2010). The calibration coefficients, H1 (amplitude of hysteresis correction), H2 (curvature function for hysteresis), and H3 (time constant for hysteresis) were determined to minimize the down-cast and up-cast data.

H1 = 0.0060, H2 = 4000.0, H3 = 2000.0 [for leg 2]

H1 = 0.0058, H2 = 4000.0, H3 = 3000.0 [for leg 3]

Outputs from RINKO are the raw phase shift data. The RINKO can be calibrated by the modified Stern-Volmer equation slightly modified from a method by Uchida et al. (2010):

$$O_2\ (\mu mol/l) = [(V_0 / V)^E - 1] / K_{sv}$$

where V is voltage, V_0 is voltage in the absence of oxygen, K_{sv} is Stern-Volmer constant. The coefficient E corrects nonlinearity of the Stern-Volmer equation. The V_0 and the K_{sv} are assumed to be functions of temperature as follows.

$$K_{sv} = c_0 + c_1 \times T + c_2 \times T^2$$

$$V_0 = 1 + d_0 \times T$$

$$V = d_1 + d_2 \times V_b + d_3 \times t + d_4 \times t \times V_b + d_5 \times t^2 \times V_b$$

where T is CTD temperature (°C) and V_b is raw output (volts). V_0 and V are normalized by the output in the absence of oxygen at 0°C, and t is working time (days) integrated from the fist CTD cast for each leg. The oxygen concentration is calculated using accurate temperature data from the CTD temperature sensor instead of temperature data from the RINKO. The pressure-compensated oxygen concentration O_{2c} can be calculated as follows.

$$O_{2c} = O_2\ (1 + cp \times P / 1000)$$

where P is CTD pressure (dbar) and cp is the compensation coefficient. Since the sensing foil of the optode is permeable only to gas and not to water, the optode oxygen must be corrected for salinity. The salinity-compensated oxygen can be calculated by multiplying the factor of the effect of salt on the oxygen solubility (Garcia and Gordon, 1992).

The post-cruise calibrated temperature and salinity data were used for the calibration. The results of the post-cruise calibration for the RINKO oxygen are summarized in Table 3.1.3 and shown in Figs. 3.1.13 and 3.1.14. The calibration coefficients are as follows:

c_0 = 4.481833626824531e-03, c_1 = 1.898732545208230e-04, c_2 = 3.186018747588371e-06,

d_0 = -4.993114971420946e-04, d_1 = -8.334758478255305e-02, d_2 = 0.3012446445865034,

d_3 = -2.736037023481914e-04, d_4 = 7.781237926511940e-04,

d_5 = -2.720297060792388e-05, E = 1.2, cp = 0.025 [for leg 2]

c_0 = 4.231278175431956e-03, c_1 = 1.586473748345674e-04, c_2 = 1.925342563039167e-06,

d_0 = -3.776889529330843e-03, d_1 = -8.075699587347064e-02, d_2 = 0.3084927182050134,

d_3 = -3.695840179696757e-04, d_4 = 5.050997085259927e-04,

d_5 = -1.146792845027660e-05, E = 1.2, cp = 0.024 [for leg 3]

Table 3.1.3. Difference between the CTD oxygen and the bottle sampled oxygen after the post-cruise calibration. Mean and standard deviation (Sdev) are calculated for the data below and above 1950 dbar. Number of data used is also shown.

Leg	Sensor	Pressure ≥ 1950 dbar			Pressure < 1950 dbar		
		Number	Mean (μmol/kg)	Sdev (μmol/kg)	Number	Mean (μmol/kg)	Sdev (μmol/kg)
2	Primary	421	–0.05	0.30	599	0.03	1.08
3	Primary	511	–0.04	0.30	826	0.06	0.77

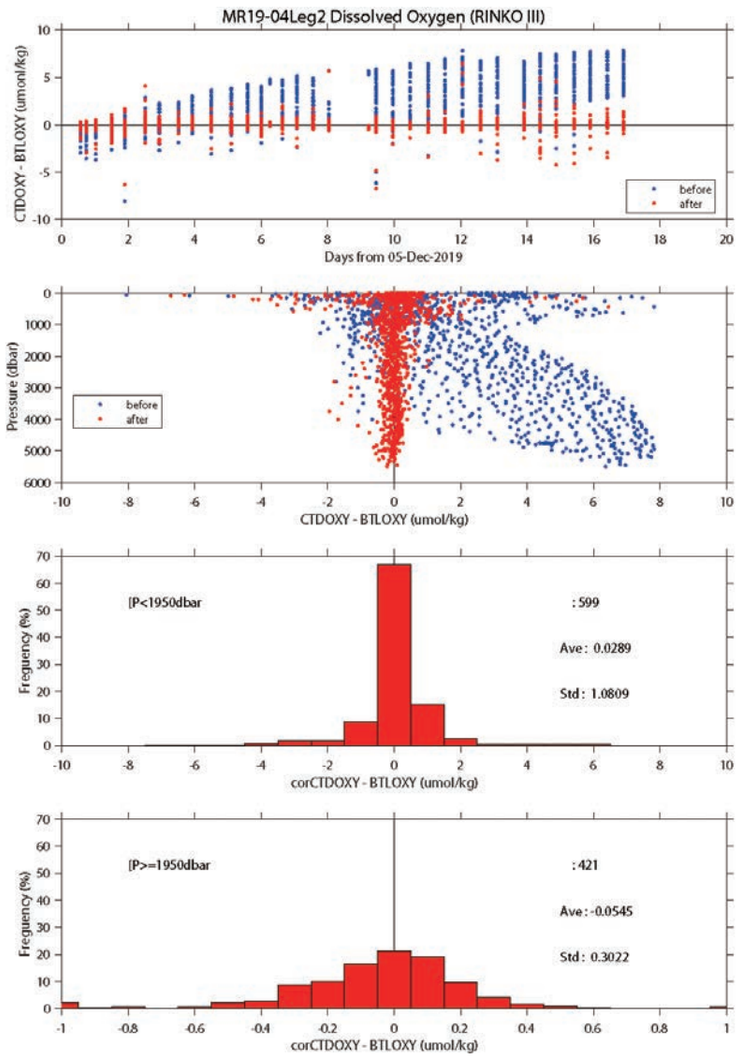

Fig. 3.1.13. Difference between the CTD oxygen and the bottle oxygen for leg 2. Blue and red dots indicate before and after the post-cruise calibration, respectively. Lower two panels show histogram of the difference after the calibration.

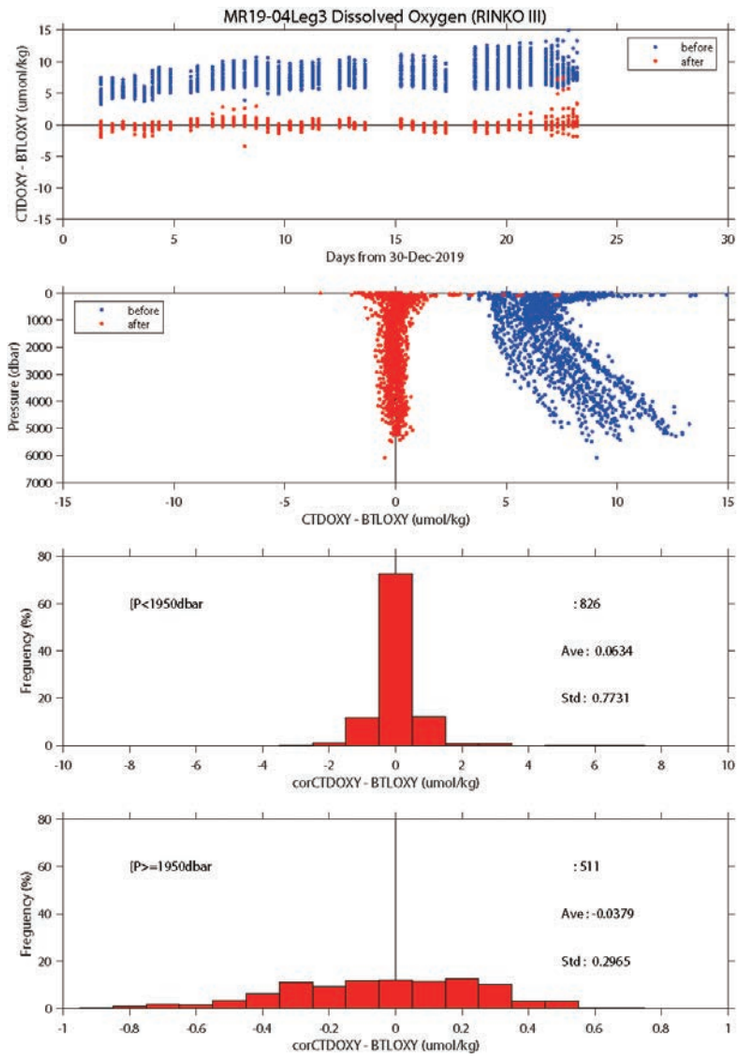

Fig. 3.1.14. Same as Fig. 3.1.13, but for leg 3.

(6.4.2) Secondary oxygen sensor, SBE 43

The primary oxygen sensor RINKO data was not available at station 132 because the cap of the sensing foil was not removed. Therefore, the secondary oxygen sensor SBE 43 was calibrated in situ for the CTD cast. The bottle sampled oxygen data were compared with the down-cast SBE 43 data extracted from the same density surfaces (Fig. 3.1.15). The SBE 43 data was calibrated by using the following equation:

$$SBE43OXY_{corr} = c_0 + c_1 \times SBE43OXY + c_2 \times P + c_3 \times T$$

$c_0 = 8.776269046135372$

$c_1 = 0.9875226996210535$

$c_2 = 3.729733540353487e\text{-}04$

$c_3 = -2.227812374383066$

where P is pressure (in dbar), T is temperature (°C) and c_0-c_3 are the calibration coefficients. Standard deviation of the difference between $SBE43OXY_{corr}$ and the bottle oxygen was 0.35 (μmol/kg) for depths deeper than 950 dbar.

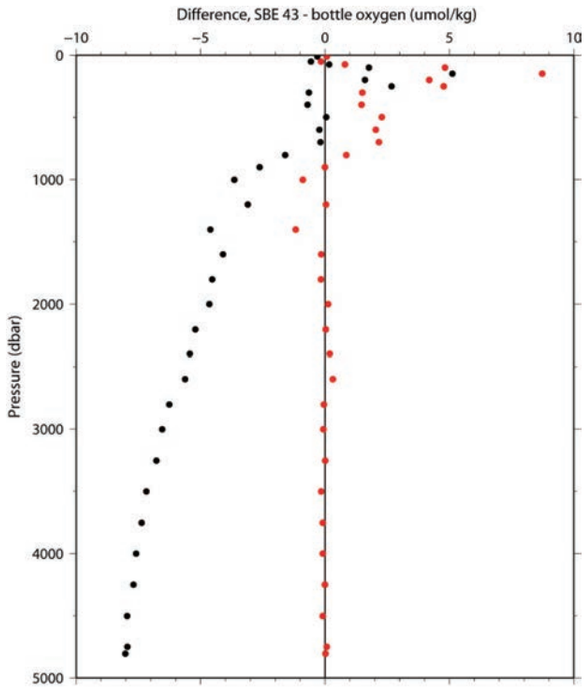

Fig. 3.1.15. Comparison of the secondary dissolved oxygen SBE 43 and the bottle sampled oxygen before the in situ calibration (black dots) and after the in situ calibration (red dots) for station 132. The down-cast oxygen sensor data were compared with the bottle sampled oxygen data.

(6.5) Transmissometer

Light transmission T_r (in %) and beam attenuation coefficient c_p are calculated from the sensor output V (in volt) as follows:

$$T_r = (V - V_d) / (V_r - V_d) \times 100$$

$$c_p = - (1 / 0.25) \ln(T_r / 100)$$

where V_d is the dark offset for the instrument, and V_r is the signal for clear water. V_d can be obtained by blocking the light path. V_d was measured on deck before each cast. V_r is estimated from the measured maximum signal in the deep ocean at each cast. Since the transmissometer drifted in time (Fig. 3.1.16), V_r is expressed as

$$V_r = c_0 + c_1 \times t + c_2 \times t^2$$

where t is working time (in days) of the transmissometer integrated from the first CTD cast for each leg, and c_0, c_1, and c_2 are calibration coefficients. Maximum signal was extracted for each cast. The calibration coefficients are as follows:

Leg 2, working time < 5.3169 days

c_0 = 4.75484110614084, c_1 = -0.00211422184747569, c_2 = 0.0

V_d = 0.0012

Leg 2, working time >= 5.3169 days

c_0 = 4.7436, c_1 = 0.0, c_2 = 0.0

V_d = 0.0012

Leg 3

c_0 = 4.741726486231039, c_1 = -2.045237713851287e-03, c_2 = 1.050489805417849e-04

V_d = 0.0012

Also, the light transmission in air $T_{rair} = (V_{air} - V_d)/(V_{ref} - V_d)$ was estimated to be 1.03553 from the measurements after the last CTD cast of leg 3.

(6.6) Turbidity meter

The turbidity meter was not calibrated in situ since there was no reference data. However, the sensor offset can be easily obtained by a dark test. The optical windows were covered by a PTFE sealing tape and a black vinyl tape. The sensor offset was estimated to be zero as the data obtained in the dark condition.

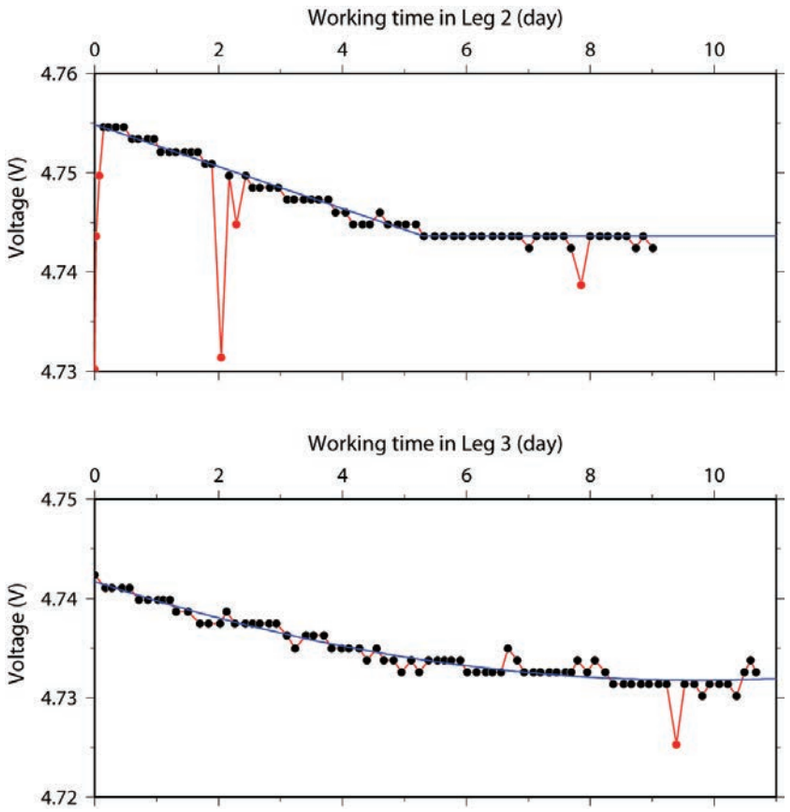

Fig 3.1.16. Time series of the maximum value of the transmissometer output at each cast. Red dots are not used in the calibration coefficients estimate and blue lines are the calibration equations.

(6.7) Chlorophyll fluorometer

The chlorophyll fluorometer data show positive biases in the deep ocean because of the interference by the fluorescent dissolved organic material (FDOM) (Xing et al., 2017). Therefore, the effect of the interference by FDOM was corrected by using the ultraviolet fluorometer data (Figs 3.1.17 and 3.1.18) as follows:

$CTDFLUOR_{fdom\_corr} = CTDFLUOR - c_0 + c_1 \times CTDUVFLUOR_{corr} \times (1.0 - 0.000013 \times P)$

$c_0 = 0.037595034491929$, $c_1 = 0.982993745243338$ [for stations 1 – 97]

$c_0 = 0.0316388799077501$, $c_1 = 0.722499476069204$ [for stations 98 – 153]

where $CTDUVFLUOR_{corr}$ is the ultraviolet fluorometer data (see below), P is pressure (in dbar), and c0 and c1 are the correction coefficients.

The chlorophyll fluorometer data thus corrected was calibrated in situ by using the bottle sampled chlorophyll-a data. The chlorophyll fluorometer data was slightly noisy so that the up-cast profile data which was averaged over one decibar more agree with the bottle sampled data than the discrete chlorophyll fluorometer data obtained at bottle-firing stops. Therefore, the CTD fluorometer data at water sampling depths extracted from the up-cast profile data were compared with the bottle sampled chlorophyll-a data. The bottle sampled data obtained at dark condition [PAR (Photosynthetically Available Radiation) < 50 μE/(m^2 sec)] were used for the calibration, since sensitivity of the fluorometer to chlorophyll *a* is different at nighttime and daytime (Figs. 3.1.19 and 3.1.20). The calibration equation is as follows:

$CTDFLUORcorr = c_0 + c_1 \times CTDFLUOR_{fdom\_corr}$

For $CTDFLUOR_{fdom\_corr} < 0.15$

$c_0 = 0.0$, $c_1 = 1.057609201250224$ [for leg 2]

$c_0 = 0.0$, $c_1 = 0.8095685935896424$ [for leg 3]

For $CTDFLUOR_{fdom\_corr} >= 0.15$

$c_0 = -9.266249192486984e\text{-}3$, $c_1 = 1.119384193144591$ [for stations 1 – 8]

$c_0 = 8.785619163927143e\text{-}2$, $c_1 = 0.4719011730479180$ [for stations 9 – 69]

$c_0 = -5.693867583263859e\text{-}2$, $c_1 = 1.189157837493829$ [for stations 70 – 71]

$c_0 = 5.686897296565606e\text{-}2$, $c_1 = 0.4304401825407885$ [for station 72 – 102]

$c_0 = 8.200539268327771e\text{-}2$, $c_1 = 0.2627010759224658$ [for stations 103 – 153]

where c_0 and c_1 are the calibration coefficients.

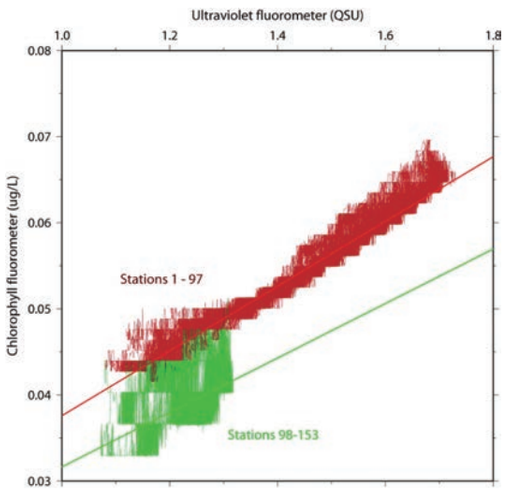

Fig. 3.1.17. Comparison between the chlorophyll fluorometer and the ultraviolet fluorometer for the deep ocean (depths deeper than 400 dbar).

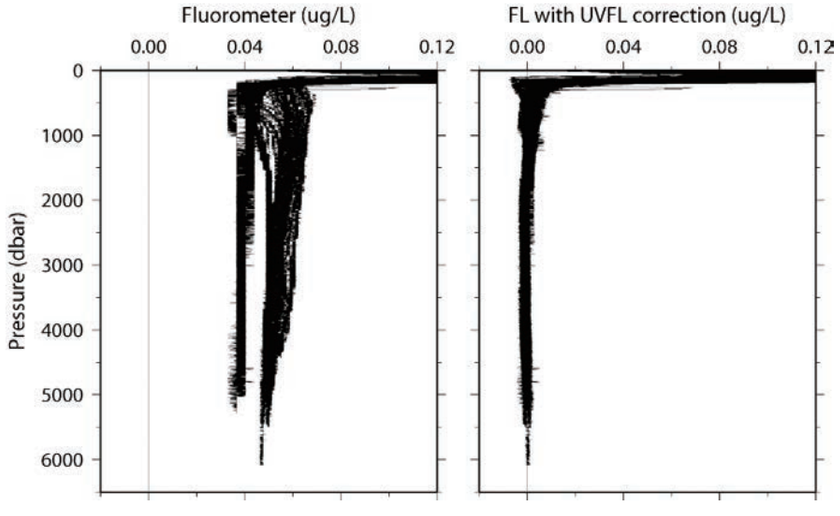

Fig. 3.1.18. Vertical profiles of the chlorophyll fluorometer before (left panel) and after (right panel) the correction for the interference by fluorescence dissolved material (FDOM).

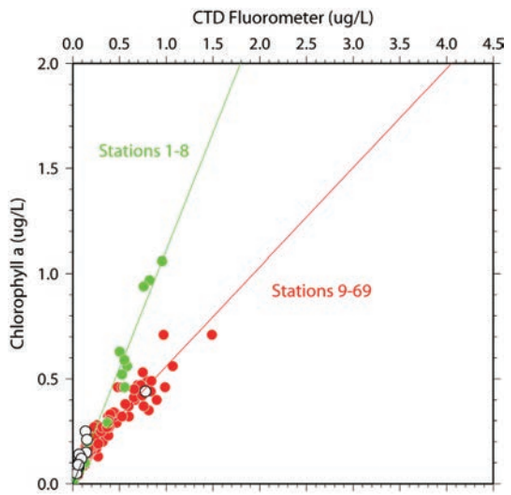

Fig. 3.1.19. Comparison of the CTD chlorophyll fluorometer and the bottle sampled chlorophyll-a for leg 2. The regression lines are also shown. Open circles were not used for the calibration because PAR was large (>= 50 $\mu E/m^2/s$).

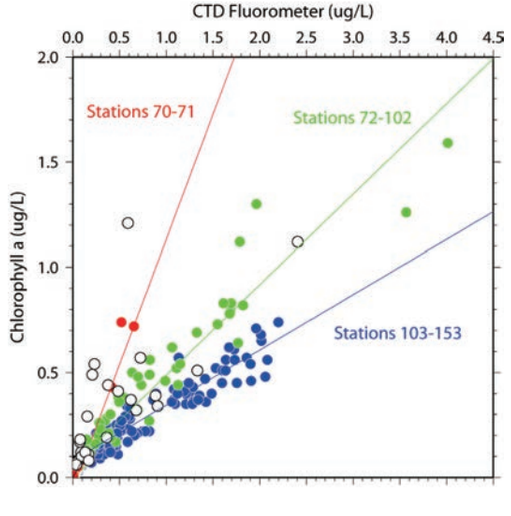

Fig. 3.1.20. Same as Fig. 3.1.19, but for leg 3.

(6.8) Ultraviolet fluorometer

The sensor output from the ultraviolet fluorometer showed difference between the down-cast and up-cast. The pressure hysteresis of the sensor output was corrected for the up-cast data by following equations:

$$CTDUVFLUOR_{corr} = CTDUVFLUOR \times (1.0 + c_0 \times [P_{lim} - P]) \quad [\text{for } P < Plim]$$

P_{lim} = 2500 dbar, c_0 = 1.5e-5 [for leg2]

P_{lim} = 2500 dbar, c_0 = 1.8e-5 [for leg 3 stations 70 – 102]

P_{lim} = 3000 dbar, c_0 = 0.4e-5 [for leg 3 stations 103 – 153]

where P is pressure (in dbar), P_{lim} is threshold value of pressure and c_0 is the correction coefficient. When the pressure P is greater than P_{lim}, c_0 was set to zero. When the maximum pressure (P_{max}) of the cast was smaller than P_{lim}, P_{lim} was set to P_{max}.

The sensor output from the ultraviolet fluorometer showed positive deviation near the surface probably because of the interference by sunlight (Fig. 3.1.21). Therefore, when the PAR data was greater than 100 μE/m^2/s, the deviated data near the surface was replaced by the surface minimum value for depths from the surface to the pressure where the minimum value was observed at each cast.

The ultraviolet fluorometer data thus corrected was calibrated in situ by using the bottle sampled fluorescence dissolved organic matter (FDOM) data (in Raman Unit [RU]) obtained at an excitation wavelength of 370 nm as follows:

$$CTDUVFLUOR\text{-}370\ [RU] = c_0 + c_1 \times CTDUVFLUOR_{corr}\ [QSU] + c_2 \times T$$

c_0 = -1.163505363380728e-02

c_1 = 1.491187270086319e-02

c_2 = -1.125715154068824e-04

where T is temperature (°C) and c_0-c_2 are the calibration coefficients. Standard deviation of the difference between CTDUVFLUOR-370 and FDOM was 0.00041 (RU) (Fig. 3.1.22).

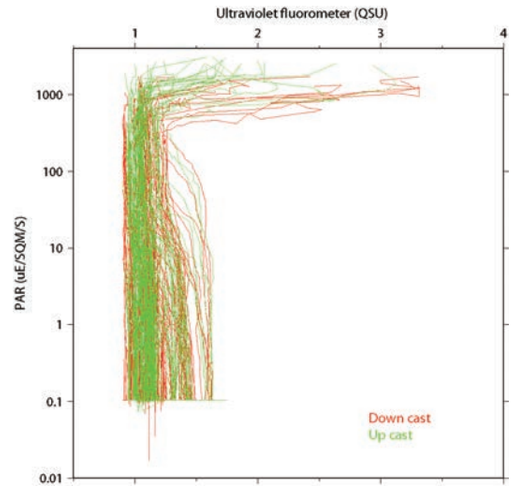

Fig. 3.1.21. Ultraviolet fluorometer data plotted against PAR data.

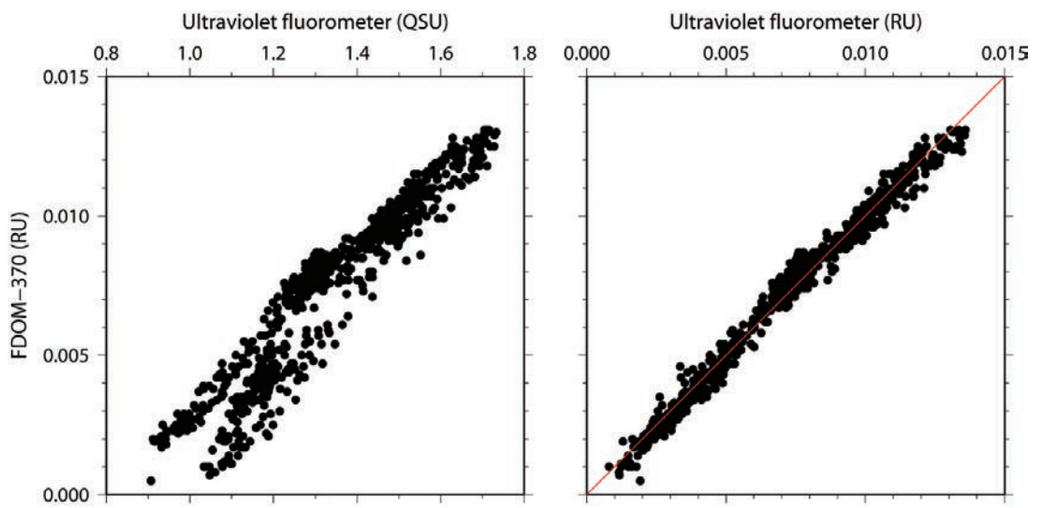

Fig. 3.1.22. Comparison of the ultraviolet fluorometer data and the fluorescent dissolved organic matter (FDOM) (left panel). The sensor data calibrated against the FDOM (Raman Unit) are also shown (right panel).

(6.9) PAR

PAR is expected to be zero in the deep ocean. Therefore, the offset measured in the deep ocean was corrected. The corrected data (PARc) is calculated from the raw data (PAR) as follows:

$$PARc\ [\mu E\ m^{-2}\ s^{-1}] = PAR - 0.104.$$

(7) References

Edwards, B., D. Murphy, C. Janzen and N. Larson (2010): Calibration, response, and hysteresis in deep-sea dissolved oxygen measurements, *J. Atmos. Oceanic Technol.,* 27, 920–931.

Fukasawa, M., T. Kawano and H. Uchida (2004): Blue Earth Global Expedition collects CTD data aboard Mirai, BEAGLE 2003 conducted using a Dynacon CTD traction winch and motion-compensated crane, *Sea Technology,* 45, 14–18.

García, H. E. and L. I. Gordon (1992): Oxygen solubility in seawater: Better fitting equations. *Limnol. Oceanogr.,* 37 (6), 1307–1312.

Uchida, H., G. C. Johnson, and K. E. McTaggart (2010): CTD oxygen sensor calibration procedures, The GO-SHIP Repeat Hydrography Manual: A collection of expert reports and guidelines, IOCCP Rep., No. 14, ICPO Pub. Ser. No. 134.

Uchida, H., T. Kawano, T. Nakano, M. Wakita, T. Tanaka and S. Tanihara (2020): An updated batch-to-batch correction for IAPSO standard seawater. submitted to J. Atmos. Oceanic Technol.

Uchida, H., Y. Maeda and S. Kawamata (2018): Compact underwater slip ring swivel: Minimizing effect of CTD package rotation on data quality, Sea Technology, 11, 30–32.

Uchida, H., T. Nakano, J. Tamba, J. V. Widiatmo, K. Yamazawa, S. Ozawa and T. Kawano (2015): Deep ocean temperature measurement with an uncertainty of 0.7 mK, J. Atmos. Oceanic Technol., 32, 2199–2210.

Xing, X., H. Claustre, E. Boss, C. Roesler, E. Organelli, A. Poteau, M. Barbieux and F. D'Ortenzio (2017): Correction of profiles of in-situ chlorophyll fluoremetry for the contribution of fluorescence originating from non-algal matter, Limnol. Oceanogr.: Methods, 15, 80–93.

Yamashita, Y., C.-J. Liu, H. Ogawa, J. Nishioka, H. Obata and H. Saito (2015): Application of an in situ fluorometer to determine the distribution of fluorescent organic matter in the open ocean, Marine Chemistry, 177, 298–305.

3.2 Bottle Salinity

February 5, 2020

(1) Personnel

Hiroshi Uchida (JAMSTEC)

Hiroki Ushiromura (MWJ) (leg 2)

Shungo Oshitani (MWJ) (leg 3)

(2) Objective

Bottle salinities were measured to calibrate the CTD salinity data.

(3) Instruments and method

Salinity measurement was conducted basically based on the method by Kawano (2010). Materials used in this cruise are as follows:

Standard Seawater: IAPSO Standard Seawater, Ocean Scientific International Ltd., Hampshire, UK

Batch P162

Salinometer: Autosal model 8400B; Guildline Instruments, Ltd., Ontario, Canada

Serial no. 62556

Serial no. 72874 (for spare: not used for the measurement of seawater samples)

A peristaltic-type sample intake pump, Ocean Scientific International Ltd.

Thermometers: PRT model 1502A, Fluke Co., Everett, Washington, USA

Serial no. B81550 (for monitoring the bath temperature) (calibration date: August 29, 2017)

Serial no. B78466 (for monitoring the room temperature) (calibration date: August 29, 2017)

Stabilized power supply: model PCR1000LE, Kikusui Electronics Co., Japan

Serial no. XH004198 (calibration date: February 15, 2018)

Sample bottles: 250 mL brown borosilicate glass bottles with screw caps (PTFE packing)

(A polyethylene inner plug was used for samples for the thermo-salinograph correction.)

Decade resistance substituter: model HARS-X-7-0.001-K, IET Labs., Inc., New York, USA

Serial no. E1-13514822 (calibration date: December 20, 2013)

Serial no. E1-19035551 (calibration date: January 17, 2019)

The bath temperature of the salinometer was set to 24 °C. The salinometer was standardized only at the beginning of the cruise by using the IAPSO Standard Seawater (SSW). The standardization dial was set to 621 and never changed during the cruise. The mean with standard deviation of the STANDBY and ZERO was 5144 ± 0.7 and 0.00000 ± 0.000001, respectively. The mean with standard deviation of the ambient room temperature was 23.0 ± 0.64 °C, while that of the bath temperature was 24.000 ± 0.0008 °C throughout the cruise.

The double conductivity ratios measured by the salinometer were used to calculate practical salinity using the algorithm for Practical Salinity Scale 1978 (IOC et al., 2010). A constant temperature of 24 °C was used in the calculation instead of using the measured bath temperature.

(4) Results

Ultra-pure water (Milli-Q water, Millipore, Billerica, Massachusetts, USA) and the IAPSO SSW were measured at the beginning and the end of the measurements (2~3 stations) for each day. Time-series of the measured double conductivity ratios are shown in Fig. 3.2.1. The mean value for the IAPSO SSW agreed with the certified value (1.99966) for leg 2, However, for leg 3, the salinometer was drifted in time and the linear time drift was estimated from the least squares method and corrected to match the mean value with the certified value. The measured double conductivity ratios for the water samples were corrected by using the estimated offset due to the time drift. The standard deviation of the IAPSO SSW measurements was 0.000016, which is equivalent to 0.0003 in salinity, after the time drift correction.

The results of the ultra-pure water and the IAPSO SSW measurement (Fig 3.2.1) suggest that the

salinometer drifted in time by changing the span of the slope. However, the salinity range of the seawater sample was close to the salinity of SSW (about 35 g/kg) as described blow. Therefore, the offset time-drift correction is adequate for the seawater samples.

A total of 2,773 (58) samples were measured for the CTD/water sampling (thermo-salinograph) measurement. Minimum and maximum value of the measured salinity was 32.7 and 35.8, respectively

As for the data quality flag, two samples (stations 103 #14 and 118_2 #13) were set to flag 4 (bad measurement) due to mis trip of the Niskin bottle, and four samples (stations 81 #3, 89 #18, 93 #20 and 122 #15) were set to flag 3 (questionable measurement) judging from relatively large deviation from the CTD sensor value.

A total of 366 pairs of replicate samples was collected and the standard deviation of the replicate samples was 0.00024 in salinity.

At station 030, duplicate samples were collected from all Niskin bottles at 4750.3 ±0.7 dbar, except for bottles #12 and #25 which were not closed properly. Mean with standard deviation for the duplicate samples was 34.7170 ± 0.00030 in salinity. For the bottles #12 and #25, duplicate samples were collected from four bottles (#6, #12, #18 and #25) at 4999.7 ± 0.2 dbar of station 039. Mean with standard deviation for the second duplicate samples was 34.7165±0.00050 in salinity.

The linearity error of the salinometer was estimated by using decade resistance substituters (see Uchida et al. [2020] for more detail). For the salinometer (serial no. 62556) used in this cruise, the linearity error was estimated to be ± 0.0005 in salinity for salinity around 35 (Fig. 3.2.2).

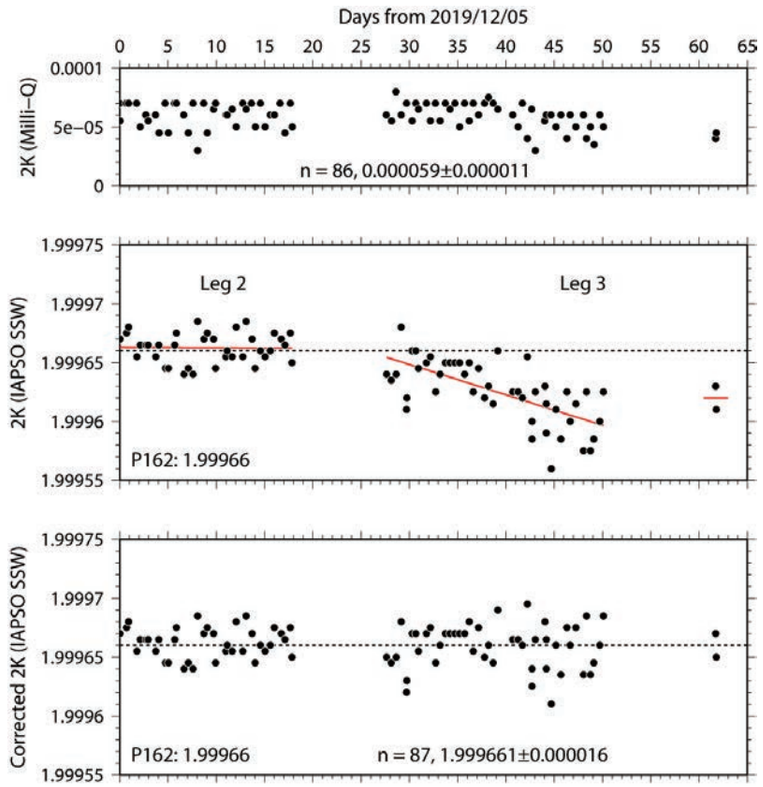

Figure 3.2.1. Time-series of the measured double conductivity ratios for the ultra-pure water (upper panel) and the IAPSO SSW (middle panel). The time-drift corrected double conductivity ratios for the IAPSO SSW were also shown (lower panel). The last two dots are the measurements only for the thermo-salinograph samples.

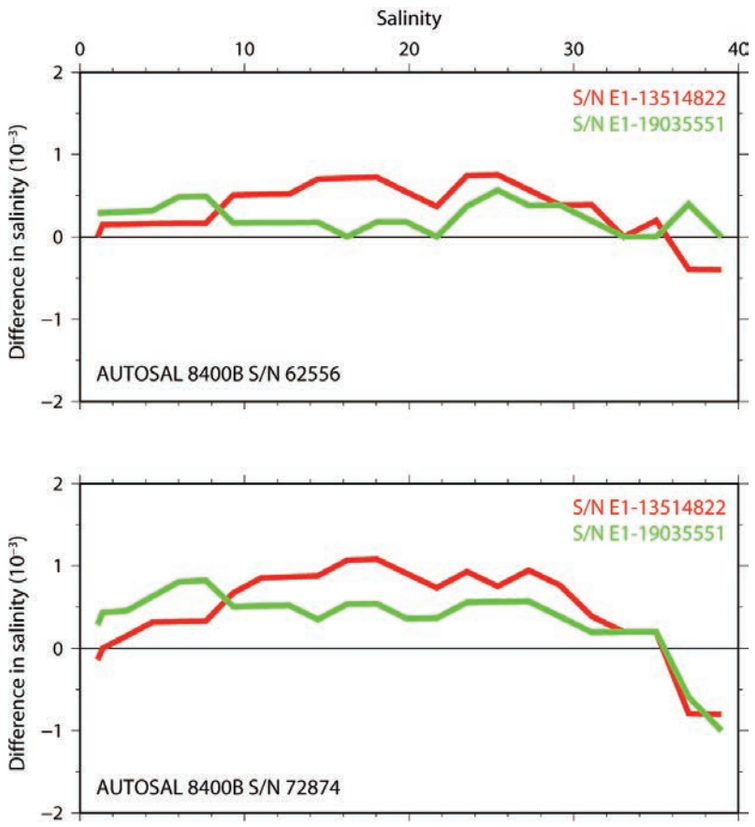

Figure 3.2.2. Linearity errors in practical salinity estimated from measurements of two decade resistance substituters for salinometers with serial numbers 62556 (upper panel) and 72874 (lower panel).

(5) References

IOC, SCOR and IAPSO (2010): The international thermodynamic equation of seawater – 2010: Calculation and use of thermodynamic properties. Intergovernmental Oceanographic Commission, Manuals and Guides No. 56, UNESCO (English), 196 pp.

Kawano, T. (2010): Salinity. The GO-SHIP Repeat Hydrography Manual: A collection of Expert Reports and Guidelines, IOCCP Report No. 14, ICPO Publication Series No. 134, Version 1.

Uchida, H., T. Kawano, T. Nakano, M. Wakita, T. Tanaka and S. Tanihara (2020): An updated batch-to-batch correction for IAPSO standard seawater. J. Atmos. Oceanic Technol., doi:10.1175/JTECH-D-19-0184.1.

3.3 Density

February 2, 2020

(1) Personnel

Hiroshi Uchida (JAMSTEC)

(2) Objective

The objective of this study is to collect absolute salinity (also called "density salinity") data and to evaluate the algorithm to estimate absolute salinity anomaly provided along with TEOS-10 (the International Thermodynamic Equation of Seawater 2010) (IOC et al., 2010).

(3) Instruments and method

Seawater density for water samples were measured with a vibrating-tube density meter (DMA 5000M [serial no. 80570578], Anton-Paar GmbH, Graz, Austria) with a sample changer (Xsample 122 [serial no. 8548492], Anton-Paar GmbH). The sample changer is used to load samples automatically from up to forty-eight 12-mL glass vials.

The water samples collected in 250 mL brown borosilicate glass bottles with screw caps (PTFE packing) for practical salinity measurement were measured by taking the water sample into two 12-mL glass vials for each bottle just before practical salinity measurement. The glass vial was sealed with Parafilm M (Pechiney Plastic Packaging, Inc., Menasha, Wisconsin, USA) immediately after filling. Densities of the samples were measured at 20 °C by the density meter two times (two vials) for each bottle and averaged to estimate the density.

The density meter was initially calibrated by measuring air and pure water according to the instrument manual. However, measured density for the IAPSO Standard Seawater deviates from density of TEOS-10 calculated from practical salinity and composition of seawater, probably due to non-linearity of the density meter (Uchida et al., 2011). The non-linearity can be corrected by measuring a reference sample simultaneously as:

$$\rho_{corr} = \rho - (\rho_{ref} - \rho_{ref\_true}) + c\ (\rho - \rho_{ref\_true}),$$

where ρ_{corr} is the corrected density of the sample, ρ is measured density of the sample, ρ_{ref} is measured density of the reference, ρ_{ref_true} is true density of the reference, and c is non-linearity correction factor.

The non-linearity factor is estimated to be 0.000411 for the density meter (serial no. 80570578). In this cruise, the non-linearity and time drift of the density meter was monitored and corrected by periodically measuring the density of the Multi-parametric Standard Seawater (MSSW) (lot PRE19) currently under development jointly by KANSO Co., Ltd., Osaka, Japan (Uchida et al., 2020) or the IAPSO Standard Seawater (batch P162) as the reference. True density at 20 °C for the PRE19 and P162 is estimated to be 1024.2186 kg/m^3 and 1024.7609 kg/m^3, respectively, from practical salinity and composition of seawater using TEOS-10. The IAPSO Standard Seawater was referred for the stations 078, 081, 083, 111, 114, 138 and 149, and the MSSW was referred for the rest of the stations.

(4) Results

Density salinity ("DNSSAL") can be back calculated from the measured density and temperature (20 °C) with TEOS-10. A total of 203 pairs of replicate samples was measured and the standard deviation of the replicate samples was 0.0014 g/kg. The measured density salinity anomalies (δS_A) are shown in Fig. 3.3.1. The measured δS_A were well agree with the δS_A estimated from Pawlowicz et al. (2011) which exploits the correlation between δS_A and nutrient concentrations and carbonate system parameters based on mathematical investigation using a model relating composition, conductivity and density of arbitrary seawaters.

(5) References

IOC, SCOR and IAPSO (2010): The international thermodynamic equation of seawater – 2010: Calculation and use of thermodynamic properties. Intergovernmental Oceanographic Commission, Manuals and Guides No. 56, UNESCO (English), 196 pp.

Pawlowicz, R., D.G. Wright and F. J. Millero (2011): The effects of biogeochemical processes on ocean

conductivity/salinity/density relationships and the characterization of real seawater. Ocean Science, 7, 363-387.

Uchida, H., T. Kawano, M. Aoyama and A. Murata (2011): Absolute salinity measurements of standard seawaters for conductivity and nutrients. La mer, 49, 237-244.

Uchida, H., T. Kawano, T. Nakano, M. Wakita, T. Tanaka and S. Tanihara (2020): An updated batch-to-batch correction for IAPSO standard seawater. J. Atmos. Oceanic Technol., doi:10.1175/JTECH-D-19-0184.1.

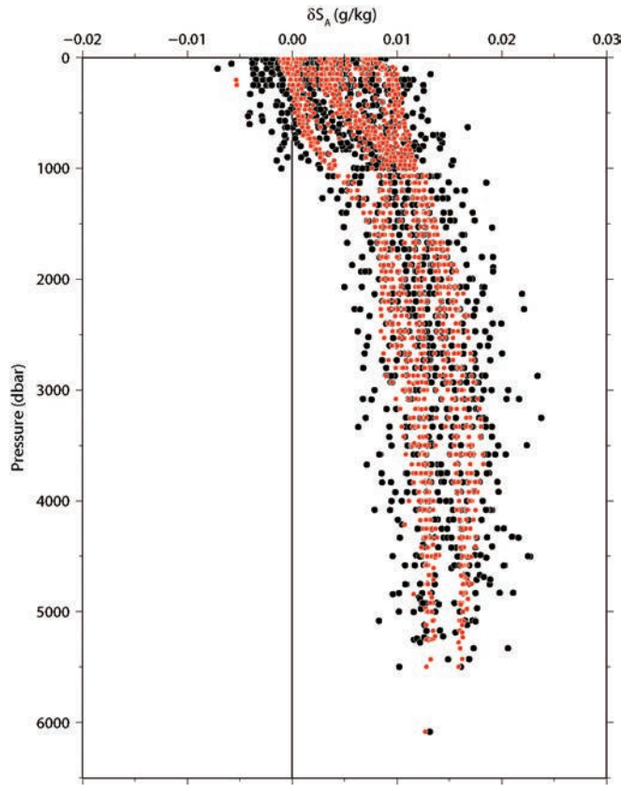

Figure 3.3.1. Vertical distribution of density salinity anomaly measured by the density meter (black dots). Absolute salinity anomaly estimated from nutrients and carbonate system parameters (Pawlowicz et al., 2011) are also shown (red dots).

3.4 Oxygen

November 23, 2020

(1) Personnel

Yuichiro Kumamoto (Japan Agency for Marine-Earth Science and Technology)

(2) Objectives

Dissolved oxygen is one of the chemical tracers for the ocean circulation. Climate models predict a decline in dissolved oxygen concentration and a consequent expansion of oxygen minimum layer due to global warming, which results mainly from decreased interior advection and ongoing oxygen consumption by remineralization. To discuss the temporal change in oxygen concentration in the water column in the Indian Ocean, we measured dissolved oxygen concentration from the surface to bottom layer at all the water sampling stations in the western Indian Ocean during MR19-04 Leg-2 and Leg-3 cruises.

(3) Reagents

Pickling Reagent I: Manganous chloride solution (3M), Lot: 1-19E

Pickling Reagent II: Sodium hydroxide (8M) / sodium iodide solution (4M), Lot: 2-19F

Sulfuric acid solution (5M), Lot: S-19C, -19D, -19F

Sodium thiosulfate (0.025M), Lot: T-19T, -19S, -19R, -19U, -19V, -19Q

Potassium iodate (0.001667M): National Metrology Institute of Japan (NMIJ), Certified Reference Material (CRM), 3006-a No.073, Mass fraction: 99.973 ± 0.018 % (expanded uncertainty)
Lot: K19E01-07 (Leg-2), K19F01-09, K19G01-03 (Leg-3)

CSK standard of potassium iodate: Lot TWJ0280, Wako Pure Chemical Industries Ltd., 0.0100N

(4) Instruments

Detector: Automatic photometric titrator, DOT-15X manufactured by Kimoto Electronic Co. Ltd., Lot: DOT-09, -10

Burette: APB-620 and APB-510 manufactured by Kyoto Electronic Co. Ltd. / 10 cm^3 of titration piston, Lot: DOT-09, MB-06/MY10-06; DOT-10, MB-01/MY10-01; KIO3, MB-11/MY10-11

Dispenser: FORTUNA Optifix 1 cm^3, Lot: Pickling Reagent I, MO-42; Pickling Reagent II, MO-27, -31, -33, -43

(5) Seawater sampling

Seawater samples were collected using 12-liter sample bottles attached to the CTD-system. The seawater was transferred to a volume-calibrated glass flask (ca. 100 cm^3) through a plastic tube. Three times of the flask volume of seawater was overflowed. Sample temperature was measured during the water sampling using a thermometer. Then the two reagent solutions (Reagent I, II) of 1.0 cm^3 each were added immediately into the sample flask and the stopper was inserted carefully into the flask. The sample flask was then shaken to mix the contents and to disperse the precipitate finely throughout. After the precipitate has settled at least halfway down the flask, the flask was shaken again to disperse the precipitate. The sample flasks containing pickled samples were stored in an air-conditioned laboratory until they were measured.

(6) Sample measurement

At least two hours after the re-shaking, the pickled samples were measured on board. A magnetic stirrer bar and 1 cm^3 of the sulfuric acid solution were added into the sample flask and stirring began. Samples were titrated by the sodium thiosulfate solution whose molarity was determined by the potassium iodate solution. The temperature of the sodium thiosulfate solution during titration was recorded by a thermometer. We measured dissolved oxygen concentration using two sets of the titration apparatus system, named DOT-09 and DOT-10. The molal concentration of dissolved oxygen (μmol kg^{-1}) was calculated by the sample temperature during the water sampling, salinity, flask volume, and concentration and titrated volume of the sodium thiosulfate solution (titrant).

(7) Standardization

The concentration of sodium thiosulfate titrant (ca. 0.025M) was determined by potassium iodate standard solution. The NMIJ-CRM potassium iodate was dried in an oven at 130°C. 1.78 g potassium iodate weighed out accurately was dissolved in deionized water and diluted to a final volume of 5 dm^3 in a calibrated volumetric flask (0.001667M). Then the aliquot (about 400 ml) of the solution was stored in a brown glass bottle (500 ml). 10 cm^3 of the standard potassium iodate solution was added to a flask using a volume-calibrated dispenser. Then 90 cm^3 of deionized water, 1 cm^3 of the sulfuric acid solution, and 1.0 cm^3 of the pickling reagent solution II and I were added into the flask in order. The amount of titrated volume of sodium thiosulfate (5 times measurements average) gave the molarity of the sodium thiosulfate titrant. Table 3.4.1 shows the results of the standardization during the cruises. The averaged coefficient of variation (C.V.) for the standardizations was 0.014 ± 0.007 % (standard deviation, n = 44).

(8) Blank determination

The oxygen in the pickling reagents I (1.0 cm^3) and II (1.0 cm^3) was assumed to be 7.6×10^{-8} mol (Murray *et al.,* 1968). The redox species apart from oxygen in the reagents (the pickling reagents I, II, and the sulfuric acid solution) also affect the titration, which is called the reagent blank. The reagent blank was determined as follows. 1 and 2 cm^3 of the standard potassium iodate solution were added to two flasks respectively. Then 100 cm^3 of deionized water, 1 cm^3 of the sulfuric acid solution, and 1.0 cm^3 of the pickling reagent II and I each were added into the two flasks in order. The reagent blank was determined by the difference between the two times of the first (1 cm^3 of KIO_3) titrated volume of the sodium thiosulfate and the second (2 cm^3 of KIO_3) one. The three results of the blank determination were averaged (Table 3.4.1). The averaged coefficient of variation (C.V.) for the reagent blank determination against the titration volume of the potassium iodate standard (about 4 ml) or 250 μmol kg^{-1} of dissolved oxygen concentration was 0.040 ± 0.030 % (standard deviation, n = 44). The redox species in the seawater sample are measured as “dissolved oxygen”, which is called the seawater blank unless they are corrected. Because we did not measure the seawater blank, the dissolved oxygen concentration reported here includes the sum of those concentrations that is less than 1 μmol kg^{-1} in the open ocean except those in suboxic and anoxic waters (Kumamoto *et al.,* 2018).

(9) Replicate sample measurement

At all the water sampling stations during Leg-2 and 3 cruises, a pair of replicate samples was collected at one or two depths. The standard deviation from the difference of pairs of replicate measurements was estimated to be 0.09 μmol kg^{-1} (n = 146), which corresponds to 0.036% of the relative standard deviation against 250 μmol kg^{-1}, using the standard operating procedure 23 of Dickson *et al.* (2007). The standard deviations of the difference between the pair of replicate measurements for the samples whose oxygen concentration is higher and lower than 150 μmol kg^{-1} are 0.08 (n = 121) and 0.15 μmol kg^{-1} (n = 25), respectively (Fig. 3.4.1). The difference between the two standard deviations is significant (F-test at 95% confidence level) and is probably due to contamination of atmospheric O_2 during the water sampling.

(10) Duplicate sample measurement

During Leg-2 the duplicate samplings were taken for all the 36 bottles at two stations (Table 3.4.2). The standard deviation of the duplicate measurements at the station 30 and 39 were calculated to be 0.09 (n = 34) and 0.13 μmol kg^{-1} (n = 4), respectively. The F-test at 95% confidence level indicates that there is no reason to believe that these standard deviations are significantly different from that of the replicate measurements (section 9). Therefore, we concluded that there is no difference in the results of the duplicate measurements, which suggests that all the bottles tripped correctly.

Table 3.4.1 Results of standardization (End Point, cm^3) and reagent blank determination (cm^3).

No	Date (UTC)	Leg	Lot	KIO_3 Lot	$Na_2S_2O_3$ Lot	DOT-9		DOT-10		Δ (%)*	Remarks
						E.P.	blank	E.P.	blank		
1	2019/Dec/02	2	1	K19E01	T-19T	3.963	-0.002	3.962	0.000	0.080	Test
2	2019/Dec/05	2	3	K19E02	T-19T	3.964	-0.001	3.963	0.003	0.136	Stn.002-014
3	2019/Dec/08	2	5	K19E03	T-19T	3.965	-0.002	3.967	0.003	0.082	Stn.017-032
4	2019/Dec/12	2	6	K19E04	T-19T	3.965	-0.002	3.966	0.004	0.12	Stn.034-046
5	2019/Dec/16	2	7	K19E05	T-19T	3.965	-0.002	3.967	0.00	0.107	$Na_2S_2O_3$ change
6	2019/Dec/16	2	8	K19E05	T-19S	3.967	-0.001	3.963	0.000	0.126	Stn.048-058
7	2019/Dec/19	2	9	K19E06	T-19S	3.966	-0.002	3.967	0.003	0.093	Stn.060-068
8	2019/Dec/22	2	10	K19E07	T-19S	3.966	-0.001	3.967	0.005	0.141	Final standardization
9	2019/Dec/31	3	1	K19F01	T-19R	3.965	-0.003	3.966	0.001	0.108	Stn.070-081
10	2020/Jan/04	3	3	K19F02	T-19R	3.970	-0.001	3.971	0.005	0.102	Stn.083-099
11	2020/Jan/08	3	4	K19F03	T-19R	3.970	0.001	3.969	0.004	0.097	$Na_2S_2O_3$ change
12	2020/Jan/08	3	6	K19F04	T-19U	3.966	0.000	3.962	0.00	0.227	Stn.101-108
13	2020/Jan/09	3	7	K19F05	T-19U	3.966	0.000	3.964	0.008	0.260	Test
14	2020/Jan/11	3	8	K19F06	T-19U	3.966	0.001	3.969	0.006	0.054	Stn.111-116
15	2020/Jan/11	3	9	K19F07	T-19U	3.967	0.001	3.969	0.006	0.099	Test
16	2020/Jan/13	3	10	K19F08	T-19U	3.966	0.000	3.968	0.005	0.074	Stn.118-124
17	2020/Jan/16	3	11	K19F09	T-19U	3.964	-0.001	3.965	0.004	0.088	$Na_2S_2O_3$ change
18	2020/Jan/16	3	12	K19F09	T-19V	3.960	-0.002	3.962	0.004	0.122	Stn.126-138
19	2020/Jan/19	3	13	K19G01	T-19V	3.966	0.000	3.967	0.005	0.107	Stn.140-147
20	2020/Jan/22	3	15	K19G02	T-19V	3.964	-0.001	3.965	0.004	0.127	Stn.148-153
21	2020/Jan/25	3	16	K19G03	T-19V	3.965	-0.001	3.962	0.001	0.103	Final standardization
22	2020/Jan/25	3	17	K19G03	T-19Q	3.963	-0.005	3.965	0.000	0.079	Test

*Difference in sodium thiosulfate concentration determined by the standardization between DOT-9 and DOT-10.

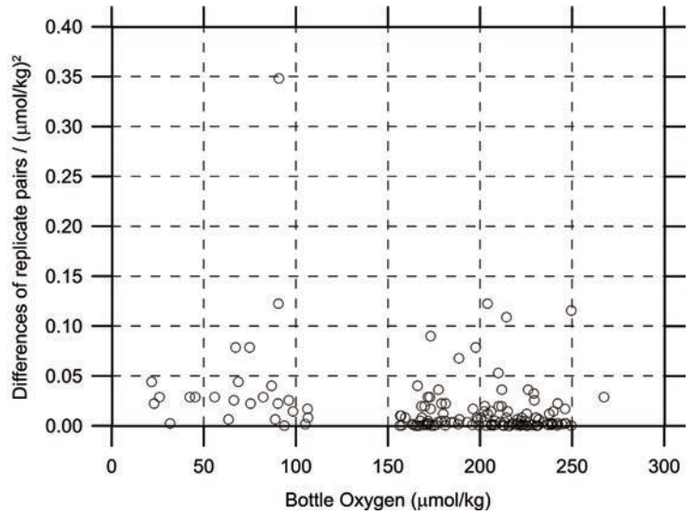

Figure 3.4.1 Oxygen difference between measurements of a replicate pair against oxygen concentration.

Table 3.4.2 Results of the duplicate sample measurements.

No.	Leg	Station	Sampling Pres. (db)	Position #	Bottle #	Dissolved oxygen (μmol/kg)
1	2	30	4750	1	X12S01	177.29
				2	X12046	177.42
				3	X12S03	177.13
				4	X12S04	177.36
				5	X12S05	177.41
				6	X12S06	177.26
				7	X12S07	177.40
				8	X12103	177.38
				9	X12S09	177.46
				10	X12S10	177.35
				11	X12S11	177.41

				12	X12S12	*
				13	X12S13	177.44
				14	X12S14	177.56
				15	X12S15	177.44
				16	X12S16	177.53
				17	X12S17	177.46
				18	X12S18	177.61
				19	X12S19	177.42
				20	X12S20	177.35
				21	X12S21	177.37
				22	X12S22	177.35
				23	X12S23	177.39
				24	X12S24	177.46
				25	X12S25	*
				26	X12S26	177.30
				27	X12S27	177.38
				28	X12S28	177.36
				29	X12S29	177.47
				30	X12S30	177.34
				31	X12S31	177.45
				32	X12S32	177.44
				33	X12S33	177.41
				34	X12S34	177.41
				35	X12S35	177.35
				36	X12S36	177.48
2	2	39	5000	6	X12S06	182.51
				12	X12S12	182.34
				18	X12S18	182.34
				25	X12S25	182.18

*Sample lost due to mis-trip (leaking).

(11) CSK standard measurements

The CSK standard is a commercial potassium iodate solution (0.0100 N) for analysis of dissolved oxygen. We titrated the CSK standard solution (Lot TWJ0280) against our KIO_3 standards as samples during the cruises (Table 3.4.3). The good agreement among them confirms that there was no systematic shift in our oxygen analyses on board.

Table 3.4.3 Results of the CSK standard (Lot TWJ0280) measurements.

Date (UTC)	KIO_3 ID No.	Conc. (N)	error (N)	Conc. (N)	error (N)	Remarks
		DOT-9		DOT-10		
2019/12/02	K19E01	0.01001	0.00001	0.01001	0.00001	Leg-2
2019/12/05	K19E02	0.01002	0.00001	0.01001	0.00001	Leg-2
2019/12/31	K19F01	0.01002	0.00001	0.01002	0.00002	Leg-3
2020/01/19	K19G01	0.01001	0.00001	0.01001	0.00000	Leg-3

(12) Quality control flag assignment

Quality flag values for oxygen data from sample bottles were assigned according to the code defined in Table 4.9 of WHP Office Report WHPO 90-1 Rev.2 section 4.5.2 (Joyce *et al.,* 1994). Measurement flags of 2 (good), 3 (questionable), 4 (bad), and 5 (missing) have been assigned (Table 3.4.4). For the choice between 2, 3, or 4, we followed a flagging procedure as listed below:

a. Bottle oxygen concentration at the sampling layer was plotted against sampling pressure. Any points not lying on a generally smooth trend were noted.

b. Difference between bottle oxygen and oxygen sensor was then plotted against sampling pressure. If a datum deviated from a group of plots, it was flagged 3.

c. Vertical sections against pressure and potential density were drawn. If a datum was anomalous on the section plots, the datum flag was degraded from 2 to 3, or from 3 to 4.

d. If there was a problem in the measurement, the datum was flagged 4.

e. If the bottle flag was 4 (did not trip correctly), a datum was flagged 4 (bad). In the case of the bottle flag 3 (leaking) or 5 (unknown problem), a datum was flagged based on steps a, b, c, and d.

(13) Uncertainty

We assume that the uncertainty of dissolved oxygen determination is derived from those of concentration/titration of potassium iodate standard solution, reagent blank determination, titration of a seawater sample, and volume of sample flask (Table 3.4.5). We found temporal variation in the standardization due to unknown causes in the titrators (section 14), whose uncertainty was also added. These uncertainties yielded 0.09% of the combined uncertainty and 0.18% of the expanded combined uncertainty. Note that this combined uncertainty does not include that derived from the temporal change in room temperature. However, that was negligible because its variation was small (17.0-21.5°C). The uncertainty due to the seawater blank (section 8) is unknown because we did not measure it. If it is assumed that the seawater blank concentration is 0.50 ± 0.50 μmol kg^{-1} and the distribution of the possible values is uniform or rectangular, its standard uncertainty is calculated to be 0.29 μmol kg^{-1} (= $0.50/\sqrt{3}$). This value corresponds to the standard uncertainty of 0.12% relative to 250 μmol kg^{-1} of dissolved oxygen concentration. The combined standard uncertainty, which includes the uncertainty of the seawater blank concentration, is calculated to be 0.15% (the extended combined uncertainty is 0.30%). These combined uncertainties, however, are applicable only for the dissolved oxygen concentration corrected by the seawater blank concentration (0.50 μmol kg^{-1}).

(14) Problem

a. The concentrations of the sodium thiosulfate solution determined using DOT-10 were higher than those determined using DOT-09 by 0.115 ± 0.047% (standard deviation, n = 22, Table 3.4.1) in average. The difference was canceled in the calculation of dissolved oxygen concentration. However, we found that it changed temporally by unknown causes, which probably affected the determination of dissolved oxygen concentration. Therefore, we added the uncertainty derived from this to the combined uncertainty of our oxygen measurement (section 13).

b. We found white turbidity in the pickling reagent II solution (Lot 2-19F). Although we replaced the dispenser (MO-43, -31, -27) two times during the cruises, the turbidity did not disappear from the reagent solution, which implies that the solution of this lot (2-19F) may have defects.

c. In some measurements, the titration did not finish automatically because the final absorbance of light through the sample flask was higher than 0.15. We believe the problem is that we cannot adjust this value of the threshold limit.

d. The titration was disturbed by air bubbles in the light path in a sample measurement, which implies that the rotation speed of the stirrer (8 rpm) is faster than the optimum one.

e. During the cruises, six samples were re-measured because of problems in the titration curve, including the problems c and d. We add 1 ml of the KIO_3 standard solution into the sample flask and the total volume of sodium thiosulfate solution titrated was recorded. Eventually, the result of the first titration was accepted in each sample measurement.

f. A sample flask was turned over by accident just before the measurement (titration), about six hours after the water sampling. There was, however, no problem in the concentration calculated from this titration.

Table 3.4.4 Summary of assigned quality control flags.

Flag	Definition	Number*
2	Good	2352
3	Questionable	18
4	Bad	2
5	Not report (missing)	0
	Total	2372

*The replicate samples (n = 146) and duplicate samples (n = 38) were not included.

Table 3.4.5 Uncertainties of estimated items for oxygen determination.

	Estimated items	Relative uncertainty to 250 μmol kg^{-1} (%)	References
1	Sodium thiosulfate concentration	0.052	2, 3, 4
2	Potassium iodate concentration	0.030	Kumamoto *et al.* (2018)
3	Titration of potassium iodate	0.014	Section 7
4	Reagent blank determination	0.040	Section 8
5	Titration of seawater sample	0.036	Section 9
6	Volume of sample flask	0.015	Kumamoto *et al.* (2018)
7	Stability of titrators	0.047	Section 14
	Combined uncertainty (k=1)	0.091	1, 4, 5, 6, 7
	Expanded combined uncertainty (k=2)	0.182	

(15) Data archives

The data obtained in the cruises will be submitted to the Data Management Group of JAMSTEC and will be opened to the public via "Data Research System for Whole Cruise Information in JAMSTEC (DARWIN)" in the JAMSTEC web site.

References

Dickson, A. G., C.L. Sabine, and J.R. Christian (Eds.) (2007) Guide to best practices for ocean CO2 measurements, PICES Special Publication 3, 191 pp.

Joyce, T., and C. Corry, eds., C. Corry, A. Dessier, A. Dickson, T. Joyce, M. Kenny, R. Key, D. Legler, R. Millard, R. Onken, P. Saunders, M. Stalcup (1994) Requirements for WOCE Hydrographic Programme Data Reporting, WHPO Pub. 90-1 Rev. 2, May 1994 Woods Hole, Mass., USA.

Kumamoto, Y., D. Sasano, H. Sato, and K. Matsumoto (2018) Dissolved oxygen, Guideline of Ocean Observations, vol. 3, chap. 1, G301EN:001-033.

Murray, C.N., J.P. Riley, and T.R.S. Wilson (1968) The solubility of oxygen in Winkler reagents used for determination of dissolved oxygen, Deep-Sea Res., 15, 237-238.

3.5 Nutrients

(1) Personnel

Michio AOYAMA (JAMSTEC/Tsukuba Univ.): Principal Investigator

Yuichiro KUMAMOTO (JAMSTEC)

Keitaro MATSUMOTO (MWJ): Operation Leader (leg 2)

Tomomi SONE (MWJ) (leg 2)

Tomoyuki TANAKA (MWJ) (leg 2)

Shinichiro YOKOGAWA (MWJ): Operation Leader (leg 3)

Tomomi SONE (MWJ) (leg 3)

Ko Morita (MWJ) (leg 3)

(2) Objectives

The objective of nutrients analyses during the R/V Mirai MR19-04 cruise in the Indian Ocean and Southern Ocean, of which EXPOCODE are 49NZ20191205 and 49NZ20191230, is as follows: Describe the present status of nutrients concentration with excellent comparability using certified reference material of nutrient in seawater.

(3) Parameters

The determinants are nitrate, nitrite, silicate, phosphate and ammonia in the Indian Ocean and Southern Ocean.

(4) Instruments and methods

(4.1) Analytical detail using QuAAtro 2-HR systems (BL TEC K.K.)

Nitrate + nitrite and nitrite are analyzed following a modification of the method of Grasshoff (1976). The sample nitrate is reduced to nitrite in a cadmium tube the inside of which is coated with metallic copper. The sample stream after reduction is treated with an acidic, sulfanilamide reagent to produce a diazonium ion. N-1-naphthylethylenediamine dihydrochloride is added to the sample stream to produce a red azo dye. With the reduction of the nitrate to nitrite, both nitrate and nitrite react and are measured. Thus, for the nitrite analysis, no reduction is performed and the alkaline buffer is not necessary. Nitrate is computed by the difference between nitrate+nitrite concentration and nitrite concentration.

The silicate method is analogous to that described for phosphate. The method used is essentially that of Grasshoff et al. (1999). Silicomolybdic acid is first formed from the silicate in the sample and molybdic acid. The silicomolybdic acid is reduced to silicomolybdous acid, or "molybdenum blue," using ascorbic acid.

The phosphate analysis is a modification of the procedure of Murphy and Riley (1962). Molybdic acid is added to the seawater sample to form phosphomolybdic acid which is in turn reduced to phosphomolybdous acid using L-ascorbic acid as the reductant.

The ammonia in seawater is mixed with an alkaline containing EDTA, ammonia as gas state is formed from seawater. The ammonia (gas) is absorbed in sulfuric acid by way of 0.5 μm pore size membrane filter (ADVANTEC PTFE) at the dialyzer attached to the analytical system. The ammonia absorbed in sulfuric acid is determined by coupling with phenol and hypochlorite to form indophenols blue.

The details of a modification of analytical methods for four parameters, nitrate, nitrite, silicate and phosphate, used in this cruise are also compatible with the methods described in nutrients section in the new GO-SHIP repeat hydrography nutrients manual (Becker et al., 2019) which is a revised version of the GO-SHIP repeat hydrography nutrients manual (Hydes et al., 2019), while an analytical method of ammonium is compatible with the determination of ammonia in seawater using a vaporization membrane permeability method (Kimura, 2000). The flow diagrams and reagents for each parameter are shown in Figures 3.5.1 to 3.5.5.

(4.2) Nitrate + Nitrite Reagents

50 % Triton solution: 50 mL Triton™ X-100 provided by Sigma-Ardrich Japan G. K. (CAS No. 9002-93-1) were mixed with 50 mL ethanol (99.5 %).

Imidazole (buffer), 0.06 M (0.4 % w/v): Dissolve 4 g imidazole (CAS No. 288-32-4), in 1000 mL ultra-pure water, add 2 mL hydrogen chloride (CAS No. 7647-01-0). After mixing, 1 mL 50 % triton solution is added.

Sulfanilamide, 0.06 M (1 % w/v) in 1.2 M HCl: Dissolve 10 g 4-aminobenzenesulfonamide (CAS No. 63-74-1), in 900 mL of ultra-pure water, add 100 mL hydrogen chloride (CAS No. 7647-01-0). After mixing, 2 mL 50 % triton solution is added.

NED, 0.004 M (0.1 % w/v): Dissolve 1 g N-(1-naphthalenyl)-1,2-ethanediamine, dihydrochloride (CAS No. 1465-25-4), in 1000 mL of ultra-pure water and add 10 mL hydrogen chloride (CAS No. 7647-01-0). After mixing, 1 mL 50 % Triton solution is added. This reagent was stored in a dark bottle.

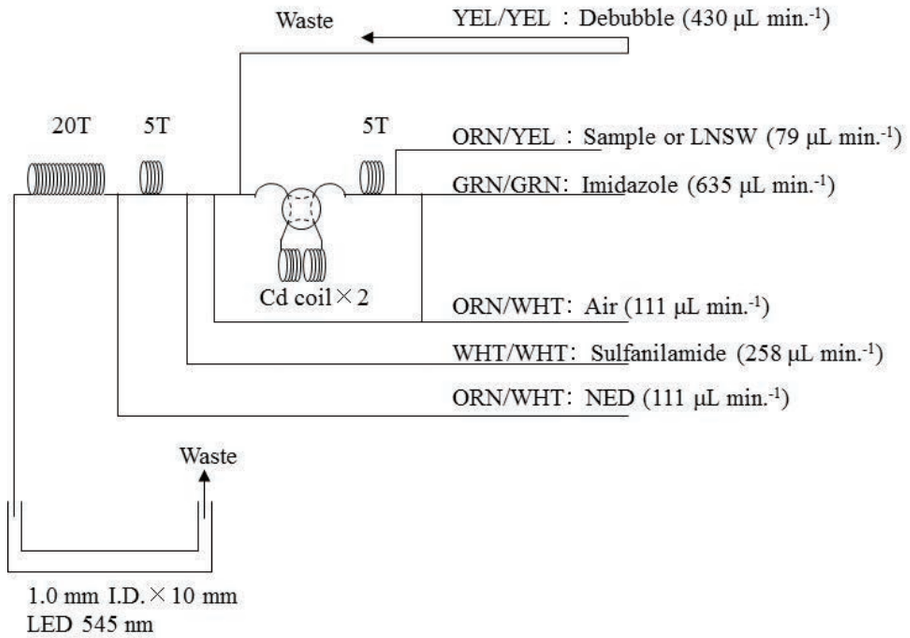

Figure 3.5.1 NO_3+NO_2 (1ch.) flow diagram.

(4.3) Nitrite Reagents

50 % Triton solution: 50 mL Triton™ X-100 provided by Sigma-Ardrich Japan G. K. (CAS No. 9002-93-1) .were mixed with 50 mL ethanol (99.5 %).

Sulfanilamide, 0.06 M (1 % w/v) in 1.2 M HCl: Dissolve 10 g 4-aminobenzenesulfonamide (CAS No. 63-74-1), in 900 mL of ultra-pure water, add 100 mL hydrogen chloride (CAS No. 7647-01-0). After mixing, 2 mL 50 % triton solution is added.

NED, 0.004 M (0.1 % w/v): Dissolve 1 g N-(1-naphthalenyl)-1,2-ethanediamine, dihydrochloride (CAS No. 1465-25-4), in 1000 mL of ultra-pure water and add 10 mL hydrogen chloride (CAS No. 7647-01-0). After mixing, 1 mL 50 % triton solution is added. This reagent was stored in a dark bottle.

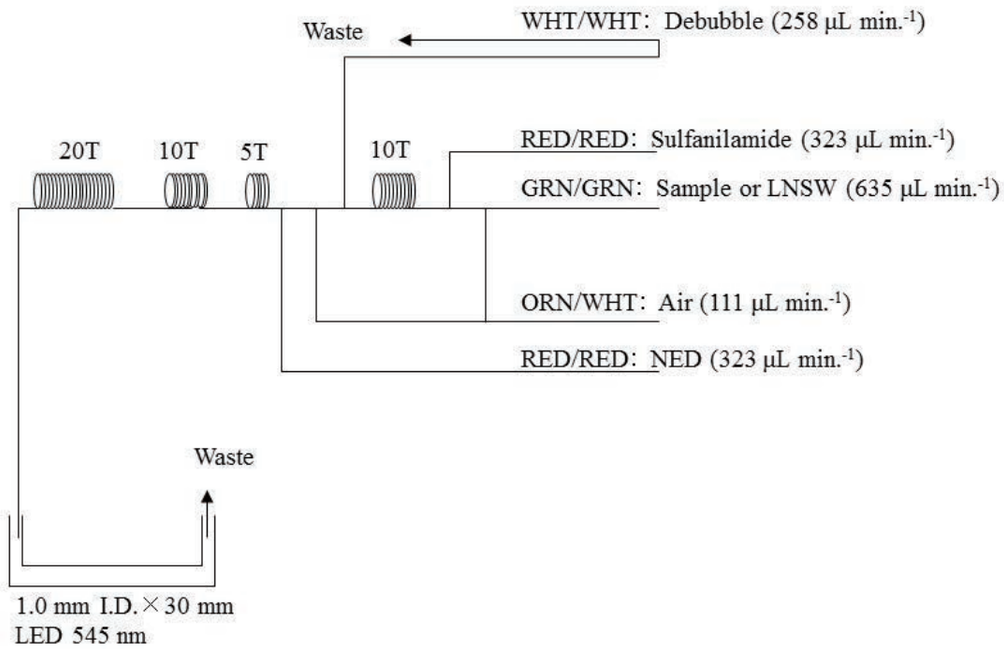

Figure 3.5.2 NO_2 (2ch.) flow diagram.

(4.4) Silicate Reagents

15 % Sodium dodecyl sulfate solution: 75 g sodium dodecyl sulfate (CAS No. 151-21-3) was mixed with 425 mL ultra-pure water.

Molybdic acid, 0.03 M (1 % w/v): Dissolve 7.5 g sodium molybdate dihydrate (CAS No. 10102-40-6), in 980 mL ultra-pure water, add 12 mL 4.5M sulfuric acid. After mixing, 20 mL 15 % sodium dodecyl sulfate solution is added. Note that the amount of sulfuric acid is reduced from previous reports because we readjusted to Grasshoff et al. (1999).

Oxalic acid, 0.6 M (5 % w/v): Dissolve 50 g oxalic acid (CAS No. 144-62-7), in 950 mL of ultra-pure water.

Ascorbic acid, 0.01 M (3 % w/v): Dissolve 2.5 g L-ascorbic acid (CAS No. 50-81-7), in 100 mL of ultra-pure water. This reagent was freshly prepared every day.

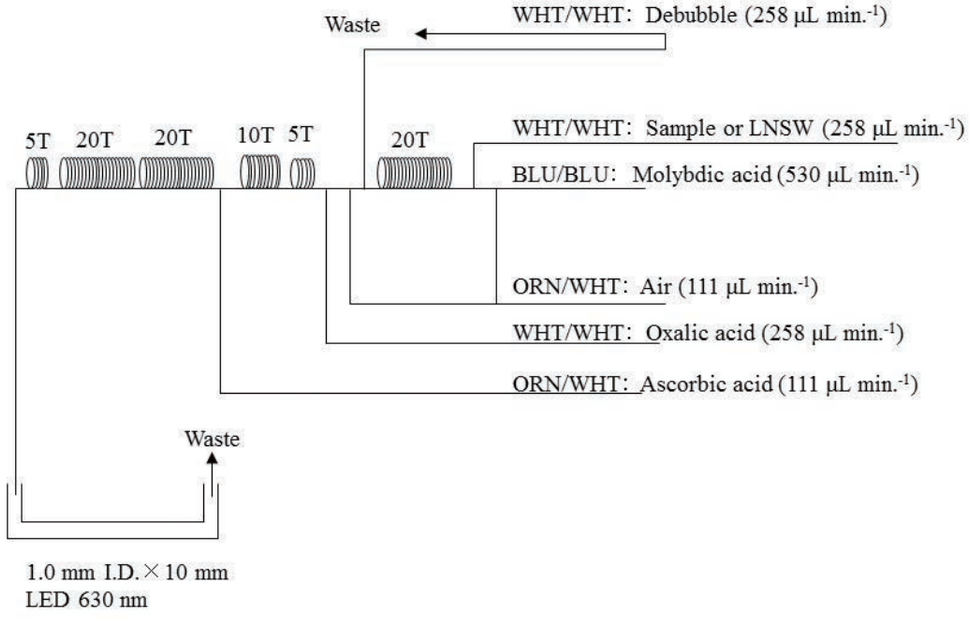

Figure 3.5.3 SiO_2 (3ch.) flow diagram.

(4.5) Phosphate Reagents

15 % Sodium dodecyl sulfate solution: 75 g sodium dodecyl sulfate (CAS No. 151-21-3) were mixed with 425 mL ultra-pure water.

Stock molybdate solution, 0.03 M (0.8 % w/v): Dissolve 8 g sodium molybdate dihydrate (CAS No. 10102-40-6), and 0.17 g antimony potassium tartrate trihydrate (CAS No. 28300-74-5), in 950 mL of ultra-pure water and added 50 mL sulfuric acid (CAS No. 7664-93-9).

PO_4 color reagent: Dissolve 1.2 g L-ascorbic acid (CAS No. 50-81-7), in 150 mL of stock molybdate solution. After mixing, 3 mL 15 % sodium dodecyl sulfate solution is added. This reagent was freshly prepared before every measurement.

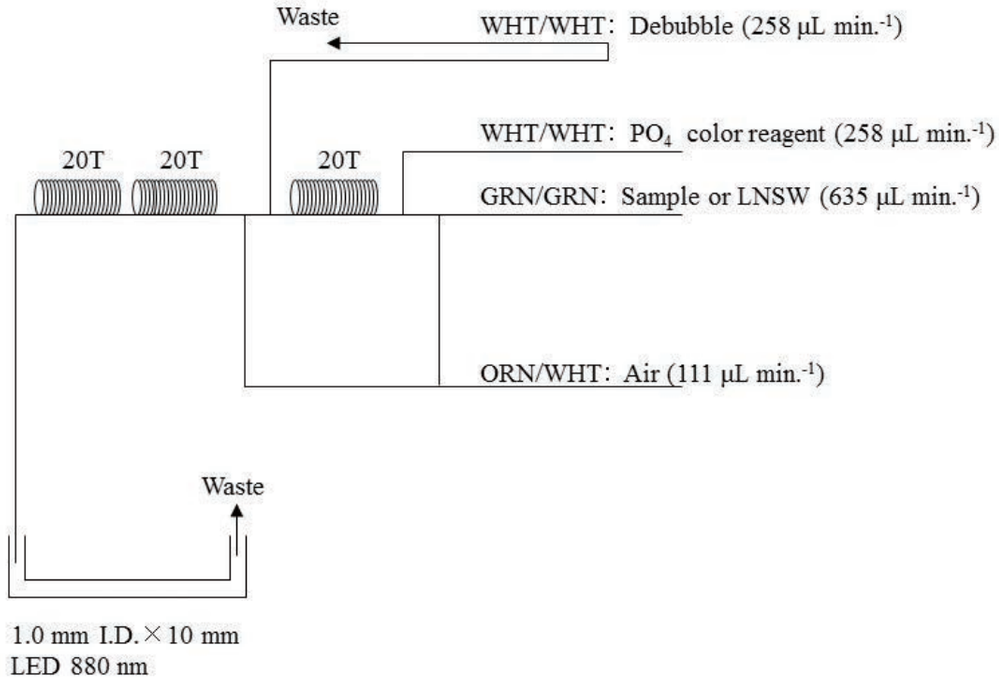

Figure 3.5.4 PO_4 (4ch.) flow diagram.

(4.6) Ammonia Reagents

30 % Triton solution: 30 mL Triton™ X-100 provided by Sigma-Ardrich Japan G. K. (CAS No. 9002-93-1) .were mixed with 70 mL ultra-pure water.

EDTA: Dissolve 41 g tetrasodium;2-[2-[bis(carboxylatomethyl)amino]ethyl-(carboxylatemethyl)amino] acetate;tetrahydrate (CAS No. 13235-36-4), and 2 g boric acid (CAS No. 10043-35-3), in 200 mL of ultra-pure water. After mixing, a 1 mL 30 % triton solution is added. This reagent is prepared a week approximately.

NaOH liquid: Dissolve 1.5 g sodium hydroxide (CAS No. 1310-73-2), and 16 g tetrasodium;2-[2-[bis(carboxylatomethyl)amino]ethyl-(carboxylatomethyl)amino]acetate;tetrahydrate (CAS No. 13235-36-4) in 100 mL of ultra-pure water. This reagent is prepared a week about. Note that we reduced the amount of sodium hydroxide from 5 g to 1.5 g because pH of C standard solutions lowered 1 due to the change of recipe of B standards solution.

Stock nitroprusside: Dissolve 0.25 g sodium nitroferricyanide dihydrate (CAS No. 13755-38-9) in 100 mL of ultra-pure water and add 0.2 mL 1M sulfuric acid. Stored in a dark bottle and prepared a month approximately.

Nitroprusside solution: Mix 4 mL stock nitroprusside and 5 mL 1M sulfuric acid in 500 mL of ultra-pure water. After mixing, 2 mL 30 % triton solution is added. This reagent is stored in a dark bottle and prepared every 2 or 3 days.

Alkaline phenol: Dissolve 10 g phenol (CAS No. 108-95-2), 5 g sodium hydroxide (CAS No. 1310-73-2) and 2 g sodium citrate dihydrate (CAS No. 6132-04-3), in 200 mL ultra-pure water. Stored in a dark bottle and prepared a week approximately.

NaClO solution: Mix 3 mL sodium hypochlorite (CAS No. 7681-52-9) in 47 mL ultra-pure water. Stored in a dark bottle and fleshly prepared before every measurement. This reagent is prepared 0.3 % available chlorine.

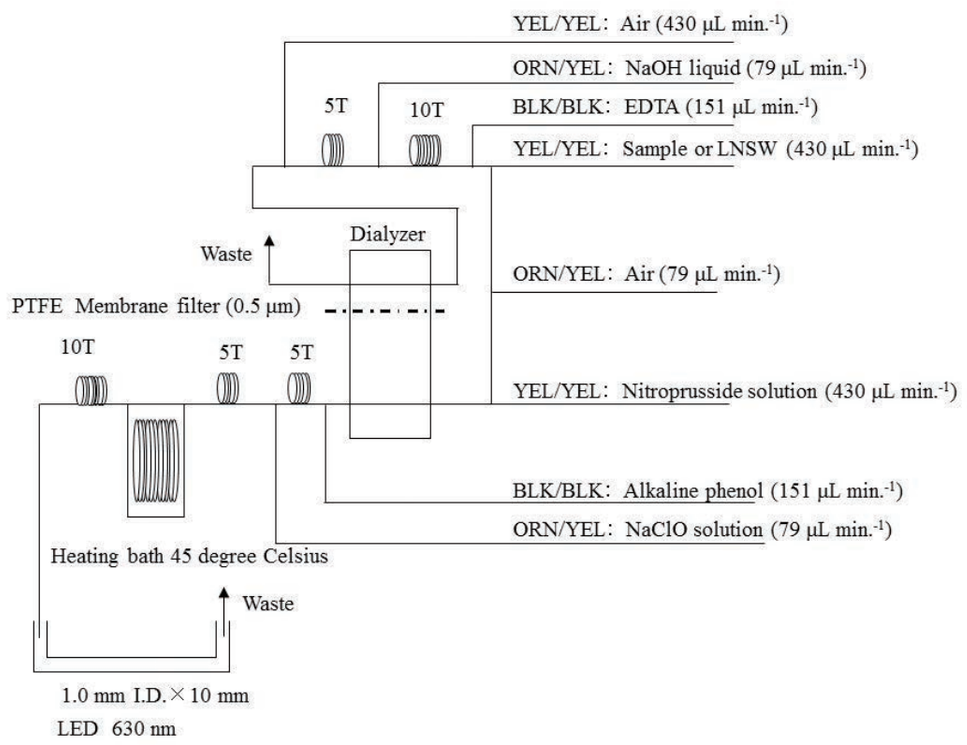

Figure 3.5.5 NH_4 (5ch.) flow diagram.

(4.7) Sampling procedures

Sampling of nutrients followed that oxygen, salinity and trace gases. Samples were drawn into a new 10 mL polyacrylates vials without sample drawing tubes. These were rinsed three times before filling and the vials were capped immediately after the drawing without headspace. The vials are put into water bath adjusted to ambient temperature, 19.9 ± 0.9 degree Celsius, in about 30 minutes before use to stabilize the temperature of samples. When we found the value of Xmiss of the sample was less than 95 % or doubtful for the particles in the sample, we carried out centrifuging (Table 3.5.12) for the samples by using a centrifuge (type: CN-820, Hsiang Tai). The conditions of centrifuging were set about 3400 rpm for 2.5 minute. We also put coolant in the

centrifuge to suppress temperature increase of samples during centrifugation.

No transfer from the vial to another container was made and the vials were set an autosampler tray directly. Samples were analyzed after collection within 24 hours.

(4.8) Data processing

Raw data from QuAAtro 2-HR were treated as follows:

- Check the baseline shift.
- Check the shape of each peak and positions of peak values taken, and then change the positions of peak values taken if necessary.
- Carry-over correction and baseline drift correction were applied to peak heights of each sample followed by sensitivity correction.
- Baseline correction and sensitivity correction were done basically using linear regression.
- Load pressure and salinity from uncalibrated CTD data to calculate density of seawater tentatively. To calculate the final nutrient concentration, we used salinity data from calibrated CTD conductivity sensor data.
- Calibration curves to get nutrients concentration were assumed second order equations.

(4.9) Summary of nutrients analysis

We made 33 QuAAtro runs for the samples collected by 37 casts at 37 stations in Leg 2 and 43 runs for the samples collected by 44 casts at 44 stations in Leg 3 as shown in Table 3.5.1 during MR19-04. The total amount of layers of the seawater sample reached to 2096 in Leg 2 and 2746 in Leg 3. We made basically duplicate measurements at all the sampling layers. The station locations for nutrients measurement are shown in Figure 3.5.6.

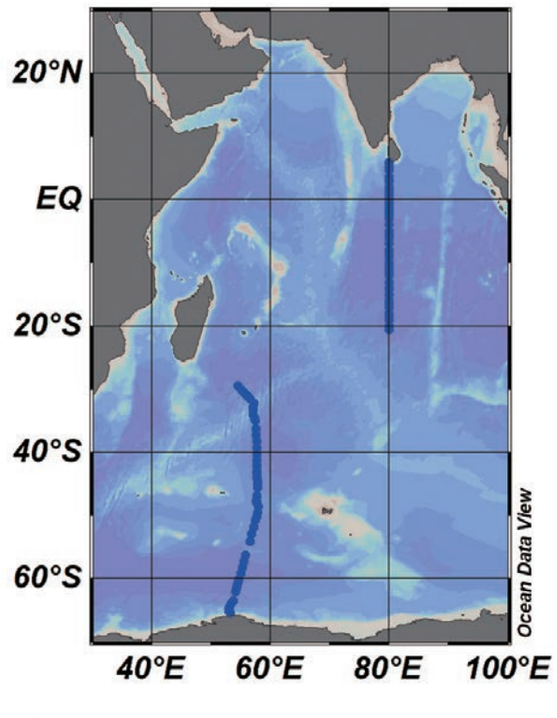

Figure 3.5.6 Sampling positions of nutrients sample.

(5) Station list

The sampling station list for nutrients is shown in Table 3.5.1.

Table 3.5.1 List of stations

Station	Cast	Date (UTC)	Position*		Depth (m)
		(mmddyy)	Latitude	Longitude	
002	1	120519	5-52.31N	79-59.22E	824
003	1	120519	5-47.51N	79-59.64E	1390
005	1	120619	5-39.95N	80-00.40E	3233
006	1	120619	5-34.97N	80-00.13E	4015
007	1	120619	5-19.97N	79-59.75E	4147
009	1	120619	4-39.95N	79-59.91E	4276
012	1	120719	3-40.31N	80-00.04E	4358
014	1	120719	3-00.04N	80-00.04E	4340
017	1	120819	2-00.07N	80-00.05E	3875
019	1	120819	1-20.05N	80-00.01E	4569
022	1	120919	0-30.16N	80-00.12E	4651
025	1	121019	0-15.07S	80-00.33E	4683
026	1	121019	0-30.04S	80-00.24E	4712
027	1	121019	0-44.93S	80-00.02E	4735
029	1	121119	1-20.05S	80-00.05E	4834
032	1	121119	2-19.99S	79-59.99E	4909
034	1	121219	2-59.96S	79-59.87E	4967
036	1	121219	4-00.12S	79-59.84E	4630
038	1	121319	4-59.96S	79-59.89E	5140
040	1	121419	5-59.99S	79-59.98E	5202
042	1	121419	7-00.02S	79-59.94E	4917
044	1	121519	8-00.13S	80-00.16E	5416
045	1	121519	8-50.00S	80-00.00E	5190
046	1	121619	9-00.02S	79-59.95E	5207
048	1	121619	10-00.01S	79-59.98E	5383
050	1	121719	11-00.00S	79-59.83E	5347
052	1	121719	12-00.01S	80-00.01E	5159
054	1	121819	13-05.81S	80-00.04E	5003
056	1	121819	13-59.90S	80-00.15E	5024
058	1	121919	14-59.93S	80-00.12E	5111
060	1	121919	15-59.94S	80-00.10E	5046
061	1	122019	16-29.83S	79-59.96E	5038
062	1	122019	16-59.91S	80-00.06E	5072
064	1	122019	17-59.93S	80-00.05E	5100
066	1	122119	18-59.82S	79-59.99E	4946
068	1	122119	20-00.01S	80-00.01E	4866
069	1	122219	20-29.77S	79-59.99E	4859
070	1	123119	29-29.64S	54-2984E	4904
072	1	010120	30-09.31S	55-11.21E	4704
074	1	010120	30-49.31S	55-52.43E	4432
076	1	010220	31-29.07S	56-33.55E	4787
078	1	010220	32-08.99S	57-15.01E	2918
080	1	010320	32-51.01S	57-07.00E	5341
081	1	010320	33-12.01S	57-02.42E	6010
083	1	010320	33-58.01S	57-02.10E	5030
085	2	010420	34-39.33S	57-17.38E	3808
086	1	010520	35-00.02S	57-25.07E	4820
089	1	010520	36-20.02S	57-32.53E	4421
091	1	010620	37-13.31S	57-37.53E	5331
093	1	010620	38-15.36S	57-39.32E	5347
095	1	010720	39-14.74S	57-41.49E	5151
097	1	010720	40-14.98S	57-44.98E	4997

099	1	010820	41-09.64S	57-44.65E	4889
101	1	010820	42-04.75S	57-45.14E	4797
103	1	010920	42-59.79S	57-45.46E	4744
105	1	010920	43-59.87S	57-45.52E	4639
107	1	010920	45-00.07S	57-47.24E	4538
108	1	011020	45-30.04S	57-47.96E	4458
111	1	011120	46-48.27S	57-40.99E	4444
113	1	011120	47-40.79S	57-35.35E	4539
114	1	011220	47-55.12S	57-41.06E	4332
116	1	011220	48-33.64S	57-55.90E	4481
118	2	011420	49-33.58S	57-49.82E	4439
120	1	011420	50-40.49S	57-29.87E	4515
122	1	011520	51-47.57S	57-10.43E	4428
124	1	011520	52-54.29S	56-50.00E	4281
126	1	011620	54-01.24S	56-29.93E	3496
132	1	011720	56-15.08S	55-50.16E	4746
134	1	011720	57-12.99S	55-33.05E	5092
136	1	011820	58-11.14S	55-15.82E	5192
138	1	011820	59-09.08S	54-58.44E	5145
140	1	011920	60-07.23S	54-41.19E	5147
142	1	011920	61-05.10S	54-23.86E	5126
144	1	012020	62-03.31S	54-06.25E	5058
147	1	012020	63-30.11S	53-40.64E	4758
148	1	012120	63-58.03S	53-25.09E	4347
149	1	012120	64-26.12S	53-04.69E	4149
150	1	012120	64-46.99S	52-59.27E	3437
151	1	012120	65-06.19S	53-00.99E	2504
152	1	012220	65-13.45S	53-07.85E	1880
153	1	012220	65-20.20S	53-15.16E	1205

* Position indicates latitude and longitude where CTD reached maximum depth at the cast.

(6) Certified Reference Material of nutrients in seawater

KANSO certified reference materials (CRMs, Lot: CE, CJ, CG, CB, BZ, CF) were used to ensure the comparability and traceability of nutrient measurements during this cruise. The details of CRMs are shown below.

Production

KANSO CRMs for inorganic nutrients in seawater were produced by KANSO Co.,Ltd. This CRM has been produced using autoclaved natural seawater based on the quality control system under ISO Guide 34 (JIS Q 0034).

KANSO Co.,Ltd. has been accredited under the Accreditation System of National Institute of Technology and Evaluation (ASNITE) as a CRM producer since 2011. (Accreditation No.: ASNITE 0052 R)

Property value assignment

The certified values are arithmetic means of the results of 30 bottles from each batch (measured in duplicates) analysed by KANSO Co.,Ltd. and Japan Agency for Marine-Earth Science and Technology (JAMSTEC) using the colorimetric method (continuous flow analysis, CFA, method). The salinity of solutions of calibration standards to get a calibration curve was adjusted to close the salinity of this CRM within ± 0.5.

Metrological Traceability

Each certified value of nitrate, nitrite, and phosphate of KANSO CRMs were calibrated versus one of Japan Calibration Service System (JCSS) standard solutions for each nitrate ions, nitrite ions, and phosphate ions. JCSS standard solutions are calibrated versus the secondary solution of JCSS for each of these ions. The secondary solution of JCSS is calibrated versus the specified primary solution produced by Chemicals Evaluation and Research Institute (CERI), Japan. CERI specified primary solutions are calibrated versus the National Metrology Institute of Japan (NMIJ) primary standards solution of nitrate ions, nitrite ions and phosphate ions, respectively.

For a certified value of silicate of KANSO CRM was determined by one of Merck KGaA silicon standard solution 1000 mg L^{-1} Si traceable to National Institute of Standards and Technology (NIST) SRM of silicon standard solution (SRM 3150).

The certified values of nitrate, nitrite, and phosphate of KASNO CRM are thus traceable to the International System of Units (SI) through the unbroken chain of calibrations, JCSS, CERI and NMIJ solutions as stated above, each having stated uncertainties. The certified values of silicate of KANSO CRM are traceable to the SI through the unbroken chain of calibrations, Merck KGaA and NIST SRM 3150 solutions, each having stated uncertainties.

As stated in the certificate of NMIJ CRMs, each certified value of dissolved silica, nitrate ions, and nitrite ions was determined by more than one method using one of NIST SRM of silicon standard solution and NMIJ primary standards solution of nitrate ions and nitrite ions. The concentration of phosphate ions as stated information value in the certificate was determined NMIJ primary standards solution of phosphate ions. Those values in the certificate of NMIJ CRMs are traceable to the SI.

One of the analytical methods used for certification of NMIJ CRM for nitrate ions, nitrite ions, phosphate ions and dissolved silica was a colorimetric method (continuous mode and batch one). The colorimetric method is the same as the analytical method (continuous mode only) used for certification of KANSO CRM. For certification of dissolved silica, exclusion chromatography/isotope dilution-inductively coupled plasma mass spectrometry and ion exclusion chromatography with post-column detection was used. For certification of nitrate ions, ion chromatography by direct analysis and ion chromatography after halogen-ion separation was used. For certification of nitrite ions, ion chromatography by direct analysis was used.

NMIJ CRMs were analyzed at the time of certification process for CRM and the results were confirmed within expanded uncertainty stated in the certificate of NMIJ CRMs.

(6.1) CRM for this cruise

60 sets of CRM lots CE, CJ, CG, CB, BZ and CF which almost cover a range of nutrients concentrations in the Indian Ocean and Southern Ocean are prepared.

These CRM assignments were done based on a random number. The CRM bottles were stored at a room in the ship, BIOCHEMICAL LABORATORY, where the temperature was maintained around 18.0 degree Celsius – 21.8 degree Celsius.

(6.2) CRM concentration

Nutrients concentrations for the CRM lots CE, CJ, CG, CB, BZ and CF are shown in Table 3.5.2.

Table 3.5.2 Certified concentration and uncertainty (k=2) of CRMs.

unit: µmol kg^{-1}

Lot	Nitrate	Nitrite	Silicate	Phosphate	Ammonia*
CE	0.01 ± 0.03	0.03 ± 0.01	0.06 ± 0.09	0.012 ± 0.006	0.69
CJ	16.20 ± 0.20	0.04 ± 0.01	38.50 ± 0.40	1.190 ± 0.020	0.77
CG	23.70 ± 0.20	0.07 ± 0.03	56.40 ± 0.50	1.700 ± 0.020	0.61
CB	35.79 ± 0.27	0.13 ± 0.01	109.20 ± 0.62	2.520 ± 0.022	0.77
BZ	43.35 ± 0.33	0.23 ± 0.01	161.00 ± 0.93	3.056 ± 0.033	0.49
CF	43.40 ± 0.40	0.09 ± 0.02	159.70 ± 1.00	3.060 ± 0.030	0.46

*For ammonia values are not certified and shown as only reference values.

(7) Nutrients standards

(7.1) Volumetric laboratory-ware of in-house standards

All volumetric glassware and polymethylpentene (PMP)-ware used were gravimetrically calibrated. Plastic volumetric flasks were gravimetrically calibrated at the temperature of use within 4 K at around 22 deg. C.

(7.1.1) Volumetric flasks

Volumetric flasks of Class quality (Class A) are used because their nominal tolerances are 0.05 % or

less over the size ranges likely to be used in this work. Class A flasks are made of borosilicate glass, and the standard solutions were transferred to plastic bottles as quickly as possible after they are made up to volume and well mixed in order to prevent the excessive dissolution of silicate from the glass. PMP volumetric flasks was gravimetrically calibrated and used only within 4 K of the calibration temperature.

The computation of volume contained by glass flasks at various temperatures other than the calibration temperatures were done by using the coefficient of linear expansion of borosilicate crown glass.

Because of their larger temperature coefficients of cubical expansion and lack of tables constructed for these materials, the plastic volumetric flasks were gravimetrically calibrated over the temperature range of intended use and used at the temperature of calibration within 4 K. The weights obtained in the calibration weightings were corrected for the density of water and air buoyancy.

(7.1.2) Pipettes

All glass pipettes have nominal calibration tolerances of 0.1 % or better. These were gravimetrically calibrated to verify and improve upon this nominal tolerance.

(7.2) Reagents, general considerations

(7.2.1) Specifications

For nitrate standard, “potassium nitrate 99.995 suprapur®” provided by Merck, Batch B1452165, CAS No. 7757-79-1, was used.

For nitrite standard solution, we used “nitrite ion standard solution (NO_2^- 1000) provided by Wako, Lot APJ6212, Code. No. 140-06451.”. This standard solution was certified by Wako using ion chromatography method. Calibration result is 1003 mg L^{-1} at 20 degree Celsius. Expanded uncertainty of calibration (k=2) is 0.8 % for the calibration result.

For the silicate standard, we changed from “Silicon standard solution SiO_2 in NaOH 0.5 M CertiPUR®” provided by Merck, to in-house Si standard solution exp64 which was produced by alkali fusion technique from 5N SiO_2 powder produced jointly by JAMSTEC and KANSO. The mass fraction of Si in the exp64 solution was calibrated based on NMIJ CRM 3645-a02 Si standard solution.

For phosphate standard, “potassium dihydrogen phosphate anhydrous 99.995 suprapur®” provided by Merck, Batch B1642608, CAS No.: 7778-77-0, was used.

For ammonia standard, “Ammonium Chloride (CRM 3011-a)” provided by NMIJ, CAS No. 12125-02-9. The purity of this standard was greater than 99.9 %. Expanded uncertainty of calibration (k=2) is 0.022 %.

(7.2.2) Ultra-pure water

Ultra-pure water (Milli-Q water) freshly drawn was used for preparation of reagent, standard solutions and for measurement of reagent and system blanks.

(7.2.3) Low nutrients seawater (LNSW)

Surface water having low nutrient concentration was taken and filtered using 0.20 μm pore capsule cartridge filter at MR18-04 cruise in August 2018. This water is stored in 20 L cubitainer with cardboard box.

Nutrients concentrations in LNSW were measured in February 2019.

(7.2.4) Concentrations of nutrients for A, D, B and C standards

The “A” standards for nitrate, nitrite, phosphate and ammonia are made separately as relatively high concentration stock standards. In this cruise we use lot exp.61 of certified silicon standard solution as A-3 standard, The "B" standard is next prepared by mixing five aliquots of single nitrate, nitrite, silicate, phosphate and ammonia A standard(s) and making the solution up to an accurately known volume. Finally, an aliquot of the B standard is made up to working, calibration-standard concentrations, or "C-5" standard for nitrate, nitrite, phosphate, silicate and ammonia, and C-7 and C-8 for ammonia typical, oceanic concentrations using LNSW. The D standards are prepared to measure the reduction rate from nitrate to nitrite.

Concentrations of nutrients for A, B, C and D standards are set as shown in Table 3.5.3.

We developed a new receipt to prepare the B standard without the addition of HCl to neutralize alkali Merck silicon standard solution. Pure water was used to prepare the B standard and to adjust salinity and

density, we add NaCl powder as appropriately.

The C standard is prepared according to recipes as shown in Table 3.5.4. All volumetric laboratory tools were calibrated prior to the cruise as stated in chapter (6.1). Then the actual concentration of nutrients in each fresh standard was calculated based on the ambient temperature, solution temperature and determined factors of volumetric laboratory-wares.

The calibration curves for each run were obtained using 6 levels, C-1, C-2, C-3, C-4, C-5 and C-6. C-1, C-2, C-3, C-4 and C-6 were the CRM of nutrients in seawater and C-5 was in-house standard.

Table 3.5.3 Nominal concentrations of nutrients for A, D, B and C standards.

Unit: μmol kg^{-1}

	A	B	D	C-1	C-2	C-3	C-4	C-5	C-6	C-7	C-8
NO_3	45000	900	900	CE	CJ	CG	CB	45.6	BZ	-	-
NO_2	21800	17	870	CE	CJ	CG	CB	0.86	BZ	-	-
SiO_2	35600	2850		CE	CJ	CG	CB	143	BZ	-	-
PO_4	6000	60		CE	CJ	CG	CB	3.0	BZ	-	-
NH_4	4000	120		-	-	-	-	6.0	-	2.4	0

Table 3.5.4 Working calibration standard recipes.

C Std.	B Std.
C-5	25 mL
C-7	10mL

(7.2.5) Renewal of in-house standard solutions

In-house standard solutions as stated in paragraph (7.2.4) were renewed as shown in Table 3.5.5(a) to (c).

Table 3.5.5(a) Timing of renewal of in-house standards.

NO_3, NO_2, SiO_2, PO_4, NH_4	Renewal
A-1 Std. (NO_3)	maximum a month
A-2 Std. (NO_2)	commercial prepared solution
A-3 Std. (SiO_2)	JAMSTEC-KANSO Si standard solution
A-4 Std. (PO_4)	maximum a month
A-5 Std. (NH_4)	maximum a month
D-1 Std.	maximum 8 days
D-2 Std.	maximum 8 days
B Std. (mixture of A-1, D-2, A-3, A-4 and A-5 std.)	maximum 8 days

Table 3.5.5(b) Timing of renewal of working calibration standards.

Working standards	Renewal
C Std. (dilute B Std.)	every 24 hours

Table 3.5.5(c) Timing of renewal of in-house standards for reduction estimation.

Reduction estimation	Renewal
36 μM NO_3 (dilute D-1 Std.)	when C Std. renewed
35 μM NO_2 (dilute D-2 Std.)	when C Std. renewed

(8) Quality control

(8.1) The precision of nutrients analyses during the cruise

The precision of nutrients analyses during this cruise was evaluated based on the 6 to 10 measurements, which are measured every 8 to 13 samples, during a run at the concentration of C-5 std. Summary of precisions is shown in Table 3.5.6 and Figures 3.5.7 to 3.5.11. During this cruise, analytical precisions were 0.16 % for nitrate, 0.22 % for nitrite, 0.12 % for silicate, 0.16 % for phosphate and 0.31 % for ammonia in terms of a median of precision, respectively.

The precisions for each parameter during this cruise are generally consistent with the analytical precisions during the R/V Mirai cruises conducted in 2009 - 2018. We also can say that time series of precision as shown in Figures 3.5.7 to 3.5.11 showed that the analytical precisions for nitrate, nitrite, silicate, phosphate and ammonia were maintained throughout this cruise except for a few runs.

Table 3.5.6 Summary of precision based on the replicate analyses.(k=1)

	Nitrate	Nitrite	Silicate	Phosphate	Ammonia
	CV %	CV %	CV %	CV %	CV %
Median	0.16	0.22	0.12	0.16	0.31
Mean	0.15	0.24	0.12	0.16	0.34
Maximum	0.32	0.60	0.24	0.69	0.69
Minimum	0.03	0.11	0.05	0.06	0.15
N	76	76	76	76	76

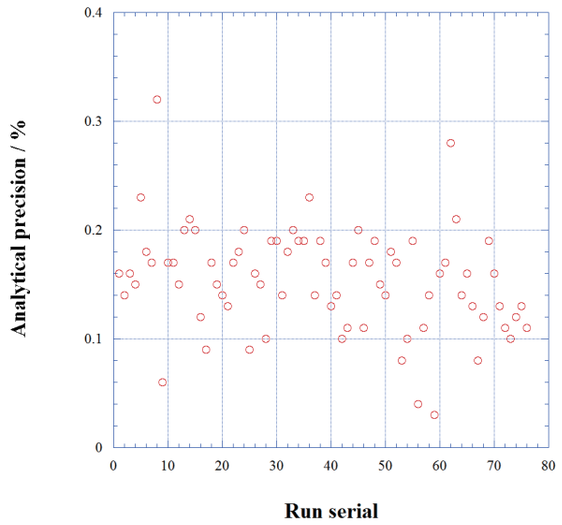

Figure 3.5.7 Time series of precision of nitrate in MR19-04.

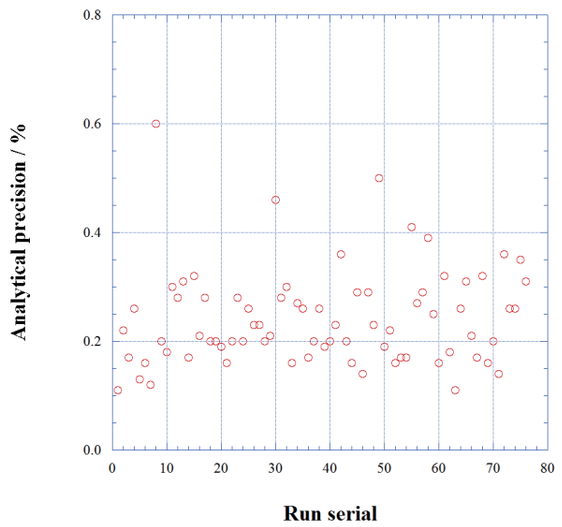

Figure 3.5.8 Same as Figure 3.5.7 but for nitrite.

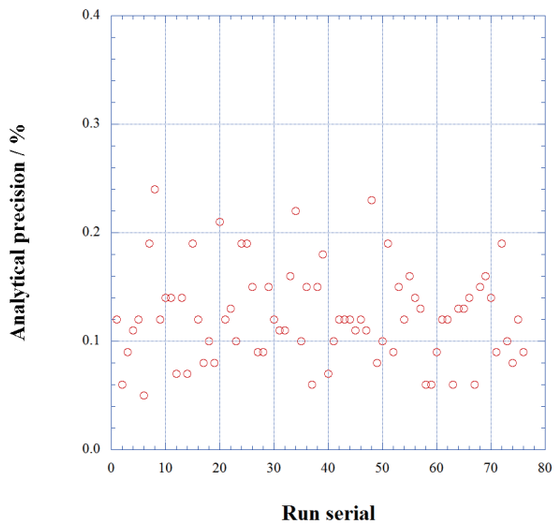

Figure 3.5.9 Same as Figure 3.5.7 but for silicate.

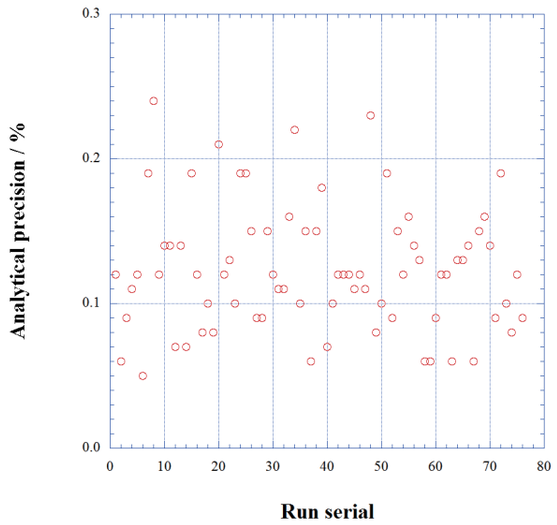

Figure 3.5.10 Same as Figure 3.5.7 but for phosphate.

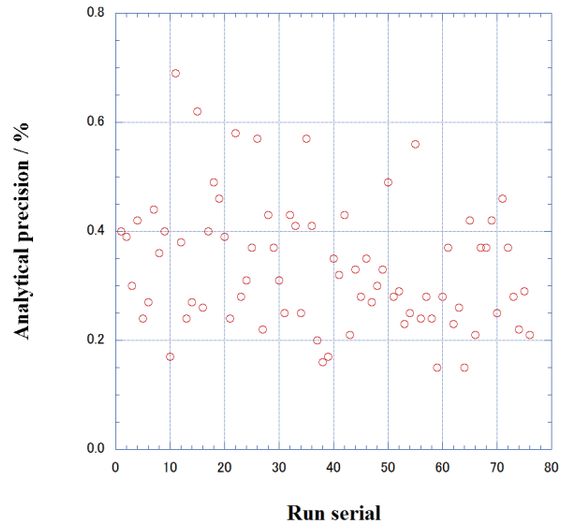

Figure 3.5.11 Same as Figure 3.5.7 but for ammonia.

(8.2) CRM lot. CF measurement during this cruise

CRM lot. CF was measured every run to evaluate the comparability tthroughout the cruise. The results of lot. CF during this cruise are shown as Figures 3.5.12 to 3.5.16. All of the measured concentrations of CRM lot. CF was within the uncertainty of certified values for nitrate, nitrite, silicate and phosphate.

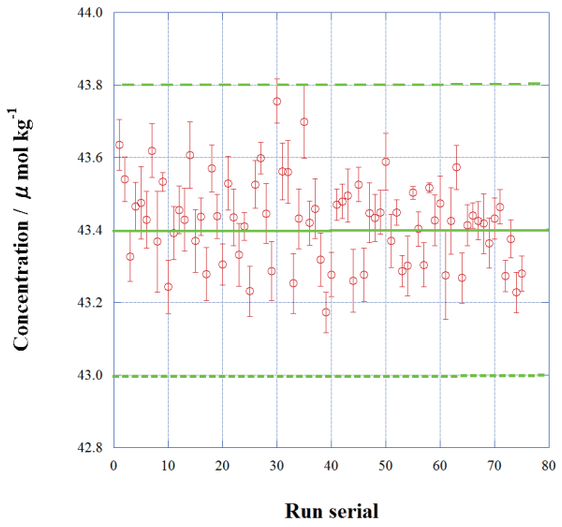

Figure 3.5.12 Time series of CRM-CF of nitrate in MR19-04. Solid green line is certified nitrate concentration of CRM and dotted green line show uncertainty of certified value at k=2.

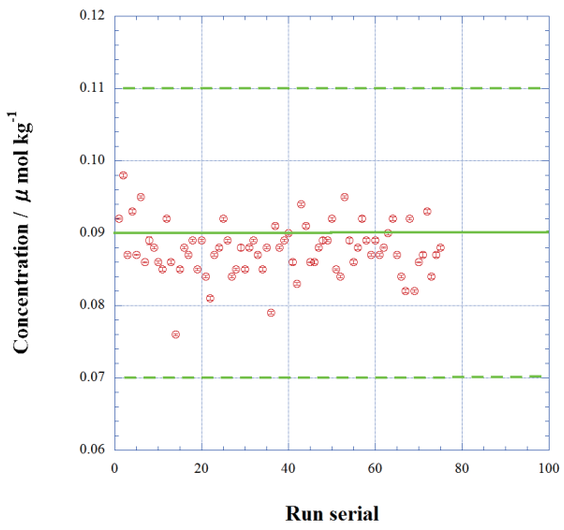

Figure 3.5.13 Same as Figure 3.5.12, but for nitrite.

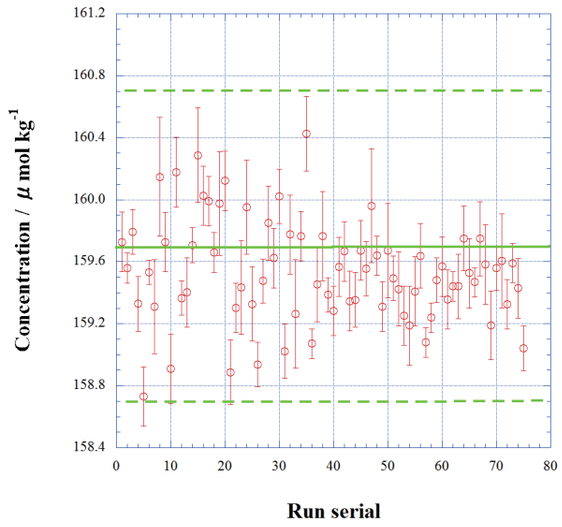

Figure 3.5.14 Same as Figure 3.5.12, but for silicate.

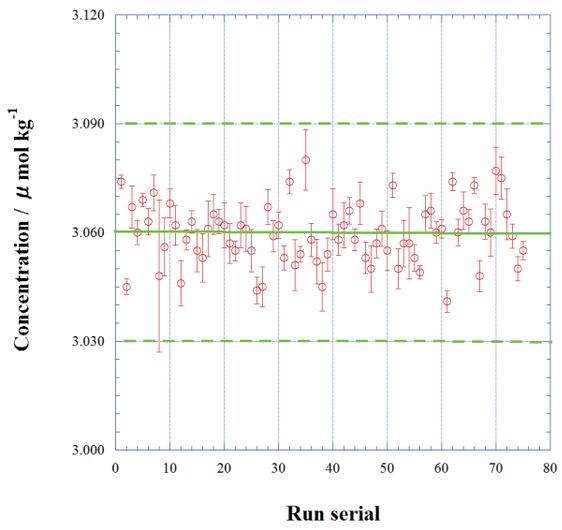

Figure 3.5.15 Same as Figure 3.5.12, but for phosphate.

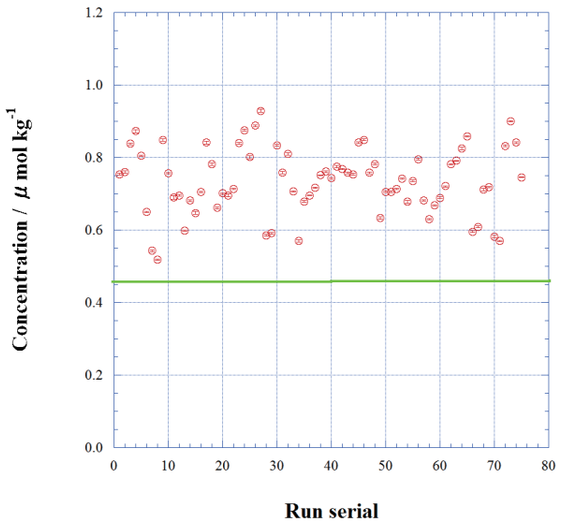

Figure 3.5.16 Time series of CRM-CF of ammonia in MR19-04. Green line is reference value for ammonia concentration of CRM-CF.

(8.3) Carryover

The carryover results from the finite and more or less incomplete flushing of the flow system between samples. Thus, an error is present in any given absorbance reading. The carryover signal can be approximated as linearly dependent upon the difference between the absorbance of a given sample and that of the preceding sample for a linear system. The carryover coefficient, k, is obtained for each channel by measuring the difference between the absorbances of the second and first full-scale standards following a near-zero standard or sample, all having the same, natural seawater matrix composition. It can equally well be calculated from the difference between the first two near-zero standards following a full-scale standard or sample. Measurement of the carryover is done in triplicate at the beginning of a cruise in order to obtain a statistically significant number. It must be checked carefully every time any change in the plumbing of a channel is done, including a simple pump tube or coil replacement. Carryover corrections for well-designed and maintained channels are usually less than 0.3%.

We summarize the magnitudes of carryover throughout the cruise. Although we observed that carryover increased in leg 3 probably due to overhaul of the analyzer, these are still small enough within acceptable levels of 0.3 % except ammonia as shown in Table 3.5.7 and Figure 3.5.17 to 3.5.21.

Table 3.5.7 Summary of carryover throughout MR19-04.

	Nitrate	Nitrite	Silicate	Phosphate	Ammonia
	%	%	%	%	%
Median	0.19	0.08	0.21	0.13	0.69
Mean	0.17	0.11	0.21	0.12	0.81
Maximum	0.31	0.53	0.31	0.30	2.30
Minimum	0.01	0.00	0.08	0.00	0.14
N	76	76	76	76	76

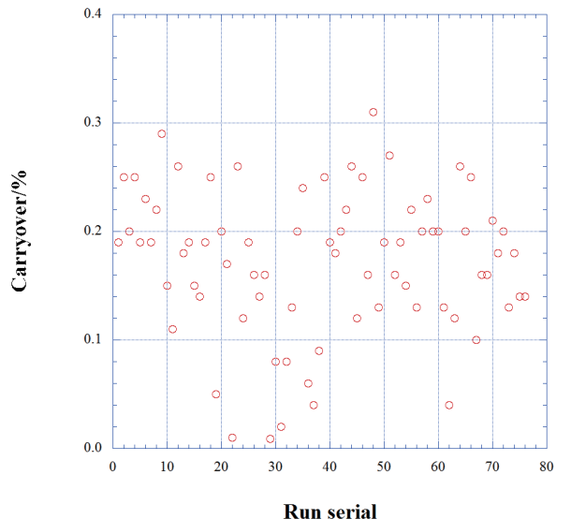

Figure 3.5.17 Time series of carry over of nitrate in MR19-04.

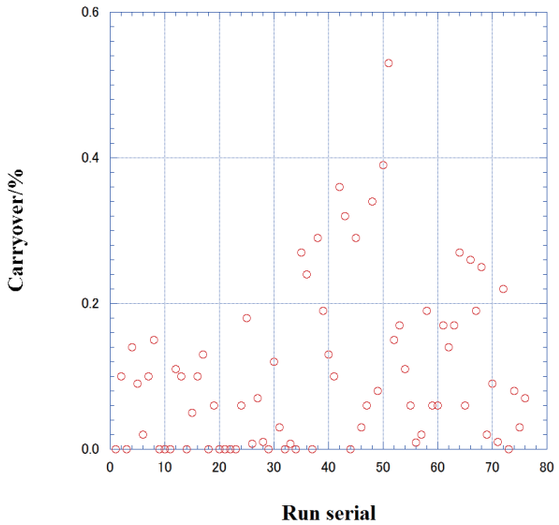

Figure 3.5.18 Same as Figure 3.5.17 but for nitrite.

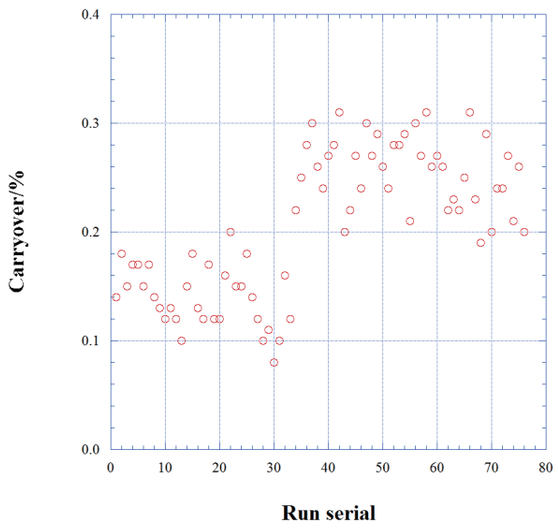

Figure 3.5.19 Same as Figure 3.5.17 but for silicate.

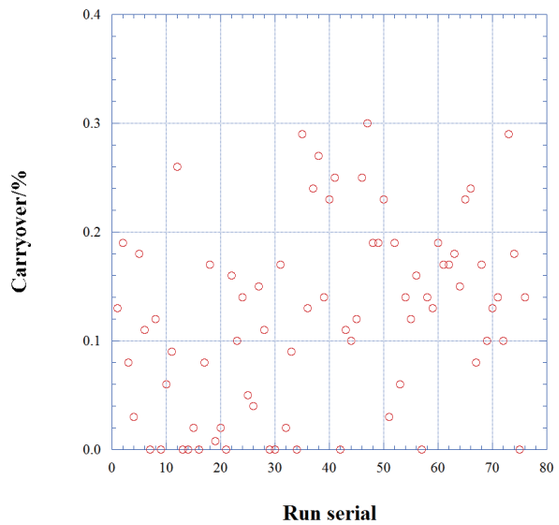

Figure 3.5.20 Same as Figure 3.5.17 but for phosphate.

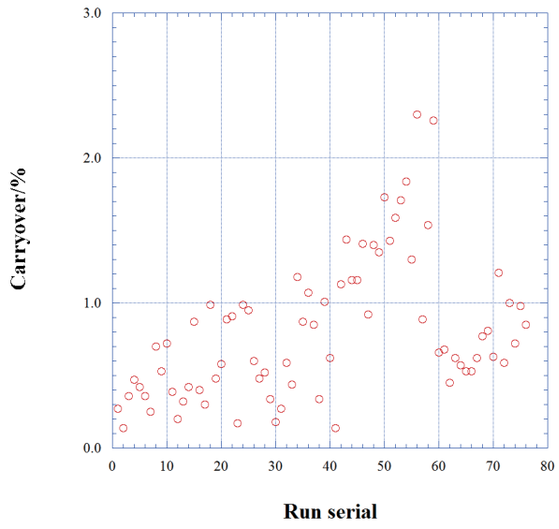

Figure 3.5.21 Same as Figure 3.5.17 but for ammonia.

(8.4) Estimation of uncertainty of nitrate, silicate, phosphate, nitrite and ammonia concentrations

Empirical equations, eq. (1), (2) and (3) to estimate the uncertainty of measurement of nitrate, silicate and phosphate are used based on 76 measurements of 52 sets of CRMs (Table 3.5.2) to obtain calibration curve during this cruise. These empirical equations are as follows, respectively.

Nitrate Concentration C_{NO3} in µmol kg^{-1}:

Uncertainty of measurement of nitrate (%) =

$$0.10303 + 7.0029 * (1 / C_{NO3}) - 0.1113 * (1 / C_{NO3}) * (1 / C_{NO3}) \quad - (1)$$

where C_{NO3} is nitrate concentration of sample.

Silicate Concentration C_{SiO2} in µmol kg^{-1}:

Uncertainty of measurement of silicate (%) =

$$0.14938 + 6.7786 * (1 / C_{SiO2}) - 0.12377 * (1 / C_{SiO2}) * (1 / C_{SiO2}) \quad - (2)$$

where C_{SiO2} is silicate concentration of sample.

Phosphate Concentration C_{PO4} in µmol kg^{-1}:

Uncertainty of measurement of phosphate (%) =

$$0.17278 + 0.28937 * (1 / C_{PO4}) \quad - (3)$$

where C_{PO4} is phosphate concentration of sample.

Empirical equations, eq. (4) and (5) to estimate the uncertainty of measurement of nitrite and ammonia are used based on duplicate measurements of the samples.

Nitrite Concentration C_{NO2} in µmol kg^{-1}:

Uncertainty of measurement of nitrite (%) =

$$- 0.027319 + 0.32334 * (1 / C_{NO2}) - 0.00019896 * (1 / C_{NO2}) * (1 / C_{NO2}) \quad - (4)$$

where C_{NO2} is nitrite concentration of sample.

Ammonia Concentration C_{NH4} in µmol kg^{-1}:

Uncertainty of measurement of ammonia (%) =

$$11.768 + 0.79428 * (1 / C_{NH4}) \quad - (5)$$

where C_{NH4} is ammonia concentration of sample.

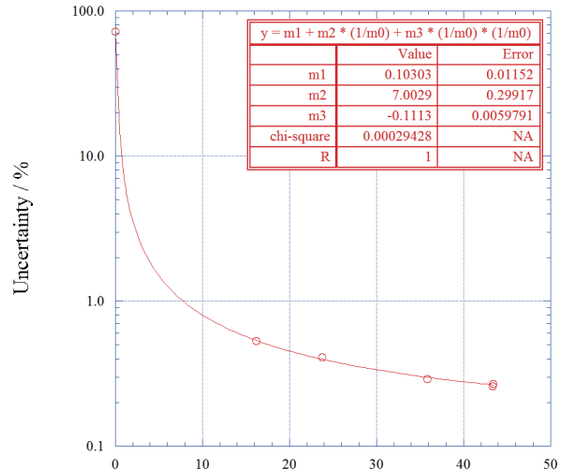

Figure 3.5.22 Estimation of uncertainty for nitrate.

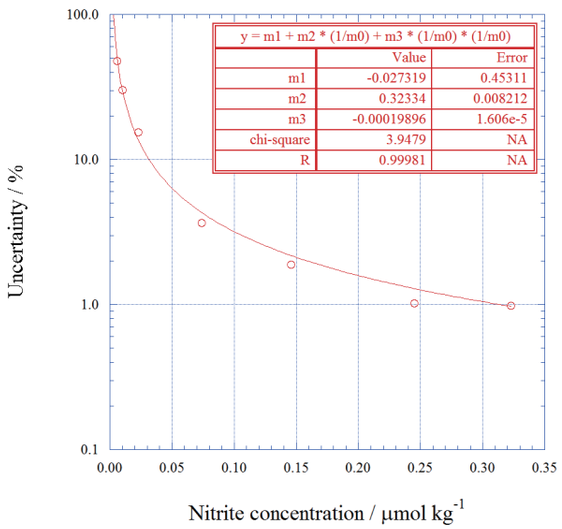

Figure 3.5.23 Estimation of uncertainty for nitrite.

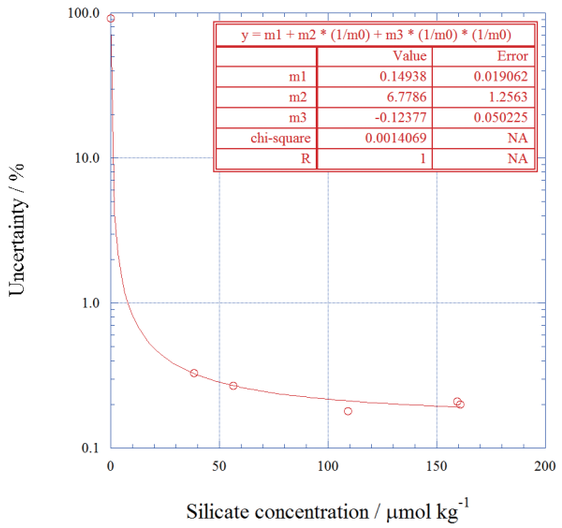

Figure 3.5.24 Estimation of uncertainty for silicate.

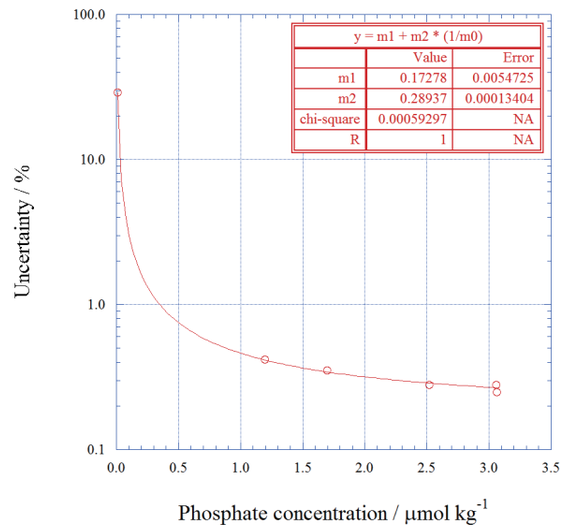

Figure 3.5.25 Estimation of uncertainty for phosphate.

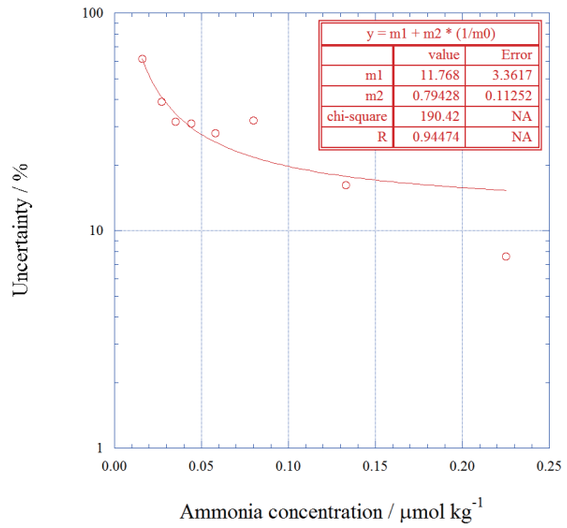

Figure 3.5.26 Estimation of uncertainty for ammonia.

(9) Problems and our actions/solutions

In this section we describe what we observed and what we did to react to solve these problems.

During this cruise, we see a few problems especially in nitrate measurements as shown below.

1, Serious nitrate contamination from the environment to the seawater samples

2. Malfunction of one of the analyzers of nutrients named #1 and nitrate concentration measured by unit #1 showed larger variability which exceeds normal analytical precision about 0.2 %.

3. We needed to replace the cadmium reduction column for nitrate measurements rather than usual operation.

We faced serious nitrate contamination from the environment to the seawater samples. We observed a larger difference of nitrate concentrations of two duplicate samples collected from the same sampling bottle for several bottles of 36 bottles throughout the cruise in general. The difference of nitrate contamination of the two samples was up to 1.6 μmol kg^{-1} during the leg 2 (stations 2-69), 2.2 μmol kg^{-1} during the first half of the leg 3 (stations 70-101), and 1.4 μmol kg^{-1} during the second half of the leg 3 (stations 103-153). As shown in Figure 3.5.27, the nitrate vs. phosphate concentration ratio became high in some samples collected at stations between 30 and 50 approximately compared with the range of natural values between 13.6 and 14.7 approximately during leg 2. We also see high ratio anomalies in some samples at stations 90-100 and 110-130 approximately during leg 3.

The magnitude of the difference between duplicate samples increased in the first half of the leg 3 and frequency we see a larger difference of nitrate concentrations between duplicate samples had also increased (Figure 3.5.27). The nitrate vs. phosphate concentration ratio in the “large-difference” sample increased and showed a linear relationship (the broken line from 14.5 of Nitrate vs. phosphate ratio at nitrate concentration difference is zero to around 15.4 of nitrate vs. phosphate ratio at nitrate concentration difference is 1.5 μmol kg^{-1}) in Figure 3.5.28a, b and c. This relationship indicated that nitrate contamination occurred one of two duplicate samples without phosphate contamination. We also observed that nitrate vs. phosphate ratio did not change while nitrate concentration difference is 1.5 μmol kg^{-1} eg. indicated as a horizontal line in Figure 3.5.28a. We guess that the malfunction of sampler we stated later may cause nitrate concentration change due to a change of the amount of intake of seawater sample compared with the intake of reagents. Furthermore, we also observed an increase of nitrate vs. phosphate ratio in spite of less difference of nitrate concentration as shown ellipses in Figure 3.5.28a for leg 2 and Figure 3.5.28c for the second half of leg 3. In leg 1 case, we guess that nitrate contamination may occur for both samples without phosphate contamination while in the second half of leg 3 case we guess that higher nitrate vs. phosphate ration were natural phenomena due to intrusion of Atlantic Ocean origin seawater at that region.

We did not observe nitrate contamination on samples taken from CRMs and C-5 standards solution, too. This may indicate that nitrate contamination occurred during a sample drawing from the environment and/or nitrate contamination inside the surface of the sampling bottles.

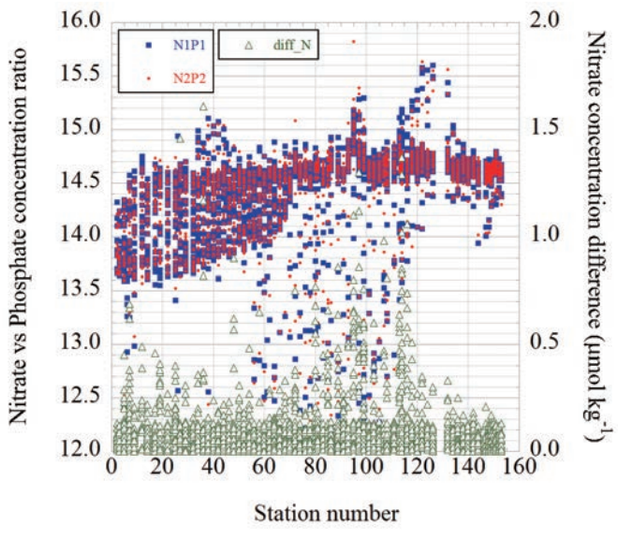

Figure 3.5.27 Nitrate/phosphate concentration ratio and difference of nitrate concentration between duplicate two samples.

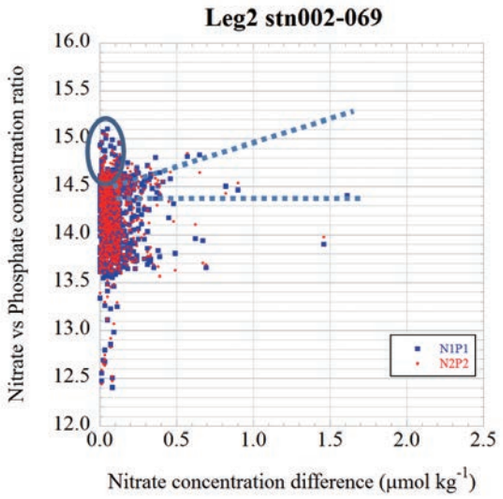

Figure 3.5.28a Relationship of nitrate concentration differences to nitrate vs. phosphate concentration ratio during the leg 2. Blue and red dots indicate the ratio in the first and second samples of duplicate pair, respectively.

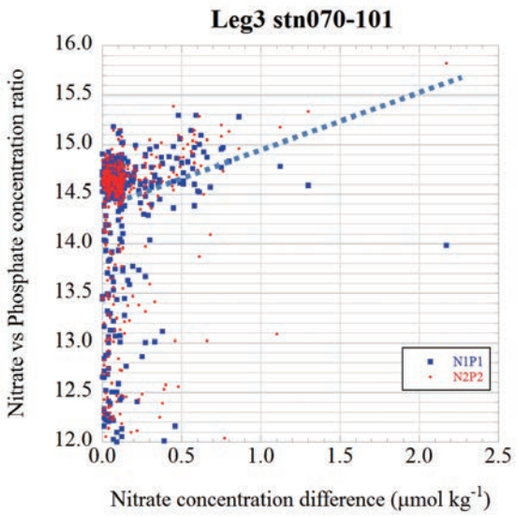

Figure 3.5.28b Same as Figure 3.5.28a but for the data at stations 70-101 in the leg 3.

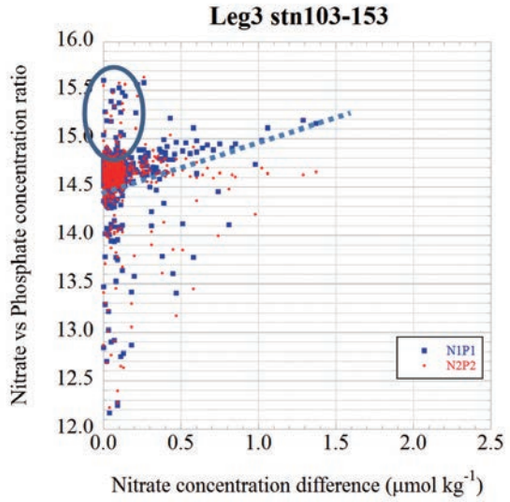

Figure 3.5.28c Same as Figure 3.5.28a but for the data at stations 103-153 in the leg 3.

We started to seek cause(es) of this nitrate contamination. We had been using latex gloves during the water sampling because of its good performance of handling. First, we checked the possibility of nitrate contamination from latex gloves on board. We also tested other gloves made from different materials as shown in Table 3.5.8. As already stated in Becker et al. (2019), the soaking tests showed that latex gloves might be a source of nitrate especially at the beginning of the use of new gloves taken from a package. Therefore, we stopped to use latex gloves and used polyvinyl chloride gloves after station 101 on 8 January 2020. The situation, however, did not change and the nitrate contamination continued, which suggests other nitrate sources in the ship. We also checked the possibility of contamination from the atmosphere by exposing tests with LNSW at the CTD room, chemical laboratory, and a few other places in the ship and by soaking small black particles collected on the deck of in the ship. The exposing tests showed that ambient air might not be a source of nitrate contamination while the small black particles could be one of the potential sources of nitrate source (Table 3.5.9). Then we cleaned up the CTD room by freshwater at station 124. As we can

see in Figure 3.5.27, the difference of two replicate samples became small gradually after that and we found a normal situation just before the end of this cruise. We believe the small particle deposited on the deck may be one of the sources of nitrate contamination.

As stated previously, we also found a linear relationship between the N/P ratio and the difference in the replicate samples in the second half of the leg 3 (Figures 3.5.28c), which is similar to that observed in the first half of the leg 3 (Figures 3.5.28b). On the other hand, we also observed the higher N/P ratio without the large difference at stations 120-130 approximately in the second half of the leg 3 (Figure 3.5.27), which was not observed in the first half of the leg 3 but in the leg 2 (Figures 3.5.28a). The high N/P ration without the large difference implies that the nitrate contamination occurred in both two replicate samples or did not occurred. The latter means that the high N/P ratios are within the natural variation. We concluded that those at station 120-130 approximately in the second half of the leg 3 are probably due to the natural variability because of Atlantic Ocean water intrusion.

Therefore, we concluded that serious nitrate contamination from the environment to the seawater samples occurred during the sample drawing although we could find the exact cause of these contaminations.

Malfunction of one of the analyzers of nutrients named #1 and nitrate concentration measured by unit #1 resulted in larger variability, which exceeds normal analytical precision about 0.2 % for the samples collected at stations 2, 7, 12, 19, 25 and 27. We found damage on a timing disk of autosampler of #1 machine and we suspect that intake of the sample seawater during the measurement was unstable. This resulted in the large nitrate concentration difference without the high N/P ratio in the early stage of the leg 2 (Figure 3.5.28a).

During this cruise, we changed the sample drawing order as shown in Table 3.5.10 due to the trail of nitrate contamination check. It is, however, the sample drawing order was not a cause of nitrate contamination.

Table 3.5.8 Results of tests for contamination from gloves.

Gloves	Methods	Measurement date	Seq.	Nitrate ($\mu mol\ L^{-1}$)	Nitrite ($\mu mol\ L^{-1}$)	Silicate ($\mu mol\ L^{-1}$)	Phosphate ($\mu mol\ L^{-1}$)	Anmonia ($\mu mol\ L^{-1}$)	Sample name
Latex A1-1	(1)	22-Dec-19	1	2.95	0.00	0.99	0.059	0.19	sample1_1_1
			2	0.38	0.01	0.98	0.051	0.09	sample2_1_1
			3	0.11	0.01	1.02	0.051	0.06	sample3_1_1
Latex A1-2		07-Jan-20	1	4.78	0.00	0.99	0.037	0.58	kuaran_1_1
			2	0.62	0.00	1.02	0.043	0.08	kuaran_1_2
			3	0.29	0.00	0.99	0.042	0.05	kuaran_1_3
Latex A2		07-Jan-20	1	1.95	0.00	0.98	0.045	0.12	kuarao_1_1
			2	0.20	0.00	0.99	0.041	0.07	kuarao_1_2
			3	0.16	0.00	1.00	0.041	0.05	kuarao_1_3
Latex B		07-Jan-20	1	1.65	0.00	0.97	0.039	0.03	positive_1_1
			2	0.43	0.00	0.98	0.040	0.03	positive_1_2
			3	0.20	0.00	0.98	0.039	0.04	positive_1_3
Latex C		07-Jan-20	1	0.34	0.00	1.01	0.037	0.03	diamond_1_1
			2	0.17	0.00	0.98	0.037	0.03	diamond_1_2
			3	0.12	0.00	1.00	0.038	0.01	diamond_1_3
Latex D-1		08-Jan-20	1	0.29	0.00	1.12	0.039	0.00	labtex_2_1
			2	0.27	0.01	1.12	0.039	0.00	labtex_2_2
			3	0.18	0.01	1.05	0.039	0.00	labtex_2_3
Latex D-2		07-Jan-20	1	0.11	0.00	1.05	0.041	0.06	labtex_1_1
			2	0.07	0.00	0.99	0.039	0.06	labtex_1_2
			3	0.07	0.00	1.00	0.041	0.07	labtex_1_3
Latex D-3		08-Jan-20	1	0.05	0.00	1.06	0.037	0.00	labtex_3_1
			2	0.08	0.01	1.09	0.036	0.00	labtex_3_2
			3	0.04	0.01	1.05	0.040	0.00	labtex_3_3
Latex D-4	(2)	09-Jan-20	replicated	4.42	0.02	1.17	0.304	0.62	labtex_4_1
				4.90	0.03	1.17	0.263	0.40	labtex_4_2
				4.17	0.02	1.11	0.256	0.48	labtex_4_3
Nitrile rubber	(1)	07-Jan-20	1	1.20	0.00	1.01	0.040	0.07	safe_1_1
			2	0.09	0.00	0.98	0.038	0.03	safe_1_2
			3	0.07	0.00	0.98	0.037	0.04	safe_1_3
Polyethylene		07-Jan-20	1	0.06	0.00	0.97	0.039	0.03	saniment_1_1
			2	0.06	0.00	0.96	0.039	0.05	saniment_1_2
			3	0.05	0.00	0.97	0.036	0.03	saniment_1_3
Polyvinyl chloride-1		07-Jan-20	1	0.02	0.00	0.99	0.039	0.02	clean_1_1
			2	0.04	0.00	1.01	0.039	0.01	clean_1_2
			3	0.03	0.00	1.02	0.043	0.04	clean_1_3
Polyvinyl chloride-2		08-Jan-20	1	0.00	0.01	1.09	0.048	0.02	clean_2_1
			2	0.00	0.00	1.03	0.041	0.00	clean_2_2
			3	0.00	0.00	1.03	0.051	0.00	clean_2_3
Polyvinyl chloride-3		10-Jan-20	1	0.00	0.00	0.96	0.043	0.05	clean_4_1
			2	0.01	0.01	0.95	0.040	0.03	clean_4_2
			3	0.00	0.00	1.01	0.041	0.02	clean_4_3
Polyvinyl chloride-4		10-Jan-20	1	0.00	0.00	0.98	0.041	0.02	clean_5_1
			2	0.00	0.00	0.98	0.041	0.01	clean_5_2
			3	0.00	0.00	0.98	0.038	0.01	clean_5_3
Polyvinyl chloride-5	(3)	09-Jan-20	replicated	0.03	0.01	1.02	0.101	0.06	clean_3_1
				0.03	0.01	1.01	0.090	0.03	clean_3_2
				0.05	0.01	0.99	0.107	0.05	clean_3_3
Blank	(4)	11-Jan-20	replicated	0.01	0.01	0.98	0.042	0.06	cap_1_1
				0.00	0.00	0.95	0.031	0.05	cap_1_2
				0.01	0.00	1.01	0.036	0.03	cap_1_3

(1) A fingertip (1 cm) of the glove was dipped into low nutrient seawater (LNSW) in the three sample tubez (10 ml) sequentially for 5 seconds each.
(2) A fingertip (2 cm) of the glove was dipped into LNSW in the sample tube (10 ml) for 1 hour.
(3) A fingertip (2 cm) of the glove was dipped into LNSW in the sample tube (10 ml) for 10 hours.
(4) LNSW in a sample tube (10 ml) with three time rinses.

Table 3.5.9 Results of tests for contamination.

Experiments		Measurement date	Nitrate (μmol L^{-1})	Nitrite (μmol L^{-1})	Silicate (μmol L^{-1})	Phosphate (μmol L^{-1})	Anmonia (μmol L^{-1})	Sample name
Exposure of low nutreint seawater (LNSW) in sample tube (10 ml) without lid for three hours.	CTD room	13-Jan-20	0.02	0.04	1.02	0.044	0.09	ctdroom_1_1
			0.00	0.05	1.00	0.042	0.08	ctdroom_1_2
			0.00	0.06	0.97	0.042	0.10	ctdroom_1_3
	No.1 buoy mooring room	13-Jan-20	0.00	0.03	0.94	0.038	0.05	no1mooring_1_1
			0.00	0.03	0.99	0.040	0.07	no1mooring_1_2
			0.00	0.03	0.96	0.039	0.08	no1mooring_1_3
	Chemical laboratory	13-Jan-20	0.00	0.08	0.97	0.037	0.38	chemicallab_1_1
			0.00	0.11	0.99	0.040	0.47	chemicallab_1_2
			0.00	0.10	1.02	0.038	0.45	chemicallab_1_3
	Within chamber for autosampler	13-Jan-20	0.00	0.05	1.01	0.040	0.29	autosampler_1_1
			0.00	0.05	0.98	0.040	0.31	autosampler_1_2
			0.00	0.06	1.01	0.042	0.33	autosampler_1_3
Exposure of LNSW in sample tube (10 ml) without lid for 1.5 hours.	Position A in CTD room	15-Jan-20	0.05	0.00	1.90	0.037	0.04	119_A_1
			0.04	0.00	1.81	0.038	0.02	119_A_2
			0.03	0.00	1.79	0.042	0.01	119_A_3
	Position B in CTD room	15-Jan-20	0.00	0.00	1.59	0.043	0.01	119_B_1
			0.00	0.00	1.61	0.032	0.01	119_B_2
			0.00	0.00	1.62	0.032	0.00	119_B_3
	Position C in CTD room	15-Jan-20	0.00	0.01	1.68	0.034	0.03	119_C_1
			0.01	0.00	1.62	0.034	0.00	119_C_2
			0.01	0.00	1.61	0.038	0.00	119_C_3
	Position D in CTD room	15-Jan-20	0.00	0.01	1.61	0.033	0.00	119_D_1
			0.00	0.01	1.57	0.040	0.00	119_D_2
			0.00	0.01	1.69	0.044	0.01	119_D_3
Dipping of sampling tube tip into LNSW in sample tube (10 ml) for 5 seconds.		10-Jan-20	0.01	0.00	0.98	0.040	0.00	tube_1_1
			0.01	0.00	0.97	0.041	0.00	tube_1_2
			0.03	0.00	1.02	0.045	0.00	tube_1_3
Pure water that flowed over the surface of paper towel	White paper towel	11-Jan-20	0.04	0.00	0.00	0.000	0.13	kim_1_1
			0.11	0.01	0.05	0.014	0.25	kim_1_2
	Brown paper towel	11-Jan-20	0.04	0.01	0.00	0.513	0.13	kim_2_1
			0.08	0.01	0.00	0.493	0.16	kim_2_2
Fresh water for general use		11-Jan-20	0.16	0.00	0.00	1.358	0.04	water_1_1
			0.19	0.00	0.01	1.439	0.04	water_1_2
Dipping of small black particulates collected in No.1 bouy mooring room into LNSW in sample tube (10 ml)		15-Jan-20	1.63	0.00	1.80	0.115	0.28	hachinohe_1_1
			0.97	0.03	1.83	0.231	0.26	hachinohe_1_2

Table 3.5.10 Sampling order.

Station	Sampling order
002-099, 103	Oxygen, CFCs, Salinity, gas, Nutrients, NO_3-Si, others
101	Oxygen, CFCs, Nutrients, Salinity, gas, others
105-153	Oxygen, CFCs, Salinity, Nutrients, NO_3-Si, gas, others

We also need to note that replacement of cadmium reduction columns for nitrate measurements had forced more frequently rather than usual operation during the Stn 118, 122, 124, 126, 132 those were located around 50-56 deg. S (Table 3.5.11).

Table 3.5.11 The number of cadmium coil in NO_3+NO_2 flow and reactivation frequency of cadmium coil.

Station	Cast	machine	cadmium coil	new cadmium coil or reactivation
2	1	unit #1	double	
3	1			
5	1	unit #2	double	
6	1	unit #1	double	
7	1			
9	1	unit #2	double	
12	1	unit #1	double	○
14	1	unit #2	double	○
17	1	unit #2	double	
19	1	unit #1	double	○
22	1	unit #2	double	
25	1	unit #1	double	
26	1	unit #1	double	
27	1			
29	1	unit #2	double	
32	1	unit #2	double	
34	1	unit #2	double	
36	1	unit #3	double	
38	1	unit #2	double	
40	1	unit #3	double	
42	1	unit #2	double	○
44	1	unit #2	double	
45	1	unit #3	double	
46	1			
48	1	unit #3	double	
50	1	unit #2	double	
52	1	unit #3	double	
54	1	unit #3	double	
56	1	unit #2	double	○
58	1	unit #2	double	
60	1	unit #2	double	
61	1	unit #2	double	
69	1			
62	1	unit #2	double	
64	1	unit #2	double	○
66	1	unit #2	double	
68	1	unit #2	double	

Station	Cast	machine	cadmium coil	new cadmium coil or reactivation
70	1	unit #3	double	○
72	1	unit #2	double	○
74	1	unit #3	double	
76	1	unit #2	single	
78	1	unit #2	single	
80	1	unit #3	double	○
81	1	unit #2	single	
83	1	unit #2	single	○
85	2	unit #2	single	
86	1	unit #3	double	
89	1	unit #3	double	
91	1	unit #2	single	
93	1	unit #3	double	
95	1	unit #2	single	○
97	1	unit #3	double	
99	1	unit #2	single	
101	1	unit #2	single	
103	1	unit #3	double	
105	1	unit #2	single	
107	1	unit #3	double	○
108	1	unit #2	single	○
111	1	unit #3	double	
113	1	unit #2	single	
114	1	unit #3	double	
116	1	unit #2	single	
118	2	unit #2	single	
120	1	unit #2	single	○
122	1	unit #2	single	
124	1	unit #2	single	○
126	1	unit #2	single	○
132	1	unit #2	single	
134	1	unit #3	single	○
136	1	unit #2	single	○
138	1	unit #2	single	
140	1	unit #3	single	
142	1	unit #2	single	
144	1	unit #3	single	
147	1	unit #2	single	
148	1	unit #3	single	
149	1	unit #2	single	
150	1	unit #2	single	
151	1	unit #3	single	
152	1	unit #2	single	
153	1			

Table 3.5.12 Centrifuged samples in leg 3.

Station	Cast	Bottle	Depth (dbar)	Trans (%)
78	1	36	10.0	98.4
78	1	35	50.1	98.4
78	1	2	88.3	97.9
78	1	34	101.7	97.1
78	1	33	151.1	99.3
81	1	36	10.7	98.6
81	1	35	50.0	98.3
81	1	2	95.2	98.2
81	1	34	101.7	98.2
81	1	33	150.5	98.8
83	1	36	9.3	97.6
83	1	35	50.0	98.2
83	1	2	76.7	98.3
83	1	34	101.2	98.8
83	1	33	150.7	99.2
80	1	36	10.8	98.8
80	1	35	49.9	98.6
80	1	2	70.7	98.7
80	1	34	100.2	99.1
80	1	33	150.0	99.4
85	2	36	10.8	96.0
85	2	35	50.4	94.2
85	2	2	77.5	97.5
85	2	34	100.9	98.7
85	2	33	149.7	99.3
86	1	36	9.7	96.9
86	1	35	50.5	97.6
86	1	2	85.5	97.2
86	1	34	100.7	98.6
86	1	33	150.3	99.2
93	1	36	10.2	92.5
93	1	2	24.8	89.6
93	1	35	50.5	95.0
93	1	34	100.1	98.8
93	1	33	150.6	99.1
89	1	36	10.0	93.9
89	1	35	49.9	93.6
89	1	2	73.4	95.4
89	1	34	100.4	98.9
89	1	33	151.0	99.1
91	1	36	10.6	95.1
91	1	35	50.3	94.0
91	1	2	65.4	96.0
91	1	34	100.7	99.0
91	1	33	150.6	99.2
95	1	36	10.3	86.9
95	1	2	23.6	91.6
95	1	35	50.6	98.1
95	1	34	100.4	99.5
95	1	33	152.3	99.6
97	1	36	9.5	88.1
97	1	2	35.9	94.9
97	1	35	49.8	97.2
97	1	34	100.9	98.6
97	1	33	151.2	99.0
99	1	36	10.7	93.8
99	1	2	37.5	95.4
99	1	35	50.0	96.3
99	1	34	98.1	99.3
99	1	33	150.7	99.3
101	1	36	10.5	91.8
101	1	2	25.2	92.2
101	1	35	50.8	98.2
101	1	34	100.6	99.0
101	1	33	150.5	99.2
103	1	36	10.1	92.2
103	1	35	50.1	93.7
103	1	34	100.3	97.0
103	1	33	151.3	98.6
105	1	36	10.3	91.7
105	1	2	30.8	91.7
105	1	35	50.2	95.9
105	1	34	99.8	99.4
105	1	33	149.5	99.6
107	1	36	10.4	94.2
107	1	2	42.8	93.9
107	1	35	50.4	96.0
107	1	34	100.9	99.5
107	1	33	150.9	99.6
108	1	36	11.0	94.5
108	1	2	45.0	95.1
108	1	35	50.6	95.8
108	1	34	100.8	98.8
108	1	33	149.9	99.6
111	1	36	11.2	93.6
111	1	35	50.8	94.1
111	1	2	58.2	94.2
111	1	34	100.2	99.0
111	1	33	150.3	99.5
113	1	36	9.8	94.9
113	1	2	30.1	95.0
113	1	35	49.6	95.2
113	1	34	100.5	98.7
113	1	33	150.6	99.4
114	1	36	11.6	95.3
114	1	2	34.7	95.3
114	1	35	49.2	95.4
114	1	34	101.0	98.5
114	1	33	151.8	99.4

Table 3.5.12 Centrifuged samples in leg 3 (continued).

Station	Cast	Bottle	Depth (dbar)	Trans (%)
116	1	36	11.3	95.2
116	1	2	25.6	95.2
116	1	35	51.1	95.4
116	1	34	100.6	98.5
116	1	33	152.4	99.5
118	2	36	11.1	95.7
118	2	35	50.2	95.8
118	2	2	84.8	95.1
118	2	34	99.9	97.0
118	2	33	150.5	99.4
120	1	36	9.3	95.4
120	1	35	50.2	95.3
120	1	2	71.8	95.4
120	1	34	100.2	98.2
120	1	33	150.2	99.2
122	1	36	10.2	95.2
122	1	35	50.8	95.1
122	1	2	62.3	95.1
122	1	34	100.5	97.9
122	1	33	150.8	99.1
124	1	36	11.2	95.8
124	1	35	51.1	95.5
124	1	2	69.5	95.4
124	1	34	101.0	97.8
124	1	33	151.0	99.4
126	1	35	10.3	95.5
126	1	33	50.2	95.2
126	1	32	74.5	95.0
126	1	31	99.0	97.2
126	1	30	147.5	99.3
132	1	36	9.9	95.7
132	1	35	50.4	95.6
132	1	2	73.1	95.7
132	1	34	99.9	98.6
132	1	33	148.5	99.5
134	1	36	9.1	95.2
134	1	2	27.8	95.2
134	1	35	50.3	95.3
134	1	34	100.6	98.7
134	1	33	151.7	99.5
138	1	36	9.4	97.0
138	1	2	41.1	96.9
138	1	35	51.0	96.9
138	1	34	98.9	99.3
138	1	33	151.8	99.6
136	1	36	9.4	95.7
136	1	35	51.2	95.9
136	1	2	61.4	96.0
136	1	34	101.4	99.2
136	1	33	151.8	99.6
140	1	36	9.9	97.2
140	1	35	49.2	97.2
140	1	2	55.5	97.7
140	1	34	99.9	99.4
140	1	33	150.0	99.7
142	1	36	10.8	97.8
142	1	2	40.0	97.7
142	1	35	50.6	97.4
142	1	34	100.7	99.3
142	1	33	150.3	99.7
144	1	36	10.7	98.0
144	1	35	50.2	97.2
144	1	2	60.8	98.2
144	1	34	100.6	99.3
144	1	33	150.4	99.6
147	1	36	10.1	98.7
147	1	35	50.1	98.5
147	1	2	58.1	98.4
147	1	34	100.6	99.2
147	1	33	150.8	99.6
148	1	36	10.3	98.3
148	1	35	50.4	98.0
148	1	2	56.6	98.7
148	1	33	150.3	99.6
148	1	32	199.5	99.7
149	1	36	10.7	98.8
149	1	35	51.2	98.6
149	1	2	84.9	99.0
149	1	34	100.4	99.3
149	1	33	150.3	99.6
150	1	36	10.4	98.4
150	1	35	50.3	97.3
150	1	2	80.2	98.8
150	1	34	100.3	99.5
150	1	33	150.9	99.6
151	1	36	10.0	98.0
151	1	35	50.0	97.8
151	1	2	69.9	97.9
151	1	34	99.6	99.4
151	1	33	149.9	99.9
152	1	36	10.3	98.2
152	1	35	50.1	97.2
152	1	2	80.1	98.1
152	1	34	100.4	99.1
152	1	33	150.3	99.9
153	1	36	9.7	97.2
153	1	35	50.4	97.7
153	1	2	87.4	98.0
153	1	34	100.4	99.1
153	1	33	150.1	99.9

(10) List of reagents

List of reagents is shown in Table 3.5.13.

Table 3.5.13 List of reagent in MR19-04.

IUPAC name	CAS Number	Formula	Compound Name	Manufacture	Grade
4-Aminobenzenesulfonamide	63-74-1	$C_6H_8N_2O_2S$	Sulfanilamide	Wako Pure Chemical Industries, Ltd.	JIS Special Grade
Antimony potassium tartrate trihydrate	28300-74-5	$K_2(SbC_4H_2O_6)_2 \cdot 3H_2O$	Bis[(+)-tartrato]diantimonate(III) Dipotassium Trihydrate	Wako Pure Chemical Industries, Ltd.	JIS Special Grade
Boric acid	10043-35-3	H_3BO_3	Boric Acid	Wako Pure Chemical Industries, Ltd.	JIS Special Grade
Hydrogen chloride	7647-01-0	HCl	Hydrochloric Acid	Wako Pure Chemical Industries, Ltd.	JIS Special Grade
Imidazole	288-32-4	$C_3H_4N_2$	Imidazole	Wako Pure Chemical Industries, Ltd.	JIS Special Grade
L-Ascorbic acid	50-81-7	$C_6H_8O_6$	L-Ascorbic Acid	Wako Pure Chemical Industries, Ltd.	JIS Special Grade
N-(1-Naphthalenyl)-1,2-ethanediamine, dihydrochloride	1465-25-4	$C_{12}H_{16}Cl_2N_2$	N-1-Naphthylethylenediamine Dihydrochloride	Wako Pure Chemical Industries, Ltd.	for Nitrogen Oxides Analysis
Oxalic acid	144-62-7	$C_2H_2O_4$	Oxalic Acid	Wako Pure Chemical Industries, Ltd.	Wako Special Grade
Phenol	108-95-2	C_6H_6O	Phenol	Wako Pure Chemical Industries, Ltd.	JIS Special Grade
Sodium citrate dihydrate	6132-04-3	$Na_3C_6H_5O_7 \cdot 2H_2O$	Trisodium Citrate Dihydrate	Wako Pure Chemical Industries, Ltd.	JIS Special Grade
Sodium dodecyl sulfate	151-21-3	$C_{12}H_{25}NaO_4S$	Sodium Dodecyl Sulfate	Wako Pure Chemical Industries, Ltd.	for Biochemistry
Sodium hydroxide	1310-73-2	NaOH	Sodium Hydroxide for Nitrogen Compounds Analysis	Wako Pure Chemical Industries, Ltd.	for Nitrogen Analysis
Sodium hypochlorite	7681-52-9	NaClO	Sodium Hypochlorite Solution	Kanto Chemical co., Inc.	Extra pure
Sodium molybdate dihydrate	10102-40-6	$Na_2MoO_4 \cdot 2H_2O$	Disodium Molybdate(VI) Dihydrate	Wako Pure Chemical Industries, Ltd.	JIS Special Grade
Sodium nitroferricyanide dihydrate	13755-38-9	$Na_2[Fe(CN)_5NO] \cdot 2H_2O$	Sodium Pentacyanonitrosylferrate(III) Dihydrate	Wako Pure Chemical Industries, Ltd.	JIS Special Grade
Sulfuric acid	7664-93-9	H_2SO_4	Sulfuric Acid	Wako Pure Chemical Industries, Ltd.	JIS Special Grade
tetrasodium;2-[2-[bis(carboxylatomethyl)amino]ethyl-(carboxylatomethyl)amino]acetate;tetrahydrate	13235-36-4	$C_{10}H_{12}N_2Na_4O_8 \cdot 4H_2O$	Ethylenediamine-N,N,N',N'-tetraacetic Acid Tetrasodium Salt Tetrahydrate (4NA)	Dojindo Molecular Technologies, Inc.	-
Synonyms: t-Octylphenoxypolyethoxyethanol 4-(1,1,3,3-Tetramethylbutyl)phenyl-polyethylene glycol Polyethylene glycol tert-octylphenyl ether	9002-93-1	$(C_2H_4O)_nC_{14}H_{22}O$	Triton™ X-100	Sigma-Aldrich Japan G.K.	-

(11) Data archives

These data obtained in this cruise will be submitted to the Data Management Group of JAMSTEC and will be opened to the public via “Data Research System for Whole Cruise Information in JAMSTEC (DARWIN)” in JAMSTEC web site.

<http://www.godac.jamstec.go.jp/darwin/e>

(12) References

Susan Becker, Michio Aoyama E. Malcolm S. Woodward, Karel Bakker, Stephen Coverly, Claire Mahaffey, Toste Tanhua, (2019) The precise and accurate determination of dissolved inorganic nutrients in seawater, using Continuous Flow Analysis methods, n: The GO-SHIP Repeat Hydrography Manual: A Collection of Expert Reports and Guidelines. Available online at: http://www.go-ship.org/HydroMan.html. DOI: http://dx.doi.org/10.25607/OBP-555

Grasshoff, K. 1976. Automated chemical analysis (Chapter 13) in Methods of Seawater Analysis. With contribution by Almgreen T., Dawson R., Ehrhardt M., Fonselius S. H., Josefsson B., Koroleff F., Kremling K. Weinheim, New York: Verlag Chemie.

Grasshoff, K., Kremling K., Ehrhardt, M. et al. 1999. Methods of Seawater Analysis. Third, Completely Revised and Extended Edition. WILEY-VCH Verlag GmbH, D-69469 Weinheim (Federal Republic of Germany).

Hydes, D.J., Aoyama, M., Aminot, A., Bakker, K., Becker, S., Coverly, S., Daniel, A., Dickson, A.G., Grosso, O., Kerouel, R., Ooijen, J. van, Sato, K., Tanhua, T., Woodward, E.M.S., Zhang, J.Z., 2010. Determination of Dissolved Nutrients (N, P, Si) in Seawater with High Precision and Inter-Comparability Using Gas-Segmented Continuous Flow Analysers, In: GO-SHIP Repeat Hydrography Manual: A Collection of Expert Reports and Guidelines. IOCCP Report No. 14, ICPO Publication Series No 134.

Kimura, 2000. Determination of ammonia in seawater using a vaporization membrane permeability method. 7th auto analyzer Study Group, 39-41.

Murphy, J., and Riley, J.P. 1962. Analytica Chimica Acta 27, 31-36.

3.6 Chlorophyll *a*

(1) Personnel

Kosei Sasaoka (JAMSTEC) (Leg 2, 3)

Misato Kuwahara (MWJ) (Leg 2, 3)

Erii Irie (MWJ) (Leg 2, 3)

Yuko Miyoshi (MWJ) (Leg 2, 3)

(2) Objectives

Chlorophyll *a* is one of the most convenient indicators of phytoplankton stock, and has been used extensively for the estimation of phytoplankton abundance in various aquatic environments. In this study, we investigated horizontal and vertical distribution of phytoplankton along the I08N section (Leg 2) in the Indian Ocean and I07S section (Leg 3) in the Southern Ocean. The chlorophyll *a* data is also utilized for calibration of fluorometers, which were installed in the surface water monitoring and CTD profiler system.

(3) Instrument and Method

Seawater samples were collected in 500 mL (Leg 2: All stations, Leg 3: Station.70–97) and 250 mL (Leg 3: Station.99-153) brown Nalgene bottles without head-space. All samples were gently filtrated by low vacuum pressure (<0.02 MPa) through Whatman GF/F filter (diameter 25 mm) in the dark room. Whole volume of each sampling bottle was precisely measured in advance. After filtration, phytoplankton pigments were immediately extracted in 7 ml of N,N-dimethylformamide (DMF), and samples were stored at –20°C under the dark condition to extract chlorophyll a more than 24 hours. Chlorophyll *a* concentrations were measured by the Turner fluorometer (10-AU-005, TURNER DESIGNS), which was previously calibrated against a pure chlorophyll *a* (Sigma-Aldrich Co., LLC) (Figure 3.6.1). To estimate the chlorophyll *a* concentrations, we applied to the fluorometric “Non-acidification method” (Welschmeyer, 1994).

(4) Results

Vertical distributions of chlorophyll *a* concentration at each stations along the I08N (Leg 2) and I07S (Leg 3) during the cruise are shown in Figure 3.6.2 and Figure 3.6.3, respectively. Cross section of chlorophyll *a* concentration along the I08N (Leg 2) and I07S (Leg 3) are shown in Figure 3.6.4 and 3.6.5, respectively. Sub-surface chlorophyll *a* maximum (SCM) was clearly seen in almost stations (Figure 3.6.2, 3.6.3). The SCM depths were deepened gradually from northern stations to around 12oS along the I08N section (Figure 3.6.4). The chlorophyll *a* concentration was highest (about 1.6 mgm^{-3}) around 40oS (the subarctic frontal zone) at the SCM depth (25m) along the I07S section (Figure 3.6.5). To examine the measurement precision, 29 (Leg 2) and 44 (Leg 3)-pairs of replicate samples were obtained from hydrographic casts at the chlorophyll *a* maximum depth. The absolute values of the difference between replicate samples were 0-0.12 mgm^{-3}, and those average relative errors were approximately 3% (Leg 2) and 4% (Leg 3).

(5) Reference

Welschmeyer, N. A. (1994): Fluorometric analysis of chlorophyll a in the presence of chlorophyll b and pheopigments. Limnor. Oceanogr., 39, 1985-1992.

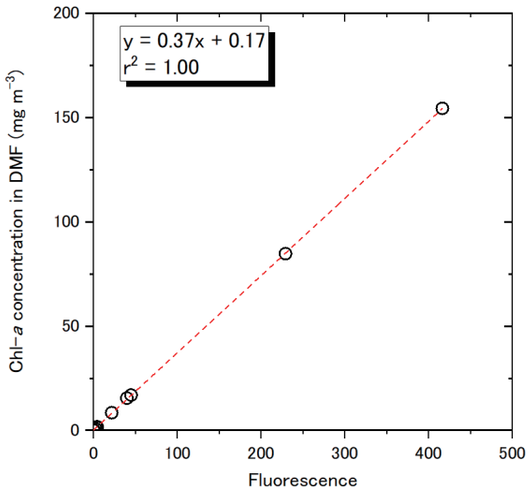

Figure 3.6.1 Relationships between pure chlorophyll *a* concentrations and fluorescence light intensity (n=10).

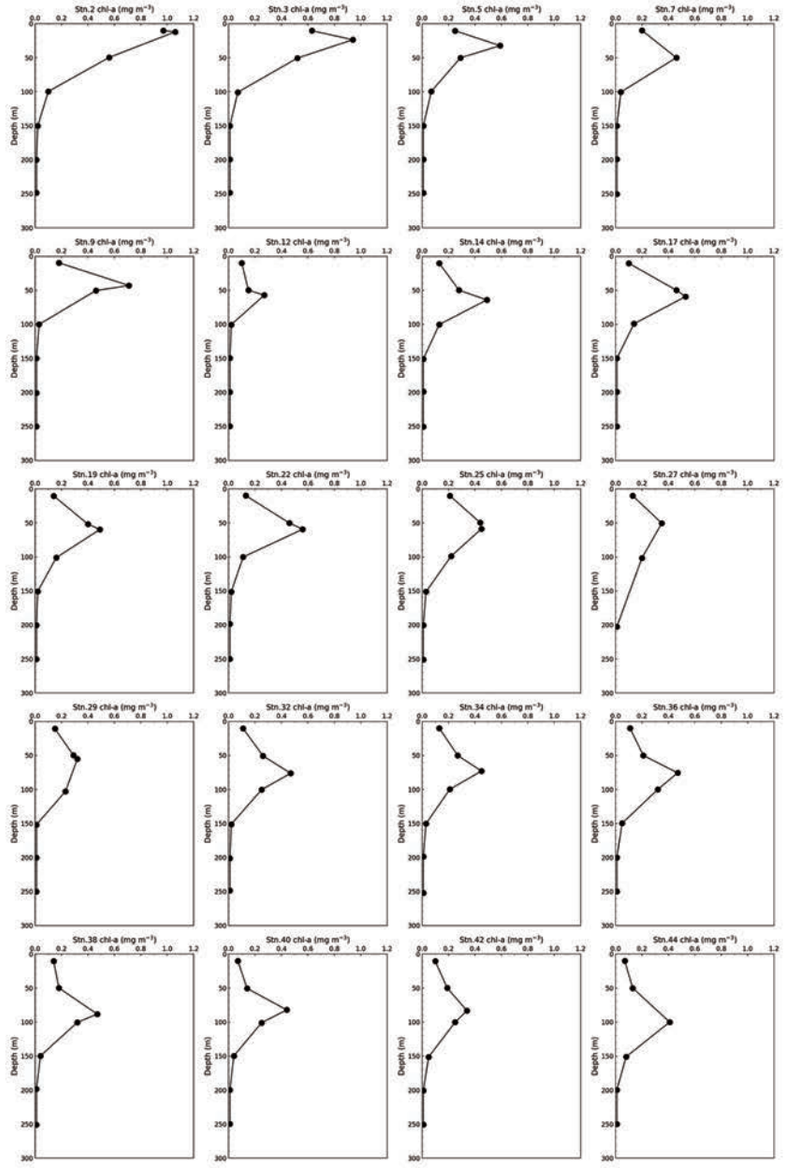

Figure 3.6.2 Vertical profiles of chlorophyll *a* concentration (32-stations) along the I08N section (Leg 2) obtained from hydrographic casts.

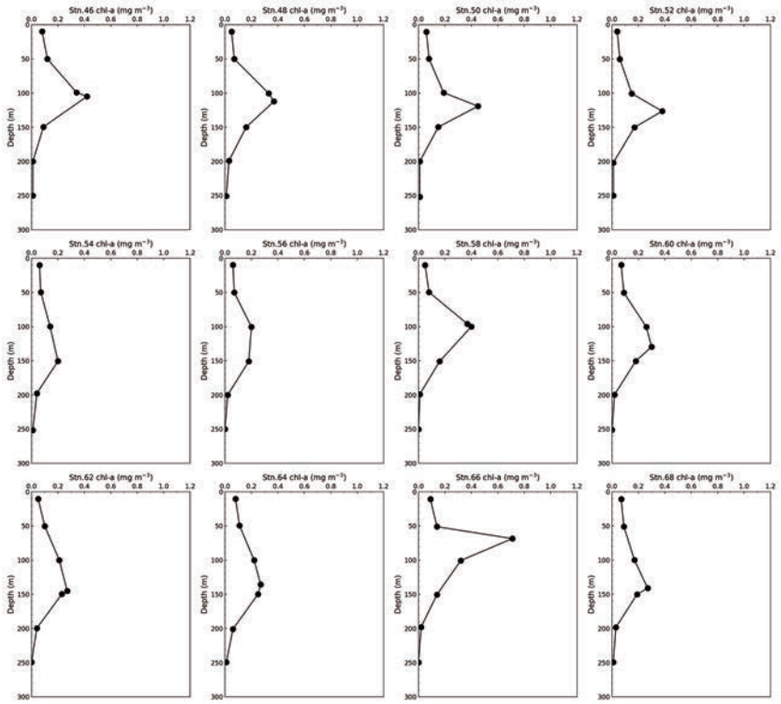

Figure 3.6.2 (Continued)

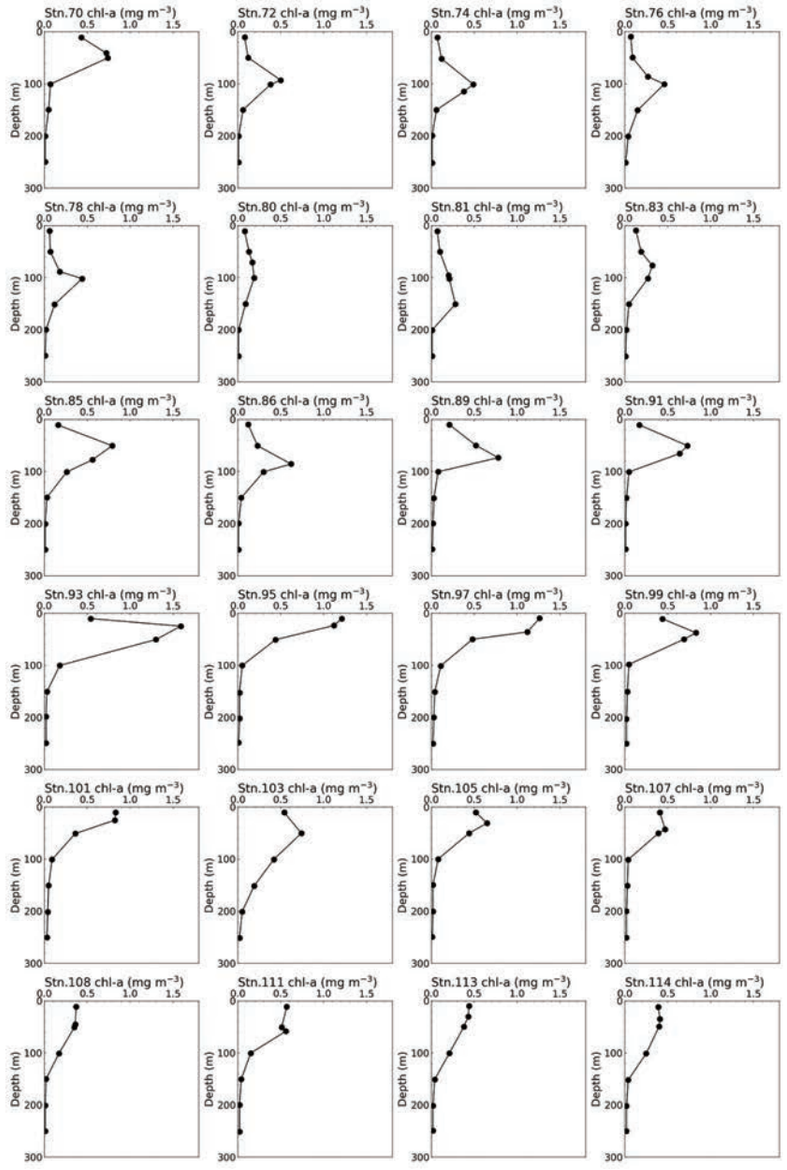

Figure 3.6.3 Vertical profiles of chlorophyll *a* concentration (44-stations) along the I07S section (Leg 3) obtained from hydrographic casts.

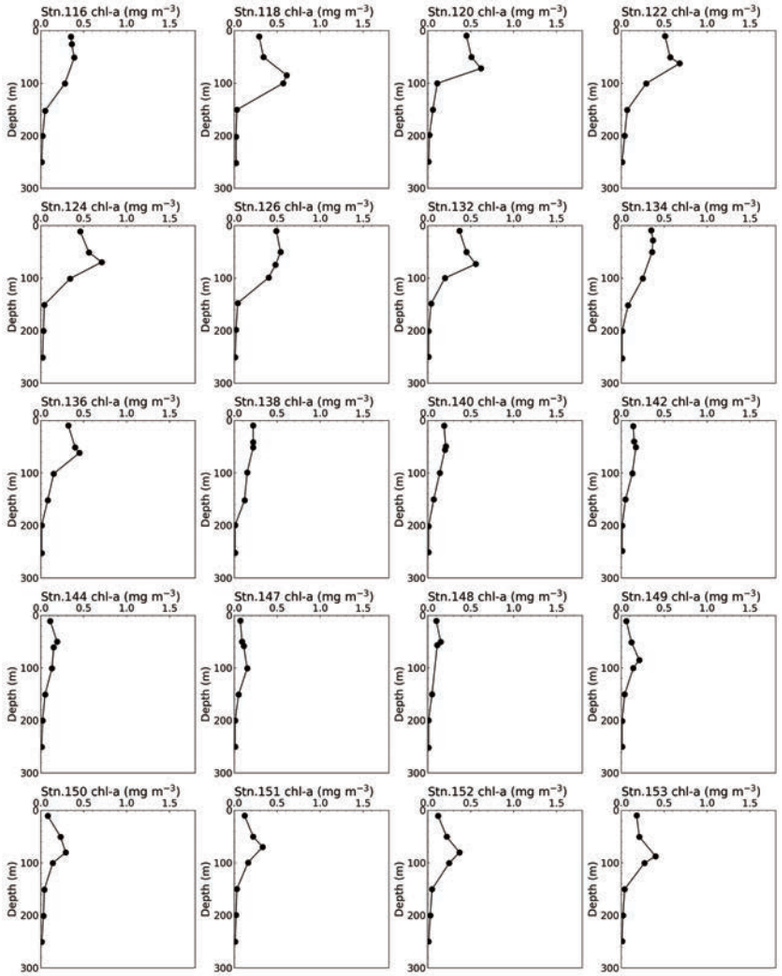

Figure 3.6.3 (Continued).

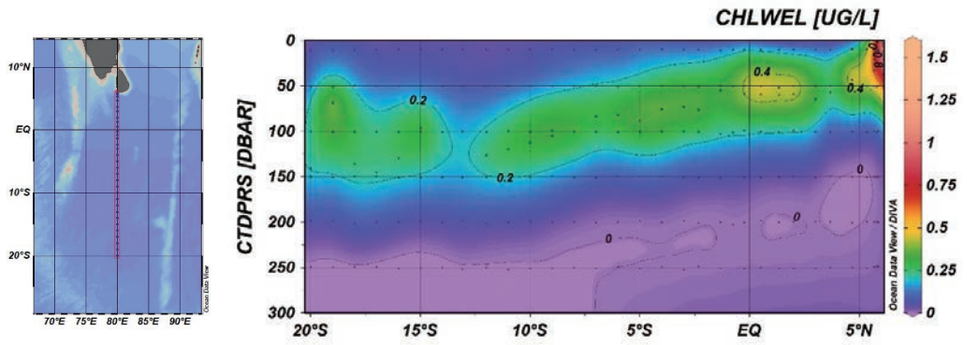

Figure 3.6.4 Cross section of chlorophyll *a* concentrations along the I08N (Leg 2) obtained from hydrographic casts.

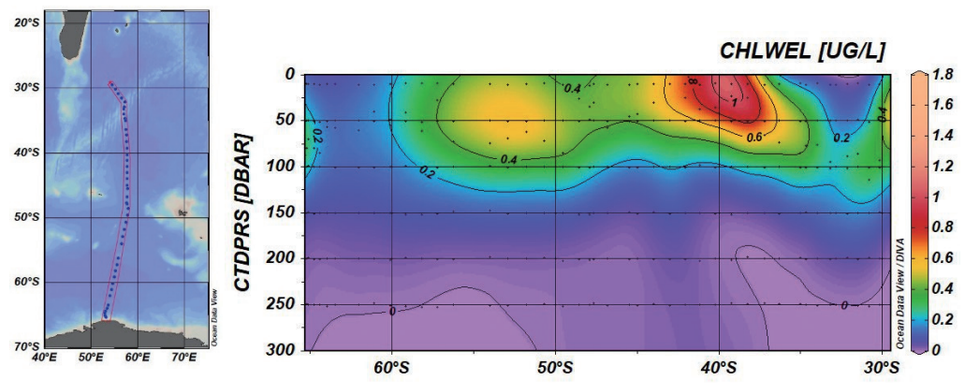

Figure 3.6.5 Cross section of chlorophyll *a* concentrations along the I07S (Leg 3) obtained from hydrographic casts.

3.7 Carbon Items

November 23, 2020

(1) Personnel

Akihiko Murata (JAMSTEC)

Nagisa Fujiki (MWJ)

Atsushi Ono (MWJ)

Masanori Enoki (MWJ)

Yuta Oda (MWJ)

Daiki Kawata (MWJ)

(2) Objectives

Concentrations of CO_2 in the atmosphere are now increasing at a rate of about 2.0 ppmv yr^{-1} due to human activities such as burning of fossil fuels, deforestation, and cement production. It is an urgent task to estimate as accurately as possible the absorption capacity of the oceans against the increased atmospheric CO_2, and to clarify the mechanism of the CO_2 absorption, because the magnitude of the anticipated global warming depends on the levels of CO_2 in the atmosphere, and because the ocean currently absorbs 1/3 of the 6 Gt of carbon emitted into the atmosphere each year by human activities.

In this cruise, we were aimed at quantifying how much anthropogenic CO_2 was absorbed in the Indian Ocean and Southern Ocean. For the purpose, we measured CO_2-system parameters such as dissolved inorganic carbon (C_T) and total alkalinity (A_T) along the WHP I08N section in the Indian Ocean and the section along the meridional line of ~56°E.

(3) Apparatus

i. C_T

Measurement of C_T was made with a total CO_2 measuring system (called as System D, Nihon ANS, Inc.). The system comprised of a seawater dispensing system, a CO_2 extraction system and a coulometer. In this cruise, we used a coulometer Model 3000, which was constructed by Nippon ANS. The systems had a specification as follows:

The seawater dispensing system has an auto-sampler (6 ports), which dispenses seawater from a 300 ml borosilicate glass bottle into a pipette of about 15 ml volume by PC control. The pipette is kept at 20 °C by a water jacket, in which water from a water bath set at 20 °C is circulated. CO_2 dissolved in a seawater sample is extracted in a stripping chamber of the CO_2 extraction system by adding phosphoric acid (~9 % v/v) of about 2 ml. The stripping chamber is approx. 25 cm long and has a fine frit at the bottom. The acid is added to the stripping chamber from the bottom of the chamber by pressurizing an acid bottle for a given time to push out the right amount of acid. The pressurizing is made with nitrogen gas (99.9999 %). After the acid is transferred to the stripping chamber, a seawater sample kept in a pipette is introduced to the stripping chamber by the same method as in adding an acid. The seawater reacted with phosphoric acid is stripped of CO_2 by bubbling the nitrogen gas through a fine frit at the bottom of the stripping chamber. The CO_2 stripped in the chamber is carried by the nitrogen gas (flow rates is 140 ml min^{-1}) to the coulometer through a dehydrating module. The module consists of two electric dehumidifiers (kept at ~2 °C) and a chemical desiccant ($Mg(ClO_4)_2$).

The measurement sequence such as system blank (phosphoric acid blank), ~1.5 % CO_2 gas in a nitrogen base, sea water samples (6) is programmed to repeat. The measurement of ~1.5 % CO_2 gas is made to monitor response of coulometer solutions purchased from UIC, Inc.

ii. A_T

Measurement of A_T was made based on spectrophotometry using a custom-made system (Nihon ANS, Inc.). The system comprises of a water dispensing unit, a HCl titration unit (Hamilton No.2), and a detection unit of a spectrophotometer (TM-UV/VIS C10082CAH, Hamamatsu Photonics, Japan) and an optical source

(Ocean Photonics, Japan). The system was automatically controlled by a PC. The water dispensing unit had a water-jacketed pipette and a water-jacketed glass titration cell.

A seawater of approx. 42 ml was transferred from a sample bottle (borosilicate glass bottle; maximum = ~130 ml) into the water-jacketed (25 °C) pipette by pressurizing the sample bottle (nitrogen gas), and was introduced into the water-jacketed (25 °C) glass titration cell. The introduced seawater was used to rinse the titration cell. After dumping the seawater used for rinse, Milli-Q water was introduced into the titration cell to rinse it. The rinse by Milli-Q water is repeated twice. Then, a seawater of approx. 42 ml was weighted again by the pipette, and was transferred into the titration cell. Then, for seawater blank, absorbances were measured at three wavelengths (730, 616 and 444 nm). After the measurement, an acid titrant, which was a mixture of approx. 0.05 M HCl in 0.65 M NaCl and bromocresol green (BCG), was added into the titration cell. The volume of acid titrant solution was changed according to expected values of AT from 1.980 ml to 2.190 ml. The seawater and acid titrant were mixed for 5 minutes by a stirring tip and bubbling by nitrogen gas in the titration cell. Then, absorbances at the three wavelengths were measured again.

Calculation of A_T was made by the following equation:

$$A_T = (-[H^+]_T V_{SA} + M_A V_A)/V_S,$$

where M_A is the molarity of the acid titrant added to the seawater sample, $[H^+]_T$ is the total excess hydrogen ion concentration in the seawater, and V_S, V_A and V_{SA} are the initial seawater volume, the added acid titrant volume, and the combined seawater plus acid titrant volume, respectively. $[H^+]_T$ is calculated from the measured absorbances based on the following equation (Yao and Byrne, 1998):

$$pH_T = -\log[H^+]_T = 4.2699 + 0.002578(35 - S) + \log((R - 0.00131)/(2.3148 - 0.1299R)) - \log(1 - 0.001005S),$$

where S is the sample salinity, and R is the absorbance ratio calculated as:

$$R = (A_{616} - A_{750})/(A_{444} - A_{750}),$$

where A_i is the absorbance at wavelength i nm. The absorbances used for the calculation are averages of 3 measurements both for seawater blank and acidified sample.

The HCl in the acid titrant was standardized on land (0.050001 mol L^{-1} and 0.050002 mol L^{-1}).

(4) Shipboard measurement

(4.1) Sampling

i. C_T

All seawater samples were collected from depth with 12 liter Niskin bottles basically at every other stations. The seawater samples for C_T were taken with a plastic drawing tube (PFA tubing connected to silicone rubber tubing) into a 250 ml DURAN® glass bottle. The glass bottle was filled with seawater smoothly from the bottom following a rinse with a seawater of 2 full, bottle volumes. The glass bottle was closed by an inner cap loosely, which was fitted tightly to the bottle mouth after mercuric chloride was added.

At a chemical laboratory on ship, a volume of about 3 mL seawater was removed with a plastic pipette from sampling bottles to have a headspace of approx. 1% of the bottle volume. A saturated mercuric chloride of 100 µl was added to poison seawater samples. The seawater samples were kept at 5 °C in a refrigerator until analysis. A few hours just before analysis, the seawater samples were kept at 20 °C in a water bath.

ii. A_T

All seawater samples were collected from depth using 12 liter Niskin bottles at the same stations as for C_T. The seawater samples for A_T were taken with a plastic drawing tube (PFA tubing connected to silicone rubber tubing) into a 100 ml DURAN® glass bottle. The glass bottle was filled with seawater smoothly from the bottom after rinsing it with a seawater of 2 full, bottle volume.

The samples were stored at about 5 °C in a refrigerator A few hours before analysis, the seawater samples were kept at 25 °C in a water bath.

(4.2) Analysis

i. C_T

At the start of each leg, we calibrated the measuring systems by blank and 5 kinds of Na_2CO_3 solutions (nominally 500, 1000 1500, 2000, 2500 μmol L^{-1}). As it was empirically known that coulometers do not show a stable signal (low repeatability) with fresh (low absorption of carbon) coulometer solutions. Therefore, we measured ~1.5% CO_2 gas repeatedly until the measurements became stable. Then we started the calibration.

The measurement sequence such as system blank (phosphoric acid blank), ~1.5% CO_2 gas in a nitrogen base, seawater samples (6) was programmed to repeat. The measurement of ~1.5% CO_2 gas was made to monitor response of coulometer solutions (from UIC, Inc.). For every renewal of coulometer solutions, certified reference materials (CRM, batch 183, certified value = 2040.25 ± 0.43 μmol kg^{-1}) provided by Prof. A. G. Dickson of Scripps Institution of Oceanography were analyzed. In addition, in-house reference materials (RM) (batch Q37) were measured at the initial, intermediate and end times of a coulometer solution's lifetime.

The preliminary values were reported in a data sheet on the ship. Repeatability and vertical profiles of C_T based on raw data for each station helped us check performances of the measuring systems.

In the cruise, we finished all the analyses for C_T on board the ship.

ii. A_T

To monitor conditions of A_T analysis, we analyzed two kinds of RM: in-house RM (batch Q37) and KRM (batch AS). The former was produced by JAMSTEC, while the latter was provided by KANSO CO., LTD. In addition, certified reference materials (CRM, batch 183, certified value = 2230.52 ± 0.28 μmol kg^{-1}) were analyzed periodically to monitor systematic differences of measured A_T. The reported values of A_T were set to be comparable to the certified value of the batch 183.

The preliminary values were reported in a data sheet on ship. Repeatability calculated from replicate samples and vertical profiles of A_T based on raw data for each station helped us check performance of the measuring system.

In the cruise, we finished all the analyses for A_T on board the ship.

(5) Quality control

i. C_T

We conducted quality control of the data after return to a laboratory on land. The repeatability of sample measurements was estimated to be 1.5 μmol kg^{-1} (n = 87) and 2.0 μmol kg^{-1} (n = 117) for legs 2 (I08N) and 3 (section along ~56°E), respectively.

ii. A_T

Temporal changes of A_T, which originate from analytical problems, were monitored by measuring A_T of RMs (in-house RM and KRM) and CRM (batch 183). We found no abnormal measurements during the cruises.

The repeatability of measurements was estimated to 1.3 μmol kg^{-1} (n = 81) and 1.3 μmol kg^{-1} (n = 102) for legs 2 (I08N) and 3 (section along ~56°E), respectively.

References

Dickson, A. G., C. L. Sabine and J. R. Christian eds. (2007) *Guide to best practices for ocean CO_2 measurements,* PICES Special Publication 3, 191 pp.

Yao, W. and R. B. Byrne (1998) Simplified seawater alkalinity analysis: Use of linear array spectrometers. Deep-Sea Research 45, 1383-1392.

3.8 Chlorofluorocarbons and Sulfur hexafluoride

(1) Personnel

Masahito Shigemitsu (JAMSTEC)

Ken'ichi Sasaki (JASMTEC)

Masahiro Orui (MWJ)

Hiroshi Hoshino (MWJ)

Atsushi Ono (MWJ)

Katsunori Sagishima (MWJ)

(2) Introduction

Chlorofluorocarbons (CFCs) and sulfur hexafluoride (SF_6) are man-made stable gases. These atmospheric gases can slightly dissolve in the sea surface water by air-sea gas exchange and spread into the ocean interior. Thus, the dissolved gases could be used as chemical tracers for the ocean circulation/ventilation. In this cruise, we try to gain insights into the ventilation rates and pathways in the Indian Ocean. To this end, we measured the concentrations of three chemical species of CFCs, CFC-11 (CCl_3F), CFC-12 (CCl_2F_2), and CFC-113 ($C_2Cl_3F_3$), and SF_6 in the seawater on board.

(3) Instrument and method

Bottle sampling

Discrete water samples for each station were collected using 12 liter Niskin bottles mounted on a CTD system. Each sample was introduced to a glass bottle of 450 ml developed in JAMSTEC by connecting a spigot of Niskin bottle through Tygon tubing. Before water sampling, each glass bottle was filled with CFCs/SF_6-free N_2. Seawater of twice the bottle volume was overflowed for each sample. The seawater samples were stored in a thermostatic water bath kept at 7 °C immediately after the water sampling, and the samples were measured as soon as possible (usually within 18 hours after sampling).

Air sampling

In order to confirm CFCs/SF_6 concentrations of the standard gases and the stabilities of the concentrations as well as to check the saturation levels in the sea surface waters, the mixing ratios in background air were periodically analyzed. Air samples were continuously led into a laboratory by an air pump. The end of 10 mm OD Dekaron tubing was put on a head of the compass deck and the other end was connected onto the air pump in the laboratory. The tubing was relayed by a T-type union which had a small stopcock. Air sample was collected from the flowing air into a 200 ml glass cylinder by attaching the cylinder to the cock.

CFCs/SF_6 measurements

The two SF_6/CFCs analyzing systems, which were based on purging and trapping gas chromatography, were used. Constant volume of water sample (approximately 200 ml) was introduced into a sample loop. The sample was first drawn into a stripping chamber and the dissolved SF_6 and CFCs were extracted by CFCs/SF_6-free N_2 gas purging for 8 minutes at 220 ml min^{-1}. The extracted gases were dried by passing them through a magnesium perchlorate desiccant tube, and concentrated in a main trap column cooled down to -80 °C. The main trap column was a 30-cm length of 1/8-in stainless steel tubing packed with 80/100 mesh Porapak Q of 5 cm and 100/120 mesh Carboxen 1000 of 5cm. Stripping efficiencies were confirmed by re-stripping of surface layer samples for every station and more than 99 % of dissolved SF_6 and CFCs were extracted on the first purge. The purging and trapping were followed by the isolation and heating to 180 °C of the main trap column. After 1 minute, the desorbed gases were transferred to a focus trap (same as the main trap, except for 1/16-in tubing) cooled down to -80 °C for 30 seconds. Then, the sample gases held in the focus trap were desorbed in the same manner as in the main trap, and were transferred into a pre-column 1 (PC 1, ~6 m of Silica Plot capillary column with i.d. of 0.53 mm and film thickness of 6 µm, held at 95 °C). The sample gases were roughly separated in the PC 1, and the SF_6 and CFCs were eluted into a pre-column 2 (PC 2, ~5 m of Molsieve 5A Plot capillary column with i.d. of 0.53 mm and film thickness of 15 µm, held at 95 °C). Then, the PC1 was connected to a cleaning line, and the remained gases with high boiling points were flushed

by a counter flow of CFCs/SF_6-free N_2. SF_6 and CFCs were quickly eluted from the PC 2 onto a main-column 1 (MC 1, ~9 m of Pola Bond-Q capillary column with i.d. of 0.53 mm and film thickness of 6 μm which is connected to ~18 m of Silica Plot capillary column, held at 95 °C) and N_2O was retained on the PC 2. The PC 2 was then connected to a back-flush carrier gas line and N_2O was sent onto a main-column 2 (MC 2, ~3 m of Molsieve 5A Plot connected to ~9 m of Pola Bond-Q capillary column, held at 95 °C). SF_6 and CFCs were further separated on the MC 1 and detected by the one ECD. N_2O sent onto the MC 2 was detected by the other ECD. However, N_2O was not targeted in this cruise. The PC1, PC2, MC1 and MC2 were in a Shimadzu GC2014 gas chromatograph with the ECDs held at 300 °C. Please note that the CFCs/SF_6-free N_2 used in the water sampling and the measurements of SF_6 and CFCs was filtered by a gas purifier column packed with Molecular Sieve 13X (MS-13X) before the gas was introduced into the system. The mass flow rates of CFCs/SF_6-free N_2 for the carrier and detector make-up gases were 10 ml min^{-1} and 27 ml min^{-1}, respectively.

(4) Performance of CFCs/SF_6 measurements

The analytical precisions were estimated from over 200 duplicate samples. The estimated precisions were ± 0.034 pmol/kg, ± 0.012 pmol/kg, ± 0.004 pmol/kg, and ± 0.047 fmol/kg for CFC-11, CFC-12, CFC-113, and SF6, respectively.

(5) Results

The results of CFCs and SF_6 during the leg 2 and leg 3 are shown in Figures 3.8.1 and 3.8.2, respectively.

(6) Data archives

These data obtained in this cruise will be submitted to the Data Management Group of JAMSTEC and will be open to the public via “Data Research System for Whole Cruise Information in JAMSTEC (DARWIN)” in the JAMSTEC web site.

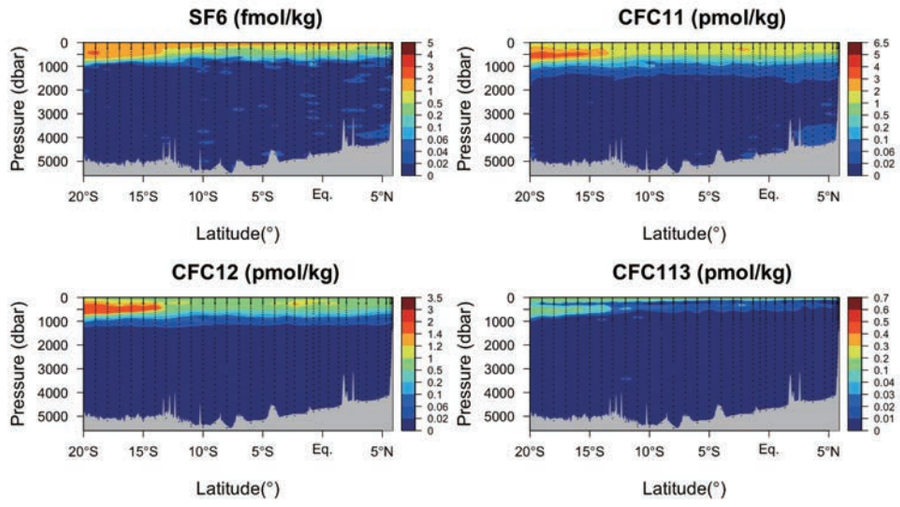

Figure 3.8.1 Vertical sections of CFCs and SF_6 during leg 2.

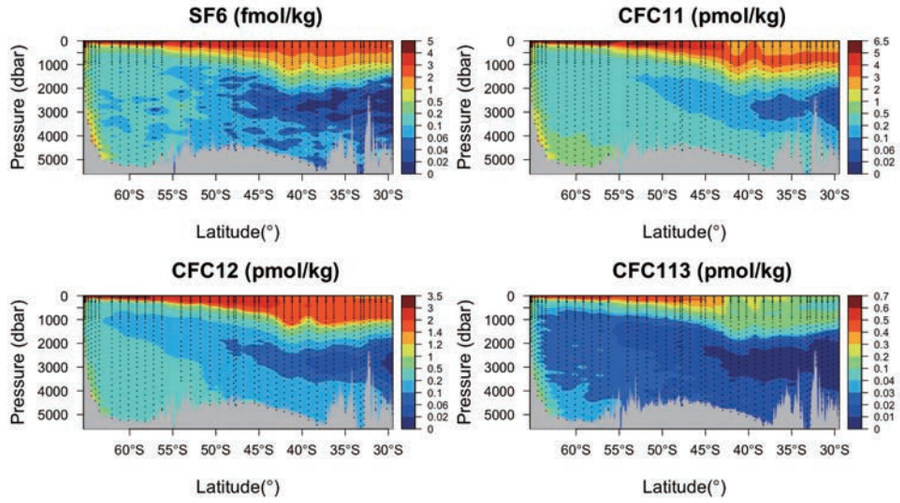

Figure 3.8.2 Vertical sections of CFCs and SF_6 during leg 3.

3.9 Dissolved Organic Carbon and Fluorescent Dissolved Organic Matter

(1) Personnel

Masahito Shigemitsu (JAMSTEC)

Masahide Wakita (JAMSTEC)

Akihiko Murata (JAMSTEC)

(2) Introduction

Marine dissolved organic matter (DOM) is known to be the largest ocean reservoir of reduced carbon, and huge amounts of the carbon exist as refractory DOM (RDOM) (Hansell et al., 2009). RDOM is thought to be generated by microbial mineralization of organic matter produced in the sunlit surface ocean, and play an important role in the atmospheric CO_2 sequestration (Jiao et al., 2010). Some components of the RDOM can be detected as fluorescent DOM (FDOM).

In this cruise, we try to gain insights into the interactions between DOM and microbial abundance, activity and diversity in the Indian Ocean. To this end, we measured dissolved organic carbon (DOC) and FDOM.

(3) Instruments and methods

Bottle sampling

Discrete water samples for each station were collected using 12L Niskin bottles mounted on a CTD system. Each sample taken in the upper 250 m was filtered using a pre-combusted glass fiber filter (GF/F, Whatman). The filtration was carried out by connecting a spigot of Niskin bottle through silicone tube to an inline plastic filter holder.

Filtrates were collected for DOC and FDOM measurements in acid-washed 60 mL High Density Polyethylene (HDPE) bottles and pre-combusted glass vials with acid-washed teflon-lined caps after triple rinsing, respectively. Other samples taken below 250 m were unfiltered. The samples for DOC and FDOM were collected at the stations 2, 5, 9, 12, 17, 22, 25, 29, 32, 36, 40, 44, 50, 52, 56, 60, 64, 68, 70, 78, 85, 93, 101, 107, 114, 118, 122, 126, 134, 138, 142, 147,149, 151, 152 and 153.

DOC measurement

The samples for DOC were immediately stored frozen onboard until analysis on land. The samples were thawed at room temperature and measured by a Shimadzu TOC-L system coupled with a Shimadzu Total N analyzer in JAMSTEC. The standardization was achieved using glucose, and the analyses were referenced against the reference deep waters collected in the western subarctic Pacific. The deep waters were calibrated with DOC Consensus Reference Waters provided by Hansell Laboratory, University of Miami. The precision through the measurements was 2.4 μmol/kg. The relatively low precision might be due to the degradation of non-dispersive infrared light source, which could not be confirmed until recently.

FDOM measurement

Fluorescence excitation-emission matrices (EEMs) were measured onboard using the Horiba Scientific Aqualog after the samples were allowed to stand until reaching near laboratory temperature. Emission scans from 248 to 829 nm taken at 2.33-nm intervals were obtained for the excitation wavelengths between 240 and 560 nm at 5-nm intervals. The fluorescence spectra were scanned with a 12-s integration time and acquired in the high CCD gain mode. The following corrections of the fluorescence spectra were carried out: 1) the inner filter effect was corrected using the absorbance spectra measured simultaneously, and 2) fluorescence intensities were corrected for the area under the water Raman peak (excitation = 350nm), analyzed daily, and were converted to Raman Units (R.U.).

(4) Results of FDOM and DOC

The results of FDOM (FDOM370/440) for the single pair of excitation and emission wavelengths (370/440 nm) are shown, which are considered to be humic-like FDOM (Coble, 2007) (Figures 3.9.1, and 3.9.2). The FDOM370/440 results were similar to the apparent oxygen utilization profiles detailed elsewhere

in this data book and indicate that this type of FDOM is produced in the ocean interior during mineralization of organic matter.

The results of DOC are shown in Figures 3.9.3 and 3.9.4. In the deep waters, the gradual decrease in DOC concentrations was confirmed the Southern Ocean to the northern Indian Ocean. As explained above, the precision of DOC measurements had been relatively low during the measurement period. Even though we consider the low precision, the decrease in DOC concentrations in the deep waters is significant. The vertical distributions of DOC are similar to the other ocean basins, i.e., high in the upper ocean and low in the deep waters.

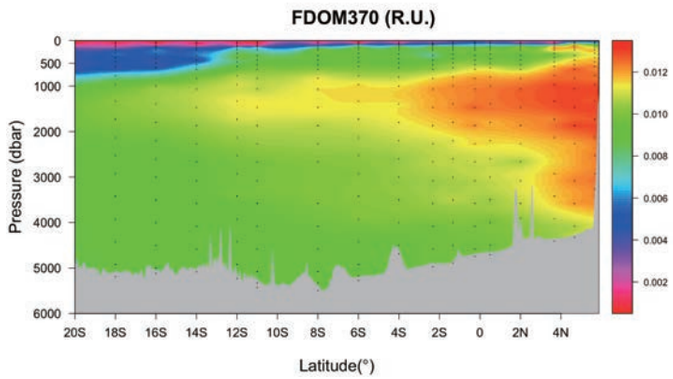

Figure 3.9.1 Contour map of FDOM370/440 during leg 2.

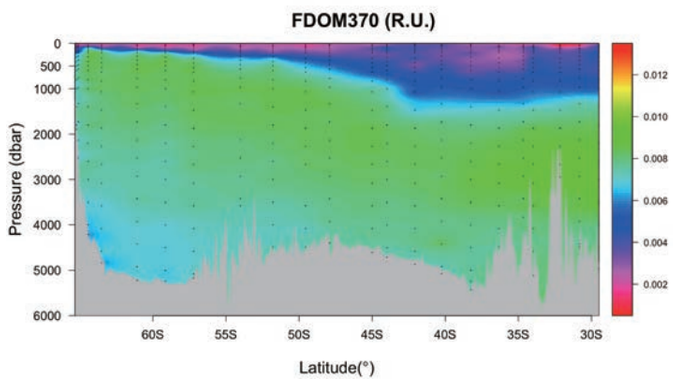

Figure 3.9.2 Contour map of FDOM370/440 during leg 3.

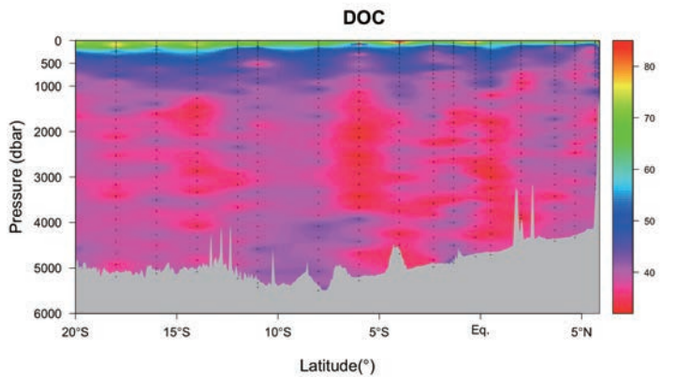

Figure 3.9.3 Contour map of DOC (μmol/kg) during leg 2.

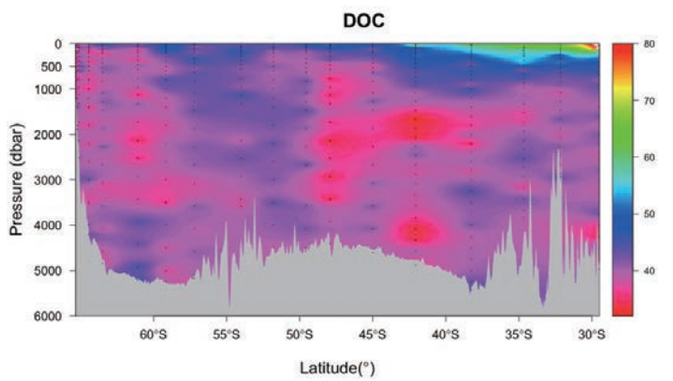

Figure 3.9.4 Contour map of DOC (μmol/kg) during leg 2.

3.10 Absorption Coefficients of Chromophoric Dissolved Organic Matter

(1) Personnel

Kosei Sasaoka (JAMSTEC) (Leg 2,3)

(2) Objectives

Oceanic dissolved organic matter (DOM) is the largest pool of reduced carbon, and its inventory in the ocean is approximately 660 Pg C (Hansell et al., 2009). Thus, investigating the behavior of oceanic DOM is important to exactly evaluate the carbon cycle in the ocean. Chromophoric dissolved organic matter (CDOM) play an important role in determining the optical properties of seawater, and the global CDOM distribution appears regulated by a coupling of biological, photochemical, and physical oceanographic processes all acting on a local scale, and greater than 50% of blue light absorption is controlled by CDOM (Siegel et al., 2002). Additionally, some investigators have reported that CDOM emerges as a useful tracer for diagnosing changes in the overturning circulation and evaluating DOM compositions, similar to dissolved oxygen (e.g., Nelson et al., 2010; Catala et al., 2015). The objectives of this study are to clarify the north-south distribution of light absorption by CDOM along the I08N (Leg 2) in the Indian Ocean and I07S (Leg 3) section in the Southern Ocean.

(3) Methods

Seawater samples for absorption coefficient of CDOM ($a_{cdom}(\lambda)$) were collected in 250ml bottles using Niskin bottles from surface to bottom at 11-24 sampling layers including a chlorophyll *a* maximum depth. CDOM samples were filtered using 0.2 μm Nuclepore polycarbonate filters on board. After filtration, optical densities of CDOM ($OD_{cdom}(\lambda)$) in seawaters between 190 and 600 nm were measured at 0.5 nm intervals by an UV-VIS recording spectrophotometer (UV-2600, Shimadzu Co.) onboard, using 10-cm pathlength quartz cells. Milli-Q water was used as a base line. The absorption coefficient of CDOM ($a_{cdom}(\lambda)$ (m^{-1})) was calculated from measured optical densities ($OD_{cdom}(\lambda)$) as follows:

$a_{cdom}(\lambda) = 2.303 \times OD_{cdom}(\lambda) / 0.1$ (0.1 is the cuvette path-length (m)).

(4) Preliminary results

Vertical profiles of CDOM (as absorption coefficient at 300 nm, unit = m^{-1}) at 18-stations along the I08N (Leg 2) section and at 23-stations along the I07S (Leg 3) section were shown in Fig. 3.10.1, and 3.10.2. Cross section of CDOM (as absorption coefficient at 300 nm, unit = m^{-1}) along the I08N (Leg 2) and I07S (Leg 3) were shown in Figure 3.10.3 and 3.10.4, respectively.

(5) References

Catala, T. S., et al., 2015, Turnover time of fluorescent dissolved organic matter in the dark global ocean, Nat. Com., 6, 1-8, doi:10.1038/ncomms6986.

Hansell, D. A., C. A. Carlson, D. J. Repeta, and R. Shlitzer, 2009, Dissolved organic matter in the ocean: A controversy stimulates new insight, Oceangr., 22, 202-211

Nelson, N. B., D. A. Siegel, C. A. Carlson, and C. M. Swan, 2010, Tracing global biogeochemical cycles and meridional overturning circulation using chromophoric dissolved organic matter, Geophys. Res. Lett., 37, L03610, doi:10.1029/2009GL042325.

Siegel, D.A., Maritorena, S., Nelson, N.B., Hansell, D.A., Lorenzi-Kayser, M., 2002, Global distribution and dynamics of colored dissolved and detrital organic materials. J. Geophys. Res., 107, C12, 3228, doi:10.1029/2001JC000965.

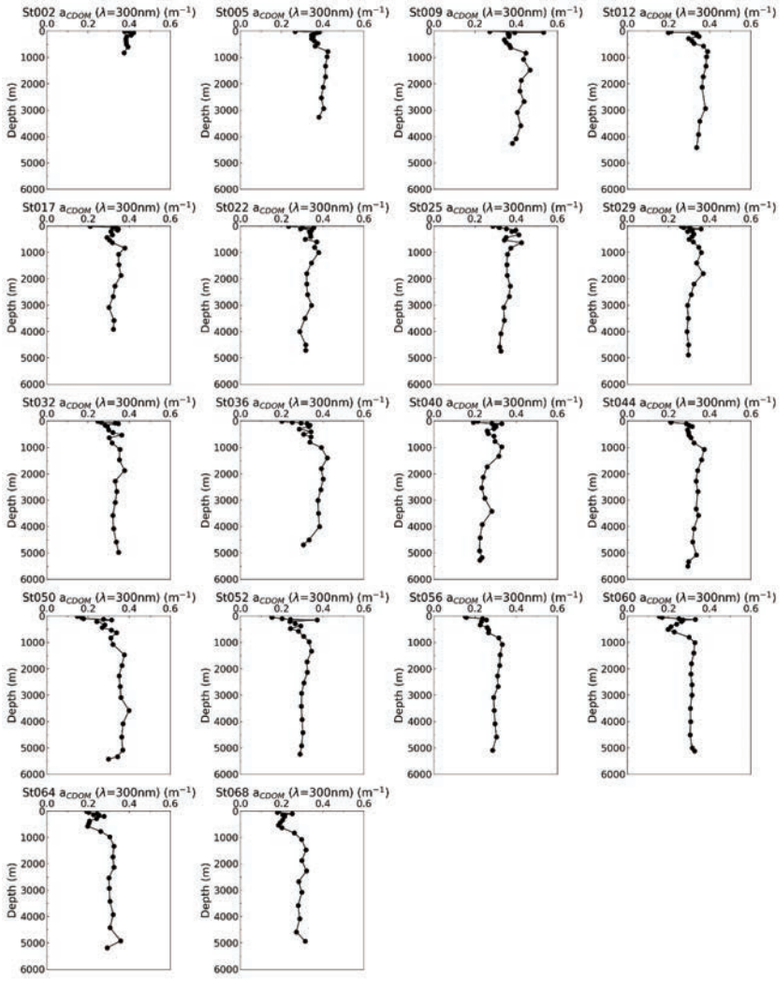

Fig.3.10.1 Vertical profiles of CDOM (as absorption coefficient at 300 nm, unit = m^{-1}) at 18-stations along the I08N section (Leg 2).

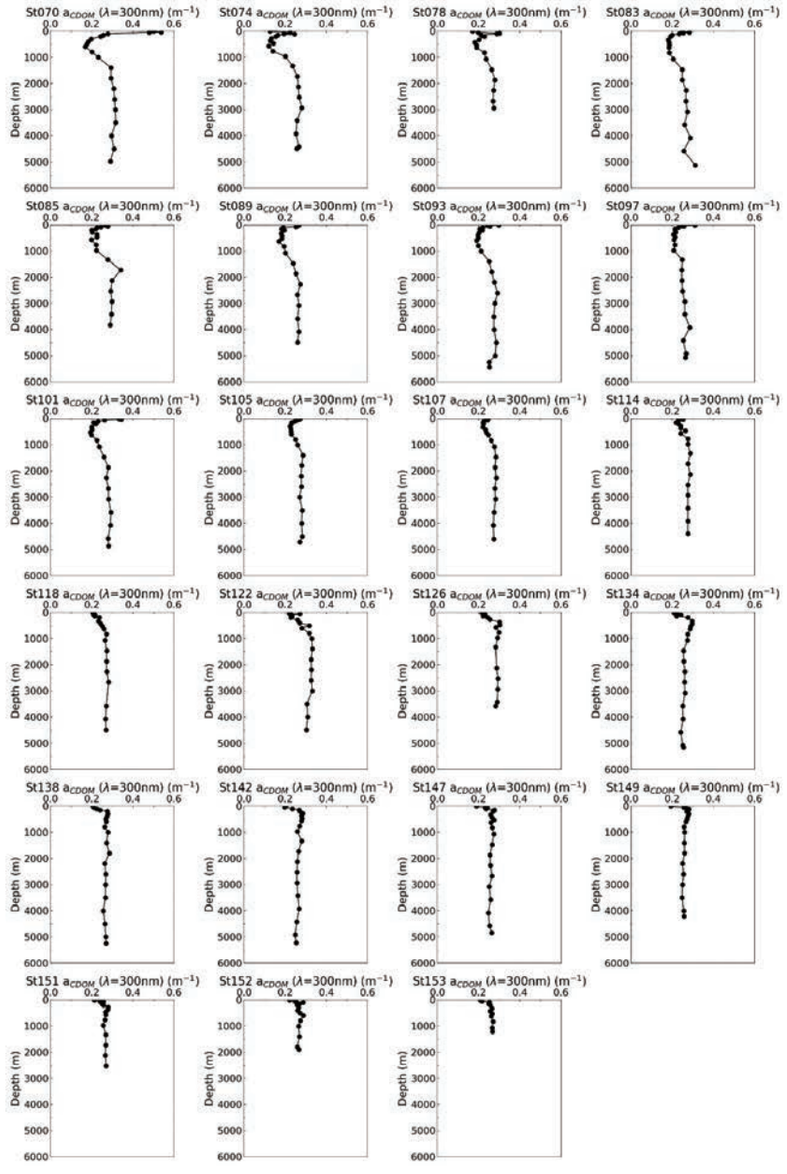

Fig.3.10.2 Vertical profiles of CDOM (as absorption coefficient at 300 nm, unit = m^{-1}) at 23-stations along the I07S section (Leg 3).

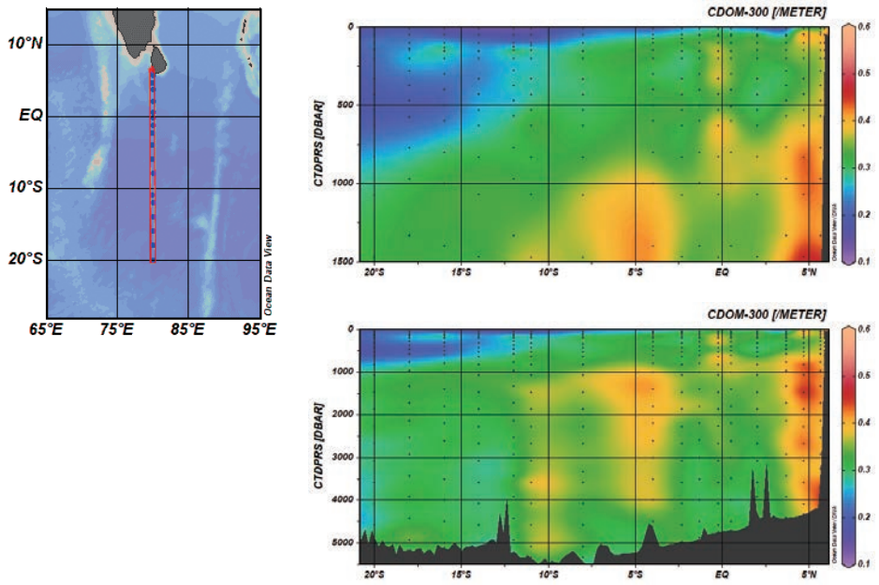

Fig.3.10.3 Sections of CDOM abundance (as absorption coefficient at 300 nm, unit = m^{-1}) along the I08N section (Leg 2) obtained from hydrographic casts. The top section covers surface to the bottom and the lower section covers the upper 1,500 m.

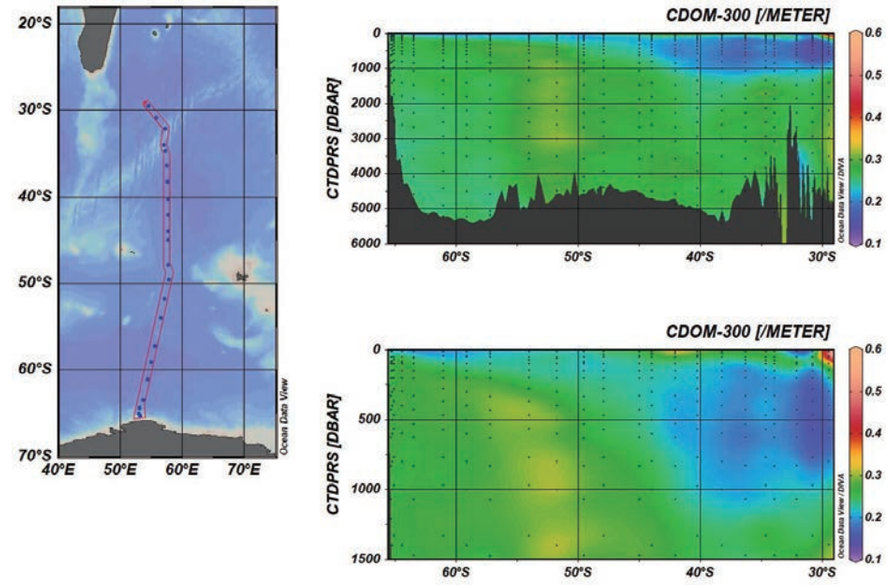

Fig.3.10.4 Sections of CDOM abundance (as absorption coefficient at 300 nm, unit = m^{-1}) along the I07S section (Leg 3) obtained from hydrographic casts. The top section covers surface to the bottom and the lower section covers the upper 1,500 m.

3.11 Lowered Acoustic Doppler Current Profiler

(1) Personnel

Shinya Kouketsu (JAMSTEC) (principal investigator)

Katsuro Katsumata (JAMSTEC)

(2) Overview of the equipment

Two acoustic Doppler current profilers (ADCP) were integrated with the CTD/RMS package. The lowered ADCP (LADCP)s, Workhorse Monitor WHM300 (Teledyne RD Instruments, San Diego, California, USA), which has 4 downward facing transducers with 20-degree beam angles, rated to 6000 m, make direct current measurements at the depth of the CTD, thus providing a full profile of velocity. The LADCP was powered during the CTD casts by a 48 volts battery pack. The LADCP unit was set for recording internally prior to each cast. After each cast the internally stored observed data were uploaded to the computer on-board. By combining the measured velocity of the sea water and bottom with respect to the instrument, and shipboard navigation data during the CTD cast, the absolute velocity profiles are obtained with the software implemented by A.Thunherr (available online at ftp://ftp.ldeo.columbia.edu/pub/LADCP; based on the method Visbeck 2002).

The instruments used in this cruise were as follows.

Teledyne RD Instruments, WHM300

S/N 24545 (downward looking), S/N 20754 (upward looking)

(3) Data collection

In this cruise, data were collected with the following configuration.

Bin size: 8.0 m

Number of bins: 12

Pings per ensemble: 1

Ping interval: 1.0 sec

The downloaded file fragmentation occurred at the stations of 41, 42, and 148 due to cable problems. The data from upward looking at the station 2, 5 and 71 and the downward looking data at the station 46 were lost due to operation problems. A part of data during the upcast was lost at station 8 due to battery shortage.

Reference

Visbeck, M. (2002): Deep velocity profiling using Lowered Acoustic Doppler Current Profilers: Bottom track and inverse solutions. *J. Atmos. Oceanic Technol.*, 19, 794-807.

3.12 Expendable Conductivity Temperature Depth profiler (XCTD)

(1) Personnel

Katsuro Katsumata (JAMSTEC) (principal investigator)

Kazuho Yoshida (NME)

Wataru Tokunaga (NME)

Satomi Ogawa (NME)

Takehito Hattori (MIRAI crew)

(2) Objective

With such restrictions as weather and shiptime, CTD/sampling observation were not performed at some stations and substituted with XCTD observations. At some CTD stations, XCTD-CTD side-by-side deployments were performed in order to calibrate the XCTD data in nearby and other stations following the method of Uchida *et al.* (2011).

(3) Instrumentation

The XCTDs used in this expedition were XCTD-4 and the deck unit was MK-150N, both from Tsurumi-Seiki Co., Ltd., Yokohama Japan. The manufacturer's specification of the accuracy is ±0.03 mS/cm, ±0.02 °C for conductivity and temperature, respectively. Depth is estimated by the elapsed time (seconds) from entry in to water as Z (m) = $at - bt^2$ with a=3.68081 (m/s) and b=4.7×10^{-4} (m/s^2). The manufacturer's specification of the accuracy for depth is the greater of 5 m or 2%.

(4) Deployments

Station numbers in the 400's are XCTD only stations. Otherwise, the XCTD were deployed side-by-side to the CTD casts which the station numbers designate. In a side-by-side deployment, an XCTD was deployed as the CTD passed approximately 250 dbar downcast. XCTD deployments were mostly performed from Auto Launcher. Due to the unfavourable wind direction, we used a hand launcher at some side-by-side stations. The Station name in the table below followed by 'H' designates those deployments with hand launcher.

The XCTD cast at Station 132 was misoperated and data from the upper 10 m were lost. The data were not used in the analysis.

Station	Date (UTC)	Time (UTC)	Latitude (deg-min)	Longitude (deg-min)	Depth [m]	SST [deg-C]	SSS [PSU]	Probe S/N
401	7/01/2020	8:36	-39:30.1462	57:42.8	5089	16.595	34.864	18117711
96	7/01/2020	10:17	-39:44.9476	57:43.5	5039	17.263	35.307	18117712
402	7/01/2020	14:18	-40:00.0431	57:44.3	4997	17.729	35.47	18117709
403	7/01/2020	21:01	-40:28.7446	57:44.9	4897	15.955	35.185	18117710
404	8/01/2020	2:47	-40:55.4518	57:44.7	4873	17.008	35.4	18117713
99H	8/01/2020	4:30	-41:09.6601	57:44.6	4889	17.06	35.472	18117714
405	9/01/2020	2:51	-42:46.2453	57:44.5	4760	15.244	35.058	18117715
103H	9/01/2020	4:42	-42:59.8214	57:43.9	4748	10.908	33.818	18117720
406	9/01/2020	9:25	-43:14.9899	57:44.4	4735	10.435	33.827	18117719
407	9/01/2020	15:15	-43:44.9967	57:45.2	4674	10.974	33.811	18117716
408	9/01/2020	21:47	-44:14.9936	57:46.0	4600	11.552	34.013	18117717
106	9/01/2020	23:29	-44:29.9881	57:46.4	4590	11.159	34.074	18117718
409	10/01/2020	3:26	-44:45.0021	57:46.8	4553	9.643	33.848	18117724
410	10/01/2020	10:05	-45:15.0196	57:47.6	4492	7.891	33.695	18117727
411	10/01/2020	16:24	-45:43.0525	57:46.7	4444	8.141	33.817	18117730
126	16/01/2020	5:40	-54:01.2103	56:30.0	3514	3.27	33.857	18117721
412	16/01/2020	10:50	-54:34.6886	56:20.1	4373	3.136	33.873	18117722
413	16/01/2020	14:17	-55:07.9922	56:10.2	3401	3.266	33.849	18117723
414	16/01/2020	17:32	-55:41.6559	56:02.3	3231	2.183	33.917	18117725
132H	17/01/2020	0:42	-56:15.0812	55:50.1	4765	1.926	33.893	18117728
137H	18/01/2020	8:31	-58:40.0252	55:07.1	5172	1.124	33.653	18117726
151	21/01/2020	18:43	-65:06.2154	53:01.0	2504	-0.195	33.727	18117729
415	22/01/2020	5:44	-65:21.9704	53:14.1	1318	-0.211	33.548	18117731
416	22/01/2020	6:05	-65:21.0914	53:14.8	1450	-0.363	33.533	18117732

(5) Calibration

The method employed here is that described in Uchida *et al.* (2011). We expect the biases in temperature and fallrate are common to all probes used in this cruise.

After smoothing and correcting the conductivity temporal delay, the comparison of fall rate from 7 side-by-side CTD casts suggests a fall rate error of -0.02 m s^{-1} in the terminal velocity, although there are some scatter amongst stations in the fall rate correction which maximised the correlation between the band-pass-filtered CTD and XCTD temperature profiles (Fig. 3.12.1). The scatter gives an impression that our expectation of uniform fallrate bias was optimistic. In fact, the grounding depths at stations 415 and 416 were respectively 1318 and 1450 m, estimated from the density corrected multibeam echo sounder. The XCTD's recorded 1319.67 and 1474.64 m, respectively, as the deepest valid measurement, were corrected to 1312 and 1465 m, respectively.

When the depth bias is corrected, the temperature difference between side-by-side CTDs and XCTDs are approximately 0.02±0.005 °C for deep layers ($z > 1800$ m). See Fig. 3.12.2. This positive bias is subtracted from all measurements.

For salinity, it is likely that the bias is different from probe to probe. If a tight TS relationship common to a side-by-side station and surrounding XCTD only stations exists within the depth of XCTD reach, it is possible to determine the probe-dependent bias, but such relationship could not be found. We therefore use the TS diagram below 1000 m from the side-by-side casts to estimate the salinity bias common to all probes used in this cruise. We identify a part of the TS curve which is smooth and shows one-to-one relationship between T and S. Namely, between 2.6 and 3.0 °C (station 96); 4.5 and 6.5 °C (station 99); 2.4 and 2.7 °C (station 103); 2.4 and 2.7 °C (station 126); 1.4 and 2.2 °C (station 126); 0.8 and 1.6 °C (station 137); and 0.12 and 0.22 °C (station 151). Depth correction and temperature bias correction have been applied to the XCTD data. The resultant salinity bias is +0.0150±0.006. This positive bias is subtracted from the XCTD salinity.

Reference

Uchida, H., K. Shimada, T. Kawano, 2011, A method for data processing to obtain high-quality XCTD data, *J. Atmospheric and Oceanic Technology*, 28, 816—826, doi:10.1175/2011JTECHO795.1.

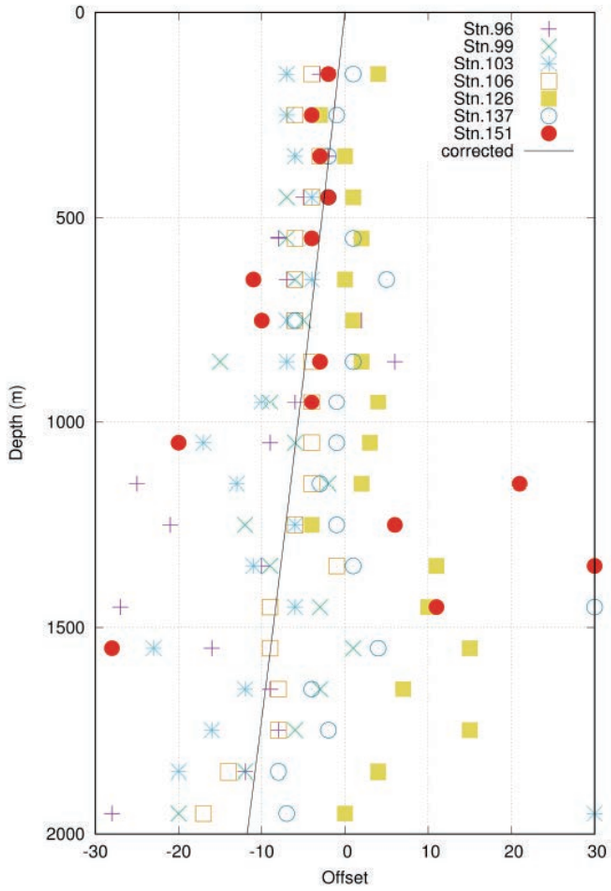

Fig. 3.12.1 Offset in meters needed to maximize correlation between the band-pass-filtered XCTD and CTD temperatures in side-by-side deployments.

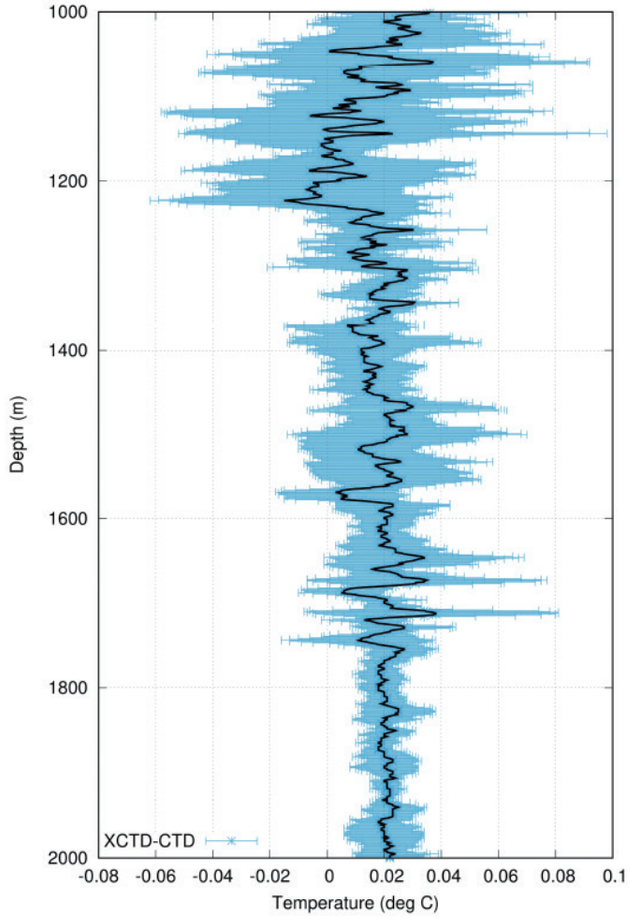

Fig. 3.12.2 After depth correction, mean (black) and standard deviation (blue) of difference between XCTD and CTD in temperature in side-by-side deployments.

3.13 Urea and Iodate Analyses

06 December 2020 ver.1.0

(1) Personnel

LEG 2

Peter CROOT (Earth & Ocean Sciences, National University of Ireland Galway, Ireland.)

LEG 3

Maija HELLER (Facultad de Ciencias del Mar y Geografía, Pontificia Universidad Católica de Valparaíso, Chile.)

(2) Objectives

The key objectives of this work were to obtain data on two less well studied chemical species, iodate (IO3-) and urea (CO(NH2)2), for which there are little or no data from the Indian Ocean nor any basin scale overview for any of the ocean basins currently available. The rationale for measuring these two species together on a GO-SHIP basin scale expedition, is that they conceptually represent different aspects (and related hypotheses), concerning nutrient regeneration in the ocean (L'Helguen et al., 2005; Tian et al., 1996) and the depths at which it is occurring. These datasets will also provide baselines for ongoing ocean and atmospheric modelling efforts into the nitrogen and iodine cycles. Importantly, both analytes can be measured at sea relatively quickly and cheaply, using spectrophotometric techniques, and this then provides a good test case for involving scientists from countries making their first steps in GO-SHIP related activities that can likely be replicated in the future with other groups.

Urea is a small nitrogen containing organic molecule, for which recent studies have shown plays an important role in the marine nitrogen cycle, as it is rapidly turned over in the environment and acts as a nitrogen shuttle within the microbial loop. Urea is mostly produced in the ocean via excretion from heterotrophic organisms of all size classes from bacteria upwards, this urea provides a source of bioavailable nitrogen for heterotrophic bacteria, cyanobacteria and eukaryotic phytoplankton. There are only a few published reports for Urea in near surface waters from the oligotrophic Indian Ocean (Baer et al., 2019) and Indian sector of the Southern Ocean (Thomalla et al., 2011) with concentrations ranging from below detection (less than 10 nM) in the oligotrophic tropics up to 2.5 µM in the region between the subtropical front and the subantarctic front. While the turnover time for urea is on the order of days and it is thus a rather transient species, this GO-SHIP expedition provides a good opportunity to obtain basic scale data on urea across a wide range of marine ecosystems with differing nitrogen dynamics.

Iodate is the thermodynamically stable form of iodine in oxygenated seawater. It is however easily reduced to iodide by UV radiation, chemical reductants and bacterial/phytoplankton metabolism (Bluhm et al., 2010). The re-oxidation of iodide to iodate is facilitated by O_2 and H_2O_2 but is significantly slower than the reduction step with a half life of around 70 days in oligotrophic tropical regions (Campos et al., 1996). The redox cycling between iodate and iodide resulting in a small but significant release of volatile halogen species of intermediate redox state (e.g. I_2, HOI, CH_3I etc) from the surface ocean to the atmosphere. Interest in the marine cycling of iodine has grown over the last decade because of discovery of the role of marine sources of iodine to the atmosphere, where upon the iodine is a major sink for ozone and the resulting IO produced is a source of new particles that can act as cloud condensation nuclei (Saiz-Lopez et al., 2011).

The development of satellite methods to measure IO in the atmosphere (Schönhardt et al., 2016; Schonhardt et al., 2008) have also highlighted the strong link between iodine speciation in seawater and atmospheric IO concentrations. Recently published overviews of iodine distributions in the ocean, show a distinct lack of data in the Indian ocean (Chance et al., 2014; Sherwen et al., 2019), while there is data for the Southern Ocean only from the Atlantic sector of the Southern Ocean (Bluhm et al., 2011; Campos et al., 1999). This lack of data is further highlighted by the publication of a recent shipboard study of IO in the Indian Ocean using a MAX-DOAS instrument (Mahajan et al., 2019) where the iodide concentrations were modelled according to algorithms based on existing datasets for other regions. Thus, the opportunity to obtain a basic scale distribution for iodate in the Indian Ocean is very timely.

The specific objectives of analyses for urea and iodate during the R/V Mirai MR1904 cruise (Leg2 – I08N) (Leg3 – I07S), were as follows;

Leg2

- Investigate if urea concentrations are elevated in the equatorial upwelling region.
- Investigate the potential relationship between urea/iodate and the deep chlorophyll maximum
- Determine if iodate concentrations are reduced in the low oxygen waters close to Sri Lanka.
- Examine the latitudinal distribution of iodate in surface waters to better understand the role of photochemistry on the reduction to iodide.
- Determine is iodate concentration varies between intermediate water masses in the central Indian Ocean.

Leg3

- Describe the distribution of urea across the Polar zones in the Indian sector of the Southern Ocean
- Investigate if urea is found at elevated concentrations in the Polar Front as has been observed in other parts of the Southern Ocean.
- Examine the relationships between urea and ammonia as to their potential for tracers of nutrient regeneration in the meso-pelagic zone.
- Investigate the relationship between iodate and other nutrients in the photic zone as a function of latitude, does Iodate behave as nutrient?

(3) Summary of analysis for Urea and Iodate

Samples were only taken from the 36 bottle CTD rosette during the expedition and we took only 18 samples from each cast covering the upper water column. Overall, we measured 18 stations during Leg 2 and 21 stations during Leg 3 for a total of 693 (336+357) samples for urea and 691 (334+357) for iodate. The station locations for urea and iodate measurement is shown in Figure 3.13.1, Figure 3.13.2, Table 3.13.1 and Table 3.13.2.

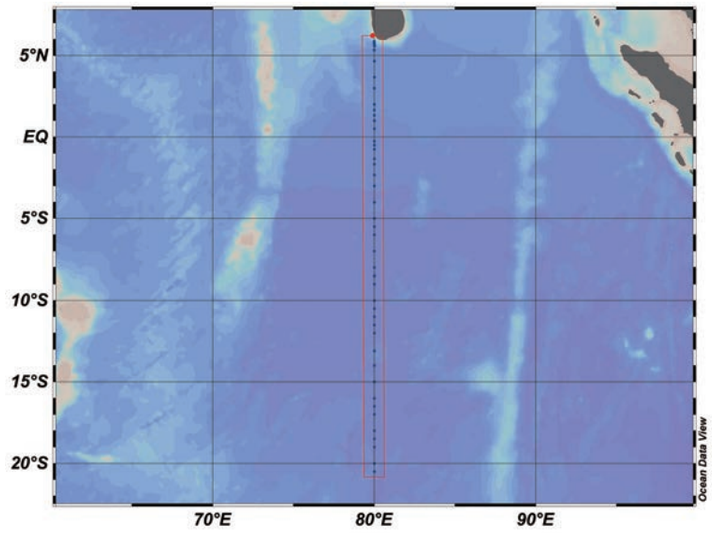

Figure 3.13.1 Sampling positions of urea and iodate samples in MR1904Leg2 (I08N).

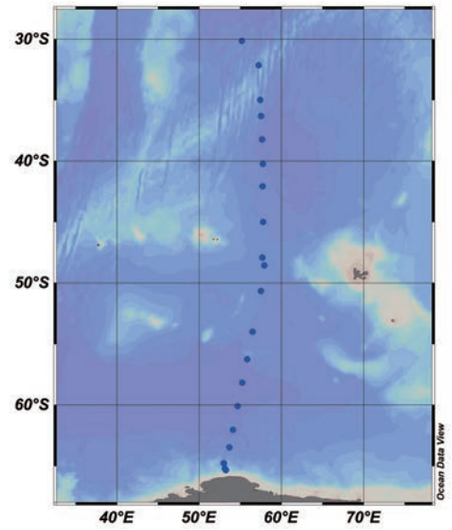

Figure 3.13.2 Sampling positions of urea and iodate samples in MR1904Leg3 (I07S).

Table 3.13.1 List of stations of MR1904Leg2 (I08N)

Station	Cast	Date (UTC)	Position*		Depth (m)
		(mmddyy)	Latitude	Longitude	
002	1	120519	5-52.31N	79-59.22E	824
005	1	120619	5-39.95N	80-00.40E	3233
007	1	120619	5-19.97N	79-59.75E	4147
012	1	120719	3-40.31N	80-00.04E	4358
017	1	120819	2-00.07N	80-00.05E	3875
022	1	120919	0-30.16N	80-00.12E	4651
025	1	121019	0-15.07S	80-00.33E	4683
029	1	121119	1-20.05S	80-00.05E	4834
036	1	121219	4-00.12S	79-59.84E	4630
042	1	121419	7-00.02S	79-59.94E	4917
046	1	121619	9-00.02S	79-59.95E	5207
048	1	121619	10-00.01S	79-59.98E	5383
052	1	121719	12-00.01S	80-00.01E	5159
054	1	121819	13-05.81S	80-00.04E	5003
058	1	121919	14-59.93S	80-00.12E	5111
062	1	122019	16-59.91S	80-00.06E	5072
066	1	122119	18-59.82S	79-59.99E	4946
068	1	122119	20-00.01S	80-00.01E	4866

Table 3.13.2 List of stations of MR1904Leg3 (I07S)

Station	Cast	Date (UTC)	Position*		Depth (m)
		(mmddyy)	Latitude	Longitude	
072	1	010120	30-09.31S	55-11.21E	4704
076	1	010220	31-29.07S	56-33.55E	4787
078	1	010220	32-08.99S	57-15.01E	2918
086	1	010520	35-00.02S	57-25.07E	4820
089	1	010520	36-20.02S	57-32.53E	4421
093	1	010620	38-15.36S	57-39.32E	5347
097	1	010720	40-14.98S	57-44.98E	4997
101	1	010820	42-04.75S	57-45.14E	4797
107	1	010920	45-00.07S	57-47.24E	4538
114	1	011220	47-55.12S	57-41.06E	4332
116	1	011220	48-33.64S	57-55.90E	4481
120	1	011420	50-40.49S	57-29.87E	4515
126	1	011620	54-01.24S	56-29.93E	3496
132	1	011720	56-15.08S	55-50.16E	4746
136	1	011820	58-11.14S	55-15.82E	5192
140	1	011920	60-07.23S	54-41.19E	5147
144	1	012020	62-03.31S	54-06.25E	5058
147	1	012020	63-30.11S	53-40.64E	4758
150	1	012120	64-46.99S	52-59.27E	3437
152	1	012220	65-13.45S	53-07.85E	1880
153	1	012220	65-20.20S	53-15.16E	1205

(4) Instrument and Method

(4.1) Analytical details

During MR19-04 all measurements were made using manual wet chemistry with subsequent spectrophotometric analysis. Chemical reagents were pre-weighed in the laboratory at the National University of Ireland Galway, before being airfreighted to Japan for loading on the vessel prior to departure.

For MR19-04 we adapted existing methods using a single reagent (COLDER) (Alam et al., 2017) for dissolved urea and that for nanomolar levels using a Liquid Waveguide Capillary Cell (LWCC) (Chen et al., 2015), applying it to small volume samples (2 mL or less) and removing the need for a 70° or 85° water bath by utilizing a thermostated dry bath (Fisher Scientific) instead. Both an LWCC-3050 (pathlength 48.9 cm) and LWCC-3250 (pathlength 252 cm) were used for this work with the following optical setup: Ocean Optics DH-Mini Light Source and an Ocean Optics Maya 2000Pro Spectrophotometer, the LWCC was connected to the light source and spectrophotometer via Ocean Optics 400 µm optical fibres (QP400-025-SR). Samples were pulled through the LWCC using a 10 mL Teflon Syringe (Savillex 700-510) connected via Teflon tubing (Upchurch) and Luer fittings (Upchurch). The use of a dry bath and small volume samples significantly reduces the risks in this analysis but does not completely eliminate them as sulfuric acid is still required in this procedure. Care was taken at all times to minimize contamination in the laboratory, particularly during filtration of the samples.

Iodate was measured using a simple spectrophotometric method (Jickells et al., 1988) based on the earlier work of Truesdale (Truesdale, 1978; Truesdale and Smith, 1979; Truesdale and Spencer, 1974) which has been adapted by us for use with small volumes (2 mL or less). Briefly sulfamic acid is added to lower the pH and destroy any nitrite that may interfere in the analysis, and after a suitable period of time (150 seconds), a 10% solution of KI is added which results in the following reaction:

$$IO_3^- + 5\,I^- + 6H^+ \rightarrow 3I_2 + 3H_2O$$

$$I_2 + I^- \rightleftharpoons I_3^-$$

The resulting I_3^- that is formed has two major absorption bands (288 and 350 nm) and we use these to quantify the iodate concentration in the sample. Previously for iodate, pathlengths of 5 or 10 cm have been used, for this work we employed an LWCC-3050 with a pathlength of 48.9 cm which allows then a higher precision analysis over the complete range of expected iodate concentrations but while still being in the linear range for the instrumental setup. The LWCC-3050 was setup with the same spectrophotometer and light source as described above for the IOP measurements, with the exception that 400 µm diameter solar resistant fiber optic cables were used instead. The resulting I_3- that is formed has two major absorption bands (288 and 350 nm) and we use these to quantify the iodate concentration in the sample. Previously for iodate, pathlengths of 5 or 10 cm have been used, for this work we employed an LWCC-3050 with a pathlength of 48.9 cm which allows then a higher precision analysis over the complete range of expected iodate concentrations but while still being in the linear range for the instrumental setup.

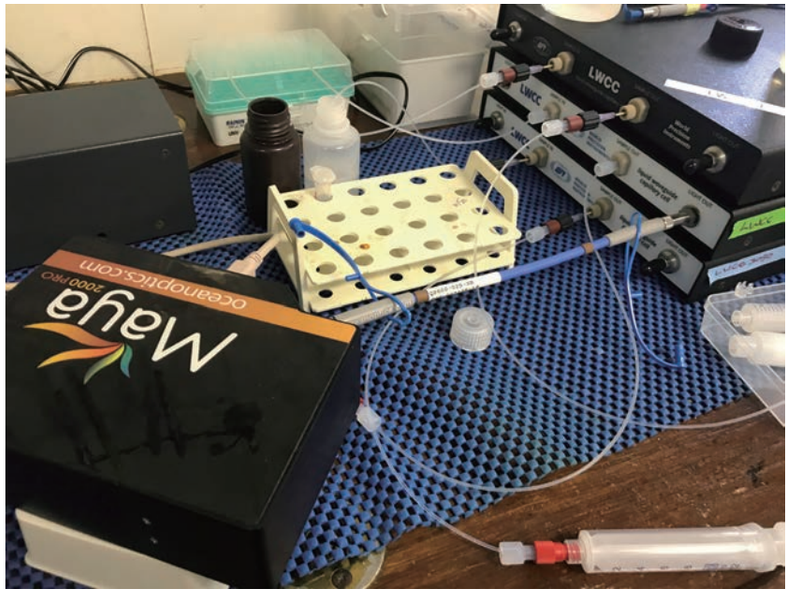

Figure 3.13.3 Set up of Analytical system for spectrophotometric analysis of Urea and Iodate employed during MR19-04.

(4.2) Urea Reagents

DAMO: Monoxime solution was prepared by dissolving 3.4 g of the pre-weighed diacetyl monoxime (CH3–CO–CNOH–CH3; Supelco 31550 Batch BCBZ8537) in 100 mL of Milli-Q (MQ) Ultrapure water.

TSC: Thiosemicarbazide solution was prepared by dissolving 0.19 g of the pre-weighed thiosemicarbazide (NH2–CS–NH–NH2; Sigma 89050 Batch BCBT8461) in 20 mL of MQ water. It apparently has not been noted in earlier works but TSC is only sparingly soluble in water: 10 mg/mL at 20°C (Santa Cruz Biotechnology). During Leg 2 the TSC was initially in the fridge but it kept precipitating out, so it was kept in the lab.

Iron solution: 0.15 g of Ferric Chloride (FeCl3; Sigma) is dissolved in 10 mL of MQ water.

Diluted Sulfuric Acid Solution: 240 mL of 95% concentrated Sulfuric acid (Wako 192-04696 Lot ECP4495) is slowly added to 188 mL of MQ in a 500 mL Teflon Bottle in the fumehood next to the laboratory. EXTREME CAUTION required: The reaction of concentrated sulfuric acid with water is an extremely exothermic reaction and the bottle will heat up very quickly, it is best to slowly add the acid to the MQ over the course of an hour or so, to reduce the risk of boiling or spitting of acid. Note that the heat generated will melt LDPE bottles so never use them with concentrated or slightly diluted sulfuric acid solutions.

Standard COLDER Preparation:

Reagent A: Reagent A was prepared by mixing 3.66 mL of the DAMO solution with 146 µL of the TSC solution (25:1 mix) in a 30 ml LDPE bottle.

Reagent B: Reagent B was prepared by adding with 90 µL of the Ferric chloride solution to 100 mL of the diluted sulfuric acid in a Teflon Bottle (125 mL capacity).

COLDER Reagent (for 30 samples): The COLDER was prepared by adding 12.2 mL of reagent B directly into the Reagent A bottle. The COLDER reagent was used immediately (see below).

For **Trace-level seawater** (< 200 nM) samples the preparation of the COLDER reagent was altered as follows:

Reagent A: Reagent A was prepared by mixing 1.83 mL of the DAMO solution with 60 µL of the TSC solution (25:1 mix) in a 30 ml LDPE bottle.

Reagent B: Reagent B was prepared as indicated above.

COLDER Reagent (for 30 samples): The COLDER was prepared by adding 12.2 mL of reagent B directly into the Reagent A bottle. The COLDER reagent was used immediately (see below).

(4.3) Iodate Reagents

10% Potassium Iodide solution: Dissolve the pre-weighed 10 g amount (Sigma 60399 Batch BCBX6003) in 100 mL of MQ water, this solution should be kept in a light tight bottle (Brown HDPE) as it will oxidize to iodine in sunlight.

1.5 M Sulfamic acid solution: Dissolve the pre-weighed ~14.565 g amount (Sigma 383120 Batch BCBX0752) in 100 mL of MQ water

(4.4) Sampling procedures – Urea and Iodate

Sampling of urea and iodate followed that of oxygen, salinity and trace gases. Samples were drawn into a single 125 mL amber HDPE Nalgene round bottle without sample drawing tubes. The bottles were rinsed three times before filling and then capped immediately after the drawing of the sample. When the rosette sampling was completed, all samples from the cast were returned to the laboratory and immediately filtered by hand through a 0.2 µm syringe filter (25 mm Sarstedt Filtropur S) into 30 or 60 mL LDPE Nalgene bottles.

(4.5) Analysis procedures - Urea

Analysis for urea was undertaken using filtered seawater according to the following protocol.

1. add 1.54 ml (2 x 770 µL) of seawater sample in an Eppendorf clear vial (2 mL)
2. add 460 µl of the freshly prepared COLDER reagent to the vial
3. Place the vials in the dry bath heater block.
4. Start the dry bath temperature cycle (heat up to 70°C and then stay at that temperature for one hour before switching off.
5. Allow 30-40 minutes to cool before measuring the absorbance using the LWCC-3050 system as described above and save the data in Spectrasuite (Ocean Optics).

(4.6) Analysis procedures - Iodate

Analysis for iodate was undertaken using filtered seawater according to the following protocol.

1. add 1.8 ml (2 x 900 µL) of sample in an Eppendorf amber vial (2 mL)
2. add 45 µl of 1.5M sulfamic acid
3. mix and allow to react for exactly 2.5 min
4. add 135 µl of a 10% potassium iodide solution
5. measure the absorbance after 2 min and save the spectra in Spectrasuite

(4.7) Data processing

Raw data for each analysis was converted from the processed Spectrasuite file into text files and then uploaded into Matlab™ (Mathworks) and analyzed using specific Matlab scripts for each analyte. Absorbance values for the respective analyte peaks were reported relative to that of a non-absorbing wavelength (for this work the absorbance at 700 nm). After this baseline correction had been applied, the standard curve was generated from the standard runs and the slope and intercept were calculated using linear regression. The concentration in each sample was then calculated using the same slope as from the standard run and corrected for the appropriate sample blank.

(5) Certified Reference Material of Urea and Iodate in seawater

There currently are no Certified Reference Materials (CRMs) available for urea or iodate in seawater at open ocean concentrations (nM levels). Accuracy of the method is therefore estimated using standard additions to seawater solutions and comparison to standards prepared in ultrapure water.

(6) Urea and Iodate standards

(6.1) Volumetric laboratory ware for use with at sea primary and working standards

The primary urea standard was produced by dilution of a pre-weighed urea standard (see below) using a calibrated 10 mL pipette (Finnpipette). Working solutions were prepared by serial dilution of the primary standard. The primary iodate standard was used as provided by the chemical supplier. Working standard for iodate were prepared by serial dilution of the primary standard.

Pipettes and pipettors: All pipettes (Finnpipette) were gravimetrically calibrated pre- and post-expedition on land. in order to verify and improve upon the nominal tolerance. Each pipette used during the expedition was identified by its lab number and manufacturers serial number.

(6.2) Reagents, general considerations

Specifications: For urea standard, ACS reagent (99.0-100.5%) U5128 provided by Sigma, Lot. SZBE0650V, CAS No.: 57-13-6, was used (Specification from Sigma 100.3%). For the iodate standard, we use 0.05 M Iodate solution 34274 provided by Sigma, Lot. SZBC0180V, CAS No.: 7758-05-6. (Specification from manufacturer is 50.0 ± 0.1 mM).

Ultra pure water: Ultra pure water (MilliQ water) freshly drawn was used for preparation of reagents, standard solutions and for measurement of reagent and system blanks.

(6.3) Concentrations of urea standards

Primary UREA Standard: A standard solution of urea ($CO(NH_2)_2$; Sigma) is prepared by dissolving 0.6 g of the pre-weighed Urea to 100 mL of MQ. This results in an 0.1 M primary solution. This solution is stored at 4 °C in an LDPE bottle; it can remain stable for more than 1 year.

Working standard (0-1 µM): A working standard solution (20 µM) is created by adding 20 µL of the primary standard to 100 mL of MQ.

Working standard low level (0-200 nM): A secondary standard (400 µM) is produced by the addition of 80 µL of the primary standard to 20 mL of MQ. A working standard (3.985 µM) is then created by the addition of 200 µL of the secondary standard to 20 mL of MQ.

(6.4) Concentrations of iodate standards

Primary Iodate Standard: The primary Iodate solution was 0.05 M as described above.

Working standard: A working standard solution (10 µM) is created by adding 20 µL of the primary standard to 100 mL of MQ.

Table 3.13.3 Nominal concentrations of urea for high level working standard solutions

Std#	MQ (µL)	Work (µL)	Reagent (µL)	[Urea] nM
1	1540	0	460	0.0
2	1520	20	460	200.0
3	1500	40	460	400.1
4	1480	60	460	600.1
5	1460	80	460	800.1
6	1440	100	460	1000.1

Table 3.13.4 Nominal concentrations of urea for low level working standard solutions

Std#	MQ (µL)	Work (µL)	Reagent (µL)	[Urea] nM
1	1540	0	460	0.0
2	1520	20	460	39.8
3	1500	40	460	79.7
4	1480	60	460	119.5
5	1460	80	460	159.4
6	1440	100	460	199.2

Table 3.13.5 Nominal concentrations of Iodate standard solutions

Std#	MQ (µL)	Work (µL)	Reagent (µL)	[Iodate] nM
1	1800	0	180	0
2	1780	20	180	101
3	1760	40	180	202
4	1740	60	180	303
5	1720	80	180	404
6	1700	100	180	505

(6.5) Renewal of in-house standard solutions.

Working standard solutions as stated above were renewed as shown in Table 3.13.6

Table 3.13.6 Timing of renewal of working standards.

Chemical Species	Renewal
Urea	Every 2 weeks
Iodate	Every week

(7) Quality control

(7.1) Reagent Blank determination, detection limits, sensitivity and linearity of response

Determination of the reagent blank for Urea is complicated by two factors: (i) the reagents themselves absorb at the analytical wavelength employed for determination of the reaction product of urea and (ii) because the MQ water used for analysis often contains significant urea at nM level as it is not removed by ion exchange nor is it destroyed by the UV irradiation employed in most systems. In the present work we found that the reagent baseline was related to the amount of TSC used in the assay and this was the reason why we decreased the TSC added to the assay for the open ocean samples. The amount of TSC present in the reagent also effected the sensitivity of the analysis (see section 4.2, absorbance reported at 525 nm): High standard setup $\varepsilon = 27150 \pm 1740$ L mol^{-1} cm^{-1} (n =8), Low standard setup $\varepsilon = 20540 \pm 4918$ L mol^{-1} cm^{-1} (n=35). Analysis of MQ blanks indicated higher concentrations of urea in the MQ than in most of the seawater samples measured during the expedition 129.3 ± 2.5 nM (n=6). A detection limit of 7.5 nM was calculated for the urea analysis.

The reagent blank for the Iodate reagents in MQ was determined to be 12.2 ± 2.4 nM (n=12) and represents a detection limit for iodate of 7.2 nM, significantly below the global mean deep water iodate concentration of approximately 450 nM. The high concentration of iodate found in deep sea water results in the signal observed using a 50 cm LWCC having an absorbance of approximately 1.69, this is still within the linear range on the instrumentation we used, as we found that the response was linear up to an absorbance of 2. The apparent sensitivity for Iodate, as determined by standard additions and the formation of I_3^- and analysis of the peak at 353 nm, was found to be $\varepsilon = 70000 \pm 5000$ L mol^{-1} cm^{-1} (n=35). This result is consistent with previous work using shorter pathlength systems for determining iodate in seawater.

(7.2) Precision of urea and iodate analyses during this cruise

The precision of urea and iodate analyses during this cruise were evaluated based on triplicate measurements of samples performed on 3-4 samples at selected stations. A summary of the results is given below in Table 3.13.7. The precision for urea was satisfactory given the very low concentrations of urea that were found in seawater throughout this expedition, where typically they were 20-80 nM, thus above the detection limit but often just at the quantification limit. In general the precision for iodate was much better as the observed signal was significantly above the detection limit.

Table 3.13.7 Summary of precision based on the replicate analyses performed during MR19-04

	Urea CV%	Iodate CV%
Median	11.4	1.7
Mean	14.6	2.4
Maximum	41.7	5.3
Minimum	1.8	0.7
N	30	12

(8) Problems / improvements occurred and solutions

(8.1) Urea Blanks – lack of CRMs

The issue of the blank in MQ for urea had not previously been reported in shipboard work, though it is well known from semi-conductor and electronics industry, and this is something that should be considered in the future along with the development of CRMs for urea in seawater.

(8.2) Generation of I_3^- due to UV photo-oxidation of I^-

The analytical system used during MR19-04 had a significant amount of UV light emitted by the Deuterium lamp employed as a light source. This UV light caused significant photo-oxidation of the I^- in the Iodate samples resulting in an increase in the observed I_3^- if the sample was left exposed in the LWCC. A flowing solution was not impacted significantly but the low volume method used here meant that the sample could easily run dry in the time span of a measurement. The use of optical filters to remove the high energy UV but retain the I_3^- analytical wavelengths could help to reduce the effect of photo-oxidation and trials on this are currently underway.

(9) Data archive

All data has been submitted to JAMSTEC Data Management Office (DMO) and is currently under its control.

References

Alam, M.S., Casareto, B.E., Suzuki, Y., Sultana, R. and Suzuki, T., 2017. Optimization of dissolved urea measurements in coastal waters with the combination of a single reagent and high temperature. Journal of Oceanography, 73(2): 249-258.

Aminot, A. and Kerouel, R., 1982. Dosage automatique de l'urée dans l'eau de mer : une méthode très sensible à la diacétylmonoxime. Canadian journal of fisheries and aquatic sciences, 39: 174-183.

Baer, S.E. et al., 2019. Carbon and nitrogen productivity during spring in the oligotrophic Indian Ocean along the GO-SHIP IO9N transect. Deep Sea Research Part II: Topical Studies in Oceanography, 161: 81-91.

Bluhm, K., Croot, P., Wuttig, K. and Lochte, K., 2010. Transformation of iodate to iodide in marine phytoplankton driven by cell senescence. Aquatic Biology, 11(1): 1-15.

Bluhm, K., Croot, P.L., Huhn, O., Rohardt, G. and Lochte, K., 2011. Distribution of iodide and iodate in the Atlantic sector of the southern ocean during austral summer. Deep Sea Research Part II: Topical Studies in Oceanography, 58(25-26): 2733-2748.

Campos, M., Farrenkopf, A.M., Jickells, T.D. and Luther, G.W., 1996. A comparison of dissolved iodine cycling at the Bermuda Atlantic Time-Series station and Hawaii Ocean Time-Series Station. Deep-Sea Research Part Ii-Topical Studies In Oceanography, 43(2-3): 455-466.

Campos, M., Sanders, R. and Jickells, T., 1999. The dissolved iodate and iodide distribution in the South Atlantic from the Weddell Sea to Brazil. Marine Chemistry, 65(3-4): 167-175.

Chance, R., Baker, A.R., Carpenter, L. and Jickells, T.D., 2014. The distribution of iodide at the sea surface. Environmental Science: Processes & Impacts, 16(8): 1841-1859.

Chen, L., Ma, J., Huang, Y., Dai, M. and Li, X., 2015. Optimization of a colorimetric method to determine trace urea in seawater. Limnology and Oceanography: Methods, 13(6): 303-311.

Helms, J.R. et al., 2008. Absorption spectral slopes and slope ratios as indicators of molecular weight, source, and photobleaching of chromophoric dissolved organic matter. Limnology and Oceanography, 53: 955-969.

Jickells, T.D., Boyd, S.S. and Knap, A.H., 1988. Iodine Cycling in the Sargasso Sea and the Bermuda Inshore Waters. Marine Chemistry, 24: 61-82.

L'Helguen, S., Slawyk, G. and Le Corre, P., 2005. Seasonal patterns of urea regeneration by size-fractionated microheterotrophs in well-mixed temperate coastal waters. Journal of Plankton Research, 27(3): 263-270.

Mahajan, A.S. et al., 2019. Observations of iodine oxide in the Indian Ocean marine boundary layer: A transect from the tropics to the high latitudes. Atmospheric Environment: X, 1: 100016.

Reay, M.K. et al., 2019. High resolution HPLC-MS confirms overestimation of urea in soil by the diacetyl monoxime (DAM) colorimetric method. Soil Biology and Biochemistry, 135: 127-133.

Saiz-Lopez, A. et al., 2011. Atmospheric Chemistry of Iodine. Chemical Reviews, 112(3): 1773-1804.

Schönhardt, A., Richter, A. and Burrows, J.P., 2016. TIBAGS: Tropospheric Iodine Monoxide and Its Coupling to Biospheric and Atmospheric Variables—a Global Satellite Study. In: D. Fernández-Prieto and R. Sabia (Editors), Remote Sensing Advances for Earth System Science: The ESA Changing Earth Science Network: Projects 2011-2013. Springer International Publishing, Cham, pp. 15-34.

Schonhardt, A. et al., 2008. Observations of iodine monoxide columns from satellite. Atmospheric Chemistry And Physics, 8(3): 637-653.

Sherwen, T. et al., 2019. A machine learning based global sea-surface iodide distribution. Earth Syst. Sci. Data Discuss., 2019: 1-40.

Thomalla, S.J. et al., 2011. Phytoplankton distribution and nitrogen dynamics in the southwest indian subtropical gyre and Southern Ocean waters. Ocean Sci., 7(1): 113-127.

Tian, R.C. et al., 1996. Iodine speciation: A potential indicator to evaluate new production versus regenerated production. Deep-Sea Research Part I-Oceanographic Research Papers, 43(5): 723-738.

Truesdale, V.W., 1978. The Automatic Determination of Iodate and Total-Iodine in Seawater. Marine Chemistry, 6: 253-273.

Truesdale, V.W. and Smith, C.J., 1979. A Comparative Study of Three Methods for the Determination of Iodate in Seawater. Marine Chemistry, 7: 133-139.

Truesdale, V.W. and Spencer, C.P., 1974. Studies on the determination of inorganic iodine in seawater. Marine Chemistry, 2(1): 33-47.

Station Summary

49NZ20191205

SHIP/CRS EXPOCODE	WOCE SECT	STNNBR	CASTNO	CAST TYPE	DATE	UTC TIME	EVENT CODE	POSITION LATITUDE	POSITION LONGITUDE	NAV	UNC DEPTH	COR DEPTH	HT ABOVE BOTTOM	WIRE OUT	MAX PRESS	NO. OF BOTTLES	PARAMETERS	COMMENTS
49NZ20191205	I08N	001	001	CTD	120519	1210	BE	5 53.44 N	79 59.40 E	GPS	-9	194						
49NZ20191205	I08N	001	001	CTD	120519	1216	BO	5 53.45 N	79 59.37 E	GPS	-9	190	10	186	190	0		
49NZ20191205	I08N	001	001	CTD	120519	1220	EN	5 53.45 N	79 59.35 E	GPS	-9	191						
49NZ20191205	I08N	002	001	ROS	120519	1308	BE	5 52.32 N	79 59.25 E	GPS	-9	816						
49NZ20191205	I08N	002	001	ROS	120519	1324	BO	5 52.31 N	79 59.22 E	GPS	-9	824	9	814	821	15	1-8,15,23,24,27,29-31,33,34,43,45,82,92,93,98,110,111,123	
49NZ20191205	I08N	002	001	ROS	120519	1406	EN	5 52.36 N	79 59.15 E	GPS	-9	826						
49NZ20191205	I08N	003	001	ROS	120519	1708	BE	5 47.50 N	79 59.71 E	GPS	-9	1384						
49NZ20191205	I08N	003	001	ROS	120519	1733	BO	5 47.51 N	79 59.64 E	GPS	-9	1390	10	1382	1395	17	1-8,20,23,24,27,30,34,93	
49NZ20191205	I08N	003	001	ROS	120519	1836	EN	5 47.53 N	79 59.44 E	GPS	-9	1445						
49NZ20191205	I08N	004	001	CTD	120519	2056	BE	5 45.51 N	79 59.33 E	GPS	-9	2562						
49NZ20191205	I08N	004	001	CTD	120519	2137	BO	5 45.51 N	79 59.32 E	GPS	-9	2568	9	2564	2594	0		
49NZ20191205	I08N	004	001	CTD	120519	2220	EN	5 45.52 N	79 59.30 E	GPS	-9	2566						
49NZ20191205	I08N	005	001	ROS	120519	2338	BE	5 39.92 N	80 0.39 E	GPS	-9	3239						
49NZ20191205	I08N	005	001	ROS	120619	0036	BO	5 39.95 N	80 0.40 E	GPS	-9	3233	10	3220	3262	27	1-8,15,20,23,24,27,29-31,33,34,43,45,82,92,93,98,100,110,123	
49NZ20191205	I08N	005	001	ROS	120619	0224	EN	5 39.92 N	80 0.30 E	GPS	-9	3241						
49NZ20191205	I08N	999	999	UNK	120619	0318	BE	5 35.45 N	79 59.73 E	GPS	-9	3947						MAGNETOMETER CALIBRATION
49NZ20191205	I08N	999	999	UNK	120619	0341	EN	5 35.85 N	79 59.25 E	GPS	-9	3898						
49NZ20191205	I08N	006	001	ROS	120619	0554	BE	5 35.03 N	80 0.01 E	GPS	-9	4006						
49NZ20191205	I08N	006	001	ROS	120619	0659	BO	5 34.97 N	80 0.13 E	GPS	-9	4015	10	3996	4058	17	3-6,30,31,33,82,100,108,111,122	
49NZ20191205	I08N	006	001	ROS	120619	0833	EN	5 35.02 N	79 59.89 E	GPS	-9	3989						
49NZ20191205	I08N	007	001	ROS	120619	1046	BE	5 19.98 N	79 59.86 E	GPS	-9	4148						
49NZ20191205	I08N	007	001	ROS	120619	1151	BO	5 19.97 N	79 59.76 E	GPS	-9	4147	8	4130	4196	36	1-8,23,24,27,30,34,91,93	
49NZ20191205	I08N	007	001	ROS	120619	1347	EN	5 19.95 N	79 59.74 E	GPS	-9	4147						
49NZ20191205	I08N	008	001	CTD	120619	1606	BE	5 0.04 N	80 0.12 E	GPS	-9	4219						
49NZ20191205	I08N	008	001	CTD	120619	1710	BO	5 0.08 N	80 0.06 E	GPS	-9	4220	8	4202	4269	0		
49NZ20191205	I08N	008	001	CTD	120619	1814	EN	5 0.08 N	80 0.03 E	GPS	-9	4219						
49NZ20191205	I08N	009	001	ROS	120619	2019	BE	4 39.95 N	79 59.96 E	GPS	-9	4274						
49NZ20191205	I08N	009	001	ROS	120619	2125	BO	4 39.95 N	79 59.91 E	GPS	-9	4276	9	4256	4326	30	1-8,15,20,23,24,27,30,34,43,45,82,92,93,98,123	
49NZ20191205	I08N	009	001	ROS	120619	2336	EN	4 39.89 N	79 59.80 E	GPS	-9	4276						
49NZ20191205	I08N	010	001	CTD	120719	0215	BE	4 20.11 N	80 0.12 E	GPS	-9	4324						
49NZ20191205	I08N	010	001	CTD	120719	0322	BO	4 20.25 N	80 0.17 E	GPS	-9	4324	9	4307	4375	0		
49NZ20191205	I08N	010	001	CTD	120719	0427	EN	4 20.45 N	80 0.34 E	GPS	-9	4322						
49NZ20191205	I08N	011	001	CTD	120719	0651	BE	4 0.24 N	80 0.38 E	GPS	-9	4343						
49NZ20191205	I08N	011	001	CTD	120719	0757	BO	4 0.35 N	80 0.55 E	GPS	-9	4341	10	4322	4394	0		
49NZ20191205	I08N	011	001	CTD	120719	0903	EN	4 0.42 N	80 0.64 E	GPS	-9	4341						
49NZ20191205	I08N	012	001	ROS	120719	1111	BE	3 40.27 N	79 59.97 E	GPS	-9	4358						
49NZ20191205	I08N	012	001	ROS	120719	1216	BO	3 40.31 N	80 0.04 E	GPS	-9	4358	8	4340	4412	30	1-8,15,23,24,27,29,30,34,43,45,82,92,93,98,110,123	
49NZ20191205	I08N	012	001	ROS	120719	1416	EN	3 40.38 N	80 0.13 E	GPS	-9	4358						
49NZ20191205	I08N	013	001	CTD	120719	1652	BE	3 19.46 N	80 0.00 E	GPS	-9	4374						
49NZ20191205	I08N	013	001	CTD	120719	1759	BO	3 19.49 N	80 0.07 E	GPS	-9	4375	9	4357	4425	0		
49NZ20191205	I08N	013	001	CTD	120719	1907	EN	3 19.63 N	80 0.12 E	GPS	-9	4373						
49NZ20191205	I08N	014	001	ROS	120719	2118	BE	3 0.12 N	79 59.90 E	GPS	-9	4336						
49NZ20191205	I08N	014	001	ROS	120719	2224	BO	3 0.04 N	80 0.04 E	GPS	-9	4340	9	4320	4385	31	1-8,23,24,27,30,34,93	

```
49NZ20191205 I08N      014    001  ROS 120819 0032    EN  3  0.07 N  80  0.17 E GPS      -9   4339
49NZ20191205 I08N      015    001  CTD 120819 0240    BE  2 40.08 N  79 59.97 E GPS      -9   4358
49NZ20191205 I08N      015    001  CTD 120819 0347    BO  2 40.17 N  79 59.96 E GPS      -9   4356        9   4342   4408        0
49NZ20191205 I08N      015    001  CTD 120819 0453    EN  2 40.22 N  79 59.95 E GPS      -9   4358
49NZ20191205 I08N      016    001  CTD 120819 0658    BE  2 20.07 N  79 59.84 E GPS      -9   4340
49NZ20191205 I08N      016    001  CTD 120819 0803    BO  2 20.11 N  79 59.86 E GPS      -9   4339        9   4319   4390        0
49NZ20191205 I08N      016    001  CTD 120819 0909    EN  2 20.17 N  79 59.89 E GPS      -9   4347
49NZ20191205 I08N      017    001  ROS 120819 1110    BE  2  0.04 N  79 59.94 E GPS      -9   3866
49NZ20191205 I08N      017    001  ROS 120819 1209    BO  2  0.07 N  80  0.05 E GPS      -9   3875        9   3855   3912       29 1-8,15,20,23,24,27,29,30,34,42,43,45,82,92,93,98,110,117,121,123
49NZ20191205 I08N      017    001  ROS 120819 1353    EN  2  0.05 N  80  0.07 E GPS      -9   3875
49NZ20191205 I08N      018    001  ROS 120819 1634    BE  1 39.96 N  80  0.03 E GPS      -9   3792
49NZ20191205 I08N      018    001  ROS 120819 1734    BO  1 39.99 N  80  0.00 E GPS      -9   3779        8   3763   3817       28 22
49NZ20191205 I08N      018    001  ROS 120819 1849    EN  1 40.07 N  80  0.05 E GPS      -9   3759
49NZ20191205 I08N      019    001  ROS 120819 2054    BE  1 20.08 N  79 59.97 E GPS      -9   4567
49NZ20191205 I08N      019    001  ROS 120819 2204    BO  1 20.05 N  80  0.01 E GPS      -9   4569        9   4552   4625       32 1-8,12,13,23,24,27,30,34,93
49NZ20191205 I08N      019    001  ROS 120919 0015    EN  1 20.17 N  80  0.12 E GPS      -9   4572
49NZ20191205 I08N      020    001  ROS 120919 0220    BE  1  0.01 N  79 59.85 E GPS      -9   4622
49NZ20191205 I08N      020    001  ROS 120919 0334    BO  1  0.04 N  79 59.91 E GPS      -9   4625        9   4606   4682       32 22
49NZ20191205 I08N      020    001  ROS 120919 0506    EN  1  0.15 N  79 59.98 E GPS      -9   4625
49NZ20191205 I08N      021    001  CTD 120919 0642    BE  0 45.09 N  79 59.85 E GPS      -9   4653
49NZ20191205 I08N      021    001  CTD 120919 0754    BO  0 45.17 N  79 59.89 E GPS      -9   4655       10   4633   4711        0
49NZ20191205 I08N      021    001  CTD 120919 0906    EN  0 45.28 N  80  0.03 E GPS      -9   4652
49NZ20191205 I08N      022    001  ROS 120919 1045    BE  0 30.12 N  79 60.00 E GPS      -9   4650
49NZ20191205 I08N      022    001  ROS 120919 1159    BO  0 30.16 N  80  0.12 E GPS      -9   4651       10   4632   4709       32 1-8,15,23,24,27,29,30,34,43,45,82,92,93,98,110,123
49NZ20191205 I08N      022    001  ROS 120919 1401    EN  0 30.33 N  80  0.40 E GPS      -9   4650
49NZ20191205 I08N      023    001  CTD 120919 1704    BE  0 14.92 N  79 59.89 E GPS      -9   4654
49NZ20191205 I08N      023    001  CTD 120919 1815    BO  0 14.96 N  79 59.99 E GPS      -9   4654        8   4640   4716        0
49NZ20191205 I08N      023    001  CTD 120919 1928    EN  0 15.02 N  80  0.13 E GPS      -9   4655
49NZ20191205 I08N      024    001  CTD 120919 2107    BE  0  0.04 S  79 59.97 E GPS      -9   4677
49NZ20191205 I08N      024    001  CTD 120919 2218    BO  0  0.00 N  80  0.15 E GPS      -9   4676        8   4658   4737        0
49NZ20191205 I08N      024    001  CTD 120919 2330    EN  0  0.14 N  80  0.32 E GPS      -9   4681
49NZ20191205 I08N      025    001  ROS 121019 0108    BE  0 15.08 S  80  0.06 E GPS      -9   4684
49NZ20191205 I08N      025    001  ROS 121019 0221    BO  0 15.06 S  80  0.33 E GPS      -9   4683        8   4670   4746       33 1-8,15,20,23,24,27,29-31,33,34,42,43,45,82,92,93,98,100,110,117,121,123
49NZ20191205 I08N      025    001  ROS 121019 0441    EN  0 14.90 S  80  0.77 E GPS      -9   4681
49NZ20191205 I08N      026    001  ROS 121019 0750    BE  0 30.12 S  80  0.01 E GPS      -9   4713
49NZ20191205 I08N      026    001  ROS 121019 0904    BO  0 30.04 S  80  0.24 E GPS      -9   4712       10   4688   4774       34 3-6,30,31,33,42,82,100,108,111,117,121,122
49NZ20191205 I08N      026    001  ROS 121019 1049    EN  0 29.60 S  80  0.95 E GPS      -9   4712
49NZ20191205 I08N      027    001  ROS 121019 1306    BE  0 45.05 S  79 59.91 E GPS      -9   4736
49NZ20191205 I08N      027    001  ROS 121019 1418    BO  0 44.93 S  80  0.02 E GPS      -9   4735        8   4717   4798       35 1-8,23,24,27,30,34,91,93
49NZ20191205 I08N      027    001  ROS 121019 1620    EN  0 44.94 S  80  0.35 E GPS      -9   4743
49NZ20191205 I08N      028    001  CTD 121019 1835    BE  1  0.01 S  79 59.88 E GPS      -9   4714
49NZ20191205 I08N      028    001  CTD 121019 1946    BO  1  0.01 S  79 59.98 E GPS      -9   4702       10   4684   4762        0
49NZ20191205 I08N      028    001  CTD 121019 2058    EN  1  0.01 S  80  0.06 E GPS      -9   4704
49NZ20191205 I08N      029    001  ROS 121019 2255    BE  1 20.02 S  79 59.92 E GPS      -9   4824
49NZ20191205 I08N      029    001  ROS 121119 0008    BO  1 20.04 S  80  0.05 E GPS      -9   4834        9   4803   4885       32 1-8,15,23,24,27,29,30,34,43,45,82,92,93,98,110,123
49NZ20191205 I08N      029    001  ROS 121119 0227    EN  1 20.08 S  80  0.21 E GPS      -9   4813
49NZ20191205 I08N      030    001  ROS 121119 0456    BE  1 39.98 S  79 59.96 E GPS      -9   4903
49NZ20191205 I08N      030    001  ROS 121119 0612    BO  1 39.96 S  79 59.98 E GPS      -9   4904        9   4882   4968       34 1,2
49NZ20191205 I08N      030    001  ROS 121119 0736    EN  1 39.98 S  80  0.03 E GPS      -9   4903
49NZ20191205 I08N      031    001  CTD 121119 0934    BE  1 59.88 S  80  0.12 E GPS      -9   4904
49NZ20191205 I08N      031    001  CTD 121119 1055    BO  1 59.81 S  80  0.17 E GPS      -9   4905       10   4883   4970        0
```

```
49NZ20191205 I08N      031    001  CTD 121119 1209    EN  1 59.79 S  80  0.15 E GPS      -9   4903
49NZ20191205 I08N      032    001  ROS 121119 1405    BE  2 19.98 S  79 59.98 E GPS      -9   4908
49NZ20191205 I08N      032    001  ROS 121119 1520    BO  2 19.98 S  79 60.00 E GPS      -9   4909        9   4888   4975        33 1-8,15,20,23,24,27,30,34,43,45,82,92,93,98,123
49NZ20191205 I08N      032    001  ROS 121119 1731    EN  2 19.99 S  80  0.02 E GPS      -9   4911
49NZ20191205 I08N      033    001  CTD 121119 2006    BE  2 40.00 S  79 59.99 E GPS      -9   4929
49NZ20191205 I08N      033    001  CTD 121119 2122    BO  2 40.00 S  79 60.00 E GPS      -9   4927       10   4910   4995        0
49NZ20191205 I08N      033    001  CTD 121119 2237    EN  2 39.99 S  79 59.99 E GPS      -9   4925
49NZ20191205 I08N      034    001  ROS 121219 0036    BE  2 59.93 S  79 59.97 E GPS      -9   4965
49NZ20191205 I08N      034    001  ROS 121219 0151    BO  2 59.96 S  79 59.87 E GPS      -9   4967       10   4945   5030        34 1-8,23,24,27,30,34,93
49NZ20191205 I08N      034    001  ROS 121219 0412    EN  2 59.87 S  79 59.67 E GPS      -9   4964
49NZ20191205 I08N      035    001  CTD 121219 0657    BE  3 29.99 S  80  0.05 E GPS      -9   5015
49NZ20191205 I08N      035    001  CTD 121219 0819    BO  3 29.91 S  80  0.01 E GPS      -9   5013       10   4997   5085        0
49NZ20191205 I08N      035    001  CTD 121219 0939    EN  3 29.87 S  79 59.89 E GPS      -9   5014
49NZ20191205 I08N      036    001  ROS 121219 1220    BE  4  0.21 S  79 59.86 E GPS      -9   4632
49NZ20191205 I08N      036    001  ROS 121219 1332    BO  4  0.12 S  79 59.84 E GPS      -9   4630       10   4612   4686        32 1-8,15,23,24,27,29,30,34,42,43,45,82,92,93,98,110,117,121,123
49NZ20191205 I08N      036    001  ROS 121219 1538    EN  4  0.11 S  79 59.88 E GPS      -9   4632
49NZ20191205 I08N      037    001  CTD 121219 1823    BE  4 30.10 S  79 59.99 E GPS      -9   4746
49NZ20191205 I08N      037    001  CTD 121219 1934    BO  4 30.01 S  79 59.99 E GPS      -9   4743        9   4729   4807        0
49NZ20191205 I08N      037    001  CTD 121219 2049    EN  4 30.02 S  80  0.00 E GPS      -9   4750
49NZ20191205 I08N      038    001  ROS 121219 2330    BE  5  0.01 S  79 59.91 E GPS      -9   5142
49NZ20191205 I08N      038    001  ROS 121319 0048    BO  4 59.96 S  79 59.89 E GPS      -9   5140       10   5120   5215        34 1-8,20,23,24,27,29,30,34,91,93,110
49NZ20191205 I08N      038    001  ROS 121319 0314    EN  4 59.94 S  79 59.85 E GPS      -9   5143
49NZ20191205 I08N      038    001  FLT 121319 0330    DE  4 59.55 S  79 59.98 E GPS      -9   5142                                                                                                DEEP APEX S/N 43
49NZ20191205 I08N      039    001  ROS 121419 0407    BE  5 30.03 S  79 60.00 E GPS      -9   5169
49NZ20191205 I08N      039    001  ROS 121419 0528    BO  5 30.08 S  80  0.02 E GPS      -9   5170        9   5153   5244        4 1,2
49NZ20191205 I08N      039    001  ROS 121419 0651    EN  5 30.11 S  79 60.00 E GPS      -9   5169
49NZ20191205 I08N      040    001  ROS 121419 0943    BE  6  0.02 S  79 59.89 E GPS      -9   5202
49NZ20191205 I08N      040    001  ROS 121419 1104    BO  5 59.98 S  79 59.97 E GPS      -9   5202       10   5182   5276        35 1-8,15,23,24,27,30,34,43,45,82,92,93,98,123
49NZ20191205 I08N      040    001  ROS 121419 1325    EN  6  0.02 S  79 59.99 E GPS      -9   5205
49NZ20191205 I08N      041    001  CTD 121419 1621    BE  6 29.98 S  80  0.01 E GPS      -9   5150
49NZ20191205 I08N      041    001  CTD 121419 1741    BO  6 30.00 S  80  0.01 E GPS      -9   5150        9   5134   5224        0
49NZ20191205 I08N      041    001  CTD 121419 1902    EN  6 29.99 S  79 60.00 E GPS      -9   5151
49NZ20191205 I08N      042    001  ROS 121419 2207    BE  6 59.97 S  79 59.83 E GPS      -9   4919
49NZ20191205 I08N      042    001  ROS 121419 2311    BO  7  0.02 S  79 59.94 E GPS      -9   4917       10   4898   4982        33 1-8,20,23,24,27,29,30,34,93,110
49NZ20191205 I08N      042    001  ROS 121519 0134    EN  7  0.00 S  79 59.98 E GPS      -9   4922
49NZ20191205 I08N      043    001  CTD 121519 0420    BE  7 29.94 S  79 59.89 E GPS      -9   5397
49NZ20191205 I08N      043    001  CTD 121519 0545    BO  7 29.97 S  79 59.92 E GPS      -9   5400        8   5375   5481        0
49NZ20191205 I08N      043    001  CTD 121519 0709    EN  7 29.92 S  79 59.93 E GPS      -9   5398
49NZ20191205 I08N      044    001  ROS 121519 0957    BE  8  0.11 S  80  0.19 E GPS      -9   5419
49NZ20191205 I08N      044    001  ROS 121519 1124    BO  8  0.13 S  80  0.16 E GPS      -9   5416        9   5396   5498        33 1-8,15,23,24,27,30,31,33,34,42,43,45,82,92,93,98,100,117,121,123
49NZ20191205 I08N      044    001  ROS 121519 1348    EN  8  0.12 S  80  0.18 E GPS      -9   5415
49NZ20191205 I08N      045    001  ROS 121519 1703    BE  8 29.99 S  79 59.98 E GPS      -9   5189
49NZ20191205 I08N      045    001  ROS 121519 1822    BO  8 30.00 S  79 60.00 E GPS      -9   5190        9   5166   5263        34 3-6,30,31,33,42,82,100,108,111,117,121,122
49NZ20191205 I08N      045    001  ROS 121519 2020    EN  8 30.00 S  80  0.01 E GPS      -9   5187
49NZ20191205 I08N      046    001  ROS 121519 2310    BE  9  0.06 S  79 59.92 E GPS      -9   5208
49NZ20191205 I08N      046    001  ROS 121619 0029    BO  9  0.02 S  79 59.94 E GPS      -9   5207       10   5190   5285        34 1-8,23,24,27,29,30,34,93,110
49NZ20191205 I08N      046    001  ROS 121619 0255    EN  9  0.02 S  79 59.96 E GPS      -9   5207
49NZ20191205 I08N      047    001  CTD 121619 0548    BE  9 29.97 S  79 59.93 E GPS      -9   5363
49NZ20191205 I08N      047    001  CTD 121619 0711    BO  9 29.97 S  79 59.93 E GPS      -9   5369        9   5340   5442        0
49NZ20191205 I08N      047    001  CTD 121619 0836    EN  9 29.95 S  79 59.97 E GPS      -9   5362
49NZ20191205 I08N      048    001  ROS 121619 1118    BE  9 59.93 S  79 59.96 E GPS      -9   5379
```

```
49NZ20191205 I08N      048    001  ROS 121619 1246    BO 10  0.00 S  79 59.97 E GPS      -9   5383       10   5357   5459        35 1-8,20,23,24,27,29,30,34,91-93,110
49NZ20191205 I08N      048    001  ROS 121619 1508    EN  9 59.97 S  79 59.98 E GPS      -9   5379
49NZ20191205 I08N      048    001  FLT 121619 1523    DE  9 59.99 S  79 59.98 E GPS      -9   5377                                                                                DEEP APEX S/N 44
49NZ20191205 I08N      049    001  CTD 121619 1806    BE 10 29.98 S  80  0.01 E GPS      -9   5369
49NZ20191205 I08N      049    001  CTD 121619 1928    BO 10 29.99 S  80  0.01 E GPS      -9   5368        8   5348   5449        0
49NZ20191205 I08N      049    001  CTD 121619 2112    EN 10 29.98 S  79 59.99 E GPS      -9   5365
49NZ20191205 I08N      050    001  ROS 121619 2353    BE 11  0.04 S  79 59.86 E GPS      -9   5346
49NZ20191205 I08N      050    001  ROS 121719 0123    BO 11  0.00 S  79 59.83 E GPS      -9   5347       10   5328   5426        35 1-8,12,13,15,23,24,27,30,34,43,45,82,92,93,98,123
49NZ20191205 I08N      050    001  ROS 121719 0352    EN 10 59.97 S  79 59.85 E GPS      -9   5347
49NZ20191205 I08N      051    001  ROS 121719 0708    BE 11 30.01 S  80  0.01 E GPS      -9   5288
49NZ20191205 I08N      051    001  ROS 121719 0833    BO 11 29.93 S  80  0.02 E GPS      -9   5295        8   5270   5369        32 22
49NZ20191205 I08N      051    001  ROS 121719 1017    EN 11 29.76 S  79 59.97 E GPS      -9   5253
49NZ20191205 I08N      052    001  ROS 121719 1259    BE 12  0.05 S  79 60.00 E GPS      -9   5157
49NZ20191205 I08N      052    001  ROS 121719 1421    BO 12  0.01 S  80  0.01 E GPS      -9   5159       10   5138   5231        34 1-8,15,20,23,24,27,29,30,34,42,43,45,82,92,93,98,110,117,120,121,123
49NZ20191205 I08N      052    001  ROS 121719 1637    EN 12  0.02 S  80  0.00 E GPS      -9   5155
49NZ20191205 I08N      052    001  FLT 121719 1654    DE 12  0.02 S  80  0.02 E GPS      -9   5149                                                                                BGC NAVIS S/N F0884
49NZ20191205 I08N      053    001  CTD 121719 1934    BE 12 29.98 S  80  0.03 E GPS      -9   5044
49NZ20191205 I08N      053    001  CTD 121719 2051    BO 12 29.97 S  80  0.04 E GPS      -9   5046        9   5031   5122        0
49NZ20191205 I08N      053    001  CTD 121719 2210    EN 12 29.97 S  80  0.03 E GPS      -9   5047
49NZ20191205 I08N      054    001  ROS 121819 0120    BE 13  5.92 S  80  0.14 E GPS      -9   5000
49NZ20191205 I08N      054    001  ROS 121819 0238    BO 13  5.81 S  80  0.04 E GPS      -9   5003        8   4995   5081        32 1-8,23,24,27,29,30,34,93,110
49NZ20191205 I08N      054    001  ROS 121819 0457    EN 13  5.81 S  79 60.00 E GPS      -9   4990
49NZ20191205 I08N      055    001  CTD 121819 1506    BE 13 30.00 S  79 59.96 E GPS      -9   4928
49NZ20191205 I08N      055    001  CTD 121819 1621    BO 13 29.99 S  80  0.00 E GPS      -9   4927        9   4906   4993        0
49NZ20191205 I08N      055    001  CTD 121819 1735    EN 13 30.00 S  79 59.98 E GPS      -9   4928
49NZ20191205 I08N      056    001  ROS 121819 2027    BE 13 59.86 S  80  0.15 E GPS      -9   5019
49NZ20191205 I08N      056    001  ROS 121819 2144    BO 13 59.90 S  80  0.15 E GPS      -9   5024        9   5000   5089        32 1-8,23,24,27,30,34,43,82,92,93,98,123
49NZ20191205 I08N      056    001  ROS 121919 0004    EN 13 59.91 S  80  0.12 E GPS      -9   5027
49NZ20191205 I08N      057    001  CTD 121919 0244    BE 14 29.91 S  80  0.12 E GPS      -9   5053
49NZ20191205 I08N      057    001  CTD 121919 0405    BO 14 29.77 S  79 59.93 E GPS      -9   5029       10   5010   5098        0
49NZ20191205 I08N      057    001  CTD 121919 0523    EN 14 29.54 S  79 59.91 E GPS      -9   5024
49NZ20191205 I08N      058    001  ROS 121919 0808    BE 14 59.94 S  80  0.08 E GPS      -9   5109
49NZ20191205 I08N      058    001  ROS 121919 0929    BO 14 59.93 S  80  0.12 E GPS      -9   5111        9   5095   5186        34 1-8,20,23,24,27,29,30,34,91,93,110
49NZ20191205 I08N      058    001  CTD 121919 1150    EN 14 59.88 S  80  0.05 E GPS      -9   5112
49NZ20191205 I08N      059    001  CTD 121919 1434    BE 15 30.01 S  80  0.04 E GPS      -9   4922
49NZ20191205 I08N      059    001  CTD 121919 1551    BO 15 30.02 S  80  0.01 E GPS      -9   4923        9   4902   4990        0
49NZ20191205 I08N      059    001  ROS 121919 1705    EN 15 30.02 S  79 59.99 E GPS      -9   4921
49NZ20191205 I08N      060    001  ROS 121919 1950    BE 15 59.94 S  80  0.08 E GPS      -9   5046
49NZ20191205 I08N      060    001  ROS 121919 2106    BO 15 59.94 S  80  0.10 E GPS      -9   5046        9   5030   5120        34 1-8,15,23,24,27,30,31,33,34,42,43,45,82,92,93,98,100,117,120,121,123
49NZ20191205 I08N      060    001  ROS 121919 2328    EN 15 59.96 S  80  0.10 E GPS      -9   5044
49NZ20191205 I08N      061    001  ROS 122019 0237    BE 16 29.95 S  80  0.03 E GPS      -9   5034
49NZ20191205 I08N      061    001  ROS 122019 0355    BO 16 29.83 S  79 59.96 E GPS      -9   5038        8   5023   5111        34 3-6,30,31,33,42,82,100,108,111,117,121,122
49NZ20191205 I08N      061    001  ROS 122019 0545    EN 16 29.67 S  79 59.85 E GPS      -9   5015
49NZ20191205 I08N      062    001  ROS 122019 0830    BE 16 59.94 S  80  0.07 E GPS      -9   5087
49NZ20191205 I08N      062    001  ROS 122019 0952    BO 16 59.91 S  80  0.06 E GPS      -9   5072       10   5051   5143        33 1-8,20,23,24,27,29,30,34,93,110
49NZ20191205 I08N      062    001  ROS 122019 1206    EN 16 59.80 S  80  0.01 E GPS      -9   5091
49NZ20191205 I08N      063    001  CTD 122019 1455    BE 17 30.03 S  79 59.97 E GPS      -9   5112
49NZ20191205 I08N      063    001  CTD 122019 1615    BO 17 30.02 S  79 59.95 E GPS      -9   5111        9   5088   5181        0
49NZ20191205 I08N      063    001  CTD 122019 1733    EN 17 30.03 S  79 59.96 E GPS      -9   5105
49NZ20191205 I08N      064    001  ROS 122019 2018    BE 17 59.93 S  79 60.00 E GPS      -9   5096
49NZ20191205 I08N      064    001  ROS 122019 2137    BO 17 59.93 S  80  0.05 E GPS      -9   5100        9   5094   5187        34 1-8,23,24,27,30,34,43,82,92,93,98,123
```

49NZ20191205	I08N	064	001	ROS	122119	0002	EN	17	59.92	S	80	0.05	E	GPS	-9	5101					
49NZ20191205	I08N	065	001	ROS	122119	0247	BE	18	29.87	S	80	0.06	E	GPS	-9	5076					
49NZ20191205	I08N	065	001	ROS	122119	0408	BO	18	29.85	S	79	59.98	E	GPS	-9	5071	9	5055	5144	32	22
49NZ20191205	I08N	065	001	ROS	122119	0548	EN	18	29.80	S	79	59.96	E	GPS	-9	5072					
49NZ20191205	I08N	066	001	ROS	122119	0837	BE	18	59.86	S	80	0.04	E	GPS	-9	4949					
49NZ20191205	I08N	066	001	ROS	122119	0955	BO	18	59.82	S	79	59.99	E	GPS	-9	4946	10	4925	5017	33	1-8,23,24,27,29,30,34,91,93,110
49NZ20191205	I08N	066	001	ROS	122119	1203	EN	18	59.81	S	79	60.00	E	GPS	-9	4947					
49NZ20191205	I08N	067	001	CTD	122119	1454	BE	19	30.00	S	79	59.89	E	GPS	-9	4874					
49NZ20191205	I08N	067	001	CTD	122119	1610	BO	19	30.03	S	79	59.99	E	GPS	-9	4871	8	4858	4943	0	
49NZ20191205	I08N	067	001	CTD	122119	1725	EN	19	30.03	S	79	59.98	E	GPS	-9	4873					
49NZ20191205	I08N	068	001	ROS	122119	2017	BE	20	0.02	S	79	59.90	E	GPS	-9	4861					
49NZ20191205	I08N	068	001	ROS	122119	2132	BO	20	0.01	S	80	0.01	E	GPS	-9	4866	9	4848	4935	34	1-8,15,20,23,24,27,29-31,33,34,42,43,45,82,92,93,98,110,117,120,121,123
49NZ20191205	I08N	068	001	ROS	122119	2345	EN	20	0.00	S	80	0.02	E	GPS	-9	4868					
49NZ20191205	I08N	068	001	FLT	122119	2357	DE	20	0.01	S	80	0.03	E	GPS	-9	4867					DEEP APEX S/N 45
49NZ20191205	I08N	069	001	ROS	122219	0301	BE	20	29.86	S	79	59.96	E	GPS	-9	4853					
49NZ20191205	I08N	069	001	ROS	122219	0417	BO	20	29.76	S	79	59.99	E	GPS	-9	4859	8	4844	4930	34	3-6,30,31,33,42,82,100,108,117,121,122
49NZ20191205	I08N	069	001	ROS	122219	0609	EN	20	29.72	S	80	0.04	E	GPS	-9	4852					
49NZ20191205	I08N	999	999	UNK	122319	1037	BE	20	22.13	S	73	35.62	E	GPS	-9	4605					MAGNETOMETER CALIBRATION
49NZ20191205	I08N	999	999	UNK	122319	1100	EN	20	21.93	S	73	35.09	E	GPS	-9	4690					
49NZ20191205	I08N	999	999	FLT	122419	1131	DE	20	15.43	S	67	59.94	E	GPS	-9	2664					APEX F0587

49NZ20191229

SHIP/CRS EXPOCODE	WOCE SECT	STNNBR	CASTNO	CAST TYPE	DATE	UTC TIME	EVENT CODE	POSITION LATITUDE			POSITION LONGITUDE			NAV	UNC DEPTH	COR DEPTH	HT ABOVE BOTTOM	WIRE OUT	MAX PRESS	NO. OF BOTTLES	PARAMETERS	COMMENTS
49NZ20191229	I07C	070	001	ROS	123119	1535	BE	29	29.63	S	54	29.88	E	GPS	-9	4901						
49NZ20191229	I07C	070	001	ROS	123119	1652	BO	29	29.64	S	54	29.84	E	GPS	-9	4904	10	4880	4972	33	1-8,20,23,24,27,30,34,42,43,82,92,93,98,117,120,121,123	
49NZ20191229	I07C	070	001	ROS	123119	1923	EN	29	29.64	S	54	29.85	E	GPS	-9	4901						
49NZ20191229	I07C			UNK	123119	1935	BE	29	30.02	S	54	30.27	E	GPS	-9	4937						MAGNETOMETER CALIBRATION
49NZ20191229	I07C			UNK	123119	1957	EN	29	30.16	S	54	30.24	E	GPS	-9	4945						MAGNETOMETER CALIBRATION
49NZ20191229	I07S	071	001	CTD	123119	2250	BE	29	49.52	S	54	50.49	E	GPS	-9	4130						
49NZ20191229	I07S	071	001	CTD	123119	2358	BO	29	49.54	S	54	50.50	E	GPS	-9	4129	10	4111	4177	0		
49NZ20191229	I07S	071	001	CTD	010120	0102	EN	29	49.50	S	54	50.57	E	GPS	-9	4119						
49NZ20191229	I07S	072	001	ROS	010120	0350	BE	30	9.42	S	55	11.18	E	GPS	-9	4699						
49NZ20191229	I07S	072	001	ROS	010120	0501	BO	30	9.31	S	55	11.21	E	GPS	-9	4704	9	4680	4765	35	1-8,23,24,27,29,30,34,40,93,110,124	
49NZ20191229	I07S	072	001	ROS	010120	0730	EN	30	9.20	S	55	11.47	E	GPS	-9	4702						
49NZ20191229	I07S	072	001	FLT	010120	0744	DE	30	9.39	S	55	11.63	E	GPS	-9	4697						DEEP APEX #46
49NZ20191229	I07S	072	001	FLT	010120	0749	DE	30	9.49	S	55	11.72	E	GPS	-9	4697						SOCCOM BGC #18299
49NZ20191229	I07S	073	001	ROS	010120	1023	BE	30	29.28	S	55	31.64	E	GPS	-9	4242						
49NZ20191229	I07S	073	001	ROS	010120	1135	BO	30	29.27	S	55	31.53	E	GPS	-9	4266	9	4266	4337	28	18,19	
49NZ20191229	I07S	073	001	ROS	010120	1253	EN	30	29.35	S	55	31.61	E	GPS	-9	4249						
49NZ20191229	I07S	074	001	ROS	010120	1533	BE	30	49.36	S	55	52.42	E	GPS	-9	4425						
49NZ20191229	I07S	074	001	ROS	010120	1642	BO	30	49.31	S	55	52.43	E	GPS	-9	4432	9	4413	4490	32	1-8,12,13,23,24,27,30,34,82,91-93,98,123	
49NZ20191229	I07S	074	001	ROS	010120	1858	EN	30	49.32	S	55	52.43	E	GPS	-9	4430						
49NZ20191229	I07S	075	001	ROS	010120	2210	BE	31	9.24	S	56	13.05	E	GPS	-9	5121						

```
49NZ20191229 I07S      075    001  ROS 010120 2332    BO 31  9.21 S  56 13.08 E GPS      -9   5116        9   5097   5197        28 22
49NZ20191229 I07S      075    001  ROS 010220 0119    EN 31  8.96 S  56 13.18 E GPS      -9   5076
49NZ20191229 I07S      076    001  ROS 010220 0410    BE 31 29.07 S  56 33.50 E GPS      -9   4772
49NZ20191229 I07S      076    001  ROS 010220 0523    BO 31 29.07 S  56 33.55 E GPS      -9   4787       10   4731   4810        33 1-8,23,24,27,30,34,93
49NZ20191229 I07S      076    001  ROS 010220 0743    EN 31 29.03 S  56 33.74 E GPS      -9   4806
49NZ20191229 I07S      077    001  CTD 010220 1027    BE 31 49.06 S  56 54.27 E GPS      -9   3103
49NZ20191229 I07S      077    001  CTD 010220 1119    BO 31 49.05 S  56 54.38 E GPS      -9   3146       10   3135   3180        0
49NZ20191229 I07S      077    001  CTD 010220 1208    EN 31 49.03 S  56 54.44 E GPS      -9   3154
49NZ20191229 I07S      078    001  ROS 010220 1451    BE 32  8.99 S  57 14.98 E GPS      -9   2871
49NZ20191229 I07S      078    001  ROS 010220 1542    BO 32  8.99 S  57 15.01 E GPS      -9   2918        9   2906   2945        25 1-8,20,23,24,27,29,30,34,43,82,92,93,98,110,123
49NZ20191229 I07S      078    001  ROS 010220 1716    EN 32  8.98 S  57 14.98 E GPS      -9   2925
49NZ20191229 I07S      079    001  CTD 010220 1923    BE 32 30.03 S  57 10.97 E GPS      -9   3617
49NZ20191229 I07S      079    001  CTD 010220 2022    BO 32 29.99 S  57 10.98 E GPS      -9   3617        8   3606   3661        0
49NZ20191229 I07S      079    001  CTD 010220 2119    EN 32 29.97 S  57 10.95 E GPS      -9   3615
49NZ20191229 I07S      080    001  ROS 010220 2326    BE 32 51.00 S  57  6.99 E GPS      -9   5344
49NZ20191229 I07S      080    001  ROS 010320 0051    BO 32 51.00 S  57  7.00 E GPS      -9   5341       10   5336   5440        35 1-8,23,24,27,30,34,93
49NZ20191229 I07S      080    001  ROS 010320 0340    EN 32 50.95 S  57  6.93 E GPS      -9   5381
49NZ20191229 I07S      081    001  ROS 010320 0616    BE 33 12.00 S  57  2.40 E GPS      -9   6014
49NZ20191229 I07S      081    001  ROS 010320 0747    BO 33 12.01 S  57  2.41 E GPS      -9   6010       10   5961   6082        36 1-8,23,24,27,30,34,92,93
49NZ20191229 I07S      081    001  ROS 010320 1034    EN 33 12.03 S  57  2.60 E GPS      -9   6087
49NZ20191229 I07S      081    001  FLT 010320 1043    DE 33 12.17 S  57  2.61 E GPS      -9   6124                                                                                                ARGO HULL#8608
49NZ20191229 I07S      082    001  CTD 010320 1317    BE 33 33.49 S  57  2.48 E GPS      -9   5843
49NZ20191229 I07S      082    001  CTD 010320 1447    BO 33 33.47 S  57  2.46 E GPS      -9   5841        9   5846   5966        0
49NZ20191229 I07S      082    001  CTD 010320 1621    EN 33 33.47 S  57  2.48 E GPS      -9   5839
49NZ20191229 I07S      083    001  ROS 010320 1843    BE 33 57.98 S  57  2.03 E GPS      -9   5029
49NZ20191229 I07S      083    001  ROS 010320 2001    BO 33 58.01 S  57  2.10 E GPS      -9   5030        8   5028   5123        33 1-8,23,24,27,30,34,82,92,93,98,123
49NZ20191229 I07S      083    001  ROS 010320 2249    EN 33 58.02 S  57  2.22 E GPS      -9   5020
49NZ20191229 I07S      084    001  CTD 010420 0140    BE 34 18.69 S  57  9.75 E GPS      -9   4175
49NZ20191229 I07S      084    001  CTD 010420 0251    BO 34 18.71 S  57  9.78 E GPS      -9   4187        9   4167   4234        0
49NZ20191229 I07S      084    001  CTD 010420 0355    EN 34 18.71 S  57  9.71 E GPS      -9   4180
49NZ20191229 I07S      085    001  CTD 010420 0605    BE 34 39.37 S  57 17.40 E GPS      -9   3799
49NZ20191229 I07S      085    001  CTD 010420 0651    BO 34 39.33 S  57 17.32 E GPS      -9   3787       99   1586   1587        0                                                   ABORTED WITH CABLE MOULD LEAK
49NZ20191229 I07S      085    001  CTD 010420 0708    EN 34 39.33 S  57 17.32 E GPS      -9   3792
49NZ20191229 I07S      085    002  ROS 010420 1709    BE 34 39.34 S  57 17.37 E GPS      -9   3806
49NZ20191229 I07S      085    002  ROS 010420 1809    BO 34 39.33 S  57 17.38 E GPS      -9   3808        9   3773   3831        29 1-6,23,24,30,34,42,43,82,92,98,117,121,123
49NZ20191229 I07S      085    002  ROS 010420 2002    EN 34 39.33 S  57 17.39 E GPS      -9   3798
49NZ20191229 I07S      086    001  ROS 010520 0009    BE 35  0.00 S  57 25.02 E GPS      -9   4817
49NZ20191229 I07S      086    001  ROS 010520 0126    BO 35  0.02 S  57 25.07 E GPS      -9   4820       10   4797   4883        36 1-8,20,23,24,27,29,30,34,40,93,110,124
49NZ20191229 I07S      086    001  ROS 010520 0357    EN 35  0.03 S  57 25.07 E GPS      -9   4815
49NZ20191229 I07S      086    001  FLT 010520 0408    DE 35  0.23 S  57 25.05 E GPS      -9   4822                                                                                                SOCCOM BGC #18082
49NZ20191229 I07S      087    001  CTD 010520 0647    BE 35 26.67 S  57 27.77 E GPS      -9   4212
49NZ20191229 I07S      087    001  CTD 010520 0758    BO 35 26.69 S  57 27.74 E GPS      -9   4209        9   4182   4251        0
49NZ20191229 I07S      087    001  CTD 010520 0903    EN 35 26.65 S  57 27.84 E GPS      -9   4215
49NZ20191229 I07S      088    001  CTD 010520 1133    BE 35 53.23 S  57 30.02 E GPS      -9   4539
49NZ20191229 I07S      088    001  CTD 010520 1246    BO 35 53.37 S  57 30.04 E GPS      -9   4515        9   4496   4575        0
49NZ20191229 I07S      088    001  CTD 010520 1355    EN 35 53.37 S  57 30.03 E GPS      -9   4518
49NZ20191229 I07S      088    001  FLT 010520 1402    DE 35 53.40 S  57 30.04 E GPS      -9   4515                                                                                                ARGO HULL#8829
49NZ20191229 I07S      089    001  ROS 010520 1629    BE 36 20.02 S  57 32.50 E GPS      -9   4422
49NZ20191229 I07S      089    001  ROS 010520 1740    BO 36 20.02 S  57 32.53 E GPS      -9   4421        7   4414   4490        31 1-8,23,24,27,29,30,34,82,93,98,110,123
49NZ20191229 I07S      089    001  ROS 010520 1946    EN 36 20.00 S  57 32.52 E GPS      -9   4429
49NZ20191229 I07S      089    001  FLT 010520 1958    DE 36 20.00 S  57 32.53 E GPS      -9   4409                                                                                                ARGO HULL#8609
```

```
49NZ20191229 I07S      090    001  CTD 010520 2218    BE 36 46.68 S  57 35.02 E GPS      -9   4749
49NZ20191229 I07S      090    001  CTD 010520 2334    BO 36 46.67 S  57 35.01 E GPS      -9   4738           4734   4819        0
49NZ20191229 I07S      090    001  CTD 010620 0047    EN 36 46.69 S  57 35.03 E GPS      -9   4733
49NZ20191229 I07S      091    001  ROS 010620 0310    BE 37 13.33 S  57 37.53 E GPS      -9   5331
49NZ20191229 I07S      091    001  ROS 010620 0432    BO 37 13.31 S  57 37.53 E GPS      -9   5331        9   5254   5353        35 1-8,23,24,27,30,34,9
49NZ20191229 I07S      091    001  ROS 010620 0657    EN 37 13.39 S  57 37.46 E GPS      -9   5364
49NZ20191229 I07S      092    001  CTD 010620 0944    BE 37 45.51 S  57 37.67 E GPS      -9   5431
49NZ20191229 I07S      092    001  CTD 010620 1110    BO 37 45.43 S  57 37.66 E GPS      -9   5430       10   5407   5511        0
49NZ20191229 I07S      092    001  CTD 010620 1236    EN 37 45.46 S  57 37.56 E GPS      -9   5435
49NZ20191229 I07S      093    001  ROS 010620 1517    BE 38 15.40 S  57 39.07 E GPS      -9   5368
49NZ20191229 I07S      093    001  ROS 010620 1642    BO 38 15.36 S  57 39.32 E GPS      -9   5347        9   5327   5429        35 1-8,20,23,24,27,29,30,34,42,43,82,92,93,98,110,117,120,121,123
49NZ20191229 I07S      093    001  ROS 010620 1905    EN 38 15.31 S  57 40.10 E GPS      -9   5318
49NZ20191229 I07S      094    001  CTD 010620 2149    BE 38 45.25 S  57 40.00 E GPS      -9   5056
49NZ20191229 I07S      094    001  CTD 010620 2309    BO 38 45.05 S  57 41.00 E GPS      -9   5074        9   5093   5149        0
49NZ20191229 I07S      094    001  CTD 010720 0027    EN 38 44.80 S  57 41.75 E GPS      -9   5095
49NZ20191229 I07S      095    001  ROS 010720 0320    BE 39 15.10 S  57 41.88 E GPS      -9   5146
49NZ20191229 I07S      095    001  ROS 010720 0438    BO 39 14.74 S  57 41.49 E GPS      -9   5151        9   5136   5230        34 1-8,23,24,27,30,34,91,93
49NZ20191229 I07S      095    001  ROS 010720 0702    EN 39 14.14 S  57 40.36 E GPS      -9   5156
49NZ20191229 I07S      401    001  XCT 010720 0836    DE 39 30.15 S  57 42.80 E GPS      -9   5089                                                                                                TSK XCTD-4 #18117711
49NZ20191229 I07S      096    001  CTD 010720 1010    BE 39 44.99 S  57 43.69 E GPS      -9   5033
49NZ20191229 I07S      096    001  XCT 010720 1017    DE 39 44.95 S  57 43.51 E GPS      -9   5039                                                                                                TSK XCTD-4 #18117712
49NZ20191229 I07S      096    001  CTD 010720 1130    BO 39 44.78 S  57 42.66 E GPS      -9   5047        9   5044   5142        0
49NZ20191229 I07S      096    001  CTD 010720 1249    EN 39 44.54 S  57 41.79 E GPS      -9   5040
49NZ20191229 I07S      402    001  XCT 010720 1418    DE 40  0.04 S  57 44.26 E GPS      -9   4997                                                                                                TSK XCTD-4 #18117709
49NZ20191229 I07S      097    001  ROS 010720 1548    BE 40 14.98 S  57 45.03 E GPS      -9   4993
49NZ20191229 I07S      097    001  ROS 010720 1707    BO 40 14.98 S  57 44.98 E GPS      -9   4997        9   4984   5076        36 1-8,20,23,24,27,29,30,34,40,82,92,93,98,110,123,124
49NZ20191229 I07S      097    001  ROS 010720 1925    EN 40 14.81 S  57 44.82 E GPS      -9   4994
49NZ20191229 I07S      097    001  FLT 010720 1936    DE 40 14.78 S  57 44.80 E GPS      -9   4988                                                                                                SOCCOM BGC #17898
49NZ20191229 I07S      097    001  FLT 010720 1941    DE 40 14.74 S  57 44.77 E GPS      -9   4990                                                                                                ARGO HULL#8844
49NZ20191229 I07S      403    001  XCT 010720 2101    DE 40 28.74 S  57 44.90 E GPS      -9   4897                                                                                                TSK XCTD-4 #18117710
49NZ20191229 I07S      098    001  CTD 010720 2234    BE 40 42.49 S  57 44.89 E GPS      -9   4936
49NZ20191229 I07S      098    001  CTD 010720 2353    BO 40 42.06 S  57 44.41 E GPS      -9   4942        9   4933   5024        0
49NZ20191229 I07S      098    001  CTD 010820 0111    EN 40 41.69 S  57 44.10 E GPS      -9   4954
49NZ20191229 I07S      404    001  XCT 010820 0247    DE 40 55.45 S  57 44.73 E GPS      -9   4873                                                                                                TSK XCTD-4 #18117713
49NZ20191229 I07S      099    001  ROS 010820 0423    BE 41  9.74 S  57 44.63 E GPS      -9   4889
49NZ20191229 I07S      099    001  XCT 010820 0430    DE 41  9.66 S  57 44.64 E GPS      -9   4889                                                                                                TSK XCTD-4 #18117714
49NZ20191229 I07S      099    001  ROS 010820 0541    BO 41  9.64 S  57 44.64 E GPS      -9   4889       10   4884   4969        33 1-8,23,24,27,30,34,93
49NZ20191229 I07S      099    001  ROS 010820 0806    EN 41  9.47 S  57 44.61 E GPS      -9   4889
49NZ20191229 I07S      100    001  CTD 010820 1051    BE 41 37.45 S  57 44.57 E GPS      -9   4747
49NZ20191229 I07S      100    001  CTD 010820 1208    BO 41 37.59 S  57 44.91 E GPS      -9   4740        9   4732   4819        0
49NZ20191229 I07S      100    001  CTD 010820 1322    EN 41 37.74 S  57 45.29 E GPS      -9   4736
49NZ20191229 I07S      101    001  ROS 010820 1613    BE 42  5.09 S  57 44.33 E GPS      -9   4788
49NZ20191229 I07S      101    001  ROS 010820 1728    BO 42  4.75 S  57 45.14 E GPS      -9   4797        9   4791   4873        32 1-8,23,24,27,29,30,34,42,43,82,92,93,98,110,117,121,123
49NZ20191229 I07S      101    001  ROS 010820 1943    EN 42  4.06 S  57 46.34 E GPS      -9   4800
49NZ20191229 I07S      101    001  FLT 010820 1955    DE 42  4.08 S  57 46.48 E GPS      -9   4798                                                                                                ARGO HULL#8827
49NZ20191229 I07S      102    001  CTD 010820 2257    BE 42 32.48 S  57 43.97 E GPS      -9   4769
49NZ20191229 I07S      102    001  CTD 010920 0013    BO 42 32.62 S  57 45.33 E GPS      -9   4767        9   4767   4839        0
49NZ20191229 I07S      102    001  CTD 010920 0127    EN 42 32.65 S  57 46.75 E GPS      -9   4771
49NZ20191229 I07S      405    001  XCT 010920 0251    DE 42 46.25 S  57 44.47 E GPS      -9   4760                                                                                                TSK XCTD-4 #18117715
49NZ20191229 I07S      103    001  ROS 010920 0425    BE 42 59.82 S  57 43.63 E GPS      -9   4747
49NZ20191229 I07S      103    001  XCT 010920 0442    DE 42 59.82 S  57 43.93 E GPS      -9   4748                                                                                                TSK XCTD-4 #18117720
```

```
49NZ20191229 I07S      103    001  ROS 010920 0538    BO 42 59.79 S  57 45.45 E GPS      -9   4744        9   4736   4810        32 1-8,20,23,24,27,30,34,93
49NZ20191229 I07S      103    001  ROS 010920 0752    EN 42 59.90 S  57 48.10 E GPS      -9   4750
49NZ20191229 I07S      406    001  XCT 010920 0925    DE 43 14.99 S  57 44.39 E GPS      -9   4735                                                                                                TSK XCTD-4 #18117719
49NZ20191229 I07S      104    001  ROS 010920 1103    BE 43 29.94 S  57 44.82 E GPS      -9   4699
49NZ20191229 I07S      104    001  ROS 010920 1219    BO 43 29.93 S  57 44.97 E GPS      -9   4699        9   4690   4774        28 18,19
49NZ20191229 I07S      104    001  ROS 010920 1346    EN 43 30.00 S  57 44.99 E GPS      -9   4699
49NZ20191229 I07S      407    001  XCT 010920 1515    DE 43 45.00 S  57 45.19 E GPS      -9   4674                                                                                                TSK XCTD-4 #18117716
49NZ20191229 I07S      105    001  ROS 010920 1650    BE 43 59.93 S  57 45.63 E GPS      -9   4639
49NZ20191229 I07S      105    001  ROS 010920 1807    BO 43 59.87 S  57 45.52 E GPS      -9   4639       10   4634   4713        32 1-8,12,13,20,23,24,27,30,34,82,91-93,98,123
49NZ20191229 I07S      105    001  ROS 010920 2017    EN 43 59.64 S  57 44.98 E GPS      -9   4638
49NZ20191229 I07S      408    001  XCT 010920 2147    DE 44 14.99 S  57 46.00 E GPS      -9   4600                                                                                                TSK XCTD-4 #18117717
49NZ20191229 I07S      106    001  ROS 010920 2323    BE 44 29.98 S  57 46.40 E GPS      -9   4588
49NZ20191229 I07S      106    001  XCT 010920 2329    DE 44 29.99 S  57 46.40 E GPS      -9   4590                                                                                                TSK XCTD-4 #18117718
49NZ20191229 I07S      106    001  ROS 011020 0035    BO 44 29.99 S  57 46.38 E GPS      -9   4588        9   4594   4670        28 22
49NZ20191229 I07S      106    001  ROS 011020 0203    EN 44 29.99 S  57 46.39 E GPS      -9   4589
49NZ20191229 I07S      409    001  XCT 011020 0326    DE 44 45.00 S  57 46.82 E GPS      -9   4553                                                                                                TSK XCTD-4 #18117724
49NZ20191229 I07S      107    001  ROS 011020 0456    BE 45  0.11 S  57 47.27 E GPS      -9   4540
49NZ20191229 I07S      107    001  ROS 011020 0606    BO 45  0.06 S  57 47.24 E GPS      -9   4538        9   4530   4607        34 1-8,20,23,24,27,29,30,34,40,43,82,92,93,98,110,123,124
49NZ20191229 I07S      107    001  ROS 011020 0818    EN 44 59.99 S  57 47.16 E GPS      -9   4539
49NZ20191229 I07S      107    001  FLT 011020 0828    DE 44 59.91 S  57 47.11 E GPS      -9   4540                                                                                                SOCCOM BGC #18739
49NZ20191229 I07S      410    001  XCT 011020 1005    DE 45 15.02 S  57 47.61 E GPS      -9   4492                                                                                                TSK XCTD-4 #18117727
49NZ20191229 I07S      108    001  ROS 011020 1145    BE 45 30.07 S  57 47.84 E GPS      -9   4457
49NZ20191229 I07S      108    001  ROS 011020 1253    BO 45 30.04 S  57 47.96 E GPS      -9   4458       10   4450   4524        32 1-8,20,23,24,27,30,34,93
49NZ20191229 I07S      108    001  ROS 011020 1453    EN 45 29.65 S  57 48.36 E GPS      -9   4458
49NZ20191229 I07S      411    001  XCT 011020 1624    DE 45 43.05 S  57 46.73 E GPS      -9   4444                                                                                                TSK XCTD-4 #18117730
49NZ20191229 I07S      109    001  CTD 011120 0007    BE 45 56.23 S  57 45.53 E GPS      -9   4435
49NZ20191229 I07S      109    001  CTD 011120 0119    BO 45 56.24 S  57 45.30 E GPS      -9   4435       10   4432   4504        0
49NZ20191229 I07S      109    001  CTD 011120 0229    EN 45 56.28 S  57 45.30 E GPS      -9   4436
49NZ20191229 I07S      110    001  CTD 011120 0503    BE 46 22.22 S  57 43.10 E GPS      -9   4489
49NZ20191229 I07S      110    001  CTD 011120 0613    BO 46 22.20 S  57 43.22 E GPS      -9   4489       10   4481   4555        0
49NZ20191229 I07S      110    001  CTD 011120 0723    EN 46 22.20 S  57 43.29 E GPS      -9   4485
49NZ20191229 I07S      111    001  ROS 011120 1000    BE 46 48.37 S  57 40.64 E GPS      -9   4447
49NZ20191229 I07S      111    001  ROS 011120 1112    BO 46 48.27 S  57 40.99 E GPS      -9   4444        9   4431   4511        31 1-8,20,23,24,27,30,34,82,92,93
49NZ20191229 I07S      111    001  ROS 011120 1308    EN 46 48.24 S  57 41.59 E GPS      -9   4447
49NZ20191229 I07S      112    001  CTD 011120 1546    BE 47 14.65 S  57 37.83 E GPS      -9   4482
49NZ20191229 I07S      112    001  CTD 011120 1658    BO 47 14.62 S  57 37.86 E GPS      -9   4482        9   4472   4550        0
49NZ20191229 I07S      112    001  CTD 011120 1806    EN 47 14.63 S  57 37.87 E GPS      -9   4481
49NZ20191229 I07S      113    001  ROS 011120 2042    BE 47 40.77 S  57 35.30 E GPS      -9   4540
49NZ20191229 I07S      113    001  ROS 011120 2154    BO 47 40.79 S  57 35.35 E GPS      -9   4539        9   4531   4612        32 1-8,20,23,24,27,30,34,93
49NZ20191229 I07S      113    001  ROS 011220 0003    EN 47 40.78 S  57 35.31 E GPS      -9   4537
49NZ20191229 I07S      114    001  ROS 011220 0223    BE 47 55.00 S  57 41.08 E GPS      -9   4332
49NZ20191229 I07S      114    001  ROS 011220 0333    BO 47 55.12 S  57 41.06 E GPS      -9   4332        9   4320   4397        34 1-8,23,24,27,29,30,34,40,42,43,92,93,98,110,117,120,121,123,124
49NZ20191229 I07S      114    001  ROS 011220 0538    EN 47 55.23 S  57 40.83 E GPS      -9   4333
49NZ20191229 I07S      114    001  FLT 011220 0548    DE 47 55.30 S  57 40.84 E GPS      -9   4335                                                                                                SOCCOM BGC #18821
49NZ20191229 I07S      115    001  CTD 011220 0841    BE 48  7.11 S  57 51.81 E GPS      -9   4334
49NZ20191229 I07S      115    001  CTD 011220 0951    BO 48  7.10 S  57 51.77 E GPS      -9   4337        9   4323   4398        0
49NZ20191229 I07S      115    001  CTD 011220 1058    EN 48  7.12 S  57 51.67 E GPS      -9   4330
49NZ20191229 I07S      116    001  ROS 011220 1331    BE 48 33.64 S  57 55.98 E GPS      -9   4481
49NZ20191229 I07S      116    001  ROS 011220 1441    BO 48 33.63 S  57 55.90 E GPS      -9   4481       10   4464   4546        30 1-8,20,23,24,27,29,30,34,93,110
49NZ20191229 I07S      116    001  ROS 011220 1639    EN 48 33.63 S  57 55.96 E GPS      -9   4479
49NZ20191229 I07S      117    001  CTD 011220 1913    BE 49  0.04 S  57 59.84 E GPS      -9   4382
```

```
49NZ20191229 I07S      117    001  CTD 011220 2022    BO 49  0.05 S  57 59.79 E GPS      -9   4382        8   4374   4451        0
49NZ20191229 I07S      117    001  CTD 011220 2130    EN 49  0.05 S  57 59.80 E GPS      -9   4381
49NZ20191229 I07S      118    001  CTD 011420 0232    BE 49 33.57 S  57 49.91 E GPS      -9   4434
49NZ20191229 I07S      118    001  CTD 011420 0243    BO 49 33.57 S  57 49.91 E GPS      -9   4434       99    400    636        0                                                    ABORTED WITH MOD ERRORS
49NZ20191229 I07S      118    001  CTD 011420 0307    EN 49 33.64 S  57 49.88 E GPS      -9   4434
49NZ20191229 I07S      118    002  ROS 011420 0442    BE 49 33.55 S  57 49.79 E GPS      -9   4441
49NZ20191229 I07S      118    002  ROS 011420 0555    BO 49 33.57 S  57 49.82 E GPS      -9   4439       11   4412   4492        36 3-6,30
49NZ20191229 I07S      118    002  ROS 011420 0801    EN 49 33.70 S  57 49.88 E GPS      -9   4432
49NZ20191229 I07S      119    001  CTD 011420 1129    BE 50  6.96 S  57 39.87 E GPS      -9   4532
49NZ20191229 I07S      119    001  CTD 011420 1241    BO 50  6.99 S  57 39.87 E GPS      -9   4533       10   4516   4600        0
49NZ20191229 I07S      119    001  CTD 011420 1354    EN 50  7.02 S  57 39.81 E GPS      -9   4536
49NZ20191229 I07S      119    001  FLT 011420 1401    DE 50  7.02 S  57 39.83 E GPS      -9   4539                                                                                ARGO HULL#8849
49NZ20191229 I07S      120    001  ROS 011420 1720    BE 50 40.48 S  57 29.90 E GPS      -9   4519
49NZ20191229 I07S      120    001  ROS 011420 1831    BO 50 40.49 S  57 29.87 E GPS      -9   4515        9   4504   4586        32 1-8,20,23,24,27,29,30,34,93,110
49NZ20191229 I07S      120    001  ROS 011420 2041    EN 50 40.49 S  57 29.95 E GPS      -9   4516
49NZ20191229 I07S      121    001  CTD 011520 0012    BE 51 13.90 S  57 19.92 E GPS      -9   4540
49NZ20191229 I07S      121    001  CTD 011520 0123    BO 51 13.92 S  57 19.95 E GPS      -9   4542        9   4524   4608        0
49NZ20191229 I07S      121    001  CTD 011520 0231    EN 51 13.90 S  57 19.76 E GPS      -9   4530
49NZ20191229 I07S      122    001  ROS 011520 0537    BE 51 47.49 S  57 10.13 E GPS      -9   4442
49NZ20191229 I07S      122    001  ROS 011520 0646    BO 51 47.57 S  57 10.43 E GPS      -9   4428       10   4407   4488        31 1-8,20,23,24,27,30,34,42,43,82,92,93,98,117,120,121,123
49NZ20191229 I07S      122    001  ROS 011520 0847    EN 51 47.65 S  57 10.50 E GPS      -9   4428
49NZ20191229 I07S      123    001  CTD 011520 1201    BE 52 20.79 S  57  0.08 E GPS      -9   4738
49NZ20191229 I07S      123    001  CTD 011520 1314    BO 52 20.77 S  56 59.98 E GPS      -9   4756       10   4713   4803        0
49NZ20191229 I07S      123    001  CTD 011520 1426    EN 52 20.76 S  56 59.91 E GPS      -9   4741
49NZ20191229 I07S      123    001  FLT 011520 1435    DE 52 20.76 S  56 59.93 E GPS      -9   4744                                                                                ARGO HULL#8843
49NZ20191229 I07S      124    001  ROS 011520 1745    BE 52 54.30 S  56 49.91 E GPS      -9   4287
49NZ20191229 I07S      124    001  ROS 011520 1851    BO 52 54.29 S  56 50.00 E GPS      -9   4281        9   4270   4347        30 1-8,20,23,24,27,30,34,91,93
49NZ20191229 I07S      124    001  ROS 011520 2056    EN 52 54.32 S  56 49.99 E GPS      -9   4285
49NZ20191229 I07S      125    001  CTD 011620 0015    BE 53 27.79 S  56 39.99 E GPS      -9   3559
49NZ20191229 I07S      125    001  CTD 011620 0115    BO 53 27.55 S  56 40.15 E GPS      -9   3663       37   3630   3684        0
49NZ20191229 I07S      125    001  CTD 011620 0212    EN 53 27.31 S  56 40.12 E GPS      -9   3712
49NZ20191229 I07S      126    001  ROS 011620 0535    BE 54  1.21 S  56 30.02 E GPS      -9   3523
49NZ20191229 I07S      126    001  XCT 011620 0540    BE 54  1.21 S  56 29.98 E GPS      -9   3270                                                                                TSK XCTD-4 #18117721
49NZ20191229 I07S      126    001  ROS 011620 0634    BO 54  1.24 S  56 29.93 E GPS      -9   3496       11   3521   3580        29 1-8,20,23,24,27,29,30,34,40,43,82,92,93,98,110,123,124
49NZ20191229 I07S      126    001  ROS 011620 0731    EN 54  1.50 S  56 29.42 E GPS      -9   4213                                                                                NISKINS TRIPPED ON THE FLY
49NZ20191229 I07S      126    001  FLT 011620 0742    DE 54  1.48 S  56 29.00 E GPS      -9   3406                                                                                SOCCOM BGC #18013
49NZ20191229 I07S      412    001  XCT 011620 1050    DE 54 34.69 S  56 20.10 E GPS      -9   4374                                                                                TSK XCTD-4 #18117722
49NZ20191229 I07S      413    001  FLT 011620 1417    DE 55  8.01 S  56 10.26 E GPS      -9   3401                                                                                ARGO HULL#8826
49NZ20191229 I07S      413    001  XCT 011620 1417    DE 55  7.99 S  56 10.23 E GPS      -9   3401                                                                                TSK XCTD-4 #18117723
49NZ20191229 I07S      414    001  XCT 011620 1732    DE 55 41.66 S  56  2.31 E GPS      -9   3231                                                                                TSK XCTD-4 #18117725
49NZ20191229 I07S      132    001  ROS 011720 0029    BE 56 15.09 S  55 50.16 E GPS      -9   4763
49NZ20191229 I07S      132    001  ROS 011720 0147    BO 56 15.08 S  55 50.16 E GPS      -9   4746       14   4714   4806        33 1-8,20,23,24,27,29,30,34,93,110
49NZ20191229 I07S      132    001  ROS 011720 0401    EN 56 14.91 S  55 50.05 E GPS      -9   4713
49NZ20191229 I07S      132    001  FLT 011720 0410    DE 56 14.92 S  55 49.88 E GPS      -9   4722                                                                                ARGO HULL#8832
49NZ20191229 I07S      133    001  CTD 011720 0659    BE 56 44.09 S  55 41.48 E GPS      -9   4931
49NZ20191229 I07S      133    001  CTD 011720 0817    BO 56 44.14 S  55 41.18 E GPS      -9   4933        8   4914   5010        0
49NZ20191229 I07S      133    001  CTD 011720 0935    EN 56 44.10 S  55 41.32 E GPS      -9   4931
49NZ20191229 I07S      134    001  ROS 011720 1241    BE 57 12.93 S  55 33.04 E GPS      -9   5087
49NZ20191229 I07S      134    001  ROS 011720 1407    BO 57 12.99 S  55 33.05 E GPS      -9   5092       14   5066   5172        34 1-8,20,23,24,27,30,34,43,82,92,93,98,123
49NZ20191229 I07S      134    001  ROS 011720 1622    EN 57 13.08 S  55 32.96 E GPS      -9   5101
49NZ20191229 I07S      135    001  CTD 011720 1937    BE 57 42.05 S  55 24.03 E GPS      -9   5196
```

```
49NZ20191229 I07S      135    001  CTD 011720 2103    BO 57 42.12 S  55 24.24 E GPS      -9   5194       10   5185   5291        0
49NZ20191229 I07S      135    001  CTD 011720 2226    EN 57 42.13 S  55 24.25 E GPS      -9   5199
49NZ20191229 I07S      136    001  ROS 011820 0133    BE 58 11.14 S  55 15.64 E GPS      -9   5186
49NZ20191229 I07S      136    001  ROS 011820 0253    BO 58 11.13 S  55 15.82 E GPS      -9   5192        8   5176   5282        36 1-8,20,23,24,27,29,30,34,40,93,110,124
49NZ20191229 I07S      136    001  ROS 011820 0511    EN 58 11.07 S  55 16.13 E GPS      -9   5190
49NZ20191229 I07S      136    001  FLT 011820 0523    DE 58 11.56 S  55 16.05 E GPS      -9   5187                                                                                SOCCOM BGC #18864
49NZ20191229 I07S      137    001  CTD 011820 0814    BE 58 40.05 S  55  7.04 E GPS      -9   5173
49NZ20191229 I07S      137    001  XCT 011820 0821    DE 58 40.03 S  55  7.08 E GPS      -9   5172                                                                                TSK XCTD-4 #18117726
49NZ20191229 I07S      137    001  CTD 011820 0932    BO 58 40.03 S  55  6.99 E GPS      -9   5170        9   5160   5267        0
49NZ20191229 I07S      137    001  CTD 011820 1053    EN 58 40.10 S  55  7.39 E GPS      -9   5172
49NZ20191229 I07S      138    001  ROS 011820 1346    BE 59  9.10 S  54 58.39 E GPS      -9   5145
49NZ20191229 I07S      138    001  ROS 011820 1507    BO 59  9.08 S  54 58.44 E GPS      -9   5145        8   5140   5242        34 1-8,20,23,24,27,30,34,42,43,82,92,93,98,117,120,121,123
49NZ20191229 I07S      138    001  ROS 011820 1717    EN 59  9.07 S  54 58.44 E GPS      -9   5153
49NZ20191229 I07S      139    001  CTD 011820 2010    BE 59 38.03 S  54 49.75 E GPS      -9   5152
49NZ20191229 I07S      139    001  CTD 011820 2129    BO 59 38.10 S  54 49.74 E GPS      -9   5152        9   5141   5245        0
49NZ20191229 I07S      139    001  CTD 011820 2249    EN 59 38.10 S  54 49.73 E GPS      -9   5152
49NZ20191229 I07S      140    001  ROS 011920 0137    BE 60  7.13 S  54 41.07 E GPS      -9   5143
49NZ20191229 I07S      140    001  ROS 011920 0254    BO 60  7.23 S  54 41.19 E GPS      -9   5147       10   5140   5240        34 1-8,20,23,24,27,29,30,34,93,110
49NZ20191229 I07S      140    001  ROS 011920 0508    EN 60  7.29 S  54 41.30 E GPS      -9   5144
49NZ20191229 I07S      140    001  FLT 011920 0517    DE 60  7.57 S  54 41.24 E GPS      -9   5152                                                                                ARGO HULL#8831
49NZ20191229 I07S      141    001  ROS 011920 0755    BE 60 36.13 S  54 32.49 E GPS      -9   5149
49NZ20191229 I07S      141    001  ROS 011920 0914    BO 60 36.17 S  54 32.66 E GPS      -9   5149       10   5137   5241        28 18,19
49NZ20191229 I07S      141    001  ROS 011920 1044    EN 60 36.11 S  54 32.79 E GPS      -9   5154
49NZ20191229 I07S      142    001  ROS 011920 1328    BE 61  5.11 S  54 23.89 E GPS      -9   5126
49NZ20191229 I07S      142    001  ROS 011920 1447    BO 61  5.10 S  54 23.86 E GPS      -9   5126       11   5120   5222        34 1-8,12,13,20,23,24,27,30,34,43,82,91-93,98,123
49NZ20191229 I07S      142    001  ROS 011920 1656    EN 61  5.08 S  54 23.85 E GPS      -9   5126
49NZ20191229 I07S      143    001  ROS 011920 1940    BE 61 34.11 S  54 15.16 E GPS      -9   5101
49NZ20191229 I07S      143    001  ROS 011920 2059    BO 61 34.10 S  54 15.22 E GPS      -9   5098        9   5093   5193        28 22
49NZ20191229 I07S      143    001  ROS 011920 2232    EN 61 34.12 S  54 15.12 E GPS      -9   5104
49NZ20191229 I07S      144    001  ROS 012020 0115    BE 62  3.19 S  54  6.42 E GPS      -9   5060
49NZ20191229 I07S      144    001  ROS 012020 0232    BO 62  3.31 S  54  6.25 E GPS      -9   5058        9   5052   5151        34 1-8,20,23,24,27,29,30,34,93,110
49NZ20191229 I07S      144    001  ROS 012020 0444    EN 62  3.30 S  54  6.22 E GPS      -9   5058
49NZ20191229 I07S      145    001  CTD 012020 0718    BE 62 32.19 S  53 57.73 E GPS      -9   5057
49NZ20191229 I07S      145    001  CTD 012020 0837    BO 62 32.17 S  53 57.44 E GPS      -9   5057       10   5051   5151        0
49NZ20191229 I07S      145    001  CTD 012020 0955    EN 62 32.19 S  53 57.28 E GPS      -9   5057
49NZ20191229 I07S      146    001  CTD 012020 1233    BE 63  1.14 S  53 49.15 E GPS      -9   4983
49NZ20191229 I07S      146    001  CTD 012020 1349    BO 63  1.07 S  53 49.14 E GPS      -9   4985       10   4980   5076        0
49NZ20191229 I07S      146    001  CTD 012020 1506    EN 63  1.08 S  53 49.28 E GPS      -9   4983
49NZ20191229 S04I      147    001  ROS 012020 1745    BE 63 30.13 S  53 40.61 E GPS      -9   4757
49NZ20191229 S04I      147    001  ROS 012020 1856    BO 63 30.11 S  53 40.64 E GPS      -9   4758       10   4750   4841        35 1-8,20,23,24,27,29,30,34,40,42,43,82,92,93,98,110,117,120,121,123,124
49NZ20191229 S04I      147    001  ROS 012020 2106    EN 63 30.08 S  53 40.65 E GPS      -9   4756
49NZ20191229 S04I      147    001  FLT 012020 2117    DE 63 30.14 S  53 40.64 E GPS      -9   4757                                                                                SOCCOM BGC #18994
49NZ20191229 S04I      148    001  ROS 012120 0006    BE 63 58.07 S  53 25.23 E GPS      -9   4350
49NZ20191229 S04I      148    001  ROS 012120 0113    BO 63 58.02 S  53 25.09 E GPS      -9   4347       11   4341   4418        29 1-8,20,23,24,27,30,34,93
49NZ20191229 S04I      148    001  ROS 012120 0315    EN 63 58.03 S  53 25.17 E GPS      -9   4348
49NZ20191229 S04I      149    001  ROS 012120 0634    BE 64 26.02 S  53  4.33 E GPS      -9   4156
49NZ20191229 S04I      149    001  ROS 012120 0739    BO 64 26.12 S  53  4.68 E GPS      -9   4149        9   4142   4214        30 1-8,20,23,24,27,30,34,43,82,92,93,98,123
49NZ20191229 S04I      149    001  ROS 012120 0931    EN 64 26.01 S  53  4.75 E GPS      -9   4137
49NZ20191229 S04I      150    001  ROS 012120 1235    BE 64 46.89 S  52 59.23 E GPS      -9   3414
49NZ20191229 S04I      150    001  ROS 012120 1331    BO 64 46.99 S  52 59.27 E GPS      -9   3437       10   3423   3480        27 1-8,20,23,24,27,29,30,34,91-93,110
49NZ20191229 S04I      150    001  ROS 012120 1522    EN 64 46.96 S  52 59.10 E GPS      -9   3432
```

49NZ20191229	S04I	151	001	ROS	012120	1836	BE	65 6.22 S	53 1.00 E	GPS	-9	2500						
49NZ20191229	S04I	151	001	XCT	012120	1843	DE	65 6.22 S	53 1.00 E	GPS	-9	2504						TSK XCTD-4 #18117729
49NZ20191229	S04I	151	001	ROS	012120	1917	BO	65 6.19 S	53 0.99 E	GPS	-9	2504	9	2492	2524	25	1-8,20,23,24,27,30,34,42,43,82,92,93,98,117,120,121,123	
49NZ20191229	S04I	151	001	ROS	012120	2041	EN	65 6.21 S	53 0.91 E	GPS	-9	2503						
49NZ20191229	S04I	152	001	ROS	012120	2349	BE	65 13.46 S	53 7.89 E	GPS	-9	1882						
49NZ20191229	S04I	152	001	ROS	012220	0021	BO	65 13.45 S	53 7.85 E	GPS	-9	1880	10	1871	1893	20	1-8,20,23,24,27,29,30,34,43,82,92,93,98,110,123	
49NZ20191229	S04I	152	001	ROS	012220	0139	EN	65 13.47 S	53 7.75 E	GPS	-9	1876						
49NZ20191229	S04I	153	001	ROS	012220	0406	BE	65 20.16 S	53 14.98 E	GPS	-9	1207						
49NZ20191229	S04I	153	001	ROS	012220	0429	BO	65 20.20 S	53 15.15 E	GPS	-9	1205	10	1196	1209	29	1-8,20,23,24,27,29,30,34,42,43,92,93,98,110,117,121,123	
49NZ20191229	S04I	153	001	ROS	012220	0521	EN	65 20.23 S	53 15.11 E	GPS	-9	1213						
49NZ20191229	S04I	415	001	XCT	012220	0544	DE	65 21.97 S	53 14.12 E	GPS	-9	1318						TSK XCTD-4 #18117731 ON ICE EDGE
49NZ20191229	S04I	416	001	XCT	012220	0605	DE	65 21.09 S	53 14.79 E	GPS	-9	1450						TSK XCTD-4 #18117732
49NZ20191229				FLT	012220	2243	DE	64 8.58 S	58 15.04 E	GPS	-9	4228						ARGO HULL#8848
49NZ20191229				UNK	012320	0100	BE	63 58.17 S	59 12.57 E	GPS	-9	4172						MAGNETOMETER CALIBRATION
49NZ20191229				UNK	012320	0121	EN	63 58.23 S	59 12.62 E	GPS	-9	4174						MAGNETOMETER CALIBRATION
49NZ20191229				FLT	012320	1814	DE	61 51.55 S	65 29.98 E	GPS	-9	4430						ARGO HULL#8833
49NZ20191229				FLT	012520	0139	DE	57 22.14 S	75 0.08 E	GPS	-9	2632						ARGO HULL#1090
49NZ20191229				FLT	012520	2245	DE	53 54.40 S	80 0.00 E	GPS	-9	3201						ARGO HULL#8845
49NZ20191229				FLT	012620	2010	DE	50 7.95 S	84 0.13 E	GPS	-9	4196						ARGO HULL#1057
49NZ20191229				UNK	012820	0117	BE	44 43.38 S	88 42.23 E	GPS	-9	3392						MAGNETOMETER CALIBRATION
49NZ20191229				UNK	012820	0141	EN	44 42.74 S	88 42.45 E	GPS	-9	3432						MAGNETOMETER CALIBRATION
49NZ20191229				UNK	012820	0211	BE	44 41.01 S	88 43.77 E	GPS	-9	3419						CESIUM MAGNETOMETER TOWING
49NZ20191229				UNK	012920	0618	EN	40 39.30 S	91 55.50 E	GPS	-9	3275						CESIUM MAGNETOMETER TOWING
49NZ20191229				FLT	012920	0652	DE	40 37.82 S	91 55.99 E	GPS	-9	3196						ARGO HULL#1064
49NZ20191229				UNK	012920	0709	BE	40 37.15 S	91 57.10 E	GPS	-9	3181						MAGNETOMETER CALIBRATION
49NZ20191229				UNK	012920	0734	EN	40 37.08 S	91 57.36 E	GPS	-9	3200						MAGNETOMETER CALIBRATION
49NZ20191229				FLT	013120	0812	DE	30 48.30 S	96 0.01 E	GPS	-9	2593						ARGO HULL#1055
49NZ20191229				UNK	020320	0737	BE	17 2.91 S	100 30.71 E	GPS	-9	5882						LARGE VOLUME PUMP SAMPLING FOR NUTRIENTS
49NZ20191229				UNK	020320	1101	UN	17 1.38 S	100 26.88 E	GPS	-9	5553						L.V.P.S. END FOR NUTS BEGIN FOR CO2
49NZ20191229				UNK	020320	1112	BE	17 0.93 S	100 27.02 E	GPS	-9	5555						MAGNETOMETER CALIBRATION
49NZ20191229				UNK	020320	1128	EN	17 0.57 S	100 26.97 E	GPS	-9	5518						L.V.P.S. FOR CO2
49NZ20191229				UNK	020320	1134	EN	17 0.88 S	100 27.08 E	GPS	-9	5555						MAGNETOMETER CALIBRATION

Water sample parameters:

Number	Parameter	Mnemonic	Mnemonic for expected error
1	Salinity	SALNTY	
2	Oxygen	OXYGEN	
3	Silicate	SILCAT	SILUNC *1
4	Nitrate	NITRAT	NRAUNC *1
5	Nitrite	NITRIT	NRIUNC *1
6	Phosphate	PHSPHT	PHPUNC *1
7	Freon-11	CFC-11	
8	Freon-12	CFC-12	
9	Tritium		
10	Helium		
11	He-3/He-4		
12	14Carbon	DELC14	C14ERR
13	13Carbon	DELC13	C13ERR
14	Kr-85		
15	Argon		
16	Ar-39		
17	Neon		
18	Ra-228		
19	Ra-226		
20	Ratio of O18 to O16	O18/O16	
21	Sr-90		
22	Cesium-137	CS-137	CS137ER *2
23	Total carbon	TCARBN	
24	Total alkalinity	ALKALI	
25	pCO2		
26	pH	PH	
27	Freon-113	CFC113	
28	Carbon tetrachloride	CCL4	
29	Iodate/Iodide		
30	Ammonium	NH4	
31	Methane	CH4	
32	Dissolved organic nitrogen	DON	
33	Nitrous oxide	N2O	
34	Chlorophyll-a	CHLORA	
35	Phaeophytin		
36	Halocarbons		
37	Biogenic sulfur compounds	DMS	
38	Hydrocarbons		
39	Barium		
40	Particulate organic carbon	POC	
41	Particulate organic nitrogen	PON	
42	Abundance of bacteria	BACT	
43	Dissolved organic carbon	DOC	
44	Carbon monoxide		
45	Nitrogen (gas)		
46	Total organic carbon	TOC	
47	Plutonium	PLUTO	PLUTOER *2
48	Primary productivity		
64	Incubation		
81	Particulate organic matter	POM	
82	15N-Nitrate	15NO3	
83	Particulate inorganic matter	PIM	
84	Dissolved organic phosphate		
85	Ratio of O-17 to O-16	O17/O16	
86	Flowcytometry		
87	Genetic analysis		
88	Nitrogen fixation		
89	Cesium-134	CS-134	CS134ER
90	Perfluoroalkyl substances	PFAS	
91	Iodine-129	I-129	
92	Density salinity	DNSSAL	
93	Sulfur hexafluoride	SF6	
94	Isoprene		
95	Pigment		
96	Microscope		
97	Calcium		
98	Colored dissolved organic matter	CDOM	
99	Absorption coefficients of particulate matter	AP	
100	Nitrification		
101	13C-CH4		
102	Prokaryotic abundance		
103	Fluorescence in situ hybridization		
104	Prokaryotic activity		
105	Viral production		
106	Microbial diversity		
107	N2O 15N-isotope		
108	Nitrogen fixation		
109	NH4 15N-isotope		
110	Urea		
111	NO2 15N-isotope		
112	Coenzyme F430		
113	Chlorophyll 15N-isotope		
114	Nitrogen isotope ratio of dissolved organic nitrogen	DO15N	
115	Abundance of phytoplankton		
116	Nitrogen isotope ratio of phytoplankton	15PHY	
117	Prokaryotic production		
118	Beryllium-isotope		
119	Transparent exopolymer particle	TEP	
120	DIC-fix		
121	DNA		
122	H2		
123	FDOM		
124	HPLC		

Figure captions

Figure 1 Station locations for (a) WHP I08N revisit in 2019 and (b) I07S in 2020 with bottom topography.

Figure 2 Bathymetry (m) measured by Multi Narrow Beam Echo Sounding system.

Figure 3 Surface wind (m/s) measured at 25 m above sea level. Wind data is averaged over 6-hour.

Figure 4 (a) Sea surface temperature (°C), (b) sea surface salinity (psu), (c) sea surface oxygen (μmol/kg), and (d) sea surface chlorophyll *a* (mg/m^3) measured by the Continuous Sea Surface Water Monitoring System.

Figure 5 Difference in the partial pressure of CO_2 between the ocean and the atmosphere, ΔpCO_2 (ppmv).

Figure 6 Surface current at 100 m depth measured by shipboard acoustic Doppler current profiler (ADCP).

Figure 7 Potential temperature (°C) cross sections calculated by using CTD temperature and salinity data calibrated by bottle salinity measurements. Vertical exaggeration of the 0-6500 m section is 1000:1, and expanded section of the upper 1000 m is made with a vertical exaggeration of 2500:1.

Figure 8 CTD salinity (psu) cross sections calibrated by bottle salinity measurements. Vertical exaggeration is same as Fig. 7.

Figure 9 Absolute salinity (g/kg) cross sections calculated by using CTD salinity data. Vertical exaggeration is same as Fig. 7.

Figure 10 Density (upper: σ_0, lower: σ_4) (kg/m^3) cross sections calculated by using CTD temperature and salinity data based on TEOS-10 definition. Vertical exaggeration of the 0-1500 m and 1500-6500 m section are 2500:1 and 1000:1, respectively.

Figure 11 Neutral density (γ^n) (kg/m^3) cross sections calculated by using CTD temperature and salinity data. Vertical exaggeration is same as Fig. 7.

Figure 12 CTD oxygen (μmol/kg) cross sections. Vertical exaggeration is same as Fig. 7.

Figure 13 CTD chlorophyll *a* (mg/m^3) cross section. Vertical exaggeration of the upper 1000 m section is same as Fig. 7.

Figure 14 CTD beam attenuation coefficient (m^{-1}) cross sections. Vertical exaggeration is same as Fig. 7.

Figure 15 CTD FDOM (RU) cross sections. Vertical exaggeration is same as Fig. 7.

Figure 16 Bottle sampled dissolved oxygen (μmol/kg) cross sections. Data with quality flags of 2 were plotted. Vertical exaggeration is same as Fig. 7.

Figure 17 Silicate (μmol/kg) cross sections. Data with quality flags of 2 were plotted. Vertical exaggeration is same as Fig. 7.

Figure 18 Nitrate (μmol/kg) cross sections. Data with quality flags of 2 were plotted. Vertical exaggeration is same as Fig. 7.

Figure 19 Nitrite (μmol/kg) cross section. Data with quality flags of 2 were plotted. Vertical exaggeration of the upper 1000 m section is same as Fig. 7.

Figure 20 Phosphate (μmol/kg) cross sections. Data with quality flags of 2 were plotted. Vertical exaggeration is same as Fig. 7.

Figure 21 Dissolved inorganic carbon (μmol/kg) cross sections. Data with quality flags of 2 were plotted. Vertical exaggeration is same as Fig. 7.

Figure 22 Total alkalinity (μmol/kg) cross sections. Data with quality flags of 2 were plotted. Vertical exaggeration is same as Fig. 7.

Figure 23 CDOM as absorption coefficient at 300 nm (m^{-1}) cross sections. Data with quality flags of 2 were plotted. Vertical exaggeration is same as Fig. 7.

Figure 24 Cross sections of current velocity (cm/s) normal to the cruise track measured by LADCP (eastward or northward is positive). Vertical exaggeration is same as Fig. 7.

Figure 1a
Station locations for WHP I08N revisit in 2019

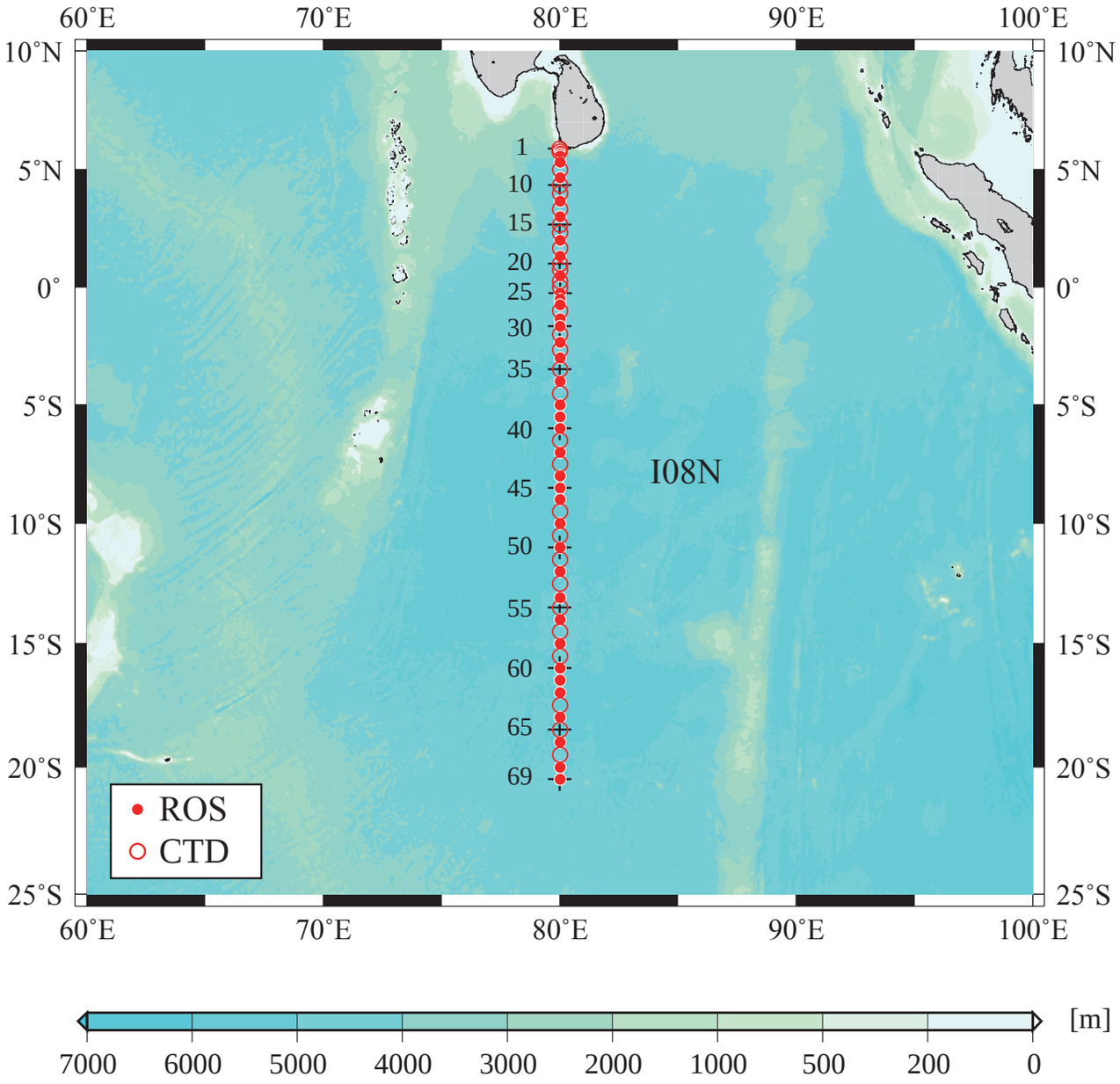

Figure 1b
Station locations for WHP I07S in 2020

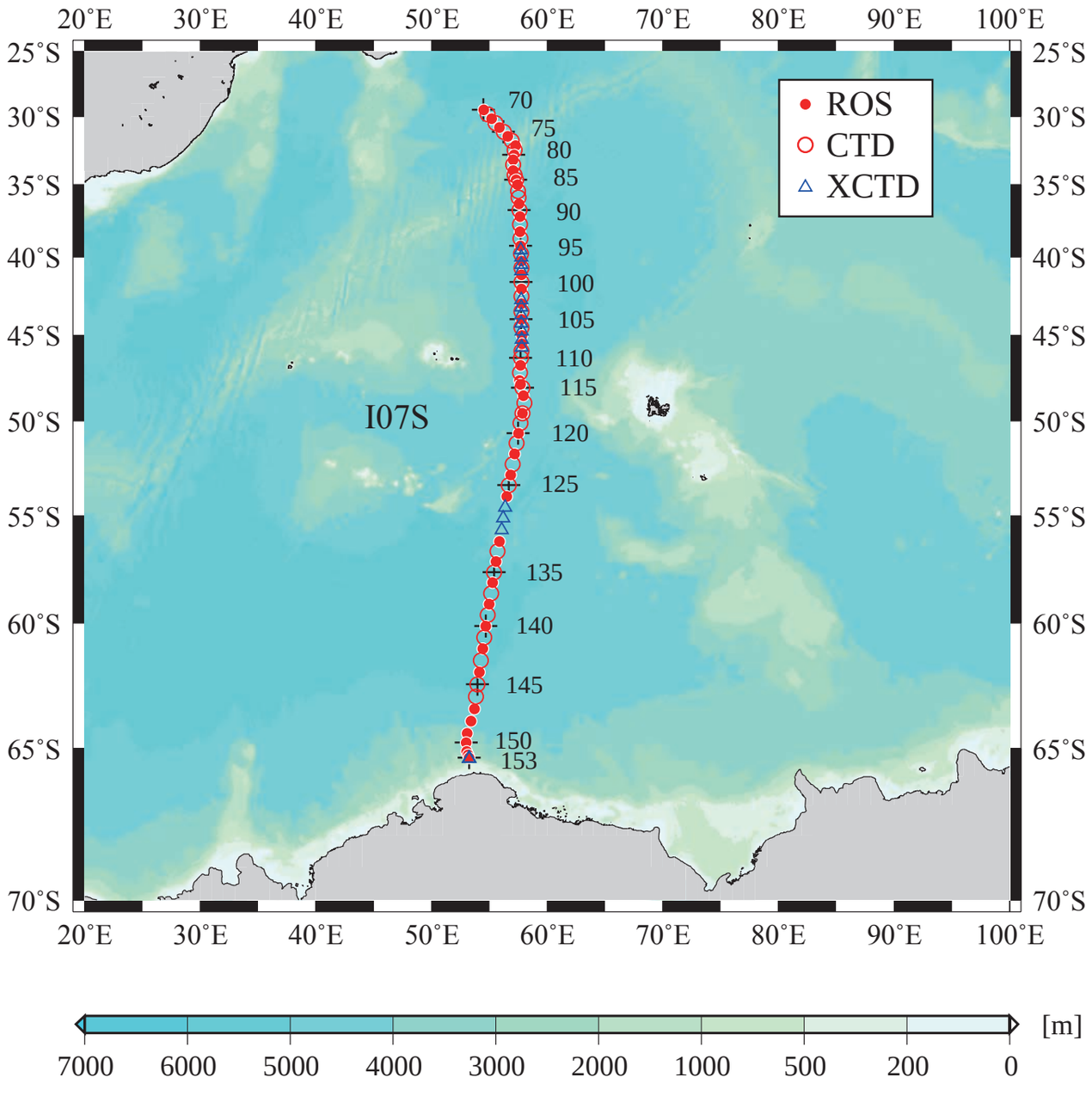

Figure 2

Bathymetry measured by Multi Narrow Beam Echo Sounding system

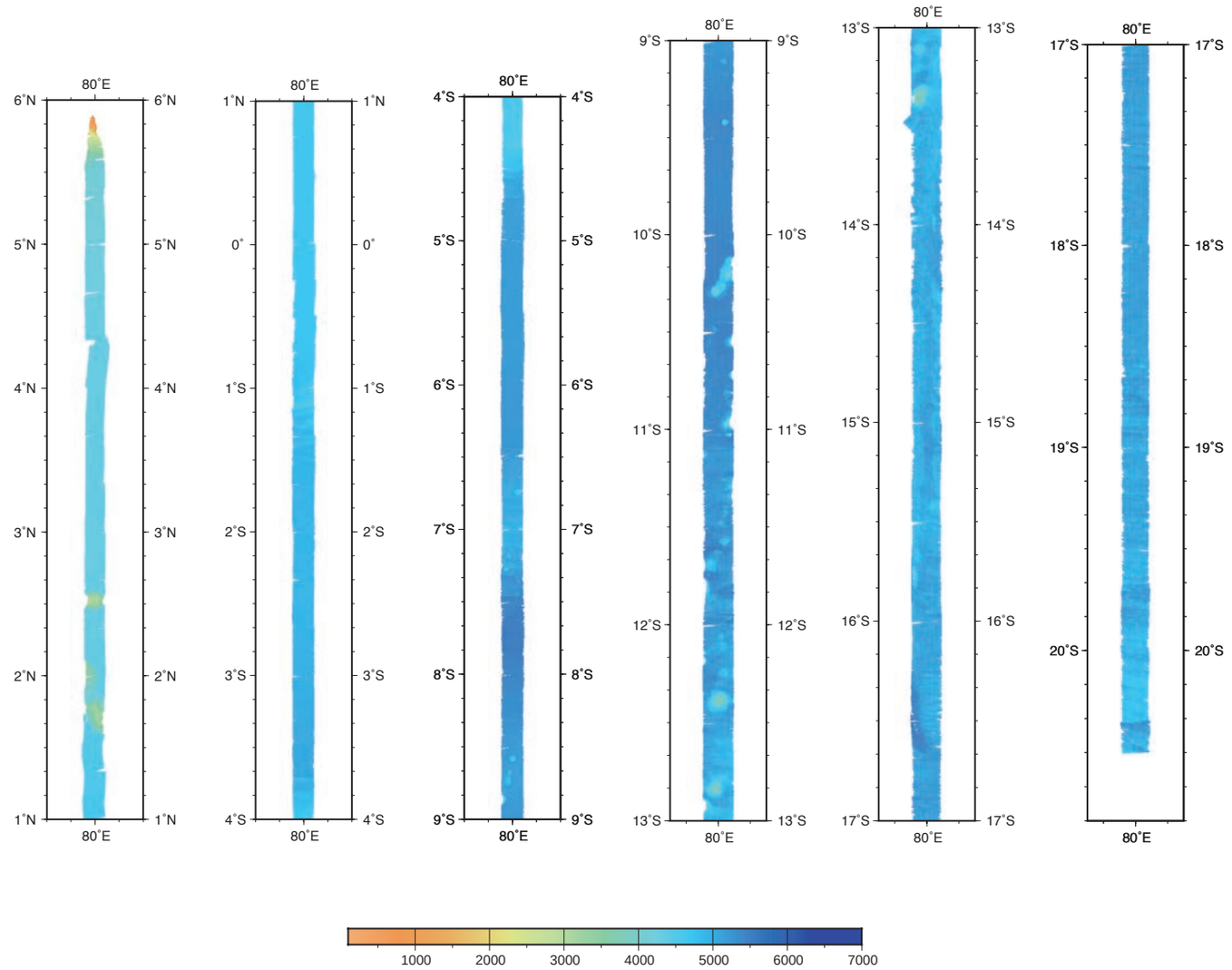

Figure 2
Continued

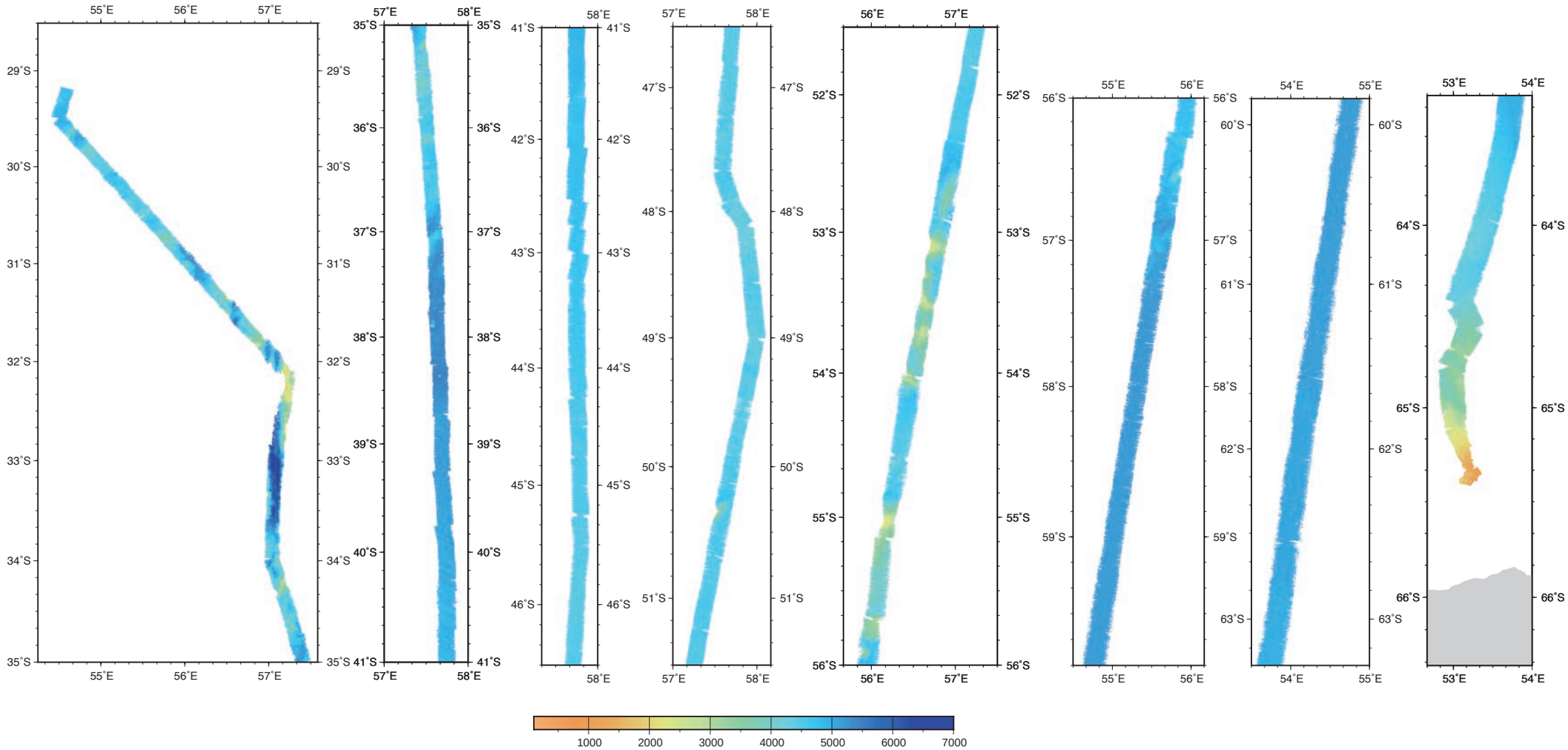

Figure 3
Surface wind measured at 25 m above sea level

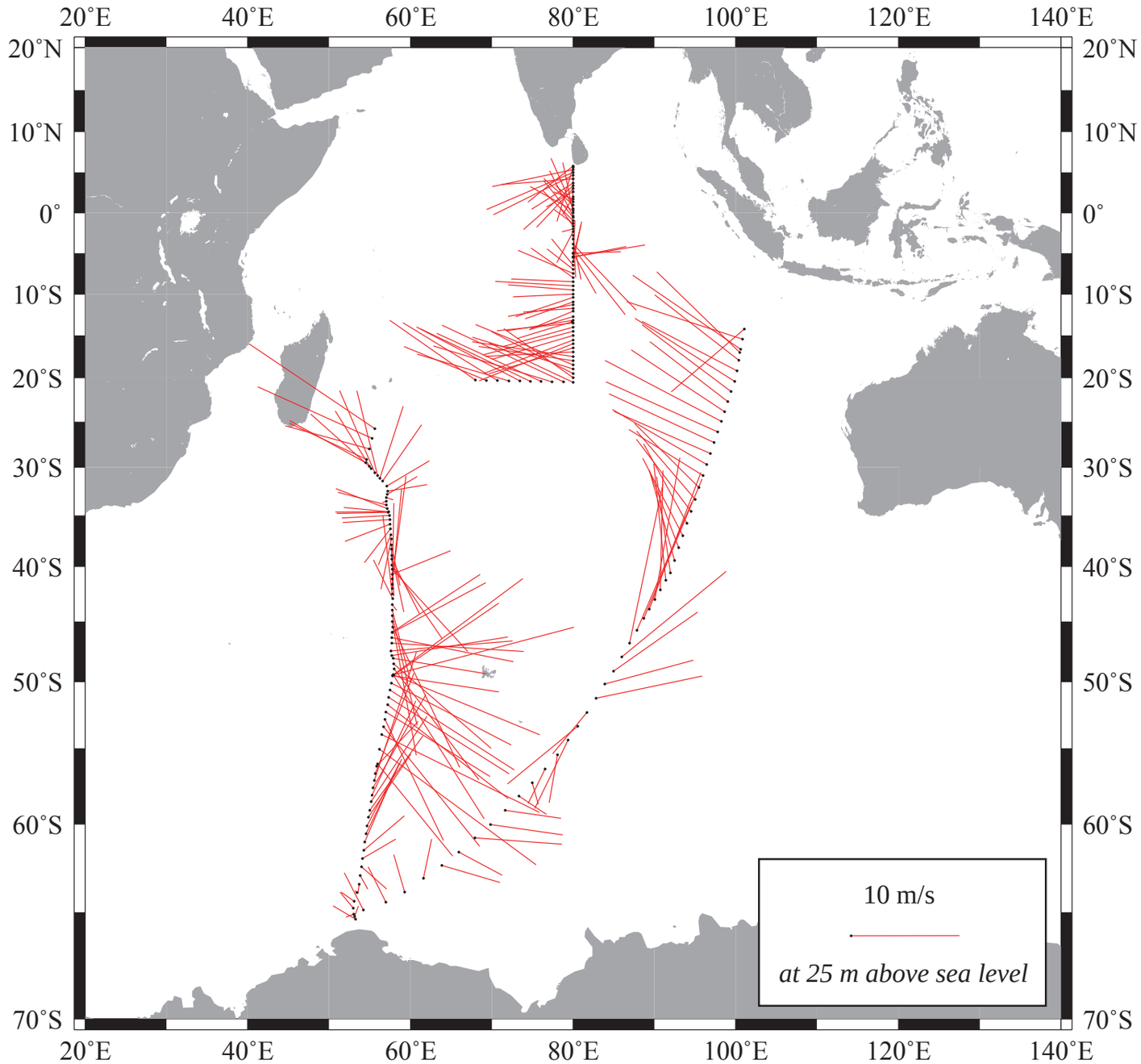

Figure 4a
Sea surface temperature (°C)

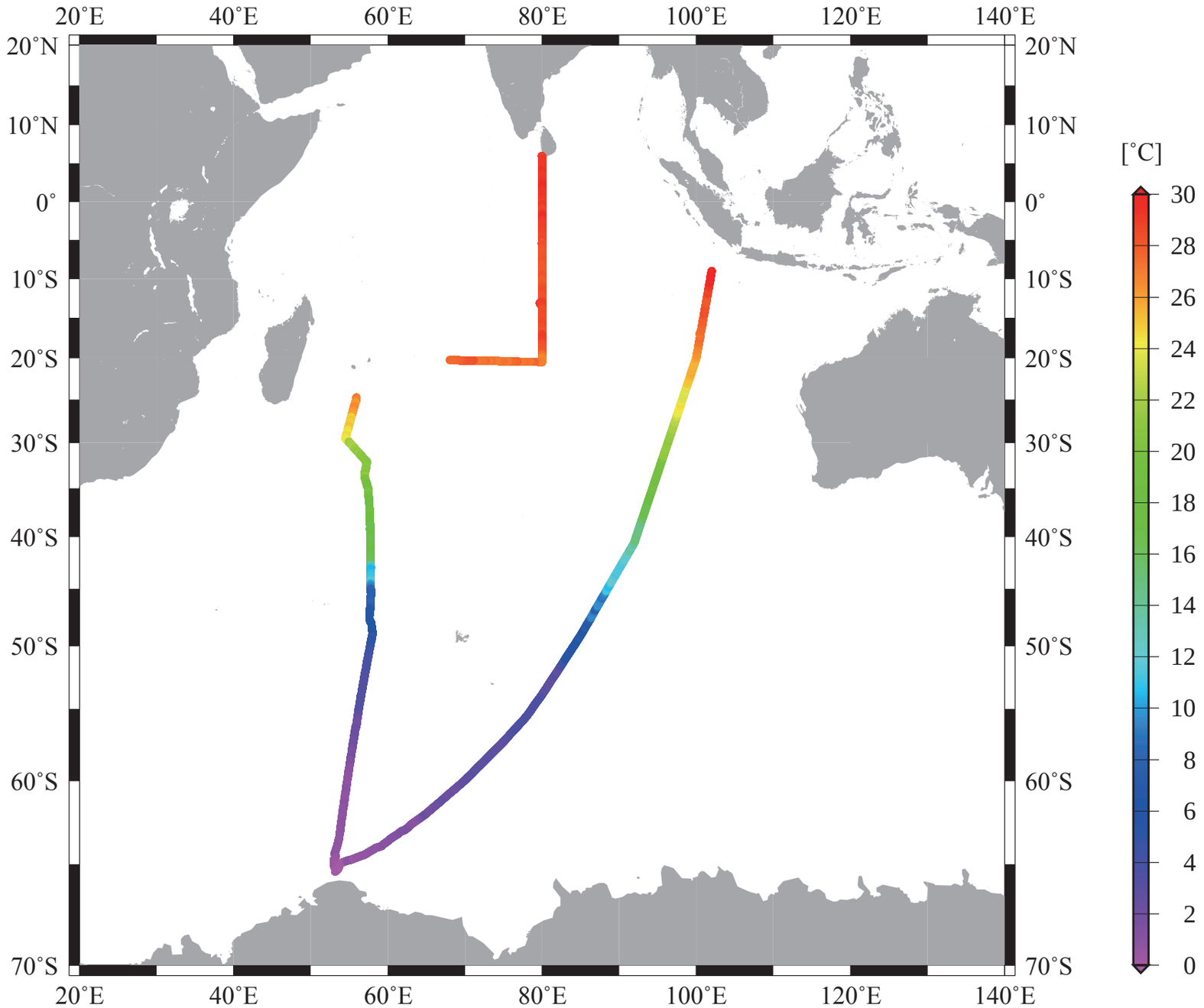

Figure 4b
Sea surface salinity (psu)

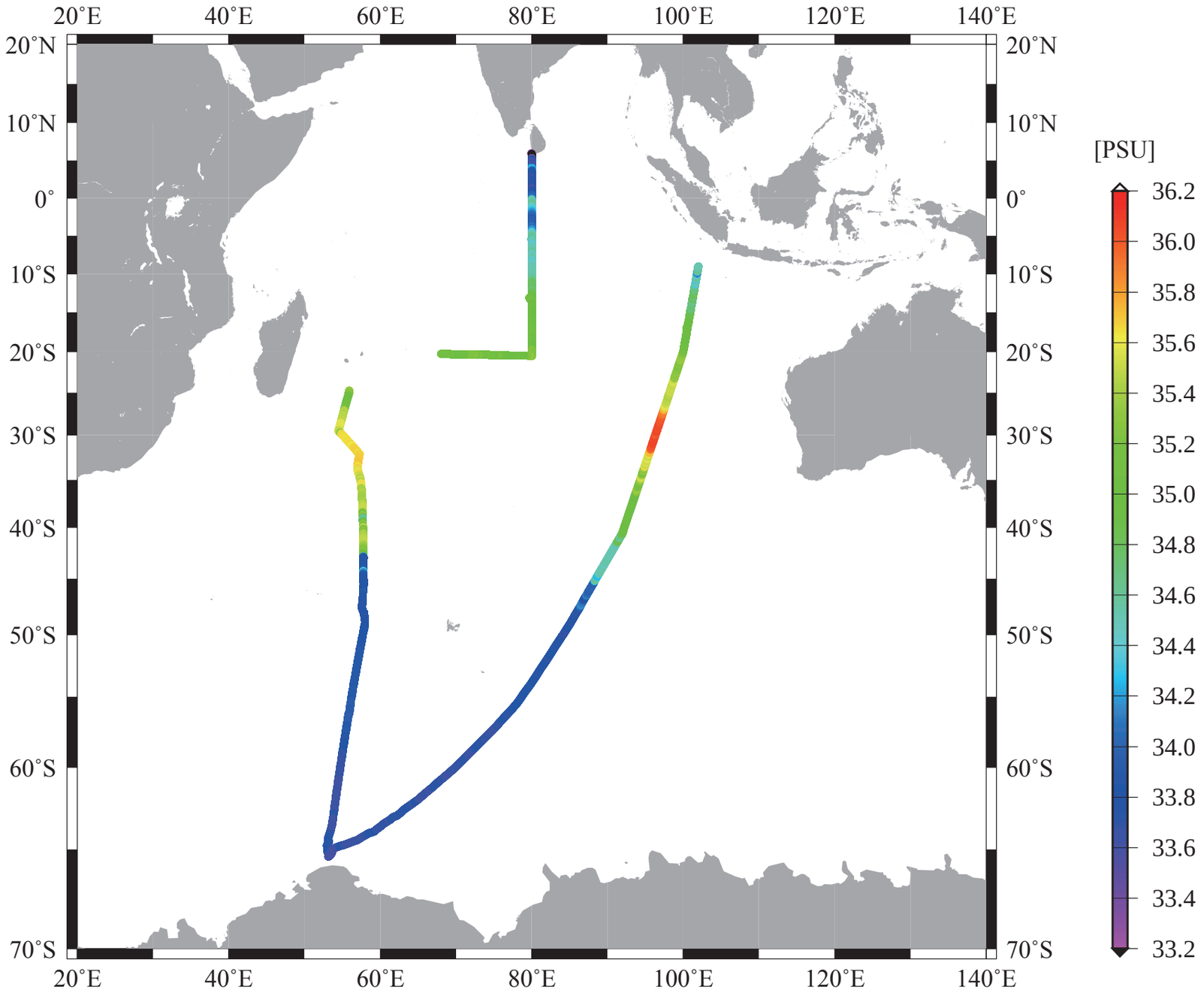

Figure 4c
Sea surface oxygen (µmol/kg)

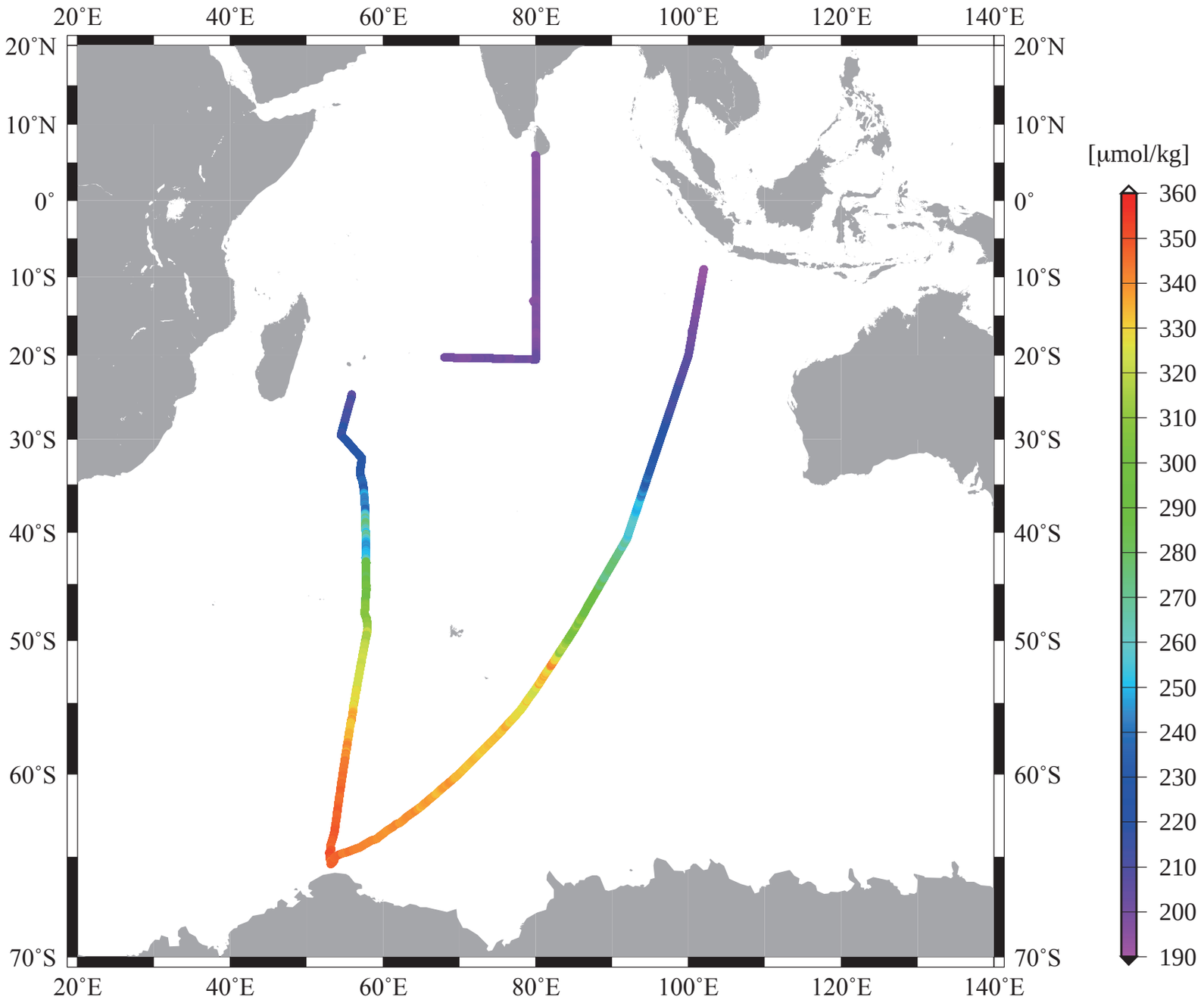

Figure 4d

Sea surface chlorophyll *a* (mg/m^3)

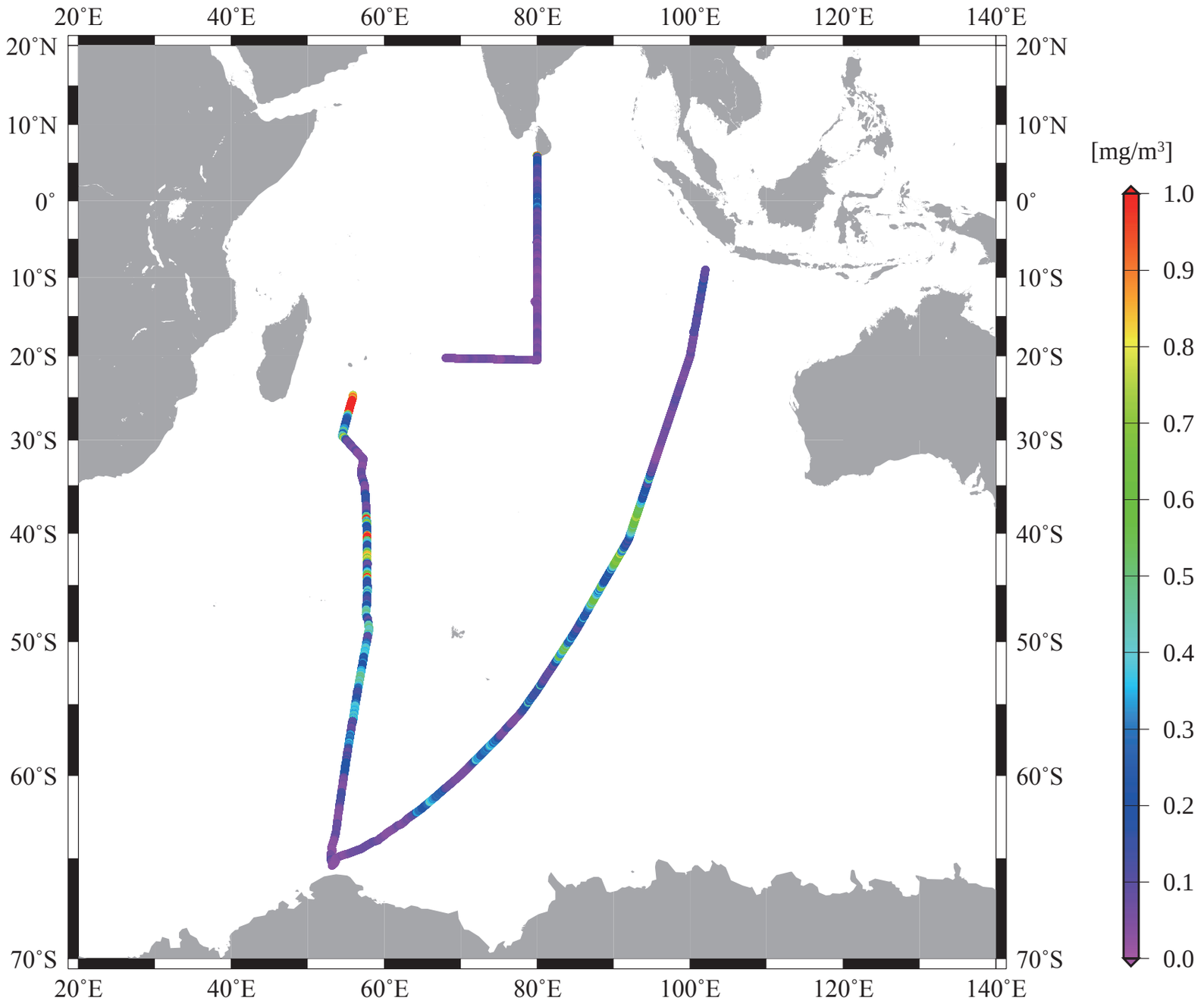

Figure 5

ΔpCO_2 (ppmv)

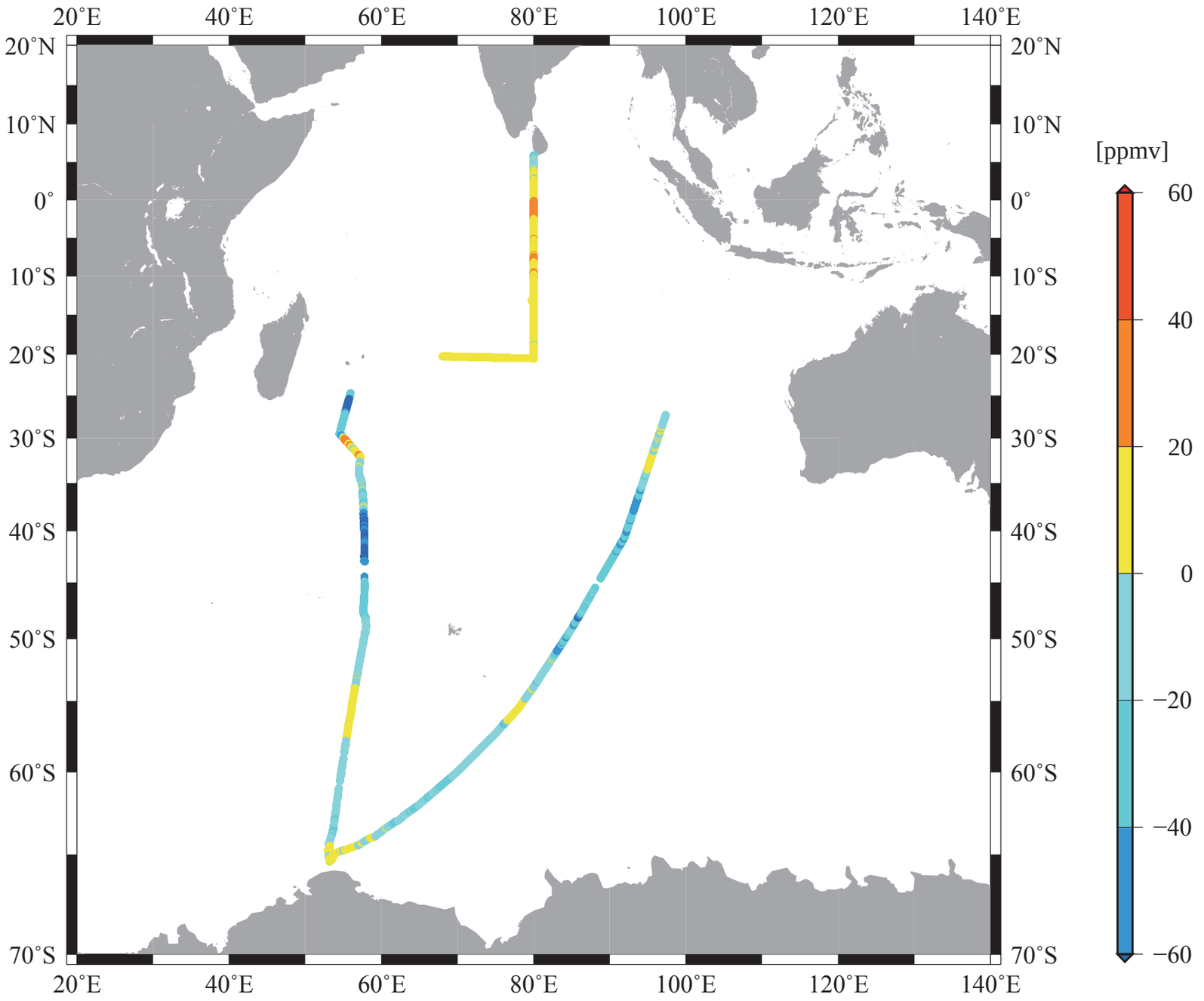

Figure 6
Surface current measured by shipboard ADCP

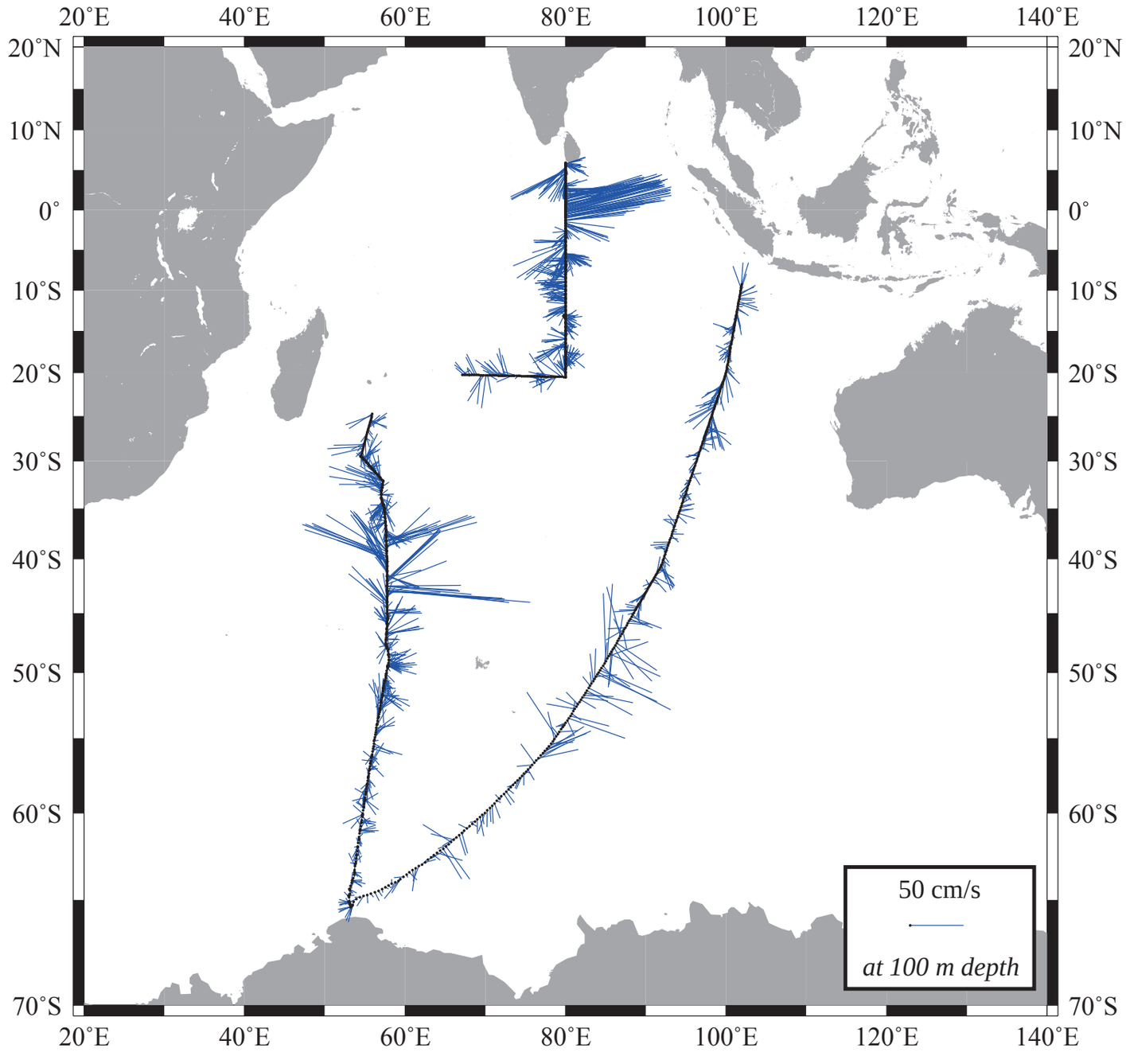

Figure 7
Potential temperature (°C)

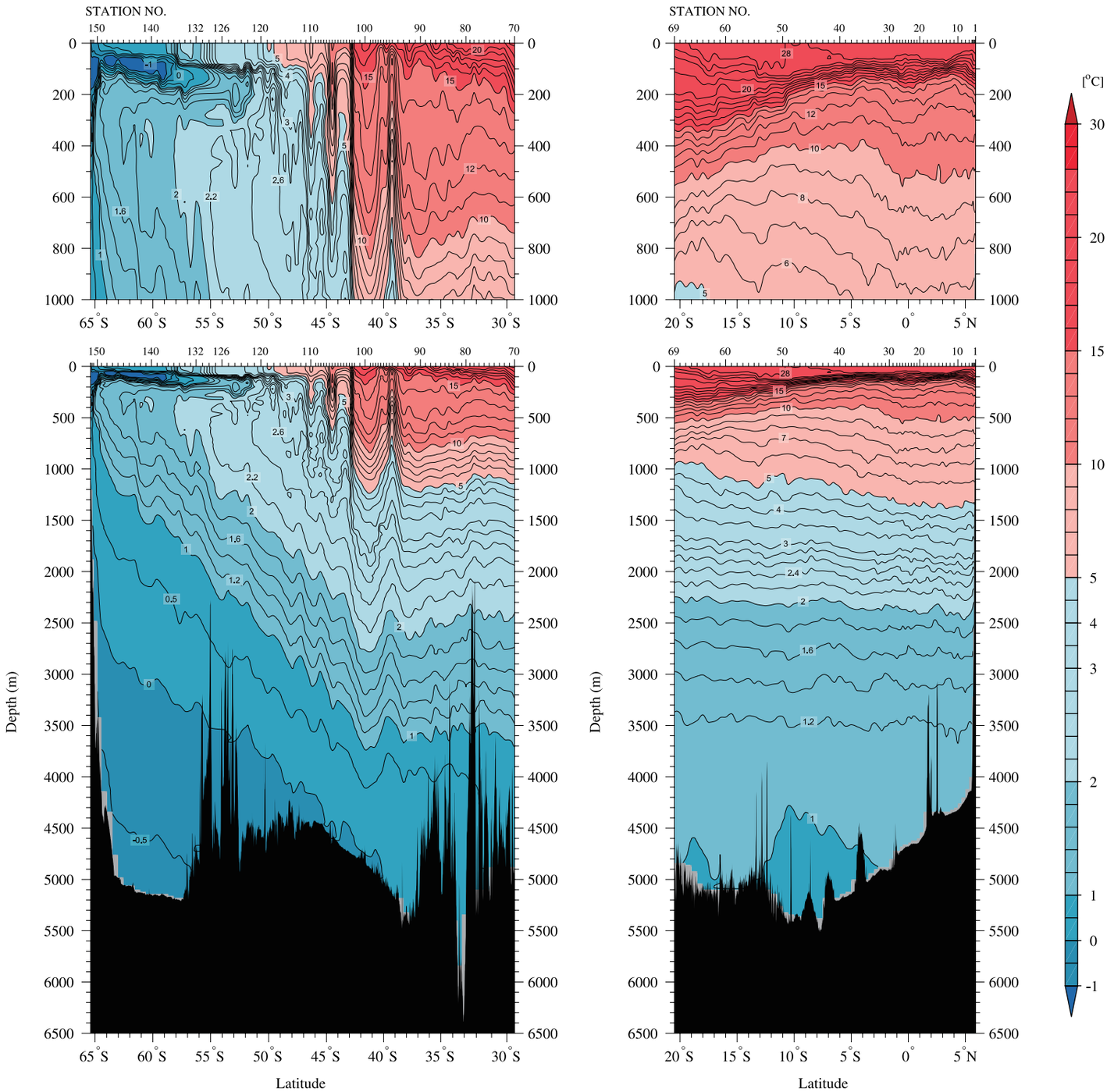

Figure 8
CTD salinity

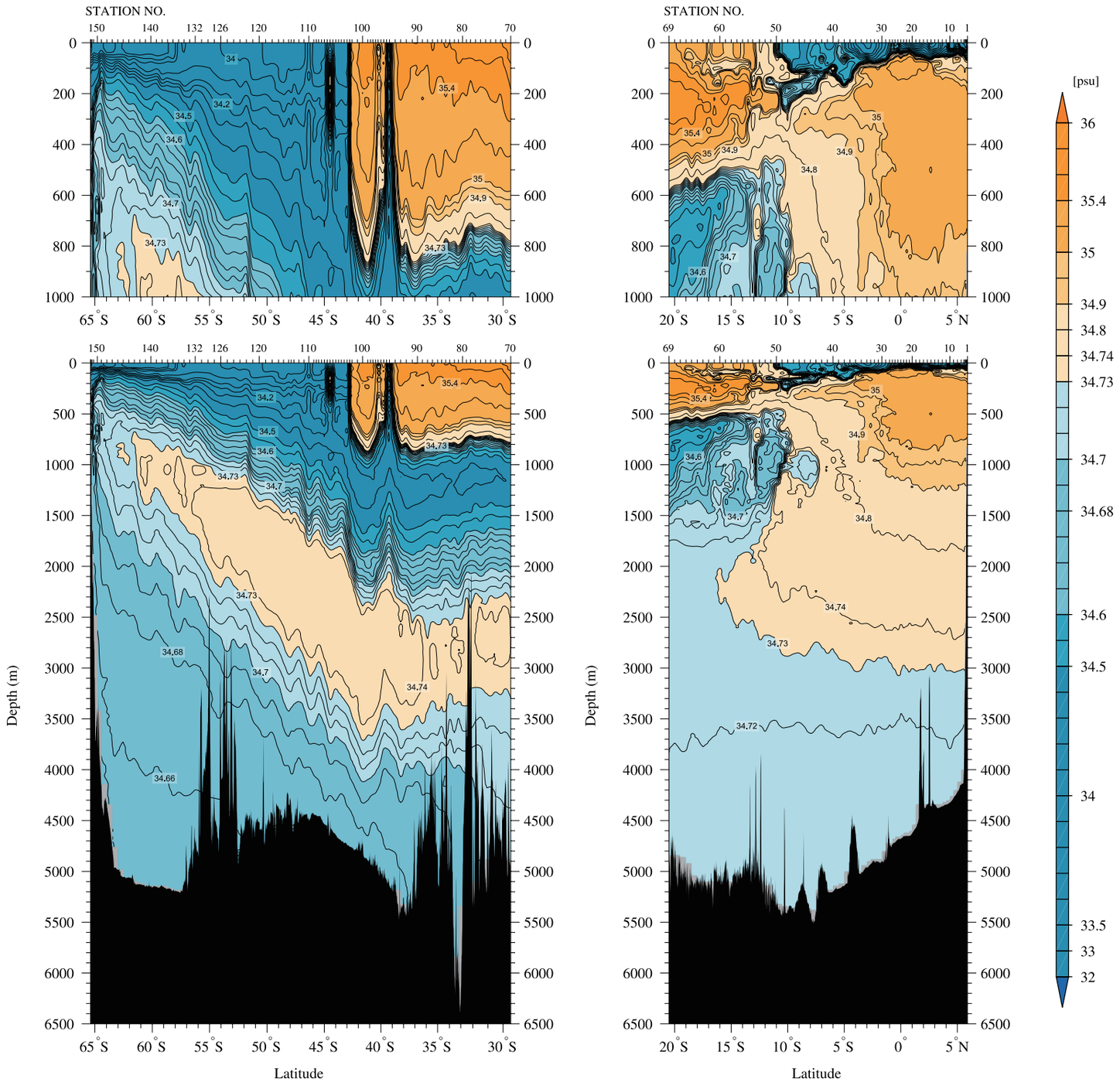

Figure 9
Absolute Salinity (g/kg)

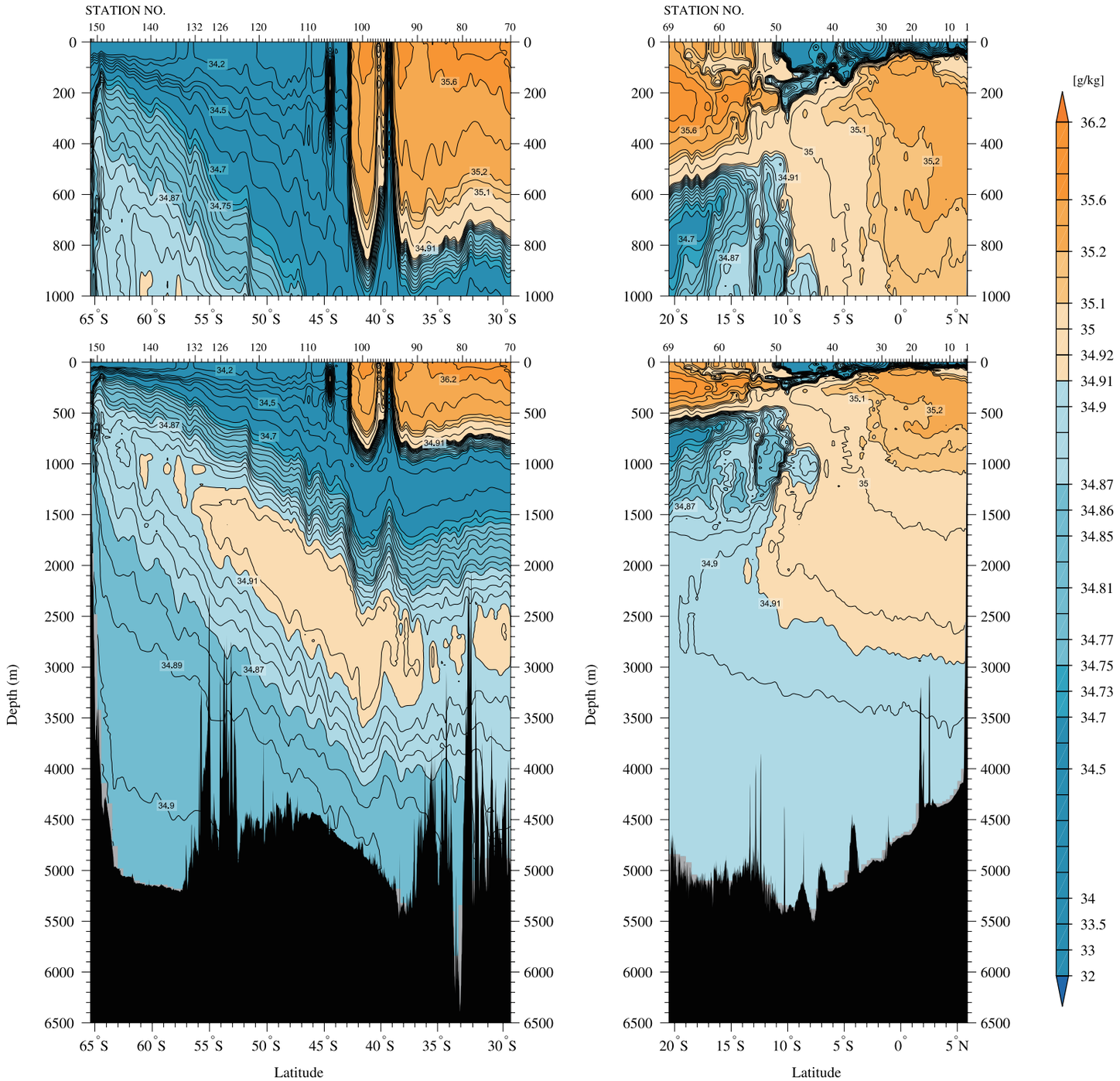

Figure 10

Density (upper: σ_0, lower: σ_4) (kg/m^3) (TEOS-10)

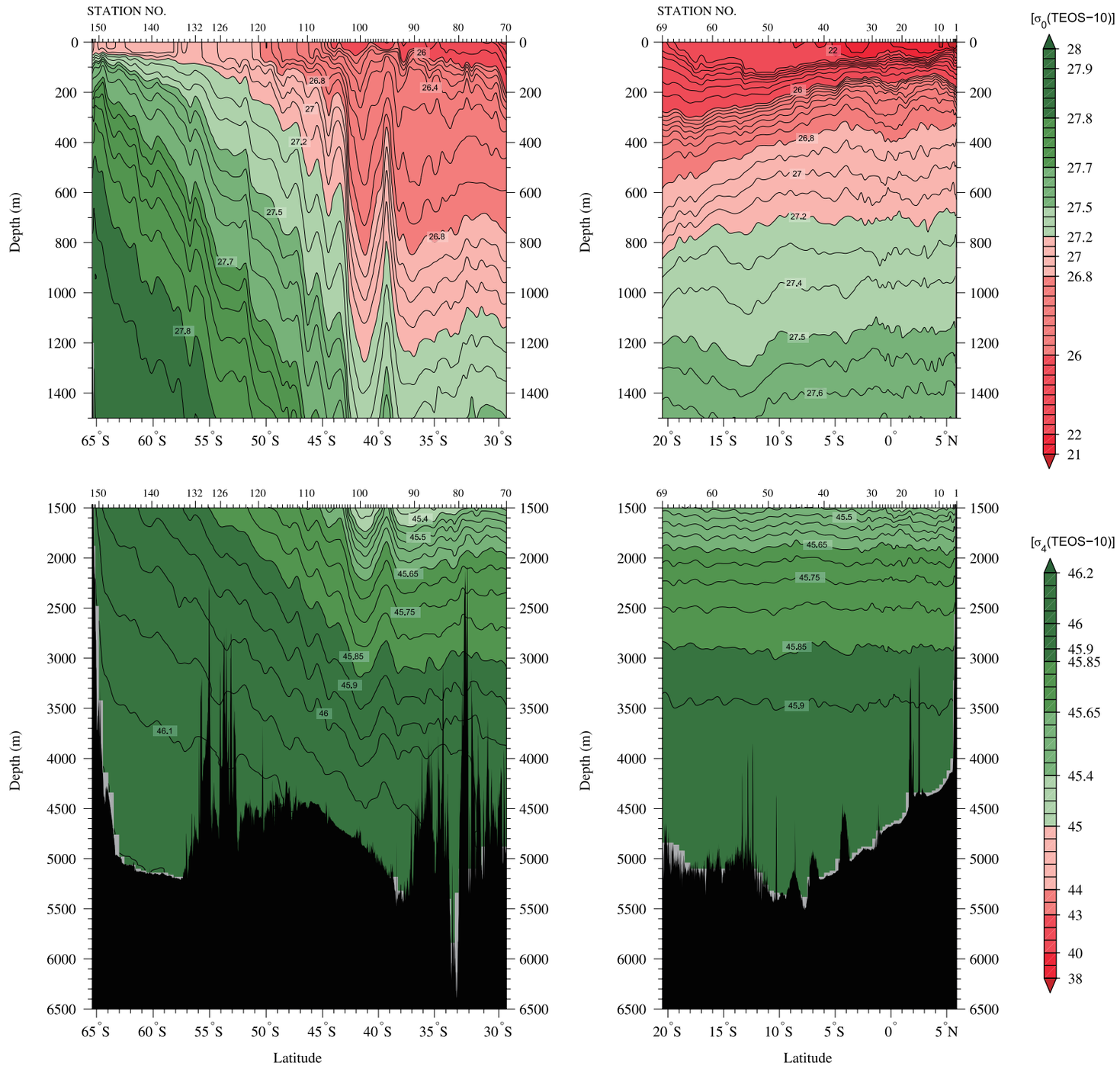

Figure 11
Density (γ^n) (kg/m^3)

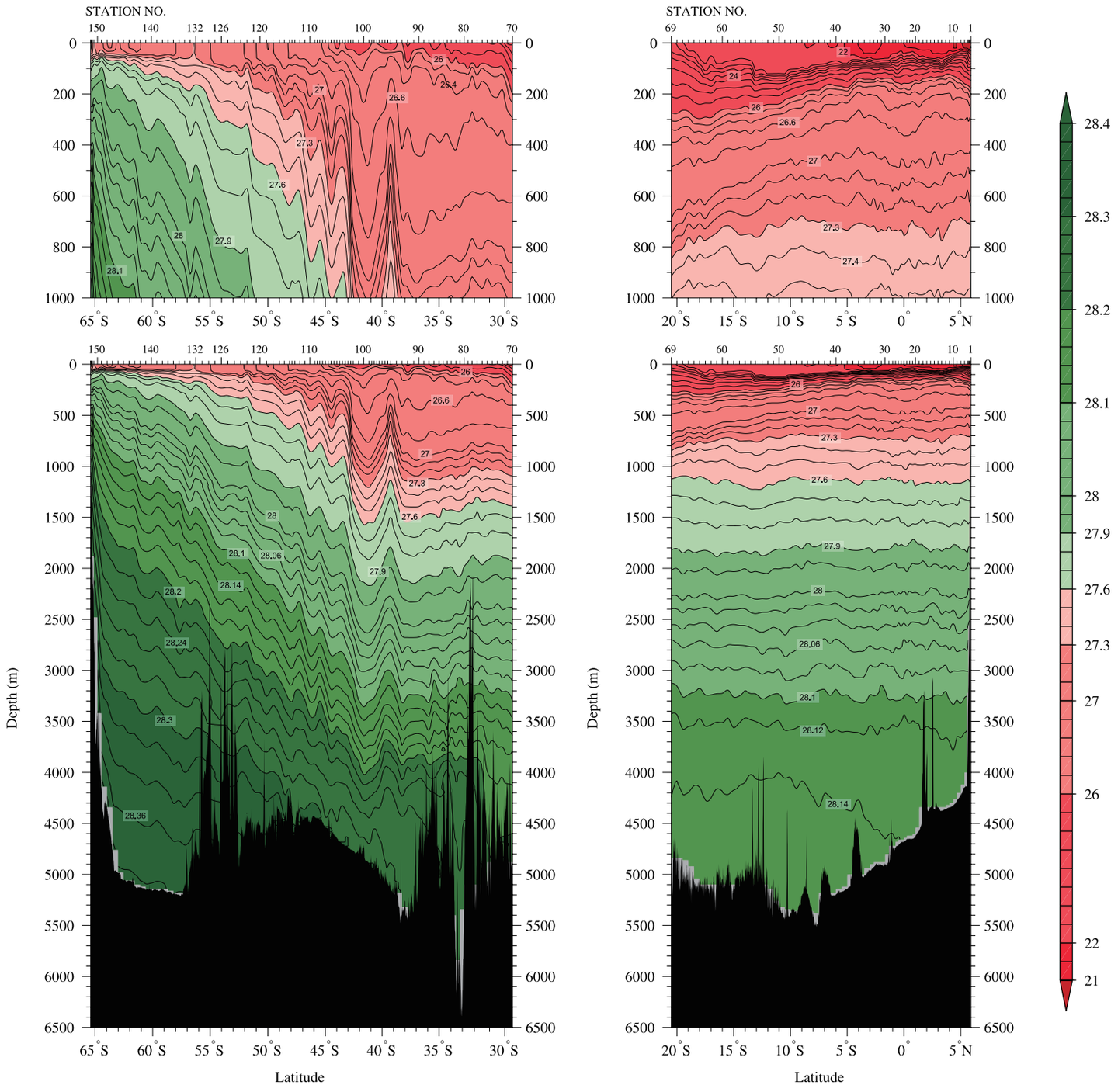

Figure 12
CTD oxygen (µmol/kg)

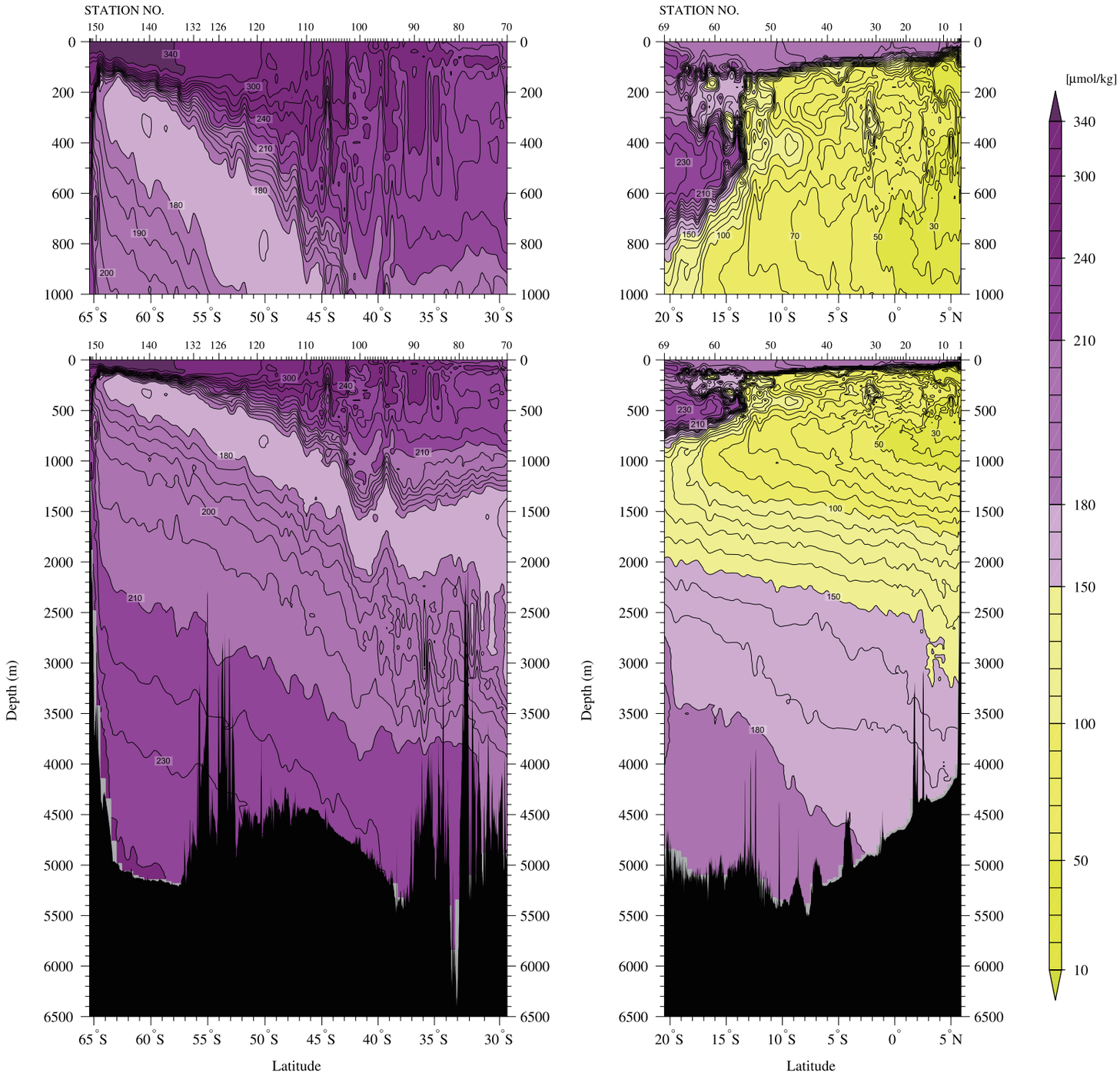

Figure 13
CTD chlorophyll *a* (mg/m^3)

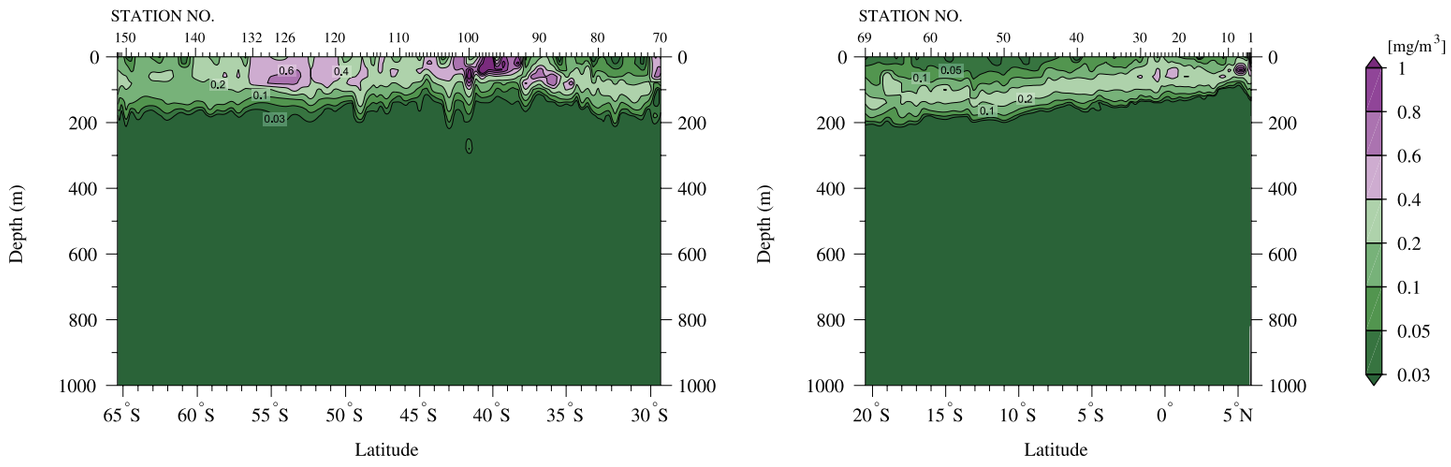

Figure 14
CTD beam attenuation coefficient (m^{-1})

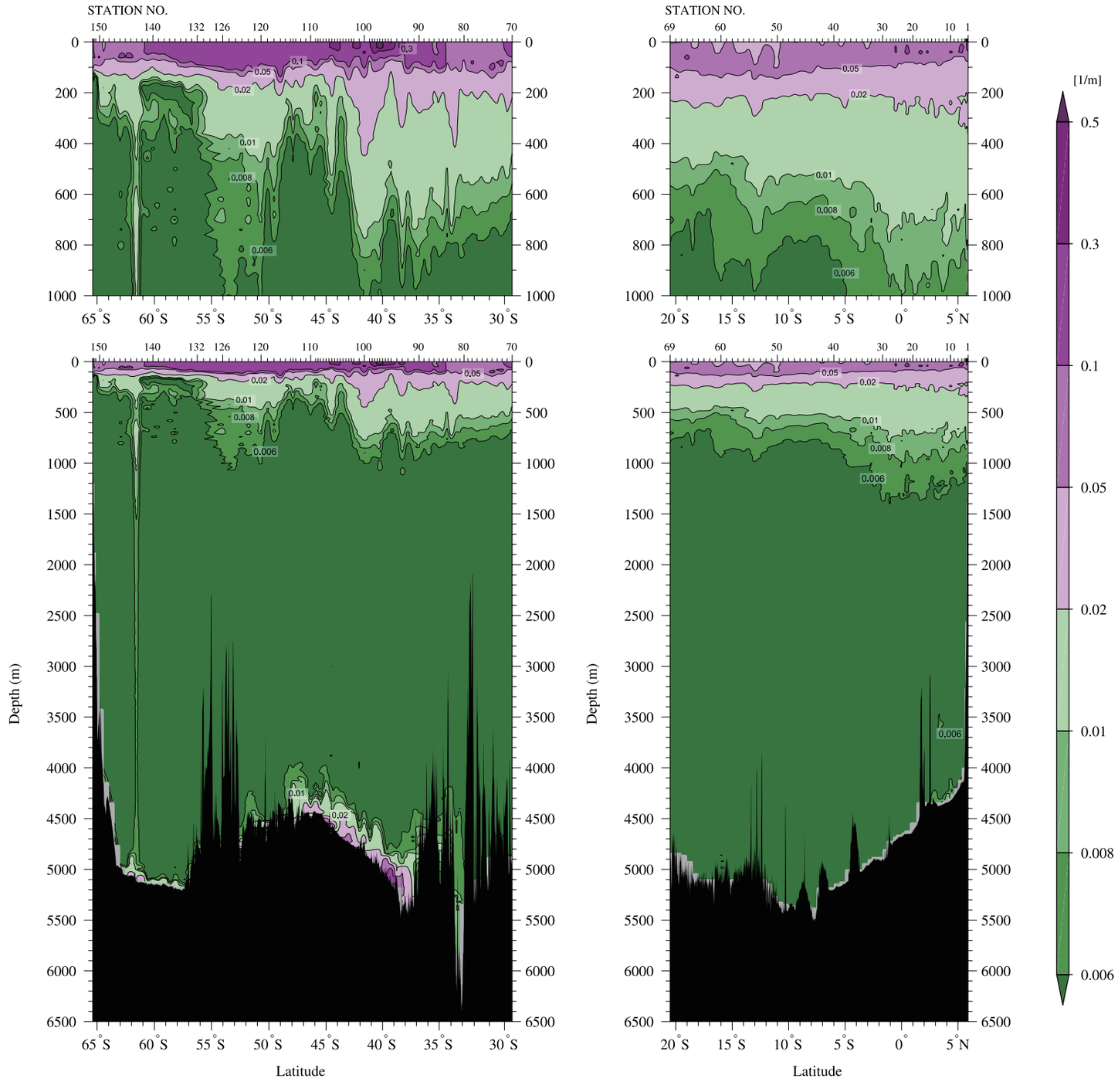

Figure 15
CTD FDOM (RU)

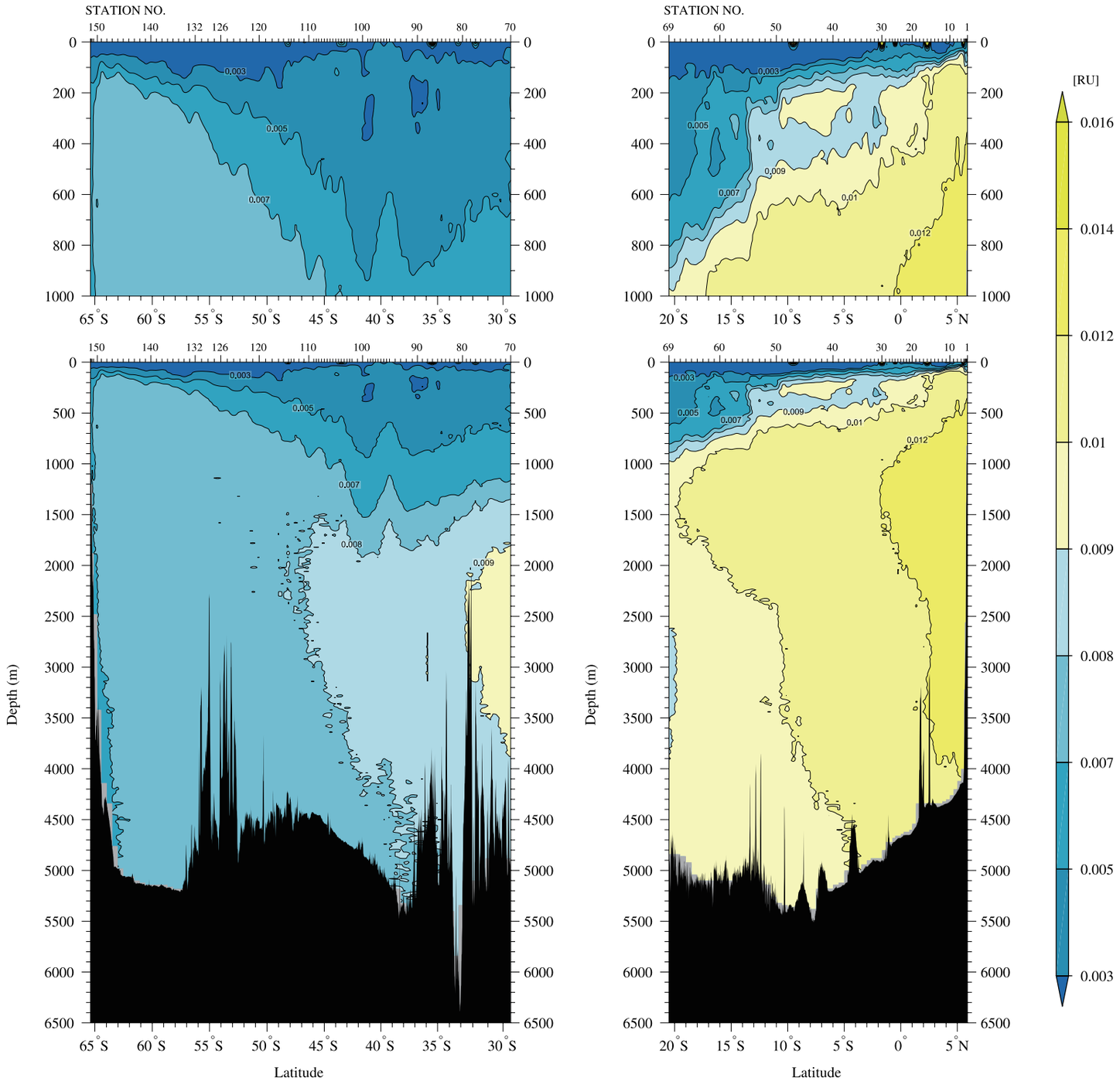

Figure 16

Bottle sampled dissolved oxygen (µmol/kg)

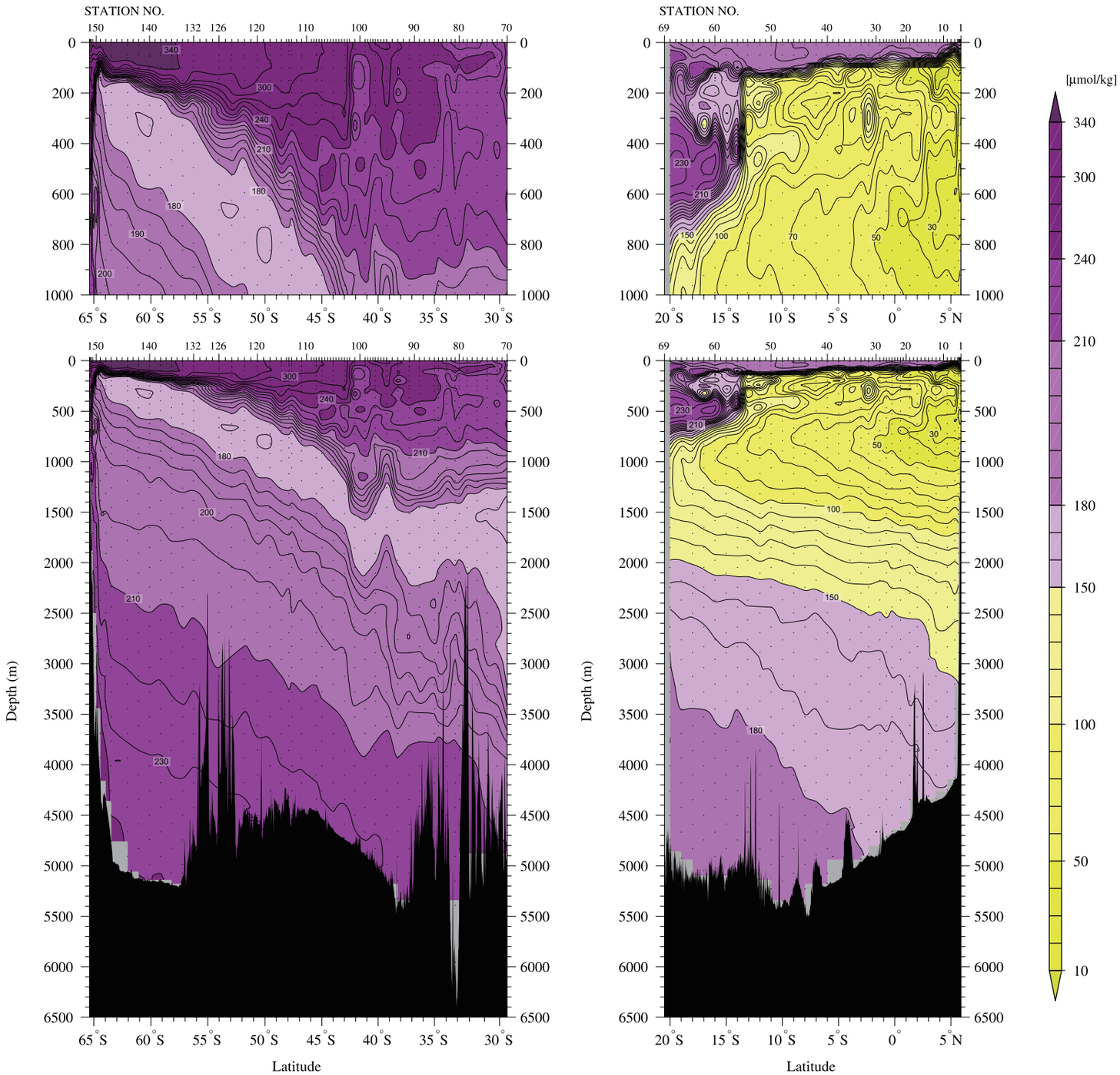

Figure 17
Silicate (µmol/kg)

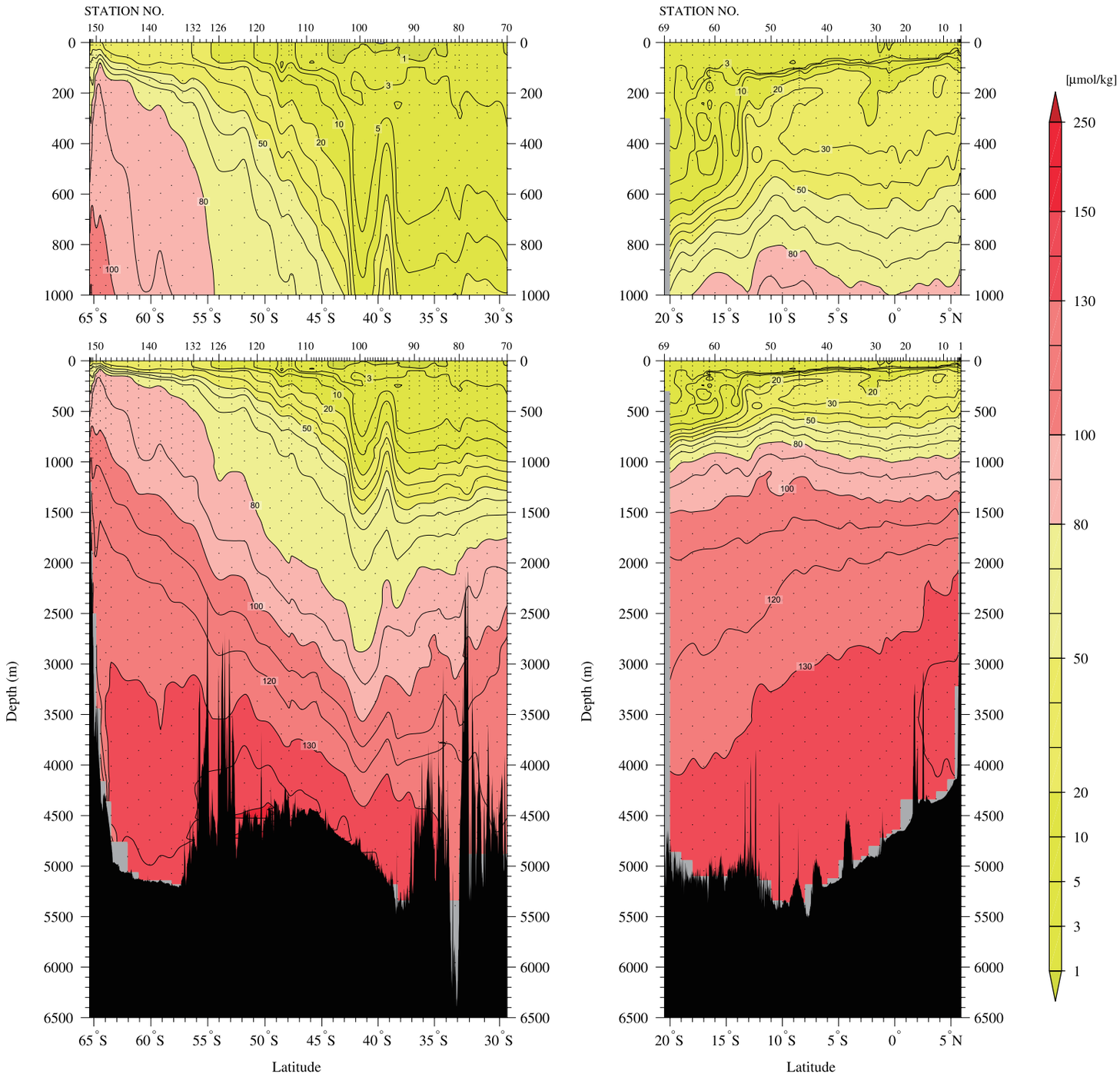

Figure 18
Nitrate (µmol/kg)

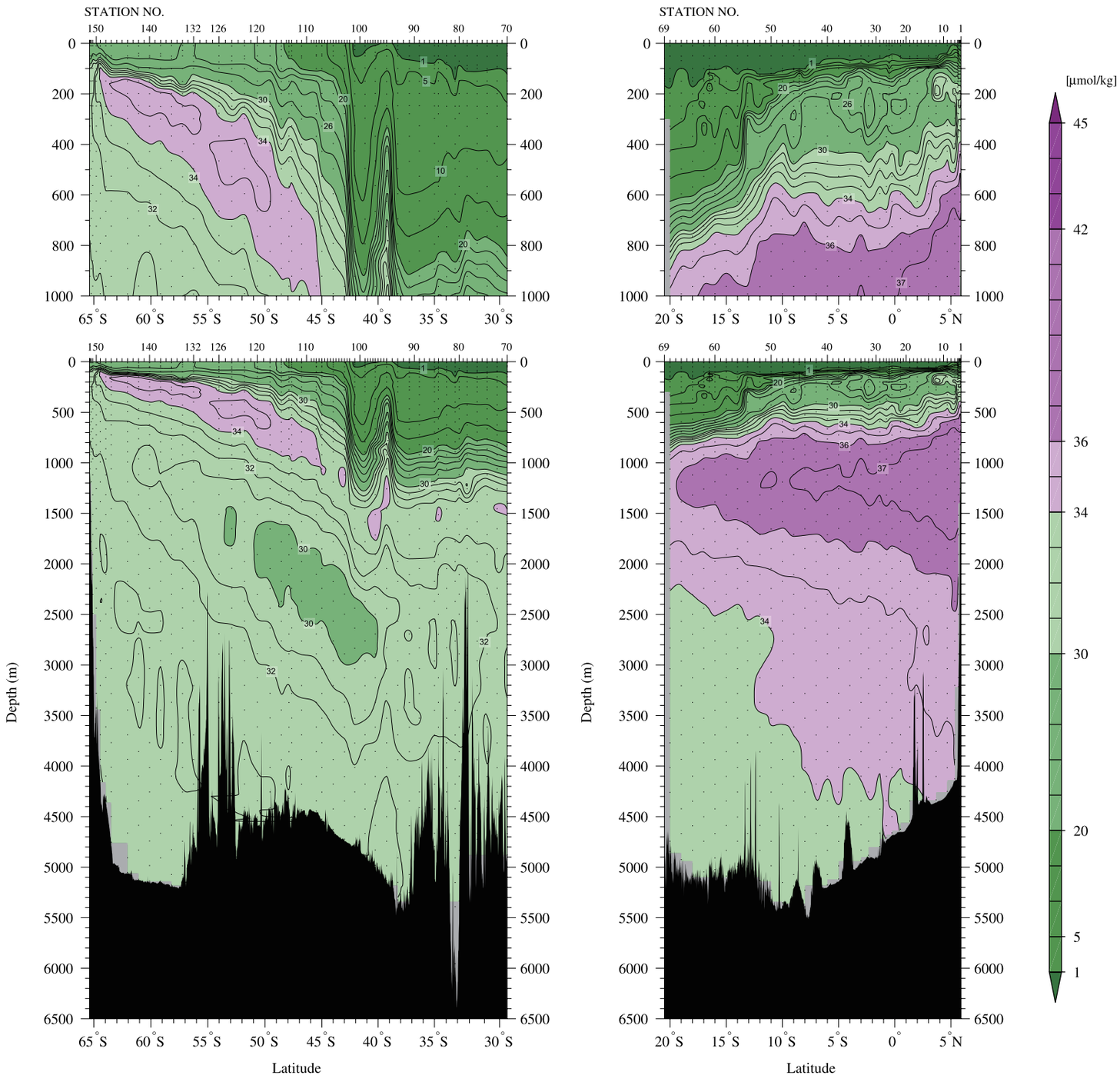

Figure 19
Nitrite (µmol/kg)

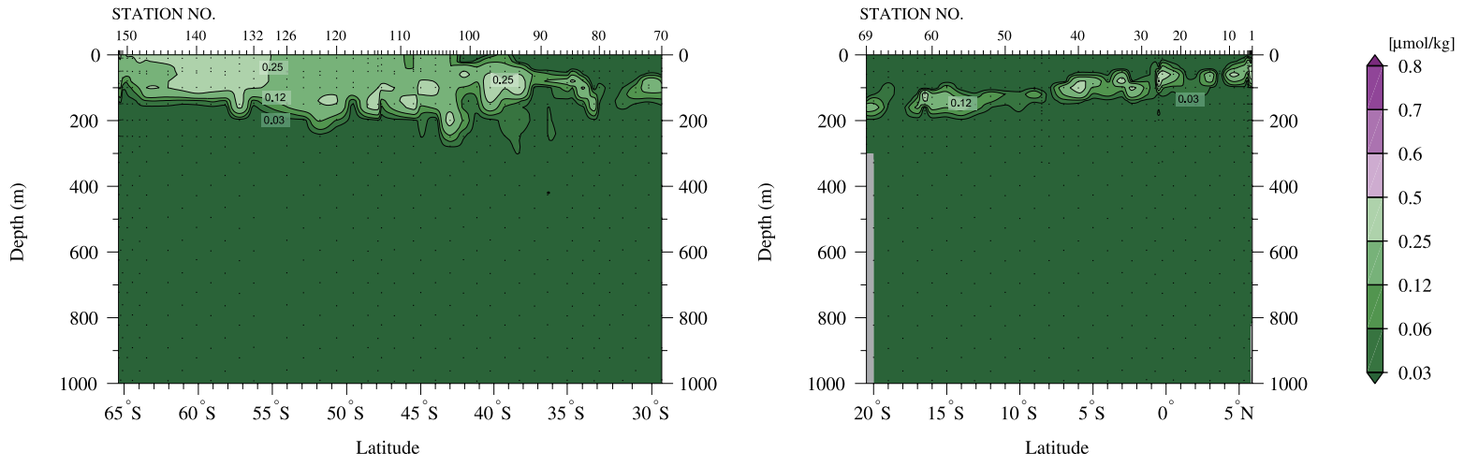

Figure 20
Phosphate (µmol/kg)

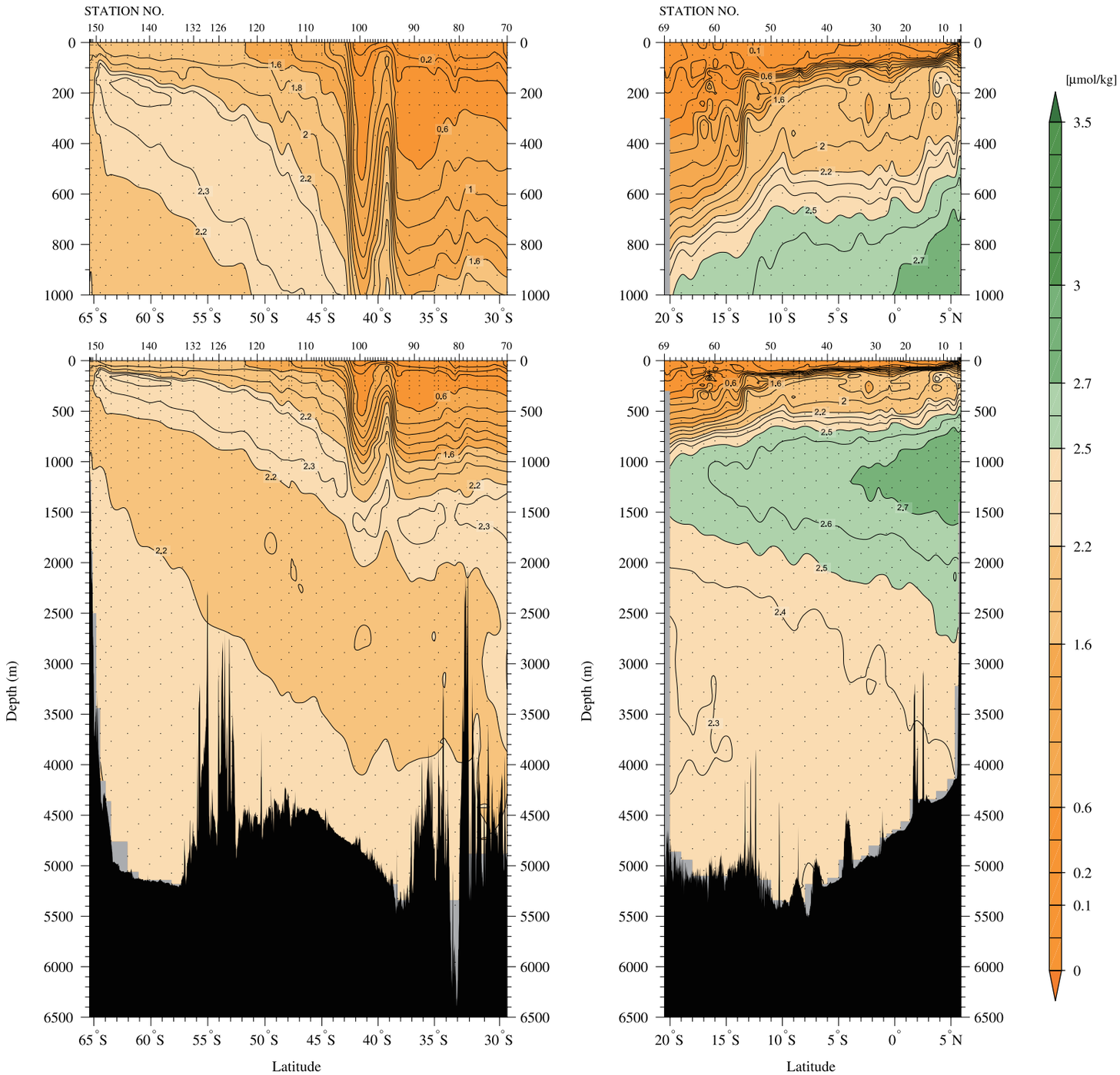

Figure 21
Dissolved inorganic carbon (C_T) (µmol/kg)

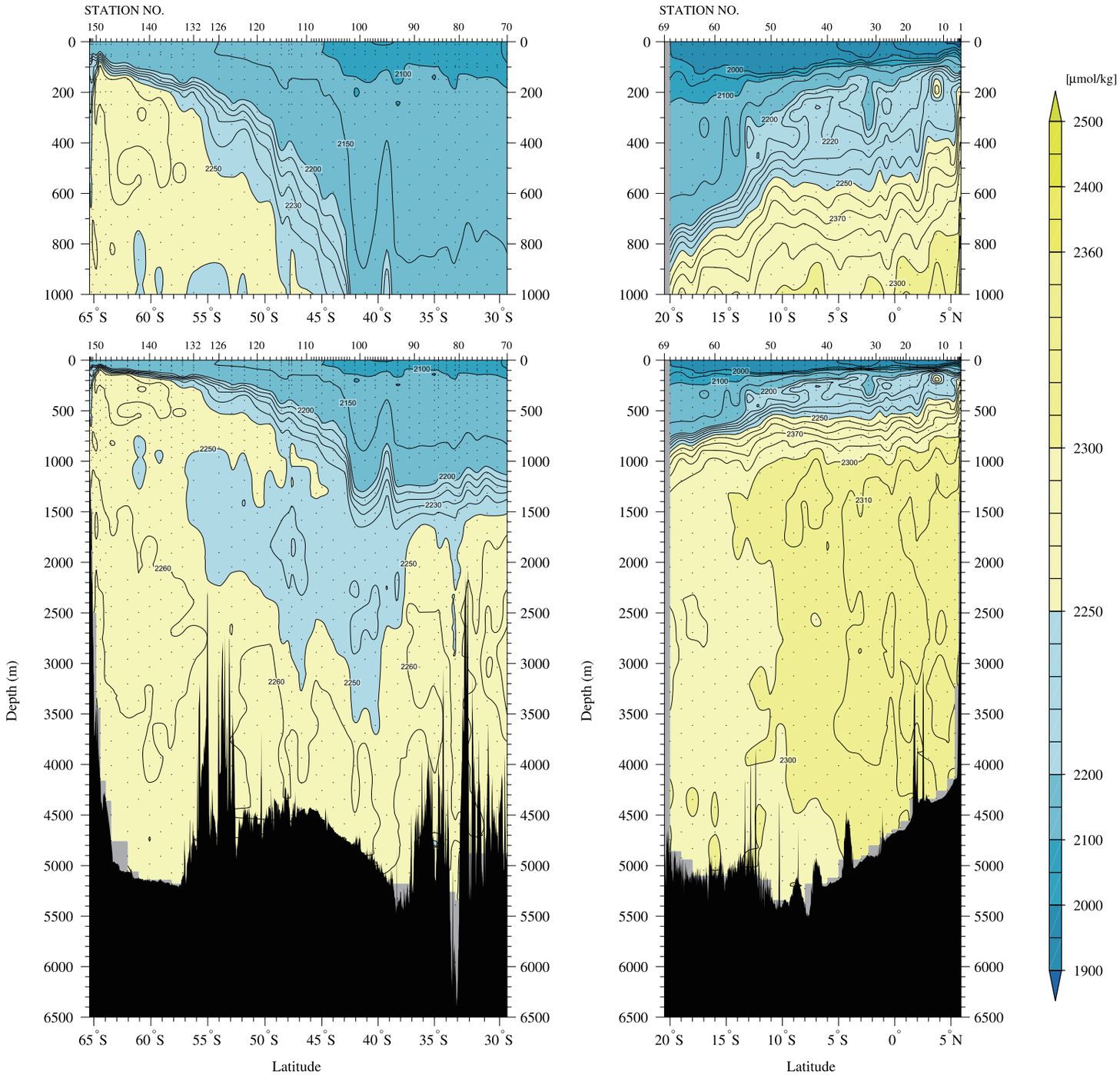

Figure 22

Total alkalinity (A_T) (µmol/kg)

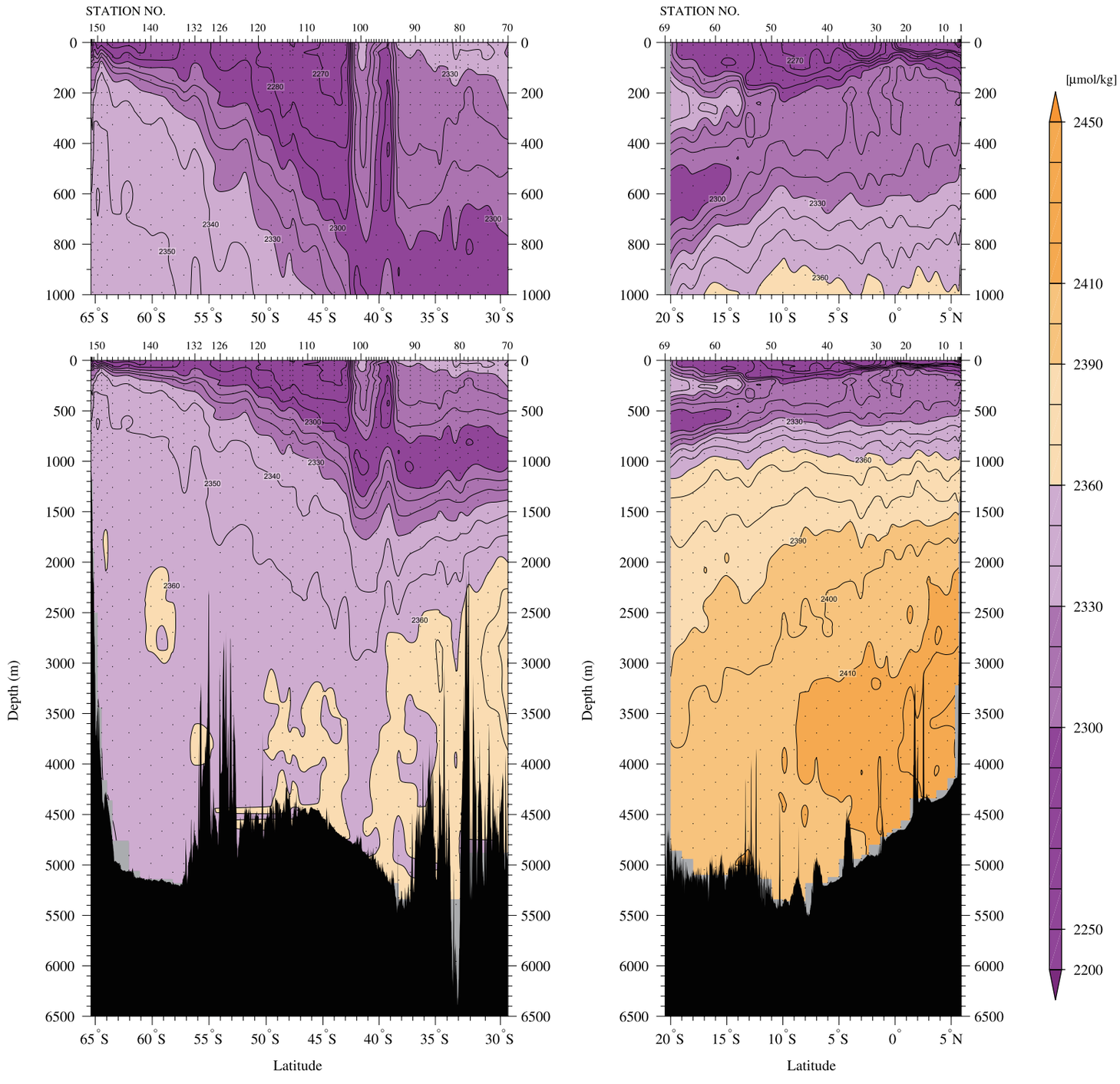

Figure 23
CDOM at 300 nm (m^{-1})

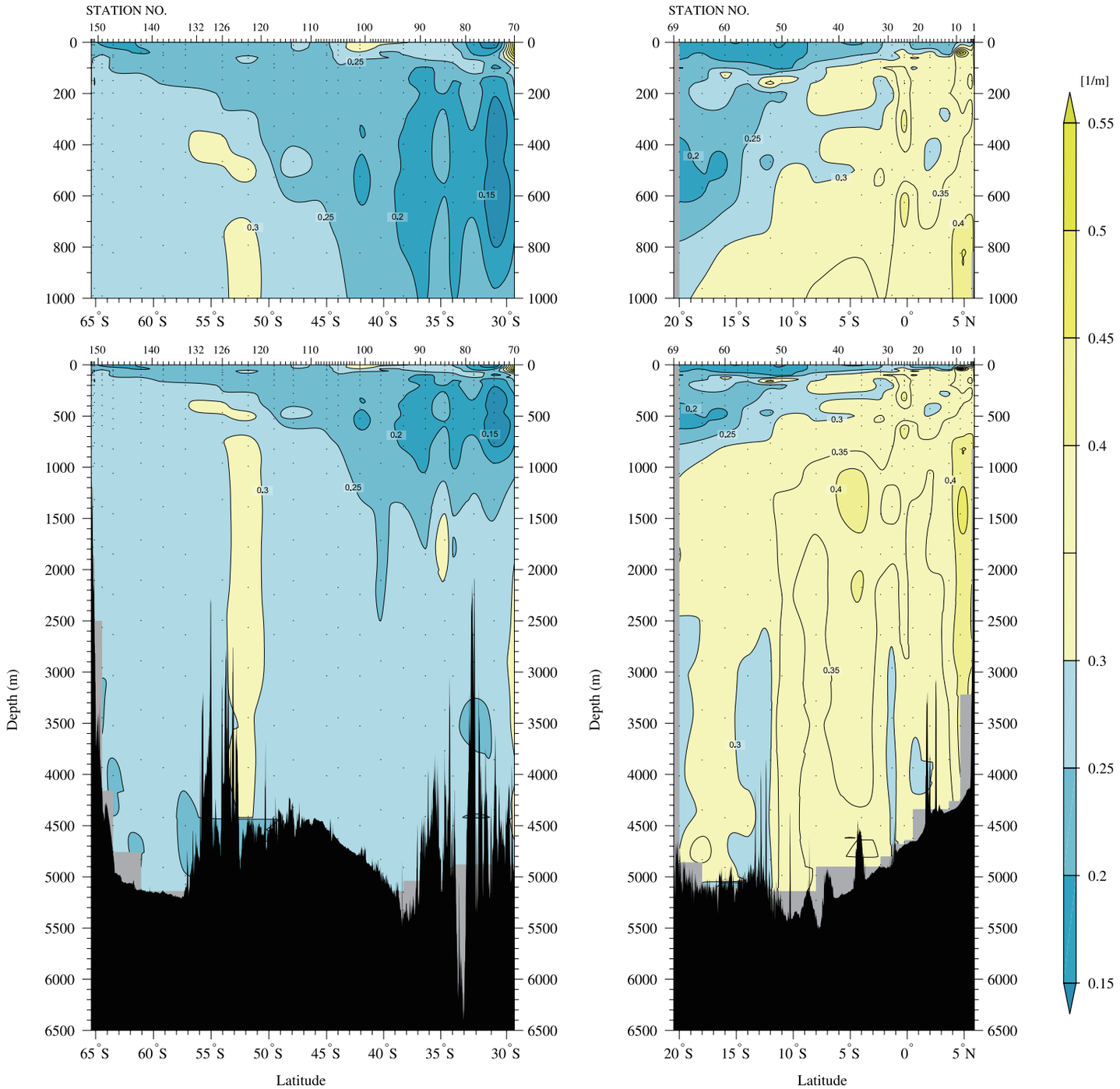

Figure 24
Current velocity (cm/s) measured by LADCP

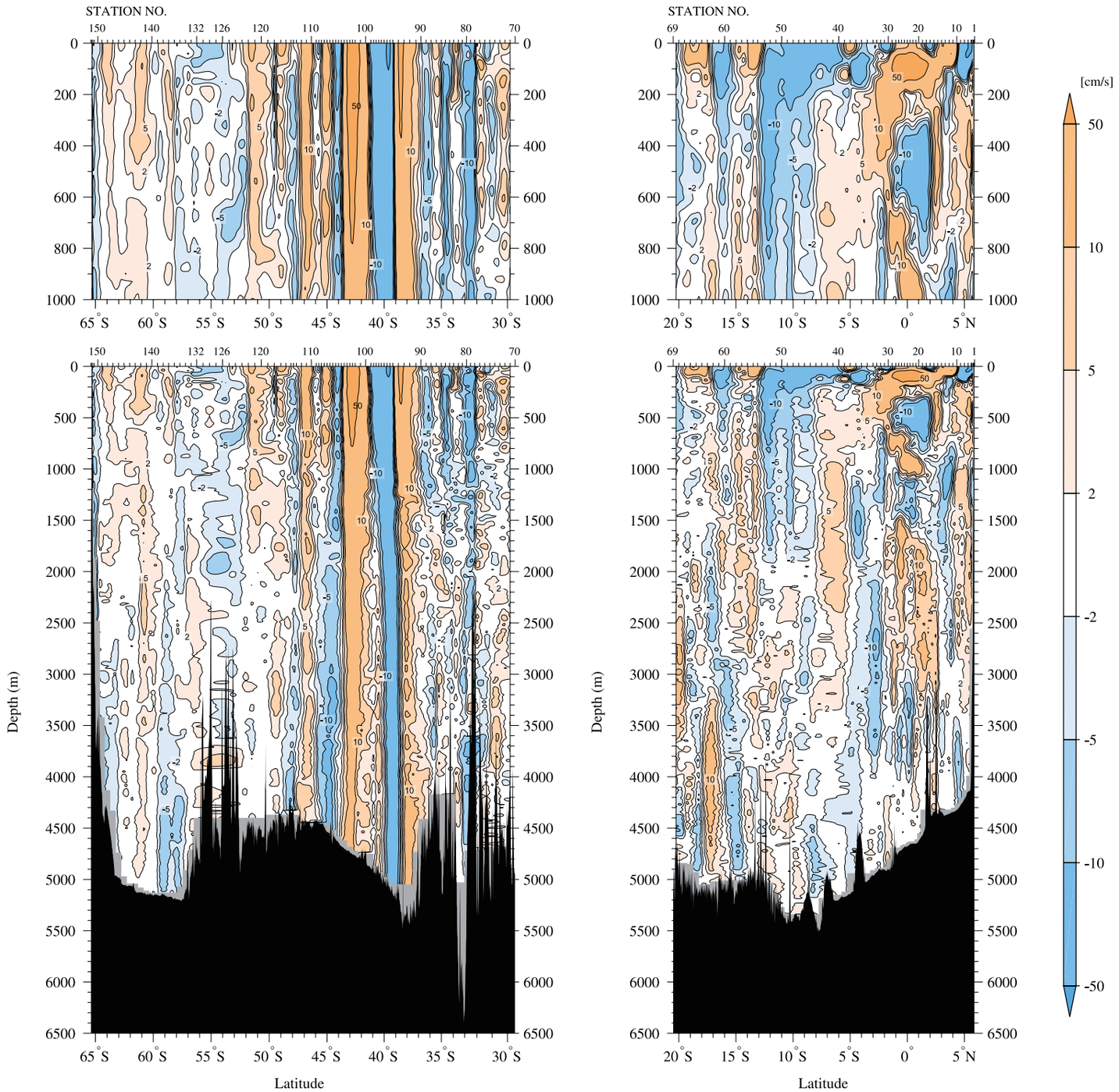

9784901833479